

IntechOpen

Electron Microscopes, Spectroscopy and Their Applications

Edited by Guillermo Huerta Cuellar



Electron Microscopes, Spectroscopy and Their Applications

Edited by Guillermo Huerta Cuellar

Published in London, United Kingdom

Electron Microscopes, Spectroscopy and Their Applications

<http://dx.doi.org/10.5772/intechopen.1000339>

Edited by Guillermo Huerta Cuellar

Contributors

Ahmed M. Hamid, Christof Jungbauer, Ghita el Mouhri, Guillermo Huerta Cuellar, Jeet Dasgupta, Josef Neumüller, Jörg Kriegsmann, Katharina Kriegsmann, Kimberly Y. Kartowikromo, Mark Kriegsmann, Naima Mammate, Nataliya Starostina, Niha Ansari, Orobola E. Olajide, Priya Rajput, Rita Casadonte, Salim Belchkar, Salma Ssouni, Sanja Cirovic, Shweta Umre, Takuya Hiratsuka, Tarik Sqalli Houssaini, Tatsuaki Tsuruyama, Thomas Wagner, Torsten Hansen

© The Editor(s) and the Author(s) 2024

The rights of the editor(s) and the author(s) have been asserted in accordance with the Copyright, Designs and Patents Act 1988. All rights to the book as a whole are reserved by INTECHOPEN LIMITED. The book as a whole (compilation) cannot be reproduced, distributed or used for commercial or non-commercial purposes without INTECHOPEN LIMITED's written permission. Enquiries concerning the use of the book should be directed to INTECHOPEN LIMITED rights and permissions department (permissions@intechopen.com).

Violations are liable to prosecution under the governing Copyright Law.



Individual chapters of this publication are distributed under the terms of the Creative Commons Attribution 3.0 Unported License which permits commercial use, distribution and reproduction of the individual chapters, provided the original author(s) and source publication are appropriately acknowledged. If so indicated, certain images may not be included under the Creative Commons license. In such cases users will need to obtain permission from the license holder to reproduce the material. More details and guidelines concerning content reuse and adaptation can be found at <http://www.intechopen.com/copyright-policy.html>.

Notice

Statements and opinions expressed in the chapters are those of the individual contributors and not necessarily those of the editors or publisher. No responsibility is accepted for the accuracy of information contained in the published chapters. The publisher assumes no responsibility for any damage or injury to persons or property arising out of the use of any materials, instructions, methods or ideas contained in the book.

First published in London, United Kingdom, 2024 by IntechOpen

IntechOpen is the global imprint of INTECHOPEN LIMITED, registered in England and Wales, registration number: 11086078, 167-169 Great Portland Street, London, W1W 5PF, United Kingdom

British Library Cataloguing-in-Publication Data

A catalogue record for this book is available from the British Library

Additional hard and PDF copies can be obtained from orders@intechopen.com

Electron Microscopes, Spectroscopy and Their Applications

Edited by Guillermo Huerta Cuellar

p. cm.

Print ISBN 978-0-85466-485-6

Online ISBN 978-0-85466-484-9

eBook (PDF) ISBN 978-0-85466-486-3

We are IntechOpen, the world's leading publisher of Open Access books Built by scientists, for scientists

7,000+

Open access books available

186,000+

International authors and editors

200M+

Downloads

156

Countries delivered to

Our authors are among the
Top 1%

most cited scientists

12.2%

Contributors from top 500 universities



WEB OF SCIENCE™

Selection of our books indexed in the Book Citation Index
in Web of Science™ Core Collection (BKCI)

Interested in publishing with us?
Contact book.department@intechopen.com

Numbers displayed above are based on latest data collected.
For more information visit www.intechopen.com



Meet the editor



Guillermo Huerta Cuellar received a Ph.D. from Centro de Investigaciones en Óptica, Mexico, in 2009. He is currently working at Centro Universitario de los Lagos, University of Guadalajara. He has been a visiting researcher at Instituto Potosino de Investigación Científica y Tecnológica (IPICYT), Mexico; the Faculty of Radiophysics, Lobachevsky State University of Nizhny Novgorod, Russia; and St. Mary's University, San Antonio, Texas, USA. He has edited six books and published eight book chapters and seventy high-impact publications. He has been an academic editor for journals such as *Complexity* and *Frontiers in Applied Mathematics* and a reviewer for several others. His research interests include the study, characterization, and dynamical behavior of fiber lasers and electronic circuits and their modeling.

Contents

Preface	XI
Section 1	
Uses of Electron Microscopy and Spectroscopy in Research	1
Chapter 1	3
Introductory Chapter: Materials Analysis by Using Electronic Microscopes and Spectroscopy <i>by Guillermo Huerta Cuellar</i>	
Chapter 2	7
Elements of Electron Microscopy Designing Laboratory Course: Examples and Applications <i>by Nataliya Starostina</i>	
Chapter 3	29
Ion Mobility Mass Spectrometry: Instrumentation and Applications <i>by Orobola E. Olajide, Kimberly Y. Kartowikromo and Ahmed M. Hamid</i>	
Section 2	
Characterization and Analysis of Samples	55
Chapter 4	57
Characterization and Enumeration of Platelet Microvesicles in Human Platelet Concentrates by Using Transmission Electron Microscopy Including Electron Tomography <i>by Josef Neumüller, Christof Jungbauer and Thomas Wagner</i>	
Chapter 5	75
The Use of Electron Microscopy for Lithiasis Research <i>by Naima Mammate, Salim Belchkar, Salma Ssouni, Ghita el Mouhri and Tarik Sqalli Houssaini</i>	
Chapter 6	89
Mass Spectrometry Analysis Using Formalin-Fixed Paraffin-Embedded Pathological Samples <i>by Takuya Hiratsuka and Tatsuki Tsuruyama</i>	

Section 3	
Applications	107
Chapter 7	109
Harnessing Electron Microscope for Trace Evidence Analysis	
<i>by Niha Ansari, Jeet Dasgupta, Shweta Umre and Priya Rajput</i>	
Chapter 8	147
Perspective Chapter: Predictive Genomics	
<i>by Jörg Kriegsmann, Sanja Cirovic, Rita Casadonte, Torsten Hansen,</i>	
<i>Katharina Kriegsmann and Mark Kriegsmann</i>	

Preface

Materials analysis plays a pivotal role in understanding the properties, behavior, and performance of various substances, from the smallest nanoparticles to the largest engineering structures. The advent of electronic microscopes and spectroscopic techniques has revolutionized the field of materials science, enabling researchers to delve deeper into the atomic and molecular structure of materials with unprecedented precision and detail.

The first part of the book introduces the topic and discusses electron microscopy, spectroscopy, and some applications. It presents a guide on designing laboratory procedures for material characterization using electron microscopy, focusing on the benefits of utilizing backscattered electrons (BSE), secondary electrons (SE), and energy-dispersive spectroscopy (EDS). The approach includes discussions on incorporating additional microscopy techniques like atomic force microscopy (AFM), ellipsometry, and optical profilometry as supplementary methods to validate electron microscopy findings. Moreover, the section presents a thorough examination of different instrument management system (IMS) platforms, including traveling wave (TWIMS), drift tube (DTIMS), trapped (TIMS), differential mobility analyzer (DMA), and Field asymmetric waveform (FAIMS). The identification of biomarkers through mass spectrometry (MS) is crucial in clinical medical research. Yet, analyzing proteins in formalin-fixed paraffin-embedded (FFPE) samples using MS has been difficult due to decreased solubility from fixation, resulting in crosslinking reactions among amino acid side chains in proteins.

The second section highlights the importance of using scanning electron microscopy coupled with X-ray energy dispersive (SEM-EDX) to analyze the surface of kidney stones for evaluating the antilithiatic properties of extracts from medicinal plants like *Saussurea costus* (Falc) Lipsch. This highlights the significant role of electron microscopy in medical research, with a focus on urinary lithiasis. Also, in a similar way and as complementary analysis, spectroscopy techniques provide valuable information about the composition, structure, and properties of materials by analyzing the way they absorb, emit, or scatter light. These techniques allow researchers to identify substances, determine their concentration, and understand their molecular and atomic structure. By examining the unique spectral fingerprints of materials, spectroscopy plays a crucial role in various scientific fields, including chemistry, physics, biology, and materials science. Additionally, various methods used for omics analysis of FFPE samples to discover disease-specific biomarkers are discussed.

The third section explains trace evidence analysis as crucial in criminal investigations because it offers critical information for linking suspects to crime scenes. In forensic investigations, scanning electron microscopy (SEM) is a vital tool, particularly in gunshot residue (GSR) analysis, where SEM helps match bullets to firearms more effectively than visual methods. Moreover, SEM is significant in examining gemstones and jewelry by distinguishing between natural and synthetic gems, studying

surface flaws, and identifying elemental compositions. Finally, the use of spectroscopy techniques in predictive genomics can assist in treatment decisions by allowing individuals to take proactive measures to prevent serious illnesses. Finally, the section examines the use of matrix-assisted laser desorption/ionization time-of-flight (MALDI-TOF) mass spectrometry technology to identify genetic variations based on their unique mass.

This book is structured to provide a comprehensive understanding of electronic microscopes and spectroscopy as powerful tools for materials analysis. It is divided into three sections, each addressing specific aspects of the topic. The chapters cover the principles underlying electron microscopy and spectroscopy, the various imaging and analytical modes available, sample preparation techniques, data interpretation and analysis, as well as a diverse range of applications spanning different material classes. Furthermore, the book explores recent advancements and emerging trends in the field, shedding light on the prospects of materials analysis using electronic microscopes and spectroscopy. In summary, this book sets the stage for an in-depth exploration of electronic microscopes and spectroscopy as indispensable tools for materials analysis. By elucidating their historical evolution, significance, and scope, the book provides a solid foundation for readers to embark on a comprehensive journey through the world of advanced materials characterization.

Guillermo Huerta Cuellar

Department of Exact Sciences and Technology,
University Center of Lagos,
University of Guadalajara,
Lagos de Moreno, Jalisco, México

Section 1

Uses of Electron Microscopy and Spectroscopy in Research

Introductory Chapter: Materials Analysis by Using Electronic Microscopes and Spectroscopy

Guillermo Huerta Cuellar

1. Introduction

Materials analysis plays a pivotal role in understanding the properties, behavior, and performance of various substances, from the smallest nanoparticles to the largest engineering structures. The advent of electronic microscopes and spectroscopic techniques has revolutionized the field of materials science, enabling researchers to delve deeper into the atomic and molecular structure of materials with unprecedented precision and detail [1].

1.1 Applications of some analysis techniques using electronic microscopes

Material analysis using electron microscopy techniques involves the study of materials at a microscopic level with high resolution and magnification. Electron microscopes use a beam of accelerated electrons to illuminate the sample, providing detailed images of the material's surface and internal structure. These techniques, such as scanning electron microscopy (SEM) and transmission electron microscopy (TEM), allow researchers to visualize the morphology, composition, and crystallographic information of materials at nanoscale dimensions. Electron microscopy plays a crucial role in various scientific disciplines, including materials science, nanotechnology, biology, and geology, enabling a deeper understanding of the properties and behavior of diverse materials [2]. In the case of materials processing analysis, atomic force microscopy (AFM) has been used to review the profile of the treated surface, as shown in (Figure 1) [3].

In Ref. [4], a guide on designing electron microscopes for material characterization is presented, focusing on the benefits of utilizing backscattered electrons (BSE), secondary electrons (SE), and energy-dispersive spectroscopy (EDS). The approach includes discussions on incorporating additional microscopy techniques like atomic force microscopy (AFM), ellipsometry, and optical profilometry as supplementary methods to validate electron microscopy findings. Applications showcased encompass eutectic alloys, thermal oxides, and nanoparticles across various industries [5]. Trace evidence analysis is crucial in criminal investigations as it offers critical information for linking suspects to crime scenes. In forensic investigations, SEM is a vital tool, particularly in gunshot residue (GSR) analysis, where SEM helps match bullets

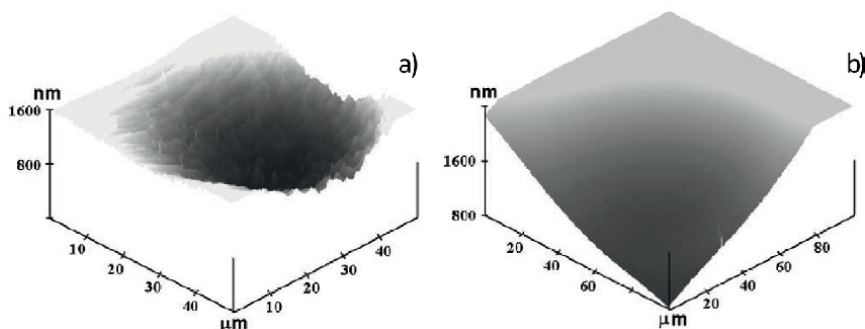


Figure 1.

AFM images of a cavity generated by photochemical etching in a GaSb sample with (a) a 1 M HCl solution having root mean square (RMS) roughness of 57 nm; and (b) in a 0.2 M H₂SO₄ solution, having an RMS roughness of 11 nm [3].

to firearms more effectively than visual methods. Moreover, SEM is significant in examining gemstones and jewelry by distinguishing between natural and synthetic gems, studying surface flaws, and identifying elemental compositions [6]. In Ref. [7], the importance of using SEM coupled with X-ray energy dispersive (SEM-EDX) to analyze the surface of kidney stones for evaluating the antilithiatic properties of extracts from medicinal plants like *Saussurea costus* (Falc) Lipsch is emphasized. This highlights the significant role of electron microscopy in medical research, with a focus on urinary lithiasis.

1.2 Applications of some analysis techniques using spectroscopy

In a similar way and as complementary analysis, spectroscopy techniques provide valuable information about the composition, structure, and properties of materials by analyzing the way they absorb, emit, or scatter light. These techniques allow researchers to identify substances, determine their concentration, and understand their molecular and atomic structure [8]. By examining the unique spectral fingerprints of materials, spectroscopy plays a crucial role in various scientific fields, including chemistry, physics, biology, and materials science.

The fusion of ion mobility spectrometry with mass spectrometry (MS), referred to as an IM-MS hybrid instrument, provides improved analytical separation and identification abilities that have greatly progressed fields such as biomedical, pharmaceutical, and forensic sciences. In Ref. [9], a thorough examination of different IMS instrument platforms is presented, which includes traveling wave (TWIMS), drift tube (DTIMS), trapped (TIMS), differential mobility analyzer (DMA), and field asymmetric waveform (FAIMS). The identification of biomarkers through MS is crucial in clinical medical research. Yet, analyzing proteins in formalin-fixed paraffin-embedded (FFPE) samples using MS has been difficult due to decreased solubility from fixation, resulting in crosslinking reactions among amino acid side chains in proteins. In Ref. [10], various methods used for omics analysis of FFPE samples to discover disease-specific biomarkers are discussed. Spectroscopy in predictive genomics has the ability to assist in treatment decisions by allowing individuals to take proactive measures to prevent serious illnesses. For matrix-assisted laser desorption/ionization time-of-flight (MALDI-TOF) MS technology identifies genetic variations based on their unique mass [11]. Apart from pharmacogenetics,

SNP variations are important in various medical fields. The importance of different SNPs in nutrigenetics is addressed in Ref. [12].

This introductory chapter provides a short but comprehensive understanding about electronic microscopes and spectroscopy as powerful tools for materials analysis, its sections address specific aspects of the topic. The content covers the principles underlying electron microscopy and spectroscopy, the various imaging and analytical modes available, sample preparation techniques, data interpretation and analysis, as well as a diverse range of applications spanning different material classes. Furthermore, the book will delve into recent advancements and emerging trends in the field, shedding light on the future prospects of materials analysis using electronic microscopes and spectroscopy. In summary, this introductory chapter sets the stage for an in-depth exploration of electronic microscopes and spectroscopy as indispensable tools for materials analysis. By elucidating their historical evolution, significance, and the scope of this book, it aims to provide a solid foundation for readers to embark on a comprehensive journey through the world of advanced materials characterization.

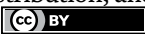
Author details

Guillermo Huerta Cuellar

Department of Exact Sciences and Technology, University Center of Lagos, University of Guadalajara, Lagos de Moreno, Jalisco, México

*Address all correspondence to: ghuertacuellar@gmail.com

IntechOpen

© 2024 The Author(s). Licensee IntechOpen. This chapter is distributed under the terms of the Creative Commons Attribution License (<http://creativecommons.org/licenses/by/3.0>), which permits unrestricted use, distribution, and reproduction in any medium, provided the original work is properly cited. 

References

- [1] Leng Y. Materials Characterization: Introduction to Microscopic and Spectroscopic Methods. Hoboken, New Jersey: John Wiley & Sons; 2013
- [2] Hayat MA. Principles and techniques of electron microscopy. In: Arnold E editor. Biological Applications. Vol. 1. 2nd ed. London: Biochemical Society Transactions; 1981. DOI: 10.1042/bst0100293
- [3] Huerta-Cuéllar G, Guel-Sandoval S, De Anda F, Méndez VH, Torres-Loredo B, Garnache A, et al. Photo-selective chemical etching of InAs and GaSb to manufacture microscopic mirrors. Journal of Applied Electrochemistry. 2008;**38**:269-271
- [4] Lencová B, Zlámál J. A new program for the design of electron microscopes. Physics Procedia. 2008;**1**(1):315-324
- [5] Starostina N, McGuire A, Rowan R. Evaluation of dihedral angle twin boundaries in Cu10 wt% Zn alloy using atomic force microscopy. Microscopy and Microanalysis. 2021;**27**(4):705-711
- [6] Desiderio VJ, Taylor CE, Daéid NN, editors. Handbook of Trace Evidence Analysis. John Wiley & Sons; 2020
- [7] Grases F, Costa-Bauzá A, Ramis M, Montesinos V, Conte A. Recurrence of renal lithiasis. Scandinavian Journal of Urology and Nephrology. 2003;**37**(6):482-486
- [8] Doumeng M, Makhoulouf L, Berthet F, Marsan O, Delbé K, Denape J, et al. A comparative study of the crystallinity of polyetheretherketone by using density, DSC, XRD, and Raman spectroscopy techniques. Polymer Testing. 2021;**93**:106878
- [9] Kanu AB, Dwivedi P, Tam M, Matz L, Hill HH Jr. Ion mobility–mass spectrometry. Journal of Mass Spectrometry. 2008;**43**(1):1-22
- [10] Donczo B, Guttman A. Biomedical analysis of formalin-fixed, paraffin-embedded tissue samples: The holy grail for molecular diagnostics. Journal of Pharmaceutical and Biomedical Analysis. 2018;**155**:125-134
- [11] Villari P, Pitini E, D'Andrea E, Rosso A, Pitini E, D'Andrea E, et al. Evaluation of predictive genomic applications. In: Personalised Health Care: Fostering Precision Medicine Advancements for Gaining Population Health Impact. Cham: Springer International Publishing; 2020. pp. 33-55
- [12] Ragoussis J, Elvidge GP, Kaur K, Colella S. Matrix-assisted laser desorption/ionisation, time-of-flight mass spectrometry in genomics research. PLoS Genetics. 2006;**2**(7):e100

Chapter 2

Elements of Electron Microscopy Designing Laboratory Course: Examples and Applications

Nataliya Starostina

Abstract

This chapter provides guidance on designing laboratory practices for material characterization using electron microscopy, with a focus on the advantages of using backscattered electrons (BSE), secondary electrons (SE), and energy-dispersive spectroscopy (EDS). The approach includes insights into using other microscopy techniques such as atomic force microscopy (AFM), ellipsometry, and optical profilometry as complementary methods to validate results from electron microscopy. Examples of applications include eutectic alloys, thermal oxides, and nanoparticles in various industries. Successful syllabuses for undergraduate and graduate courses are illustrated, and the laboratory teachings' results were presented at a conference and published in peer-reviewed journals.

Keywords: secondary electrons, backscatter electrons (BSE), atomic contrast, energy-dispersive spectroscopy (EDS), energy-dispersive X-ray (EDX), scanning probe microscopy (SPM), atomic force microscopy (AFM), ellipsometry, optical profilometry, eutectic alloys, thermal oxides (TOX), nanoparticles, carbon nanotubes (CNT), laboratory practicum, teaching lab, lab syllabus, materials science, material characterization

1. Introduction

The design and teaching implementation of material characterization laboratory practicums present a challenge to many teaching professionals. There are many variables in that task:

1. scientific instrumentation availability
2. technical difficulty of the lab (graduate or undergraduate level)
3. number of students per class
4. goals or what we want students to accomplish by the end of the quarter or semester
5. desired assistance or how many student assistants one can get.

The design thinking approach shared in this chapter is based on my experience developing and teaching both graduate and undergraduate level courses with labs at Santa Clara University, CA, USA. The inspiration for syllabus development came from a couple of sources: “Elements of X-ray diffraction” by Cullity and Stock [1] and “The design of everyday things” by Norman [2]. Design thinking should not be an after-thought, but rather a guiding principle for syllabus development. Conceptual understanding is just as important as attention to technical details. Our experience and knowledge of product management have been applied to the development of new laboratory practicums. Examples of syllabuses taught along with students reported results are shared below. The goal of this chapter is to be a useful practical guide for teaching technical labs with electron microscopes.

The structure of the chapter follows the flow of my materials characterization lecture. We start with the assumption we have a scanning electron microscope (SEM) and atomic force microscope (AFM) at our disposal, Section 2 and Section 3 respectively. The SEM and the AFM are two fundamental pillars for teaching materials, science and nanotechnology [3, 4]. The core idea for the lab teaching is complementary characterization, verification, of the results obtained by one technique with an independent measurement by a second method. SEM and AFM pair very nicely in the micro-nano range. SEM is well-established 2D or XY imaging technique [5, 6], while only AFM is truly 3D [7–9]. One of the main advantages of SEM besides million times magnification is the benefit of large depth of field, see Getty images [10] of insects. The perception of the three dimensions is most remarkable. AFM, however, provides direct height measurement and 3D visualization from atomic scale as it can be seen in IBM images [11] of atoms and molecules as well as pioneering work toward nanomanipulation. Both AFM and scanning tunneling microscopy (STM) are the members of a larger family named scanning probe microscopy (SPM) [3–5, 8, 9]. SPM generally stands for a technique where a probe, a stylus, is being used to measure variations of topography while raster scanning.

The core of a student’s project is in dual measurements. For example, first practice XY dimensions measurements with SEM, confirm with AFM and then determine Z height with AFM. The choice of samples can range from mechanically polished alloy to thermally grown oxides to nanoparticles, see Sections 7 and 8 of this chapter. XYZ measurements project facilitates the learning of SEM and AFM in the topography modes. The ultimate goal of the lab is to learn how to run the microscopes or how to acquire and analyze the data, is entirely up to the teaching instructor, the idea of dual measurements is central for my syllabuses. In addition, we use an approach of “station rotation” that has proven to be beneficial by allowing students to gain more hand-on experience during the lab and reduce number of students per group.

The idea of dual measurements can be expanded into various operating modes of both SEM and AFM. For example, elemental composition mapping or EDX imaging is a standard mode in SEM [7, 8] that can be complemented by AFM phase imaging or frictional mode. Lateral force mode (LFM or friction) and phase mode are usually acquired simultaneously with topography AFM. The standard materials sensing properties modes, although, are electrical, magnetic, thermal, and mechanical (force-distance based) modes [9, 10]. Depending on whether you are teaching future electrical, mechanical, or bioengineers, one can adjust according to the needs of the major.

Teaching the “Introduction to Nanotechnology” lab, an undergraduate course, to a broad spectrum of engineering students was designed with one more idea in mind, utilizing all equipment SCU has at the Center for Nanostructures (CNS). Sections 4

and 5 give a general introduction to optical profilometry and ellipsometry. Section 6 is dedicated to transmission electron microscopy (TEM). TEM concludes the list of measurement techniques in this chapter. Section 7 provides examples of syllabus and students' reports on the topic of "Electron Microscopy". A graduate-level guided research course for students with a concentration in materials science was developed with a focus mainly on SEM and AFM, see Section 8.

2. Imaging with electron microscope

2.1 Basic topography

Secondary electron (SE) or reflected electron beam, is a default operating mode for commercial SEMs. The physical origin of the term belongs to the fact that when the primary electron beam hits the surface of the material, primary electrons interact with the outer shell electrons and reflect back as secondary electrons [7, 8]. The nature of image formation is frequently described in analogy to sunlight shining on the mountains producing good image contrast depending on the tilt angle of the specimen and or topography variation (see **Figure 1**).

Cross-sectional SEM imaging can reveal a wealth of information about the quality of fabrication and the root cause of failure [12]. Sample preparation for cross-sectional examination is the key to successful imaging; therefore it is essential to introduce students to this topic. For teaching purposes in undergraduate labs, the process of cross-sectional sample preparation can be simplified. It can be as simple as braking, or cutting, a wafer with a diamond knife and mounting a piece in a vertical position rather than laying it flat, see **Figure 2**. Students can learn how to demonstrate different types of information that can be extracted from semiconductor samples depending on how it is prepared, see Section 7 for a project example.

Nanoparticle analysis is a valid option for a characterization project as well. An electron beam can be focused down to 1–2 nm, providing ultimate lateral resolution imaging of nano-scale objects with SEM (see **Figure 3(a)**). Unlike AFM [13, 14], SEM does not have tip artifacts associated with the size of the scanning tip, which can be an idea for a project to compare SEM resolution vs. AFM lateral resolution, see **Figure 3**.

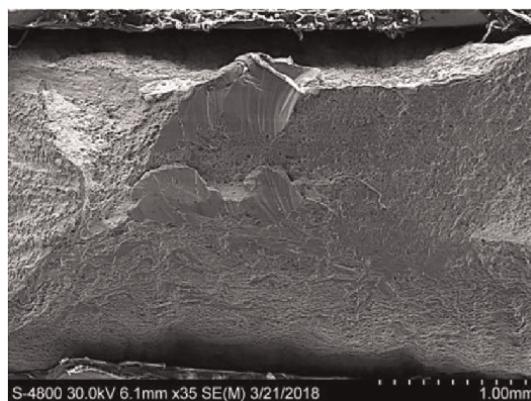


Figure 1.
2.5 mm × 2 mm SEM scan of fractured CuZn alloy specimen after tensile testing.

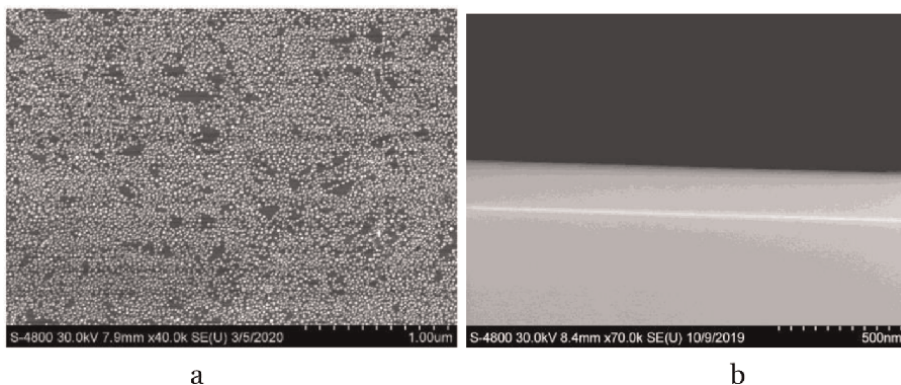


Figure 2. Top view (a) and cross-sectional SE SEM images (b). (a) 2–5 nm cobalt nanoparticle (TedPella sample) and (b) cross-section of a silicon wafer showing 200 nm layer of TOX. Our measurements indicate 191.56 ± 2.12 nm.

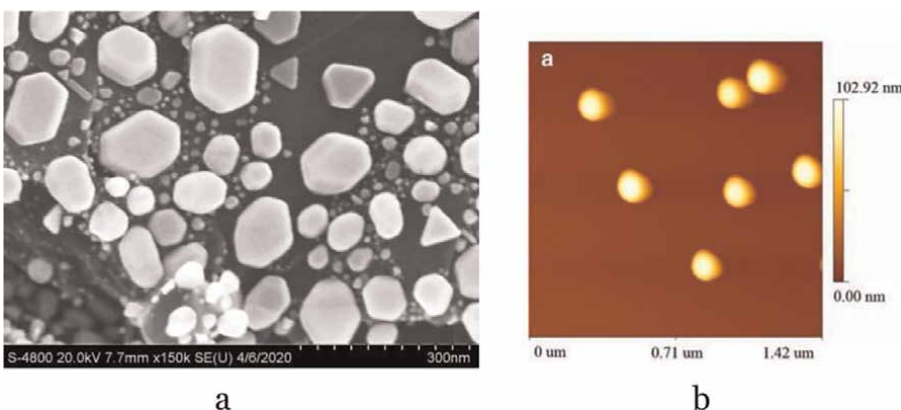


Figure 3. (a) $5 \mu\text{m} \times 2 \mu\text{m}$ topography, SE SEM, scan of gold particles (TedPella Inc. sample) and (b) $1.4 \mu\text{m} \times 1.4 \mu\text{m}$ AFM topography scan of 100 nm diameter polystyrene spheres on mica.

The topic of resolution can be expanded toward transmission electron microscopy (TEM), where the theoretical resolution of the electron beam can be achieved [1, 7].

The standard operating voltage for SEM is between 10 keV and 30 keV, with 20 keV as a typical accelerating voltage, allowing students to stay focused on learning basic modes of operations without going too deep into imaging modes of electron microscopy [8], see **Figures 1–3(a)**.

2.2 Atomic number contrast

Atomic number contrast or backscattered electron imaging (BSE), arises from the interaction of the primary electron beam with the atomic nucleus rather than with electron shells [7, 8]. This provides an opportunity to observe contrast based on the difference in atomic number. The higher the difference in atomic number, A , the greater the contrast. Gold nanoparticles ($A = 79$) deposited on graphite ($A = 6$) are a good reference sample for successful demonstration of BSE imaging (see **Figure 4**). An eutectic alloy where the difference in atomic numbers between lamellas is large enough to provide visible contrast, is another good candidate for demonstration

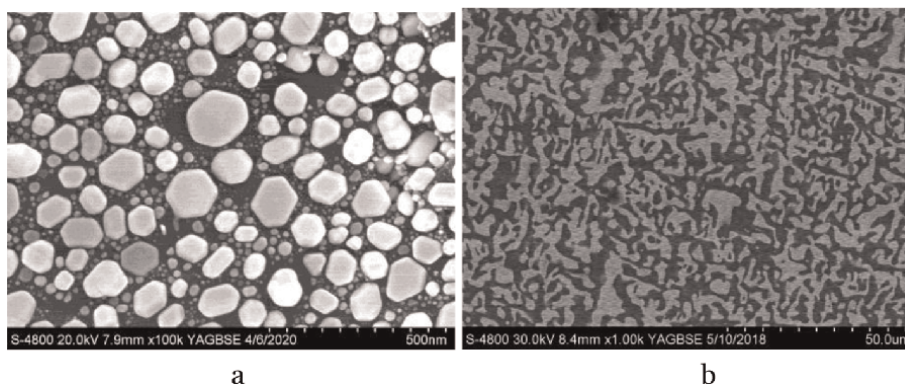


Figure 4. (a) BSE SEM image of gold nanoparticles deposited on carbon substrate (TedPella sample) and (b) SnBi eutectic alloy showing lamellar microstructure. Brighter regions are Bi-rich ($A = 83$) because heavier elements dominate the composition of lamella. Darker regions are Sn-rich ($A = 50$) because lighter elements dominate the composition of lamella.

atomic contrast, see Section 8. A CuZn substitutional alloy, in comparison, provides essentially no BSE contrast because atomic numbers for Zn and Cu are 30 and 29, respectively.

Most of the commercial SEMs are equipped with a BSE detector which is easy to operate. BSE contrast could provide compositional insights that are otherwise not visible with SE SEM. BSE imaging can be paired with EDS as a nice project for students to learn the pros and cons of both techniques.

2.3 Elemental mapping

Elemental mapping with EDS is a powerful tool for composition analysis. Image formation is based on X-rays emitted due to the interaction of the incident e-beam with the surface electrons [1, 7, 8]. This method allows visualization of inhomogeneities and X-ray spectrum analysis (see **Figure 5**). The information obtained from EDS usually compliments BSE contrast, which in its own right can be an additional project for students to do—i.e., homogeneity verification, impurities segregation and lamella microstructure study (see Sections 7 and 8).

The smaller elements of microstructure become the more one needs to be aware of the size of the volume interaction in comparison to the size of inhomogeneities or nanoparticles to avoid false interpretation of elemental composition. The size of the volume of interaction is generally thought of as $1\ \mu\text{m}^3$, meaning the radius of the particle should be less than $0.62\ \mu\text{m}$ to provide meaningful measurements with EDX. The reported critical size is actually around $5\ \mu\text{m}$ according to NIST studies referenced by Goldstein et al. [8]. If the size of the nanoparticle is smaller than the critical value, there is a good chance, the EDX image analysis software may miscalculate the composition (see **Figure 6**). According to the sample specification, the deposited islands are 100% gold. The substrate is 100% carbon (graphite). However, the software calculations for selected particles are 5% Au, 27% C, and oxygen is the rest (see onset **Figure 6b**). Nanoparticle particle size distribution, in conjunction with composition verification, is a good project for undergraduate students. You choose to use SE SEM vs. EDX or SEM vs. AFM (see Chapters 8 and 9).

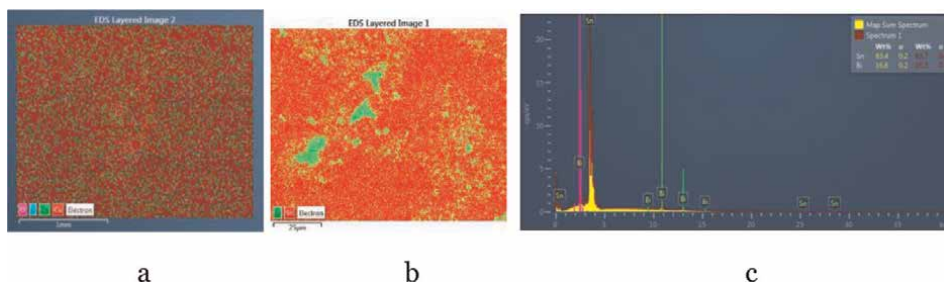


Figure 5.

(a) EDX map of CuZn alloy, showing homogeneity of elemental distribution in solid solution and some presence of surface contaminations (C and O). (b) EDS map of SnBi alloy showing inhomogeneous distribution of Bi in Sn solid solution. (c) SnBi alloy X-ray spectrum and calculated composition of the alloy (small onset on c).

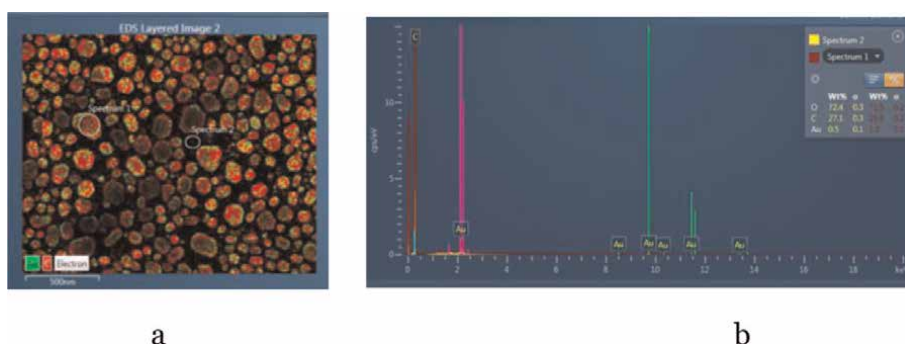


Figure 6.

(a) EDX map of gold particles on graphite showing false result from selected area analysis due to size of the particle not being taken into account (b) Spectrum 1, selected area composition, particle (in red) is 1.8% Au, 26.8% C, 71.5% O. Spectrum 2, selected area composition, substrate (in yellow) is 0.5% Au, 27.1% C, 72.4% O. A nominal composition is 100% gold for particles and pure graphite as substrate.

3. Imaging with AFM

AFM is a subset of SPM that does not require a vacuum nor the probe and or sample to be conductive [5, 6, 9–11, 15]. The physics, fundamentals of operation, and modes are extensively covered in the literature [7–9]. Imaging with AFM implies a smaller scan size compared to SEM, usually less than 150 μm scans compared to a few mm, respectively (see **Figure 1** for SEM and **Figure 7** for AFM). The height variation is also limited to less than 8 μm due to the maximum piezo extension of the AFM scanner head. Overall sample size should be small enough to fit under the AFM scanner head, $\sim 2 \times 0.25$ inches maximum.

Novice users of AFM should be aware of AFM tip artifacts [13, 14]. The phenomenon manifests itself when the size of the features of the interest becomes comparable to the diameter of the AFM probe. The typical value for the tip radius for the most commercially available probes is ~ 20 nm (compared to the size of the electron beam of 1–2 nm). This means the measured XY distances will be dilated by approximately the size of the probe. It is possible to correct for tip dilation and reconstruct the shape of the tip of the probe by running your data through the tip dilation algorithm [14] (see **Figure 8**).

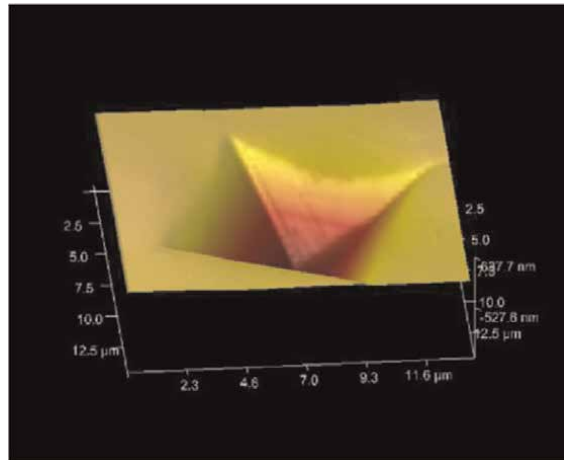


Figure 7.
 $14.5 \mu\text{m} \times 14.5 \mu\text{m}$ 3D AFM images of the Vickers hardness indent on CuZn surface.

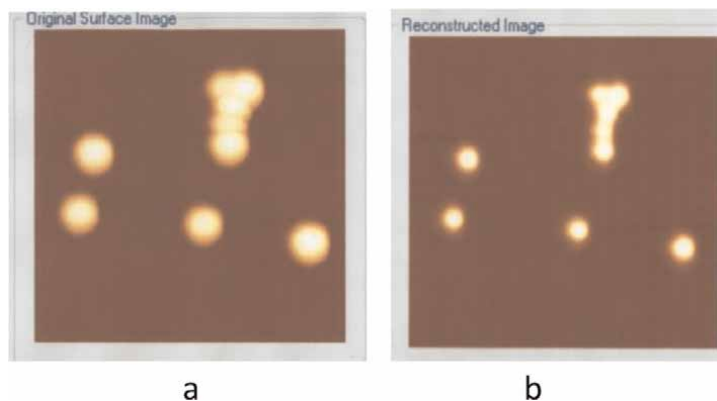


Figure 8.
 (a) $1.6 \mu\text{m} \times 1.6 \mu\text{m}$ original AFM scan of 102 nm diameter spheres (b) reconstructed image of the spheres without tip dilation effect. Reproduced with permission of Springer Nature. Images are courtesy to Wong et al. [14].

3.1 Basic topography

There are three main AFM topography modes:

1. contact mode or non-vibrating mode
2. non-contact vibrating mode
3. in-and-out of contact vibrating mode, commonly referred as Tapping mode (the term coined and trademarked by Veeco in about 2000–2010).

The AFM probe, or stylus, moves over the surface of the sample tracking the topography similar to a mechanical profiler that metallurgists used to measure surface roughness on the macro and micro scale. The benefits of the light lever amplification being used to discern up-down motion on a position-sensitive photodetector to acquire topography data. The probe is kept in feedback with the electronics maintaining either force of interaction between the sample and the probe constant or distance from the tip to the sample constant [9, 10, 15, 16]. It usually takes an experienced user to prefer one type of feedback loop versus another. The software makes it easy to switch from one feedback setting to another.

The choice of the most appropriate mode of operation, as well as the AFM probe, depends mainly on your sample. If the sample is hard and dry (metals, alloys, ceramics, and hard plastics), then contact mode and contact probe will do a good job. If your sample is a delicate soft polymer or integrated circuit or some biological tissues, then oscillating modes and probes will be your choice. It is easier for students to start with contact mode first and then switch to vibrating mode while practicing on the same reference samples, see **Figures 9–11**. Once students master routine imaging, they can switch to actual samples and do projects (see **Figures 3b, 8, 12 and 13**).

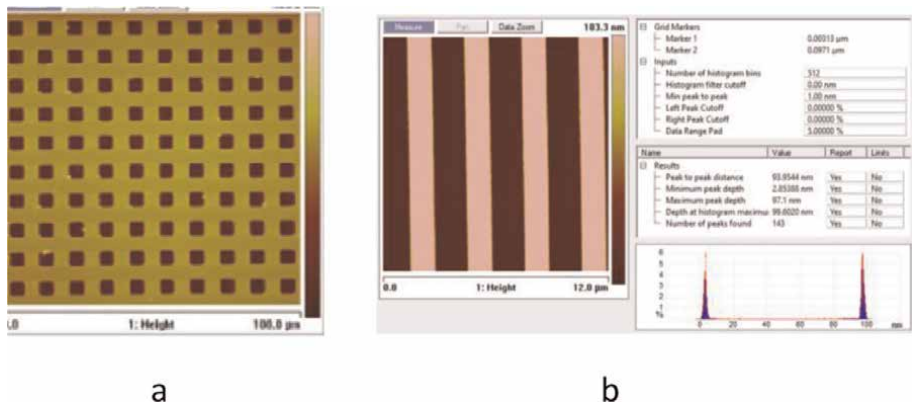


Figure 9. (a) $100\ \mu\text{m} \times 100\ \mu\text{m}$ AFM scan of Veeco reference sample. Pitch size is $10\ \mu\text{m}$, depth is $100\ \text{nm}$. (b) $13\ \mu\text{m} \times 13\ \mu\text{m}$ AFM image of a reference sample (TedPella, $3\ \mu\text{m}$ pitch size, nominal step height = $100\ \text{nm}$). Step height measurements, $94\ \text{nm}$, are shown with histogram method.

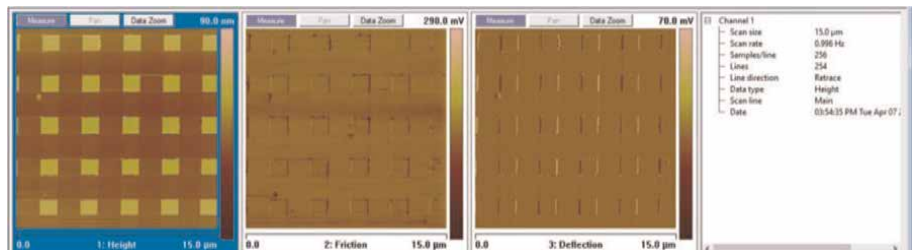


Figure 10. A typical selection of channels recommended for contact mode scanning. From left to right: topography, LFM or friction, deflection, or error channel and scan parameters tab. Both LFM and error data should be monitored in both scan directions for good image quality.

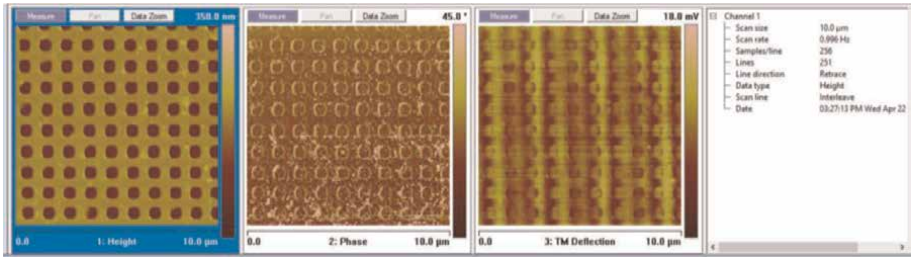


Figure 11.
A typical selection of channels recommended for vibrating mode scanning. From left to right: topography, phase, deflection, or error channel, and scan parameters tab. Both Phase and error data should be monitored in both scan directions for good image quality.

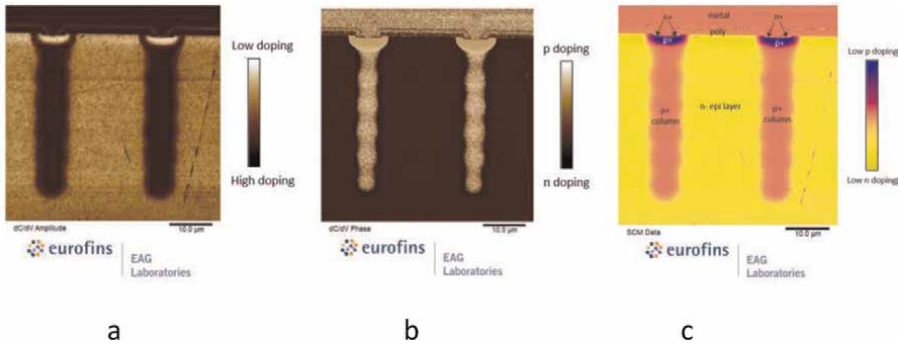


Figure 12.
50 µm × 50 µm scanning capacitance mode (SCM) images of the cross-sectioned MOSFET (a) relative dopant levels contrast, bright-low dopant level (b) dopant type contrast, brown—n-type, white—p-type, (c) combined SCM image. Images are courtesy to Eurofins EAG Laboratories.

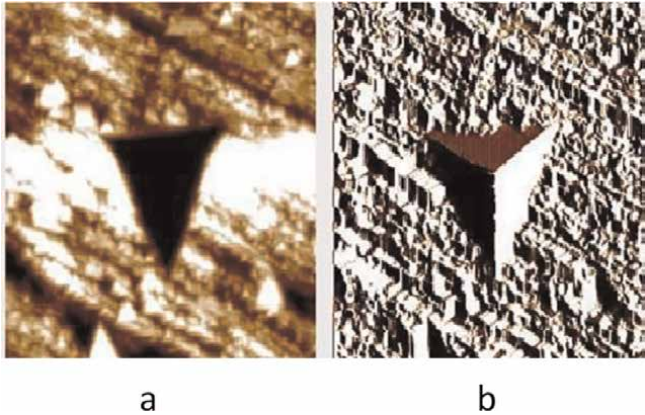


Figure 13.
(a) 10 µm × 10 µm topography image of an indent done with Berkovitch tip by a Nanoindenter. Scanning is performed with a Nanoindenter right after indentation and (b) error channel image acquired simultaneously with topography channel.

3.2 Lateral force mode (LFM)

There are two built-in additions to topography imaging: lateral force, or friction, mode (LFM) and phase mode, which can be acquired simultaneously with topography. LFM and phase images are related to the physical properties of the materials under investigation.

The signal that feeds the LFM channel is associated with the lateral twist of the probe: Left-right motion as opposed to the up-down motion associated with the topography channel. The amount of twist or the difference in intensities between left and right quadrants in position-sensitive photodetector can be correlated to drag force or the friction coefficient of the material [9, 10]. LFM contrast can represent the difference in friction coefficients of the materials or the amount of twist due to large height variation (see **Figure 10**). The error (deflection) channel should not be forgotten during the acquisition as it represents the quality of feedback loop parameters adjustment. It is good practice for students to acquire data having topography, LFM, and error channels open.

3.3 Phase contrast in vibrating modes

In vibrating mode, the simultaneous data acquisition channel is called the phase channel. The feedback loop in oscillating mode can work either on amplitude or on phase signal, therefore the phase channel (usually the default setting) records the phase delay of the signal made with the material of interest [9, 10]. The topography channel represents recording of height variation on constant amplitude with respect to the driving signal. It is easy to switch the setting from phase to amplitude feedback and record amplitude attenuation while having topography imaging done in constant phase. Triblock polymer sample is usually the best candidate for phase image verification. However, even a mildly contaminated reference sample can do a good job (see **Figure 11**). Phase image represents the phase signal delay associated with differences in hardness, elastic modules and adhesion of the material and results in corresponding image contrast.

3.4 Material sensing modes

The material sensing modes are the next generation of AFM capabilities. AFM can visualize the mechanical, magnetic, electrical (see **Figure 12**), and thermal properties of materials [9, 10]. An in-depth discussion of material sensing mode is beyond the scope of this chapter; however, we would like to illustrate a couple of important applications: electrical mode and indentation.

AFM can measure long-range interaction forces, such as electrostatic force and force gradient. One of the variations of electrical AFM (EFM) is scanning capacitance microscopy (SCM). SCM maps charge distribution with a lateral resolution sufficient for the needs of the semiconductor industry (see **Figure 12**).

Indentation studies are a promising domain of AFM-based techniques. The best way to measure nanohardness and elastic modulus is to use a Nanoindenter. Nanoindenter is an instrument, specifically designed to perform hardness measurements on the nanoscale. If a Nanoindenter is at your disposal, then it is very useful for teaching students about the difference between AFM and Nanoindenter. **Figure 13** shows images of an indent performed with a Nanoindenter. Nanoindents have a distinct triangular pyramid shape reflecting the geometry of a diamond indenter, Berkovich tip. Vickers hardness indents have the characteristic shape of a square pyramid while Berkovich indenter is 3-sided pyramid (compare

Figure 7 and Figure 13). Hardness mapping of bonding areas of micro and nano interconnects is of interest in the semiconductor industry [17, 18].

4. Imaging with optical profilometer (complimentary method)

A profilometer is a device similar to a phonograph that measures a surface as the surface is moved relative to the contact profilometer's stylus. A profilometer is an instrument used to measure a surface profile, to quantify its topography. Critical dimensions as step height, curvature, flatness, and surface roughness are computed from the surface topography. Profilometry branches out to SPM where the stylus is a scanning probe or cantilever of very small size. SEM utilizes an electron beam as a scanning probe [5–8]. Optical profiler is based on light and light interferometry [19, 20].

Optical interferometry is a physical phenomenon when the wavefront of light reflected from the surface of the material interferes with a reference wavefront. By introducing a slight tilt to one wavefront, a pattern of interference fringes is created. The departure from the straightness of these fringes is a deviation from a reference. Sophisticated software can reconstruct the 3D topography of the surface based on the difference in interferometry patterns.

4.1 Step height and surface roughness measurements

Metrology parameters, such as step height and surface roughness, can be quantified with the optical profiler (see **Figure 14**). The scan range overlaps nicely with SEM and AFM. Pairing the optical profiler technique, either with SEM or AFM, represents a valuable teaching opportunity where students can explore the limits of resolution for different techniques and merge substantial characterization data sets together (see Sections 8 and 9).

4.2 Advantages and disadvantage of optical interferometry

An optical profiler is a non-contact and fast method to visualize surface topography from micro- to upper nano-range. The techniques were most suitable for delicate and, or, organic samples that cannot be touched by a mechanical stylus. 3D image is reconstructed from interference patterns. The imaging may be problematic for transparent, highly reflective materials and true nanoscale features.

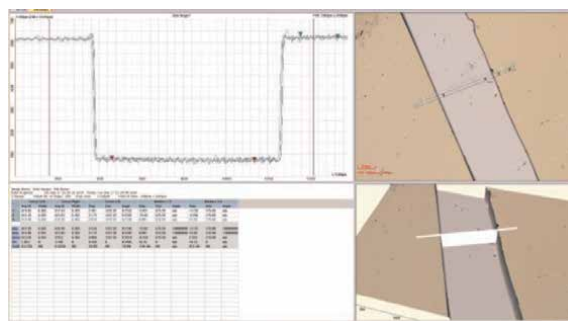


Figure 14. Screenshot of optical profilometry images (2D, top right, and 3D, down right) with line profile and surface roughness measurements (top left). The height measurements result in $615 \pm 2 \mu\text{m}$ tall silicon trench. The average surface roughness $S_a = 5.3 \mu\text{m}$. RMS surface roughness $S_q = 6.9 \mu\text{m}$.

5. Ellipsometry (complimentary method)

Ellipsometry is a standard industry technique to measure the thickness and other properties of thin layers of dielectrics and semiconductor materials [21]. The fundamental principle of ellipsometry is the phase difference between two mutually perpendicular polarized light beams. The information about the sample is contained in total reflection coefficients. The quantities such as thickness and optical constants are calculated based on assumed theoretical models.

5.1 Optical properties evaluation and film thickness measurements

Both thickness of a film, or layer, in layered structure and refractive index can be evaluated with ellipsometer, if the films are optically transparent (see **Figure 15**).

5.2 Advantages and disadvantages of ellipsometry

An ellipsometer is simple to use. The measurements are highly reproducible and very sensitive to the presence of ultrathin films (down to a monolayer or native thermal oxide on silicon). An ellipsometer can be used to analyze multiple layers and determine the optical constants of unknown materials. Ellipsometry is not an imaging technique.

6. Transmission electron microscopy

TEM is considered to be a more difficult technique than SEM requiring preparation of a very small and delicate sample. Visualization and image interpretation requires an understanding of geometrical optics and diffraction fundamentals [1, 7]. There are three basic mechanisms of TEM contrast formation: mass-thickness contrast, diffraction contrast, and phase contrast [7]. All three contributing factors may form an image. The resolution of TEM is near the theoretical limit (0.2Å) for an electron beam at 100 kV [7]. TEM compliments high-resolution SEM (1–2 nm) and is much better

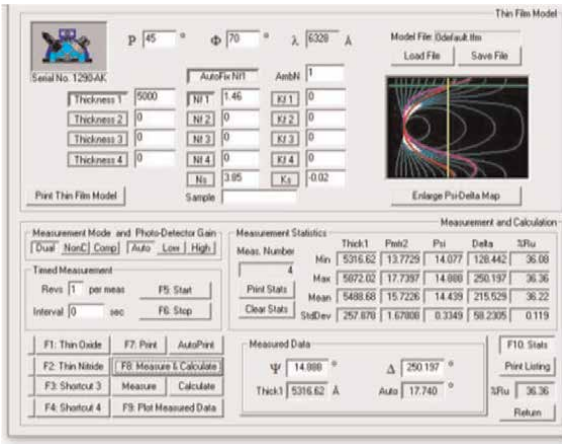


Figure 15. Ellipsometry user interface for TOX wafer reporting thickness $549 \text{ nm} \pm 26 \text{ nm}$ and refractive index $n = 1.4 \pm 0.2$.

than AFM, which has limited lateral resolution (~ 20 nm) due to tip artifacts [14]. Mass-thickness contrast is most frequently used as images are relatively easy to interpret (see **Figure 16**). Diffraction and phase contrast has been extensively used by physical metallurgists to study dislocations, stacking faults and other crystallographic phenomena [7, 23]. A combined TEM/SEM/AFM project can be a suitable candidate for graduate lab or guided research [24]. We plan to outline briefly only the importance of diffraction patterns for practical applications and discuss a special case of using superlattice reflections from a diffraction pattern to form dark field image [7].

6.1 Bright field imaging: mass-thickness contrast

Mass-thickness contrast results from electrons that pass through the specimen. The electrons having no obstacle, or a very thin layer of material, on their way after passing the objective aperture result in a bright (white) color appearance of the recording film. A thicker specimen will allow the transmission only a portion of electrons and will result in a darker color of the film due to less exposure to electrons. The layer, or specimen that are too thick will block electron beam and film will appear dark, because all electrons are blocked by the specimen (see **Figure 16**). Biologists usually prefer mass-thickness contrast by taking advantage of staining cells with heavy elements. CNTs, graphene, precipitates and nanoparticles can be successfully studied with TEM [25–29].

6.2 Use of diffraction patterns

Diffraction patterns by themselves can be very useful to indicate if partial crystallinity is present in the compound. A single crystal will form dots on a diffraction pattern (see **Figure 17**), polycrystalline material will produce rings and amorphous materials will result in a fuzzy halo [7]. Indexing the diffraction patterns is a routine job of a crystallographer requiring knowledge of both crystallography and the physics

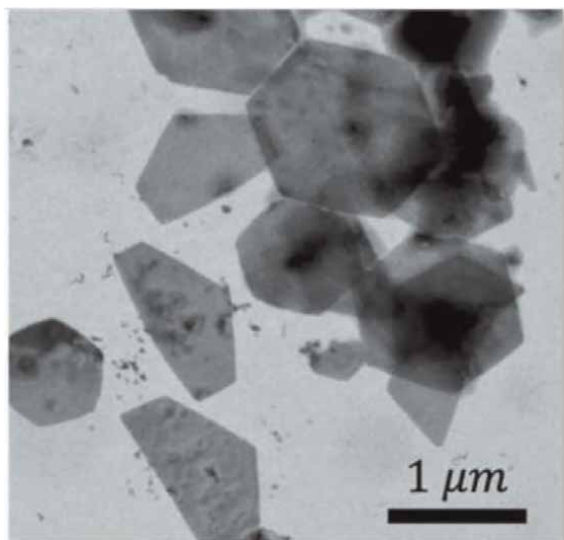


Figure 16.
Bright field TEM images showing lead dioxide particles with hexagonal shape, deposited on silicon. Reproduced with permission of the International Union of Crystallography. Image is courtesy to Kabbara et al. [22].

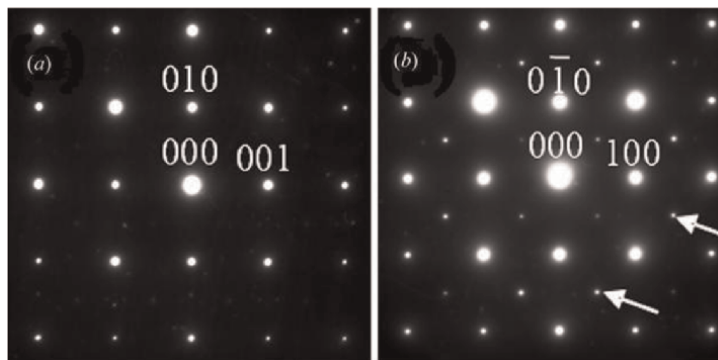


Figure 17. (a) Indexed TEM diffraction pattern in $[100]$ orientation and (b) indexed TEM diffraction pattern showing superlattice reflections, see arrows pointing at weaker reflections. Reproduced with permission of the International Union of Crystallography. Images are courtesy to Woodward and Reaney [23].

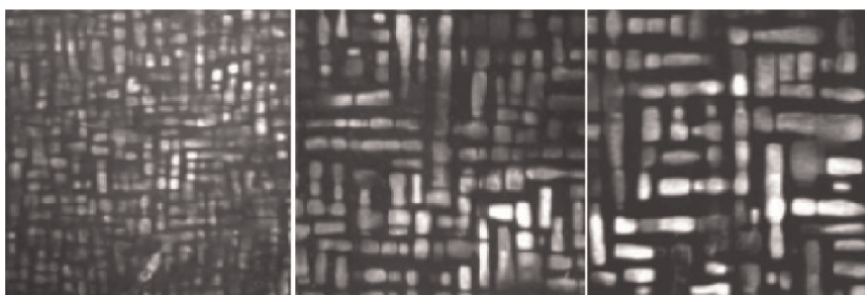


Figure 18. $500\text{ nm} \times 500\text{ nm}$ dark field TEM images of Ni_3Ga precipitates in NiGa single-crystal alloy as a function of aging time. Left image is the shortest aging time, right image is the longest aging time for the same alloy composition. See data analysis in [27]. TEM images are courtesy to Dr. Starostina.

of electron diffraction [1, 7]. The project involving indexing or use of the diffraction patterns would be a good candidate for a graduate research assignment.

6.3 Dark field imaging

Dark field imaging in general means that in the absence of the specimen, the background appears dark because all electrons are blocked by the shifting objective aperture of the TEM microscope [7]. This is a special case of kinematic diffraction contrast when only electron “light” resulting from super reflections is used for image formation (see **Figure 18**). Dark filed imaging is an essential technique to study morphology and kinetics of coarsening of ordered precipitates in a disordered alloy matrix [25–27].

7. “Introduction to Nanotechnology” course example

Course description: “Introduction to the field of nanoscience and nanotechnology. Properties of nanomaterials and devices. Nanoelectronics: from silicon and beyond. Measurements of nanosystems. Applications and implications. Laboratory experience is an integral part of the course.”

7.1 Lab syllabus example for undergraduate course

“MECH/ECEN 156 “Introduction to nanotechnology” lab.

Course type: elective, undergraduate level engineers, contribute to engineering topics.

Learning outcomes:

- hands-on experience operating scientific instrumentation
- hands-on experience acquiring data on nanoscale
- being able to choose a proper material characterization technique(s) to meet the requirements of the project
- technical presentation design: ability to create technical presentation
- presentation skills: ability to communicate technical results of your project

Instrumentation: The course is based on the instrumentation available at CNS and other laboratories. It includes optical profiler, AFM, electron microscope, probe station, and other equipment.

Group size: 2–3 people per group, no more than 5 groups (15 people max).

Projects (examples):

1. Electrical and ellipsometry characterization of the thermal oxides and MOS-structures.
2. Ellipsometry and SEM/EDX of the thermal oxides in cross-section.
3. Nanoparticles morphology and particle size distribution characterization.
4. Metrology and surface roughness characterization from micro to nano.
5. Electrical and SEM characterization of MOS-structures.

Preliminary schedule

Week 1 Introduction and safety training at CNS.

Week 2–week 6 Group training on instruments, hands-on practice on test samples (rotating stations every week; one week per instrument, if done earlier can start doing a project).

Week 7–9 projects measurements—done on at least two different instruments/different types of complementary measurements.

Week 10 field trip if arrangements with nanotechnology company are possible.

7.2 Lab reports, SEM example

The video recordings of “Introduction to Nanotechnology” final exam, mini-conference, can be seen online [30–34]. The video recording of Ph.D. student poster presentation, “Influence of Crystallographic Orientation on the Growth of

Thermal Oxide of Silicon”, inspired by teaching this lab is available on the official AAAFM YouTube channel [35].

“Scanning electron microscope laboratory report”

Instrumentation description

Hitachi S4800 Scanning Electron Microscope. The SEM works, primarily, by sending a beam of high-energy electrons from an electron gun, through electromagnetic lenses and apertures which manipulate the electron beam (alignment, stigma, and focus) onto the target sample. The electrons interact with the sample in various ways to produce secondary electrons, backscattered electrons, and X-rays. The signals from these interactions are collected by one or more sensors and processed into an image for viewing. In the case of the X-rays, information about the elemental makeup of the sample can be determined and superimposed on a secondary electron image. This is a non-destructive process that can produce great information about the surface of a sample in a relatively short amount of time. *(Description of my own based on information from Wikipedia and Nanoscience Instruments.)*

Results

The initial image at 15K magnification, see **Figure 19a**, was clear and as expected with great care taken during the alignment phase. However, an issue arose a short while later that caused the image from the SEM to shift erratically. This nuisance shifting made further alignment very difficult. The 100K magnification image, see **Figure 19b**, likely suffered some resolution quality due to this and the image capture used for the EDX was mostly unrecognizable. But the EDX was able to provide some good information on the sample surface, see **Figure 19c**. Carbon was present due to the carbon nanotubes, silicon and nickel were present as they are the substrate elements upon which the nanotubes are grown, and oxygen was present perhaps due to some oxide layer on the substrate or oxygen contamination from sample exposure to the atmosphere. The nanotubes appear to range from 50 to 200 nm and have an approximate density of $1.24\text{E}10/\text{cm}^2$.

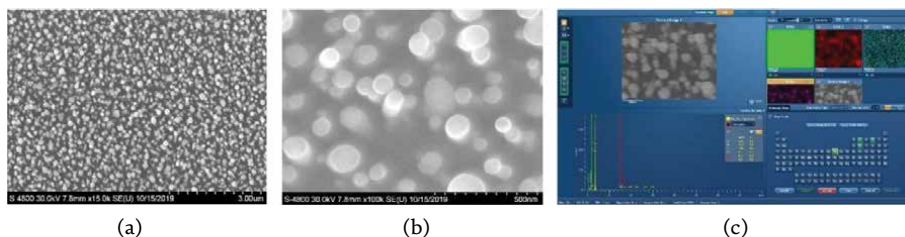


Figure 19.

(a) Low magnification, 15K, SE SEM image of MWCNTs grown by PVD method. (b) High magnification, 100K, SE SEM image of MWCNTs grown by PVD method. (c) Screenshot of EDS window analysis showing elements detected.

8. “Experiments in materials science” guided research lab example

Course description: “This course consists of research-oriented assignments involving heavy use of scientific instrumentation mainly at the center of nanostructures (CNS) and is equivalent to culminating experience. The projects are sample/materials-based. The assignments may involve hands-on sample preparation,

instrumentation calibration verification on the reference samples, imaging and measurements followed by data analysis. The research may include hands-on examination of surface morphology/roughness and elemental composition and mechanical properties. Students are expected to correlate obtained data of structural and compositional changes on micro/nano scale to changes in materials properties. The results of the assignments are expected to be written up in a scientific paper format and presented thereafter. An off-campus tour may be organized if arrangements are possible.”

8.1 Syllabus example for graduate course

“333B “Experimental Analysis in Materials Science”

Course type: elective, graduate-level engineers, contribute to engineering topics.

Course learning outcomes:

Students who successfully complete MECH 333AB will be able to:

- choose a proper material characterization technique(s) (optical-light microscopy, AFM, electron microscopy) to meet the requirements of your research project
- hands-on experience operating scientific instrumentation
- technical writing: ability to write in a technical paper format
- technical presentation: ability to create technical content for a public presentation
- presentation skills: ability to communicate technical results of your project

Group size: 2–3 people per group, no more than 5 groups (15 people max).

Examples of research assignments:

- SnBi alloy micro/nanostructure morphology, chemical composition, and mechanical properties evaluation
- Grain size, morphology, chemical composition examination, and dihedral angle of twin boundary measurements in CuZn alloy
- Gold nanoparticles size distribution, morphology and chemical composition characterization

8.2 Example of students reports abstracts and results

The video recordings of “Experiments in materials science” final exam, mini-conference, can be seen on-line [36–38]. Dihedral angle measurement with AFM project and morphology measurements of eutectic in SnBi alloy resulted in publications in peer-reviewed journals [24, 39].

“Characterization of Gold and Cobalt Nanoparticles using AFM and SEM”

Authored by Brian Chen, Raymond Chen, Mohamed Sabry

Abstract

Understanding nanoparticle morphology and chemical composition is critical to predict the behavior of these particles in various applications. In this chapter, SEM,

EDX, and AFM were used for characterization. Gold and cobalt particles were purchased from Ted Pella and are known to be deposited using thermal evaporation method. Cobalt spec is 5–7 nm for height distribution. As for gold, there were two samples used, 2–30 nm and 30–500 nm. SEM was used to determine the morphology parameters of gold particles such as size, aspect ratio, and sphericity. Average size was 14 and 18 μm for smaller and larger particles respectively. The aspect ratio was 1.37–1.48 for smaller to larger particles. Sphericity is 0.827 and 0.69 for smaller and larger particles. The values are an average value based at least 50 measured particles. EDX was used for elemental composition analysis of different areas as well. AFM was implemented for cobalt topography measurements using two different scan areas $1 \times 1 \mu\text{m}$ and $375 \times 375 \mu\text{m}$. A total of 30 particles are measured to calculate the average height and PSD. The average height measured is 13.9 nm. Particle size distribution (PSD) is between 10.8 and 16.89 nm. The measured data for cobalt were found to be outside of the vendors specifications, while gold seems to deviate from the normal distribution. In this chapter, some of the suspected reasoning for this discrepancy will also be discussed. After all the data was analyzed, recommendations for best techniques to characterize the properties of nanoparticles is given.

9. Conclusions

The product management approach proved to be a very useful tool for designing and developing a laboratory practicum. Our ultimate goal was to utilize SEM in all modes available at CNS to verify the measurements done with AFM. Our second priority was to use all scientific instrumentation at CNS to compliment both SEM and AFM, enhancing the dual, or complementary, measurement idea. Our third priority was to make the undergraduate lab as well-rounded as possible in order to be able to include students from Physics, Mechanical, Electrical, and BioEngineering departments. The priority for the graduate course was to be able to generate a sufficient amount of data for further analysis and ultimately publication in a peer-reviewed journal. We also are very mindful of students having hands-on experience with microscopes by implementing “stations rotation” mechanism to move a cluster of students from one microscope (characterization technique) to another characterization technique. By doing that we were able to train students on five instruments, enabling them to conduct research projects with minimum assistance.

The outcomes of our product-oriented approach resulted in two successful courses based primarily on SEM and AFM with publications in peer-reviewed journals with students as co-authors. The dual design idea can be expanded to AFM materials sensing modes with complements of Scanning TEM and or to the fields of chemistry and biology. Both SEM and AFM can be integrated into projects involving nanomanipulation.

Acknowledgements

We acknowledge the contributions of Prof. Drazen Fabris and Prof. Shoba Krishna for setting ultimate goals and funding the MECH/ECEN156 and MECH 333B courses, Dr. Stephen Hudgens for fruitful discussions, Dr. Michael McElfresh for proofreading the manuscript, Dr. Robert Marks for supplying SnBi and CuZn samples. We acknowledge the contributions of Eurofins EAG Laboratories for sharing SCM images. Copyright Eurofins Scientific. www.eag.com


A special thanks for the commitment and dedication of our Student Assistants for these course—Parth Shah for SEM/EDS, Dongmeng Li for Optical Profiler and SEM/BSE/EDS and Vinay Krishnan for AFM. We also would like to thank SCU School of Engineering Dean's Office and Office of Diversity & Inclusion for funding this publication.

Author details

Nataliya Starostina
Mechanical Engineering Department, Santa Clara University, Santa Clara, CA, USA

*Address all correspondence to: nstarostina@scu.edu

IntechOpen

© 2023 The Author(s). Licensee IntechOpen. This chapter is distributed under the terms of the Creative Commons Attribution License (<http://creativecommons.org/licenses/by/3.0>), which permits unrestricted use, distribution, and reproduction in any medium, provided the original work is properly cited. 

References

- [1] Cullity B, Stock S. Elements of X-ray Diffraction. 3rd ed. Noida, India: Pearson; 2016. p. 652
- [2] Norman D. The Design of Everyday Things. New York, USA: Basic Books; 2021. p. 347. DOI: 10.15358/9783800648108
- [3] Getty Images SEM Insects [Internet]. 2023. Available from: <https://www.gettyimages.com/photos/sem-insect>
- [4] Atom and Molecule Manipulation [Internet]. 2023. Available from: <https://www.zurich.ibm.com/st/atomicmanipulation/>
- [5] Binns C. Introduction to Nanoscience and Nanotechnology. 2nd ed. New Jersey, USA: John Wiley & Sons, Inc.; 2022. 405 p. DOI: 10.1002/9780470618837
- [6] Poole C, Owen F. Introduction to Nanotechnology. John Wiley & Sons, Inc; 2003. p. 388
- [7] Goodhew P, Humphreys J, Beanland R. Electron Microscopy and Analysis. 3rd ed. New York, USA: Taylor and Francis; 2001. p. 251. DOI: 10.1201/9781482289343
- [8] Goldstein J, Newbury D, Joy D, Lyman C, Echlin P, Lifshin E, et al. Scanning Electron Microscopy and X-Ray Microanalysis. 3rd ed. New York: Springer; 2007. 690 p. DOI: 10.1007/978-1-4939-6676-9
- [9] Haugstad G. Atomic Force Microscopy: Understanding Basic Modes and Advanced Applications. 1st ed. New Jersey, USA: Wiley; 2012. p. 464. DOI: 10.1002/9781118360668
- [10] Bonell D. Scanning Probe Microscopy and Spectroscopy. 2nd ed. New York, USA: Wiley-VCH; 2001. p. 493
- [11] Bowen R, Hilal N. Atomic Force Microscopy in Process Engineering. 1st ed. Burlington: Elsevier; 2009. p. 283
- [12] Sullivan D, Carleton E. Failure analysis: High technology devices. Boston/Berlin: De Gruyter; 2022. p. 120. DOI: 10.1515/9781501524790
- [13] West P, Starostina N. How to recognize and avoid AFM image artifacts. Microscopy Today. 2003;3:20-26
- [14] Wong C, West P, Olson K, McCartney M, Starostina N. Tip dilation and AFM capabilities in the characterization of nanoparticles. Journal of Materials. 2007;1:12-16. DOI: 10.1007/s11837-007-0003-x
- [15] West P, Starostina N. Atomic force microscopy. Advanced Materials & Processes. 2004;162:35-37
- [16] How Atomic Force Microscope Works [Internet]. 2023. Available from: https://en.wikipedia.org/wiki/Atomic_force_microscopy
- [17] Ogasawara N, Chiba N, Chen X. Measuring the plastic properties of bulk materials by single indentation test. Scripta Materialia. 2006;54:65-70. DOI: 10.1016/j.scriptamat.2005.09.009
- [18] Schuh C. Nanoindentation studies of materials. Materials Today. 2006;9:5. DOI: 10.1016/S1369-7021(06)71495-X
- [19] How Interferometer Works [Internet]. 2023. Available from: <https://en.wikipedia.org/wiki/Interferometry>
- [20] Hariharan P. Basics of Interferometry. 2nd ed. Amsterdam: Elsevier; 2006. p. 248. DOI: 10.1063/1.2808787

- [21] Tompkins H, McGahan W. Spectroscopic Ellipsometry and Reflectometry: A user's Guide. New York, USA: Wiley; 1999. p. 220
- [22] Kabbara H, Ghanbaja J, Redjaïmia A, Belmonte T. Crystal structure, morphology and formation mechanism of a novel polymorph of lead dioxide, γ -PbO₂. Journal of Applied Crystallography. 2019;**52**:304-311. DOI: 10.1107/S1600576719001079
- [23] Woodward D, Reaney I. Electron diffraction of tilted perovskites. Acta Crystallographica. 2005;**B61**:387-399. DOI: 10.1107/S0108768105015521
- [24] Starostina N, McGuire A, Rowan R. Evaluation of dihedral angle twin boundaries in Cu₁₀wt%Zn alloy using atomic force microscopy. Microscopy and Microanalysis. 2021;**27**:1-7
- [25] Prikhodko S, Starostina N, Ardell A. Retardation of the coarsening kinetics of Ni-Al and Ni-Ge alloys under uniaxial elastic stress. Microscopy and Microanalysis. 2004;**10**:696-697
- [26] Prikhodko S, Starostina N, Ardell A, Prasad S. Coarsening of Ni₃Ge precipitates in Ni-Ge alloys aged under uniaxial compression. Materials Science and Engineering A. 2005;**409**: 264-270
- [27] Prikhodko S, Starostina N, Ardell A, Prasad S. TEM study of morphology and kinetics of coarsening of coherent Ni-Ga alloy under uniaxial compression. Microscopy and Microanalysis. 2006;**12**: 1046-1047
- [28] Du W, Ahmed Z, Wang Q, Yu C, Feng Z, Li G, et al. Structures, properties, and applications of CNT-graphene heterostructures. 2D Materials. 2019;**6**:042005. DOI: 10.1088/2053-1583/ab41d3
- [29] Zhou C, Zhang M, Yang CY. Nanocarbon Electronics. New York: Jenny Stanford; 2020. p. 374. DOI: 10.1201/9781003043089
- [30] Video 1. Film thickness determination of metallized and thermal oxide layers on silicon. Final exam presentation. Available from: <http://bit.ly/41xxpXr>
- [31] Video 2. TLM and cross-sections SEM characterization of the MOS structures. Final exam presentation. Available from: <http://bit.ly/41xxpXr>
- [32] Video 3. Nanoparticles morphology and size distribution characterization. Final exam presentation. Available from: <http://bit.ly/41xxpXr>
- [33] Video 4. Film thickness determination and elemental composition characterization. Final exam presentation. Available from: <http://bit.ly/41xxpXr>
- [34] Video 5. Surface metrology. Final exam presentation. Available from: <http://bit.ly/41xxpXr>
- [35] Ph. D student presentation "Influence of Crystallographic Orientation on the Growth of Thermal Oxide of Silicon" [Internet]. Available from: <https://www.youtube.com/watch?v=9GjhdBZuJgU>
- [36] Video 6. Grain size, chemical composition examination and dihedral angle of twin boundary grooves measurements in CuZn alloy. Final exam presentation. Available from: <http://bit.ly/41xxpXr>
- [37] Video 7. Characterization of gold and cobalt nanoparticles. Final exam presentation. Available from: <http://bit.ly/41xxpXr>
- [38] Video 8. SnBi alloy micro/nanostructure morphology, chemical

composition and mechanical properties
characterization. Final exam
presentation. Available from: <http://bit.ly/41xxpXr>

[39] Starostina N, Hartman A, Cole R,
Li D, Park W. Hardness-strength linear
correlation coefficients in eutectic SnBi
alloy. Materials Research Express, IOP
Science. 2023 (submitted)

Chapter 3

Ion Mobility Mass Spectrometry: Instrumentation and Applications

*Orobola E. Olajide, Kimberly Y. Kartowikromo
and Ahmed M. Hamid*

Abstract

The integration of ion mobility spectrometry with mass spectrometry (as an IM-MS hybrid instrument) provides additional analytical separation and identification capabilities that have greatly advanced various fields, including biomedical, pharmaceutical, and forensic sciences. In this chapter, a comprehensive exploration of various IMS instrumentation platforms is discussed, including Drift tube (DTIMS), Traveling wave (TWIMS), Trapped (TIMS), Field asymmetric waveform (FAIMS), and Differential mobility analyzer (DMA). Their respective advantages and limitations are evaluated in the context of distinct applications, including isomer separation, signal filtering to increase signal-to-noise ratio, and collision cross section (CCS) measurements in targeted and untargeted omics-based workflows. The scanning rate compatibility between various IMS devices and different mass analyzers resulted in various IM-MS hyphenation platforms. Higher sensitivity and selectivity are further achieved with the introduction of tandem IMS such as TIMS-TIMS-MS. IMS separations occur in the millisecond range and can therefore be easily incorporated into the liquid chromatography-mass spectrometry workflows and coupled with ambient ionization MS for metabolomics, lipidomic, proteomics, etc. The emergence of high-resolution IMS instruments such as Cyclic Ion Mobility Spectrometry (cIMS) and Structures for lossless ion manipulations (SLIM) is also discussed for the improvement of separation of isomers and increased predictive accuracy of CCS by machine learning models.

Keywords: ion mobility mass spectrometry, CCS experimental measurements, CCS prediction models, ambient ionization, omics

1. Introduction

Compounds with the same mass-to-charge ratio (m/z) but differ in configurations and conformations exhibit significant variations in potency, pharmacodynamics, and toxicology [1, 2]. In metabolomics, lipidomics, and proteomics studies, the existence of isomers poses significant challenges to effective separation. Analytical methods for isomer separation and characterization include chromatographic separation and differences in tandem mass spectrometry (MS/MS) fragmentation patterns. However, similar retention behavior during chromatography and fragmentation patterns in

mass spectrometry techniques reduce the accuracy of both qualitative and quantitative structural analysis of compounds [3, 4]. Ion mobility spectrometry (IMS) is an effective solution for addressing the intricate structural challenges presented by isomers in omics studies. In addition to isomer separation and signal filtering, IMS facilitates the annotation of features via CCS values thereby enhancing the identification of compounds in non-targeted omics analysis that share common properties (e.g., tandem mass spectrometry (MS/MS), retention time (RT), m/z) [5]. This chapter focuses on the commercially available IMS instrumentation platforms and their integration with other separation methods, sample introduction, and detection techniques for all-omics studies. Furthermore, the applications of computational and machine learning models for the calculation and prediction of CCS are also discussed. Moreover, a detailed examination of novel high-resolution IMS systems, including cyclic IMS (cIMS) and Structures for lossless ion manipulations (SLIM), and their technological advancements is provided.

2. IM-MS: Instrumentation and experimental CCS measurement

IMS separate ions based on their mobility rates (K or K_0 ; K is usually reported as K_0 under standard pressure and temperature) through the combined action of an electric field and neutral buffer gas. The mobility of the ions depends on characteristics of the ions such as mass, size, shape, and charge number, leading to the separation of compounds with the same m/z but different structures (isomers) due to the combined influence of the collisions of the ions with neutral buffer gas and applied electric field [5]. Although IMS can detect the size of an ion, it cannot determine its exact molecular weight. Therefore, IM-MS is more valuable, combining complementary size selection and quality mass separation into a single analysis platform [3]. IMS separations typically occur on a timescale of 10^{-3} – 10^{-2} s, hence, are well-suited for incorporation between LC (10^2 – 10^3 s timescale) and mass spectrometry techniques (10^{-6} – 10^{-4} s timescale), thereby providing three-dimensional orthogonal separation based on polarity, size, and mass of the analytes. This results in a four-dimensional dataset including RT, drift time (DT), m/z , and fragmentation patterns, all captured in a single sampling event [3, 5, 6]. The supplementary advantages of IMS separation when coupled with MS, such as separation of isomers, signal filtering, and CCS fingerprinting, depend on the resolution of the IMS technique and its accuracy of collision cross section (CCS) measurements. These parameters must be considered when selecting IMS instruments. According to separation mechanisms, IMS platforms can be classified into temporal dispersive, spatial dispersive, and confinement and selective release; and based on electric field applications, they can be classified into static and dynamic fields [7, 8]. In temporal dispersive IMS, all ions drift along similar paths colliding with the neutral buffer gas under the influence of electric fields, resulting in different arrival times (mainly DTIMS and TWIMS), while in spatial dispersive IMS, ions are separated along different drift paths (mainly DMS, FAIMS, Aspiration IMS (AIMS), and DMAs). In confinement and selective release IMS (mainly TIMS), ions are trapped within a pressurized region by a precisely adjustable electrodynamic field and are then selectively released based on differences in their mobility [3]. Static field IMS instruments employ linear and constant electric fields (mainly DTIMS and DMA), whereas dynamic field IMS instruments utilize non-uniform electric fields (mainly FAIMS, TWIMS, and TIMS) [8].

2.1 Drift tube ion mobility spectrometry (DTIMS)

A distinctive feature of DTIMS is the uniform application of a weak electric field (10–20 V/cm) that propagates through the drift tube, which is filled with a neutral buffer gas such as nitrogen or helium that has no directional flow, as shown in **Figure 1A**. The two working states of DTIMS are the reduced pressure (~4 Torr e.g., Agilent 6560 IM-QTOF) and atmospheric pressure (760 Torr e.g., TOFWERK-IMS-TOF) [9]. The choice between low-pressure and high-pressure systems involves trade-offs; while low-pressure systems offer higher sensitivity and improved ion focusing due to reduced collisions frequency with the buffer gas, high-pressure IMS systems yield enhanced separation capacity due to more frequent collisions, but often experience significant ion losses [10]. Radiofrequency (RF) confinement in low-pressure DTIMS (3.5 Torr) has been reported for excellent ion transmission resulting in increased sensitivity [11]. The ability to calculate CCS from first principles using the Mason-Schamp equation is perhaps the most significant advantage of DTIMS. The utilization of a low and uniform electric field enables DTIMS to measure K as a primary method, enabling it to calculate the corresponding CCS values. In fact, DTIMS is the only ion mobility paradigm that can provide precise CCS measurement without the need for external calibrants. This is achieved through a method known as step-field, which is the “gold standard” for CCS measurements with a remarkable 0.29% relative standard deviation (RSD) [12]. However, using the step-field method for experimental CCS measurements can be time-consuming and is not practically compatible with the analytical timescale of the chromatographic separation [5]. In contrast, the single-field method (calibrant dependent) is compatible with

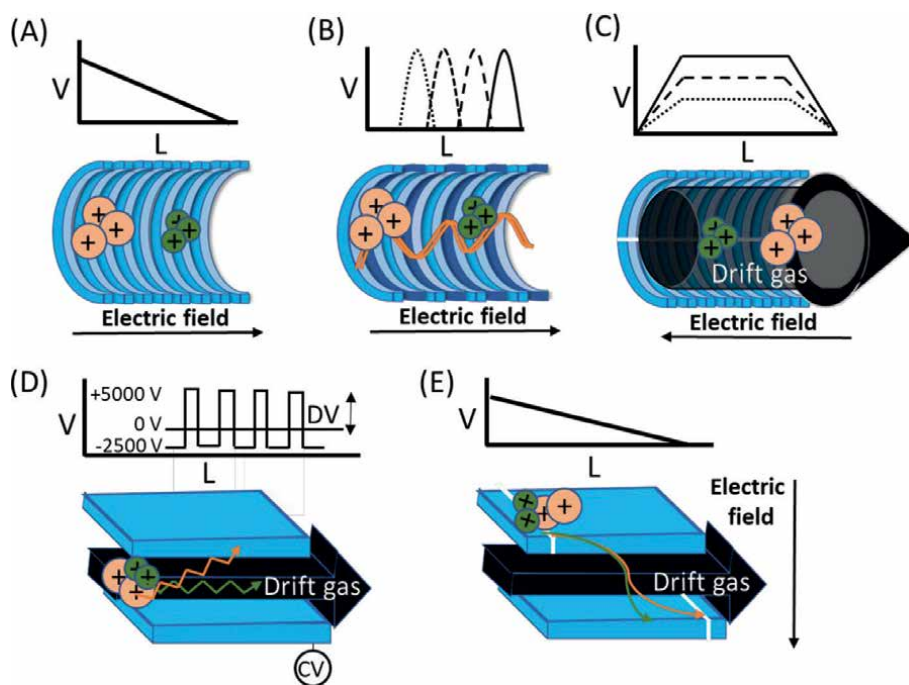


Figure 1.
 Schematic diagram of various IMS technology and separation mechanisms: (A) DTIMS, (B) TWIMS, (C) TIMS, (D) FAIMS, and (E) DMA.

	DTIMS	TWIMS	TIMS	DMA	FAIMS
Separation mechanism	Temporal	Temporal	Trap & Release	Spatial	Spatial
Gas flow to ion motion	No net flow	No net flow	Parallel	Perpendicular	Parallel
Electric field	Static	Oscillating	Static	Static	Oscillating
Ion injection	Pulsed ion packet	Pulsed ion packet	Variable	Continuous filter	Continuous filter
Ion analysis	All ion analysis	All ion analysis	All ion & scannable	Scannable	Scannable
CCS	Direct	Calibrated	Calibrated	Direct	No CCS
Common calibrants	Agilent tune mix	Polyalanine, Waters CCS Major Mix	Agilent tune mix		
Resolving power	60–80 ^a	~40 ^b	~200	<100	~40 ^c
Vendors	Agilent, ToFwerk, Excellims	Waters	Bruker	SEADM, TSI	Owlstone, Thermo, Heartland, Sciex
Mass analyzers	TOF, Quadrupole	TOF	TOF, FTICRs, Orbitraps	TOF, FTICRs, Orbitraps	TOF, FTICRs, Orbitraps

^a180–250 with HRdm.^bcIMS and SLIM: >400.^cUp to 500 with the doping of the N₂ carrier gas with light gases such as He or H₂.**Table 1.**

General information on each IMS technology.

chromatographic separation. It utilizes calibrant ions to produce highly reproducible CCS values with 0.54% RSD compared to the step-field method [12]. Other IMS platforms (e.g., TWIMS) use this single-field method using calibrants that have well-characterized CCS values previously determined with DTIMS instruments to create a calibration curve for CCS measurements of unknown analytes [5, 13, 14]. Calibrant compounds used in DTIMS include the Agilent Tune mix (**Table 1**).

While DTIMS systems enable comprehensive ion collection, i.e., the arrival time of all ions is recorded during each measurement cycle, particularly valuable for the analysis of complex biological samples, ions are not continuously injected. Instead, ion packets are introduced as ion pulses into the drift tube using an ion gate [15] or an ion funnel [16]. The time scale of the ion release time and IMS separation time is 25–400 μ s and 25–100 ms respectively, resulting in an experimental duty cycle of ~0.04–1%. Consequently, only a fraction (0.1–1%) of the generated ions are transmitted to the drift tube for separation, resulting in a low sensitivity [17]. To improve the DTIMS sensitivity, an ion multiplexing approach is utilized, involving the pulsing of multiple packets of ions into the drift region at defined times. The multiplexing strategy results in an overlapping ion mobility spectrum, which is subsequently deconvoluted to the correct arrival times using schemes such as the Hadamard Transformation algorithm, achieving improvements as high as 50% duty cycle [5, 18]. An additional challenge of DTIMS systems is the low resolving power which can be improved using

a post-acquisition data reconstruction technique or modifying the DTIMS instrumentation [5, 19]. An example of a reconstruction technique is the High-resolution demultiplexing tool (HRdm, Agilent Technologies), which effectively increases the resolving power from ~60 to a range between 180 and 250 [20]. This involves passing multiple ion packets through the drift tube, giving each ion packet a shorter accumulation time to improve the duty cycle while reducing the negative effects of space charge. The spectrum obtained is then deconvoluted and demultiplexed using the Hadamard transform algorithm, resulting in an improved signal-to-noise ratio and lower detection limits. The increase in the resolving power through instrumentation is accomplished by increasing the voltage drop across the drift cell and decreasing temperature [5]. For precise DTIMS measurements, it is essential to keep the ions in the low field limit. Therefore, to increase the voltage drop either the length of the drift cell or pressure needs to be increased [5, 21]. Examples include DTIMS systems of 2 m by Bowers et al. [22] and ~2.9 m by Clemmer et al. [23], as well as atmospheric pressure DTIMS systems yielding resolving power between 100 and 250 [9].

2.2 Traveling wave ion mobility spectrometry (TWIMS)

The drift region of TWIMS is very similar schematically to the DTIMS platform; it contains a stacked set of ring electrodes. However, in TWIMS, an RF voltage is applied across consecutive electrodes to confine the ions radially, and pulse differential current (DC) voltage is applied to push ions axially as shown in **Figure 1B**. Similarly to the RF-confining drift cell, the RF confinement in TWIMS focuses the ions, leading to increased analyte signals attributed to reduced ion diffusion. Under the combined actions of the applied voltages, traveling electric field waves are formed to propel the ions through the IMS tube under reduced pressure of ~2–4 Torr. The amplitude and speed of the electric waves determine the ion separation in TWIMS [14]. Due to the existence of RF voltage, ions are not in a constant field in TWIMS mode, requiring prior calibration of TWIMS instruments with ions of known mobility before determining CCS values of unknowns (analogous to the single-field CCS measurements in DTIMS) [5, 14]. Various compounds are used as calibrants in TWIMS, including polyalanine and Waters CCS Major Mix (**Table 1**). Since the accuracy of CCS measurement in TWIMS depends on the type of calibrants being used, class-specific calibrants are needed for more accurate CCS measurements. For example, calibrating instruments to obtain CCS values using peptides in lipid analyses has demonstrated a significant error [5, 24]. TWIMS shares both advantages and disadvantages with DTIMS, such as the full ion mobility spectrum acquisition and pulsed ion packet delivery by ion gating. Two primary advantages distinguish TWIMS: the low voltage requirements due to constant wave heights, and the ability to manipulate ion motion to long path lengths without significant ion losses. These attributes were the key to the development of two platforms with extremely long path lengths leading to very high resolving power: cIMS from Waters Corporation with a resolving power of ~750 for 100 passes [25] and SLIM, developed at PNNL and commercialized by MOBILion Systems (Chadds Ford, PA) with a path length of 13 m in a device measuring 45.9 cm × 32.5 cm, with a separating power of ~1860 [26].

Commercial TWIMS instruments are produced by Waters Corporation, which includes the Synapt G2 and Vion series (**Table 1**). The Synapt G2 model is designed with an IM tube positioned behind the quadrupole. The collision cell is situated both before and after the drift tube (in DTIMS the collision cell can be connected only after the IMS), enabling TWIMS-MS to perform time-aligned parallel fragmentation [3].

The Vion series moved the IM tube and its frontally connected collision cell to the front of the quadrupole. For comprehensive compound structure elucidation, in addition to the collision-induced dissociation (CID), TWIMS can combine surface-induced dissociation (SID) or electron capture dissociation (ECD), essential tools for structural details of both ligand-bound and unbound [3]. Compared to DTIMS, the resolving power of TWIMS is not significantly improved as it is less than 100.

2.3 Trapped ion mobility spectrometry (TIMS)

The separation principle of TIMS is effectively inverted from traditional ion mobility modalities. While DTIMS and TWIMS methods maintain, the essentially stationary gas flow, with an electric field parallel to the ion movement, TIMS utilizes a unidirectional buffer gas parallel to the ion motion, accompanied by an opposing electric field (ca. 70 V/cm) [3]. The TIMS analyzer is comprised of a set of electrodes that form three regions: the entrance funnel, the TIMS mobility region (ion mobility analyzer), and the exit funnel. The entrance and exit regions serve to control ion deflection and focusing, while the TIMS mobility region is utilized to accumulate, trap, and elute ions of interest which effectively increases the measurements' duty cycles. In the TIMS mobility region, different plates along its length modulate the potential of ions as a function of distance. Consequently, ions with larger CCS values will be pushed further along the TIMS analyzer due to the energy they receive from the carrier gas as shown in **Figure 1C**. The accumulated ions can then be eluted from the TIMS analyzer by sequentially lowering the position-dependent plate potential as a function of time. This sequence of accumulation and elution processes can be adjusted to optimize for fast scans (tens of ms) or high-resolution separations (hundreds of ms) [5]. Optimized stepping scan functions can provide IMS resolving power of >300 while reducing overall experiment time and increasing the duty cycle [10]. An additional main difference between TIMS and the previously described DTIMS and TWIMS techniques lies in its operational scanning mode. In DTIMS and TWIMS, all ions are observed under the same experimental conditions, while TIMS requires changes to experimental parameters to elute all ions. Though TIMS instruments can indeed measure K as a primary method (thus obtaining CCS values), calibrating TIMS with analytes of known mobility prior to analysis (similar to TWIMS) is needed [5]. An example of calibrant ions used in TIMS CCS measurement is the Agilent tune mix (**Table 1**).

2.4 Field asymmetric waveform ion mobility spectrometry (FAIMS)

Both DTIMS and TWIMS separate ions by the gas-phase mobility inherent in an ion for a given gas under low electric field conditions. At high electric fields (i.e., > 10^4 V/cm), ion mobility begins to change due to non-elastic ion-gas collisions (e.g., reactive, or interactive ion-gas collisions). An IM technique that exploits this differential mobility behavior at high fields is FAIMS operating at atmospheric pressure and near-ambient conditions [14]. Two ions with different chemical compositions can have the same ion mobility at a low electric field, but completely different mobilities at a high field, allowing them to be differentiated in the FAIMS measurement. FAIMS's current commercial instruments include Thermo Fisher Scientific, Owlstone Medical, Heartland MS, and Sciex (**Table 1**). FAIMS utilizes an asymmetric waveform voltage known as Dispersion Voltage (DV) which comprises high-field components of short duration and low-field components of a longer time. As a result, ions oscillate between two electrodes in an up-and-down motion, as illustrated in **Figure 1D**.

The dispersion voltage alone would ultimately cause all ions to contact the electrodes and be neutralized. To account for this, a second voltage – a variable compensation voltage (CV) is applied during the experiment. For ions at a specific K value, a given CV value enables ions, under the influence of parallel gas flow, to keep a straight-lined trajectory and exit the chamber to the mass analyzer [3]. In fact, FAIMS acts like a quadrupole mass analyzer and in this way contrasts temporal dispersive IMS instruments in which all ions are transmitted simultaneously. FAIMS can be used in two ways: [1] by scanning a range of CVs to create a fingerprinting in global analyses, or (ii) by selecting CVs values related to the analytes of interest for targeted analysis [14]. Due to the challenging nature of characterizing ion mobility behavior under high fields, FAIMS instruments are unable to provide CCS values. Moreover, the ion structure itself can change from low to high field strengths during oscillation. The different mobility behavior in FAIMS may result from the dipole orientation and the clustering and declustering of the ions. FAIMS devices can be fabricated in different geometries, such as cylindrical, planar, and chips [5]. Differential mobility spectrometry (DMS), differential ion mobility spectrometry (DIMS), along with FAIMS operate under the same electronic mechanism, differing primarily in the geometry of their respective electrodes. Furthermore, these devices do not pulse ions into the mobility region as seen in DTIMS, TWIMS, and TIMS [3]. The continuous ion injection enables FAIMS/DMS/DIMS devices to increase the signal-to-noise ratio for the ions of interest by greatly removing unwanted chemical noise in MS spectra.

2.5 Differential mobility analyzer (DMA)

DMA operates similarly to DTIMS; both systems use a constant electric field and can measure CCS directly. However, DMA instruments introduce distinct features, including unidirectional gas flow (as opposed to the no-directional gas flow in DTIMS), operation at ambient pressure, and scanning for target analytes [10]. This scanning capability makes DMA a narrow bandpass IM technique, analogous in concept to FAIMS, where ions travel between two parallel electrodes in the presence of a gas flow. In DMA a constant electric field is applied between two cylindrical and concentric metal electrodes and ions are introduced at the entrance electrode where they are pushed towards the exit electrode through orthogonal sheath gas flow, as shown in **Figure 1E**. Only ions with the appropriate mobility will reach the cell exit, while others collide with the electrode, thus preventing their detection [8]. By scanning the electric field, an ion spectrum based on the different ion mobilities can be recorded. The well-defined nature of the electric allows for high-precision measurements of ion CCS using DMA. Notably, DMA can be utilized for analyses that are not possible with DTIMS; DMA detects very large analytes, such as antibodies, aerosol particles, viruses, and other macromolecules (~ 10 's to 100 's of nm^2); and is not commonly used in screening applications for small molecules (e.g., lipids and metabolites) [5]. DMA instruments are currently marketed by SEADM and TSI (**Table 1**).

3. Ion mobility mass spectrometry hyphenation

3.1 Mass analyzers interfaced with IM

The difficulty of coupling an IM device to a mass analyzer is caused by the need for scanning rate compatibility of both instruments. Time of flight (TOF) mass

analyzers due to their microsecond acquisition timescale are readily hyphenated with all types of IM devices, facilitating the recording of several mass spectra per mobility scan [27]. For higher MS performances in terms of dynamic range, mass resolving power, and mass accuracy, Fourier transform mass spectrometry (FTMS) analyzers (e.g., Orbitrap-based or FTICR instruments) are required. FTMS analyzers can be readily coupled with spatial dispersive IM instruments, for instance, the coupling of FAIMS with LTQ-orbitrap and FTICR instruments is routinely used [14]. Hyphenation of FTICR or orbitrap-based instruments with temporal dispersive IM systems is less straightforward due to the time scale difference between the rapid IM separation and the slow FTMS acquisition rate (up to 1 s for FTICR). To circumvent this limitation, the IM separation is “slowed down” to make it suitable for the FTMS scan rate [14]. Examples include the coupling of DTIMS with an Orbitrap-based instrument using a dual gate approach [28]. The scan rate in TIMS in theory can be conducted at any speed and synchronized with any analyzer. For instance, TIMS coupling with TOF analyzer, FTICR coupling with gated TIMS, selective accumulation-TIMS (SA-TIMS), and oversampling selective accumulation TIMS (OSA-TIMS) [14, 27]. However, TOF mass analyzers are used in all the commercial IM-MS platforms (e.g., DTIMS, TWIMS, and TIMS) due to the complexity nature of coupling with FTMS analyzers.

3.2 Front-end separations coupling with IM-MS

The incorporation of front-end separation techniques such as LC with IM-MS results in an enhanced peak capacity, detection of more features, separation of co-eluting compounds and isobaric components, and increasing S/N ratios due to the orthogonality of the separation techniques [5]. Notably, the addition of IM to LC-MS workflow has been shown to yield a 15% increase in peak capacity, as reported by Pacini et al. [29]. In the context of lipid mapping of human plasma, the implementation of 2D-LC coupled with MS (LC \times LC-MS) enabled the detection of 1100 features, with 100 lipids identified. Comparatively, the LC-IM-MS approach provided 800 features, identifying 55 as lipids. Despite the fewer features detected by LC-IM-MS, it offers better structural identification and higher throughput (190- and 20-min analysis time for LC \times LC-MS and LC-IM-MS, respectively) [30]. Olajide et al. utilized a multidimensional LC-IM-MS/MS method to detect features that served as strain-indicating biomarkers for efficiently discriminating *E. coli* strains [4]. Paglia et al. used LC-IM-MS^E for metabolomic and lipidomic analyses of frontal cortex samples from Alzheimer’s Disease (AD) patients [31]. Other front-end separation techniques coupled with IMS include gas chromatography (GC) as GC-IMS for fingerprinting volatile organic compounds (VOCs) from the feces and urine of AD-model mice [32]. Furthermore, 2D GC (GC \times GC) coupled to IM-MS was used to analyze *Calendula officinalis* plant extracts, with the IM dimension effectively separating isobaric compounds not resolved by the 2D-GC [33]. Capillary zone electrophoresis (CZE) was coupled with TWIMS-MS to resolve glycan isomers [34]. Supercritical fluid chromatography (SFC) and TWIMS devices were coupled to detect and quantify four nonsteroidal androgen receptor modulators from bovine urine samples [14]. The absence of front-end separations leads to severe matrix interferences and ionization suppression which is a challenge to conventional IM-MS [4]. Solid-phase extraction (SPE) coupled with IM-MS is a promising alternative, such as the SPE-IM-MS method proposed by Zhang et al. for

the simultaneous targeted and untargeted measurements of metabolites in complex human fluids [35].

3.3 Ambient Ionization Coupling with IM-MS

Ambient ionization MS is a technique for direct analysis by ionizing analytes at ambient pressure and temperature conditions without sample preparation. The advantages of ambient ionization techniques include minimal sample preparation, low sample and solvent volume utilization, and direct rapid analysis [36]. Ambient ionization can be largely categorized into three main classes primarily based on their desorption methods: liquid extraction, plasma desorption, and laser ablation [37]. An extensive description of each ambient ionization technique under each classification and their applications in forensics, biomedical, environmental, bioanalysis, in vivo analysis, food and agriculture, and reaction monitoring and catalysis have been detailed in previous reviews [37, 38]. The direct sample analysis using ambient ionization MS suffers severe matrix interference and chemical noise due to no chromatographic separation and reduced selectivity as isomers cannot be separated [4].

The coupling of IM-MS to ambient ionization has proven to increase the technique selectivity due to isomer separation [39]. In addition, ambient ionization IM – MS is very rapid compared to classic LC – IM – MS workflows. Desorption electrospray ionization (DESI) was coupled to DTIMS to investigate charge state distributions and cross sections for protein ions in a single experiment [40]. DESI was also coupled with FAIMS to effectively increase the image quality of targeted compounds in sea algae and mouse brain tissue sections [41]. The capability of DESI to produce ions directly from tablets and creams was explored in combination with hyphenated IMS for the analysis of pharmaceutical drugs [42]. The signal filtration capability of TWIMS was demonstrated in a selective surface analysis when coupled with Desorption atmospheric pressure photoionization (DAPPI) and Direct analysis in real-time (DART) resulting in a low limit of detection (LOD) [43]. Liquid extraction surface analysis (LESA) and FAIMS were integrated to image proteins in mouse brain and liver tissue samples [44]. FAIMS has also been coupled with paper spray (PS) to obtain metabolomic and liposome characteristics in breast tissues [45]. Olajide et al. coupled PS and leaf spray (LS) to DTIMS for the separation of geometric and constitutional isomers [39]. Furthermore, the PS-IM-MS/MS developed by Olajide et al. was utilized to distinguish five *Bacillus* species and seven *E. coli* strains [4, 20].

3.4 Tandem ion mobility (IMS/IMS)

The coupling of multiple ion mobility cells allows low-intensity features to be detected. Tandem ion mobility separations have been achieved either by hyphenation of the FAIMS device with conventional ion mobility geometry or by combining ion mobility cells of the same geometry [14]. Examples include FAIMS-DTIMS-MS with the FAIMS increasing the S/N ratio and the DTIMS providing accurate CCS measurement [46], DTIMS-DTIMS-MS [47], and TIMS-TIMS-MS [48]. In a study on the tryptic peptide, IMS provided a peak capacity of 60–80 while tandem IMS provided a peak capacity of 480–1360 indicating the advantage of using tandem IMS in the analysis of complex mixtures, especially in metabolomics, lipidomics, and proteomics [49]. The history of tandem IM instruments, recent developments, and detailed applications to biological systems can be found in a recent review [50].

4. High-resolution ion mobility and new technologies

The development of high-resolution IMS (HRIMS) has emerged as a solution to the low resolving power of conventional IM techniques (~ 60), which limits the separation of difficult isomers such as cis/trans. Achieving a resolving power of at least 300 is considered essential for effectively resolving such challenging isomers [51]. HRIMS involves advancements in technology and techniques to improve the separation and characterization of ions in complex samples. This is particularly important as samples become more complex and require more precise separation methods [52]. IMS platforms that offer high resolving power include Waters' cyclic ion mobility spectrometry (cIMS), MOBILion Systems' SLIM device, and the previously-described Bruker's TIMS [10].

4.1 Cyclic ion mobility spectrometry (cIMS)

cIMS is an innovative platform that uses the TWIMS concept but has a closed-loop design with a 98 cm path length. It is comprised of an IMS separator, ion entry, and ion exit regions. This model utilizes opposite phases of RF voltage to adjacent plates in the y-axis for a pseudopotential barrier and ion confinement in the z-direction. The applied DC voltage on the "repeller" band electrodes gives ion confinement in the x-axis and TWs in a repeated pattern are supplied to the RF electrodes to propel ions forward which gets them separated as a function of their respective mobilities (**Figure 2**). During the injection of ions, the DC bias of the array electrodes is lower than that of the cIM electrodes, the prearray store (prior to the entrance), and the exit array regions. During IM separation, the DC offset applied to the array electrodes is increased to be similar to the cIM electrodes while being lower than that of the entrance and exit regions. Then the ions are guided through the circular path using the TW voltages applied to the cIM and array electrodes and are subsequently separated based on their ion mobility. After the separation period, the mobility-separated ions are ejected (towards the mass spectrometry) by lowering the DC offset of the array electrodes with respect to that of the cIM. However, this DC offset is still higher than the exit and postarray (after the exit). In addition, separated ions can also move

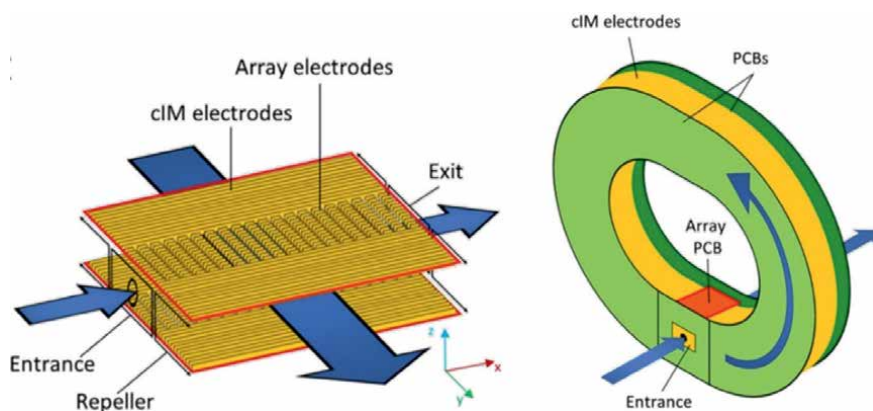


Figure 2. cIMS instrument design. (Adapted with permission from Ref. [25], Copyright (2019) American Chemical Society, Note: further permissions related to the material excerpted should be directed to the ACS).

to the prearray store if needed by adjusting the voltages accordingly. In short, this model provides a “multifunction” option for mobility selection, activation, storage, IMSⁿ, as well as custom combinations of these functions.

Interestingly, cIMS provides a resolving power of around 80 for a single pass while 750 for 100 passes, but also loses its transmission ion efficiency with each pass (~2.4% per pass) [25]. Additionally, much work on cIMS has been conducted showing promising separation results [53–55]. For example, Williamson et al. utilized mass distribution-based isotopic shift separation for the characterization of isomeric species and conformers with very good reproducibility [56]. Harrison et al. reported the use of cIMS coupled with a temperature-controlled electrospray ionization source to analyze large biomolecular systems, temperature-induced protein aggregation, and oligonucleotide complexes [55]. Another study incorporated liquid extraction surface analysis with cIMS for the analysis of intact proteins in mouse brains and rat kidneys, increasing the number of proteins being detected with each pass using multipass experiments [54].

4.2 Structures for lossless ion manipulations (SLIM)

Nearly a decade ago, SLIM platforms were developed to demonstrate their application in high-resolution IM separation. A SLIM device consists of two parallel boards which are fabricated using printed circuit board (PCB) technology, which is fast and inexpensive. SLIM boards can also be fabricated using 3D printing or other processes. Ion motion within SLIM is driven by the action of net forces caused by the electric field (DC and/or TW) and collision with a buffer gas while efficient ion confinement is achieved by applying a combination of high frequency (RF) and DC “guard” voltages. The applied fields in SLIM create “an ion-pipe” in which the ions are transmitted “losslessly” through the device (**Figure 3**). Therefore, the ions can travel different paths in the SLIM by changing or removing the electric field [57]. In addition, simulations of ion motion and the applied electric fields within the SLIM with the choice of fields RF and DC are investigated using computational methods such as SIMION [58, 59].

Different SLIM concepts are used for ion mobility separation based on the constant field SLIM and the traveling wave SLIM (TW-SLIM). In the constant field SLIM, the first generation of SLIM, constant DC fields (e.g. DTIMS) are used for ion motion and ion mobility separation with a resistor divider network to establish a voltage gradient across the electrodes and a capacitor chain for the superimposed Ref. [57]. However, the disadvantage of the constant field SLIM is the limitation of ion path

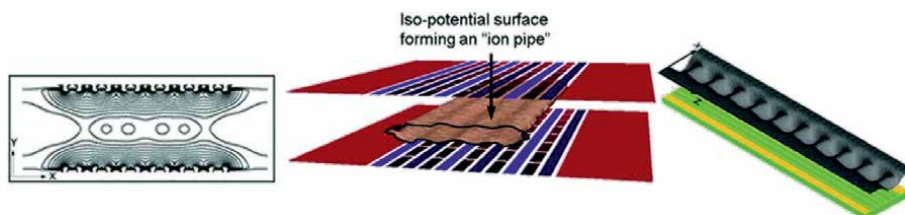


Figure 3. The RF potentials are presented by the contour lines on the left. The central plane shows the ion confinement region (iso-potential surface forming an “ion pipe”). The right plane represents the TW potential distribution between two SLIM boards and the ion confinement region. (Adapted with permission from Ref. [57], Copyright (2017) Royal Society of Chemistry).

length and field strength because longer ion path lengths (e.g., 13 m) would require extremely high voltages. In contrast, since TW-SLIM repeatedly uses the same TW sequence across the device utilizing a low voltage (e.g., 30 V) enabling the extension of the IM path length significantly without the need for high voltages. In addition, the advantages of TW-SLIM include that it does not require many electronic components (resistors and capacitors). It uses phase-shifted RF waveforms for adjacent electrodes that are in the direction of the ion path, and segmented TW electrodes that are interleaved [60, 61]. Recently, the TW-SLIM model has been modified to a multi-level TW-SLIM where multiple dual-surface SLIM boards are stacked vertically, and each level contains “ion escalators” and “ion elevators” between the SLIM levels [62]. Moreover, a resolving power of ~ 400 was obtained with a multilevel ion path of only 43.2 m [63]. In addition, other parameters, such as plate spacing, thickness, velocity, and amplitudes can affect the ion transfer efficiency [2, 63]. Many SLIM studies are still being studied on improvement (i.e., the charge capacity), modification of SLIM designs, and coupling with different MS platforms [64–67].

5. Theoretical approaches for CCS

Even though ion mobility experiments are rapid, they still have some limitations, such as the CCS accuracy, which is affected by the calibrant mixtures available for CCS calibration and the calibration method. Another limitation is the ability to identify compounds in untargeted analysis when no reference CCS values are available for the specific chemical class of interest. To solve this problem, theoretical approaches such as computational and machine-learning prediction models have been used as alternatives. More details on different CCS prediction theoretical models were recently summarized by Kartowikromo et al. [51].

5.1 Computational models

Computational models have been used for decades to calculate CCS values. CCS Predictions using these models require conversion to 3-dimensional (3D) structures to obtain all possible conformers with consideration of variables such as bond length, and protonation/deprotonation sites [68, 69]. These conformers are then optimized to the minimum energy, which is used to calculate the CCS values on a computational software platform, such as IMoS [70–72], MOBCAL [73, 74], and Sigma [75]. Some of the recent computational platforms are Rosetta online server that includes everyone (ROSIE) [76], IMPACT [77], and colloidoscope [78]. The optimization of the conformers is performed using various theoretical approaches, including density functional theory (DFT), molecular dynamics, and molecular mechanics, while the calculation of CCS is performed using algorithms, such as projection approximation (PA), exact hard-sphere scattering (EHSS), and trajectory method (TM) [68]. One of the earliest CCS prediction methods in helium gas was based on the PA algorithm using the average projected area of a large number of orientations of the analyte [79]. Furthermore, other computational CCS calculation methods have been developed, showing some improvement compared to the previous methods, such as superposition approximation (PSA) [80], diffuse hard-sphere scattering (DHSS) [70], and colloidoscope TM [78]. Olajide et al. applied the IMoS TM method to structurally characterized two conformers of verapamil based on their calculated CCS [39].

Recently, a web application (<https://rosie.graylab.jhu.edu>) for CCS calculations using the projection approximation rough circular shapes (PARCS) algorithm on ROSIE was reported where the projection area of each atom with a nine points rough circle was studied. However, computational approaches usually require high CPU power (computationally intensive) to generate a whole set of compounds which can even take days even though it can accurately calculate CCS values. In addition, it is also prone to larger CCS errors, especially for flexible molecular structures [81].

5.2 Machine learning (ML) models

Machine learning-based models have the advantage of less time and CPU power for predicting multiple connections with fewer errors compared to computational methods. In fact, errors of less than 10% are obtained compared to the computational methods. These models require a training set with data obtained from experimental measurements and a validation dataset divided into an internal and an external dataset [69]. In addition, molecular descriptors (MDs) are determined for the compounds in the dataset, which are numerical values obtained from molecular structures using mathematical algorithms, such as measured values (polarity, logP, dipole moment, etc.) and theoretical values (constitution, geometry, physical chemistry, etc.). These MDs are calculated or determined using computer software or programs such as Dragon, or online databases such as Lipid Maps and the Human Metabolome Database (HMDB) [82]. The combination of different MDs can provide a “finger-print” for the chemical property of a compound. However, these MDs do not always correctly reflect the features of a compound’s structure [83]. Moreover, the MDs are preprocessed, selected, and optimized using the preferred ML algorithm. ML algorithms can be divided into nonlinear and linear methods, such as regression models, neural networks (NN), random forest (RF), or Gradient Boosting Machine (GBM) [82]. Several ML CCS prediction models that can be used for lipidomics and metabolomics studies are publicly available and are based on support vector regression such as MetCCS [84], LipidCCS [85], AllCCS [69], CCSbase [83], etc. Bijlma et al. were the first to present an ML-based model for predicting the CCS values for small molecules based on the ANN algorithm (a type of NN algorithm) [86]. Subsequently, many neural network algorithm methods and comparisons between different neural network algorithms have been reported to be used for different omics (lipidomics, metabolomics, and proteomics), in which some methods are publicly available such as DeepCCS [87], DarkChem [88], AlphaPeptDeep [89], etc. Although ML models provide fast CCS predictions with lower errors, they still have some limitations due to the availability of databases for a variety of chemical classes, the low resolving power of IMS instruments, and the calibration methods for more accurate experimental CCS values.

6. Applications of IM-MS to lipidomics, metabolomics, and proteomics

6.1 Lipidomics

Lipids are structurally diverse with various isomers performing different biological functions which has necessitated the use of IMS for their structural elucidation and isomeric separation. IM-MS separates various lipid categories, with each

category occupying a distinct m/z -drift time or (m/z -CCS) trendlines, mainly due to their unique backbones. For instance, Sphingolipids (e.g., Cer, SM, and HexCer) have more extended structures and longer drift times than glycerophospholipids (e.g., PC, PA, PE, PG, etc.) [90]. Within each category, IM-MS further separate the lipids into classes according to their headgroups. A longer fatty acids chain in a lipid class induces a more extended structure, and the high number of double bonds generates a bend and compact structure. In fact, there is a 1–5% reduction in drift time with the addition of one double bond in the acyl chain of PC, PS, PE, etc. [90]. Lipid species exist as different isomers, such as positional isomers (e.g., sn- and double-bond positional isomers), stereoisomers (e.g., cis/trans isomers and enantiomers), and acyl chain isomers. These different isomeric systems differ by less than 1% in their CCS values, requiring high-resolution IM instruments for their baseline resolution [90]. Groessl et al. utilized AP-DTIMS with an IM resolving power of ~ 250 to separate sn-positional isomers (PC (16:0/18:1) vs. PC (18:1/16:0)) and double-bond positional isomers (PC(18:1(9Z)/18:1(9Z)) vs. PC(18:1(6Z)/18:1(6Z)) through specific adduct formations (e.g., Ag^+) [9]. The Agilent DTIM-MS 6560 instrument was used to partially distinguish cis/trans isomeric pairs (FA(18:1(9Z)) vs. FA(18:1(9E))) while the Waters TWIM-MS enabled the separation of carotenoid cis/trans isomers, such as cis- β -carotene and all trans- β -carotene [91, 92]. Serpentine ultralong path with extended routing (SUPER) enabled baseline separation of cis/trans isomers of glycerophospholipids (e.g., PC (16:1(9Z)/16:1(9Z)) vs. PC (16:1(9E)/16:1(9E))) and partially separated the stereoisomers of sphingolipids (e.g., GlcSphingosine (d18:1) vs. Gal-Sphingosine(d18:1)) [93]. High-resolution TIMS-MS was used to successfully identify lipid isomers that differ in the double bond locations/geometries as well as in the position of the acyl chain with resolving power up to ~ 410 [94]. A FAIMS study showed that about 75% of triacylglycerol (TG), and PC isomers could be separated at high electric fields, including regio-, sn-, positional, and geometric pairs [95]. In theory, if an IM resolving power of 500 and above is utilized, most lipid isomers would be resolved [90]. Moreover, IM improves lipid identification accuracy through the measurement of its CCS values. Several research groups have experimentally measured lipid CCS to confidently support lipid identification. Groessl et al. [9] and May et al. [96] acquired the CCS values of 112 and 294 lipids with DTIMS, respectively covering glycerophospholipids and sphingolipids. Picache et al. developed a curated CCS database with more than 3800 CCS values using DTIMS with 810 of those CCS values being lipids [97]. CCS values of 244 lipids from 13 lipid classes were acquired with TWIMS by Paglia et al. [98]. Hines et al. developed a lipid CCS database with 148 lipids and 258 CCS values using biological samples with further expansion in their subsequent work [99]. Hernández-Mesa et al. measured 1080 CCS values from 300 steroids using TWIMS [100]. The full details of these experimental CCS measurements can be found in previous reviews [14, 90] and a summary is provided in a review by Kartowikromo et al. [51]. The limited experimental lipid CCS values compared to a large number of possible lipid structures have necessitated the development of Machine Learning models for the prediction of lipid CCS values such as LipidCCS [85].

6.2 Metabolomics and proteomics

Metabolomics is a large-scale study of metabolites, that is, small molecules (<1500 Da) involved in cell function and various regulatory pathways.

Biological processes often produce metabolite isomers during metabolism which common analytical methods often fail to distinguish. Hines et al. successfully determined the nitrogen CCS values of 1425 drug or drug-like metabolites using TWIMS, resolving drug metabolites protomers such as fluoroquinolone protomers in her study [101]. DTIMS was utilized in the isomeric separation of steroid metabolites [102], isomeric bile acid [103], and isobaric/isomeric biomarkers in newborn screening [104]. The Zheng-Jiang Zhu group collected more than 5000 empirical metabolites CCS values from literature to predict the CCS for more than 1.6 million small molecules thereby improving unknown metabolites annotation in untargeted metabolomics [105]. Multiplexing strategy in DTIMS has significantly improved sensitivity in metabolomics with applications such as the analysis of contaminants of emerging concerns (CECs) in human urine samples. This study introduces the first comprehensive database of $^{DT}CCS_{N_2}$ values of 148 CECs, and their metabolites collected utilizing the Agilent 6560 platform [106]. PNNL Preprocessor, developed by the Smith group is used for the simplification of the multiplexed data through data interpolation, demultiplexing, multidimensional smoothing, and saturation repair functions [107]. Twenty seven diverse metabolites covering a mass range of m/z 90–788 demonstrate the suitability of DTIMS in the multiplexed mode for non-targeted metabolomics in difficult matrices [108]. TIMS has also been used successfully to analyze isomeric opioid metabolites in human urine and does so with better precision and reproducibility than standard multiple reaction monitoring (MRM) techniques [109]. TIMS has been used to study human colorectal cancer utilizing metabolomics and multi-omics approaches [110]. Traditional untargeted metabolomics studies have detailed the utility of FAIMS in the separation and distinction of metabolites [10]. Metabolites isomer separation by cIMS includes separation of diastereomeric pairs of enantiomeric dimers [111], characterization of protomers of fluoroquinolone antibiotic residues [112], and separation of positional isomers of Diclofenac Acyl Glucuronide [113]. Three glycol-BA isomers (glycodeoxycholic acid (GDCA), glycochenodeoxycholic acid (GCDCA), and glycoursoxycholic acid (GUDCA)) were separated by SLIM SUPER IM-MS as both their cyclodextrin complexes and as their potassiated adducts as shown in **Figure 4** [114]. The CCS values collected on IM-MS platforms including 400 metabolites (DTIMS) by Zhou et al., more than 500 metabolites and xenobiotics (DTIMS) by Zheng et al., 417 metabolites (DTIMS) by Nichols et al., 125 metabolites (TWIMS) by Paglia et al., and 510 metabolites (TWIMS) by Nye et al., have been detailed in a recent review [14].

Protein conformers have been studied using TIMS which was used for conformational analysis of several model peptides [115]. DTIMS was utilized to measure the gas-phase conformational populations of three proteins: ubiquitin, cytochrome c, and myoglobin reporting over 260 helium and nitrogen cross section values for the three proteins [116]. cIMS has been utilized to study the gas-phase stability of protein ions and found that the native protein conformation is stable on the order of hundreds of milliseconds [117]. The applications of DTIMS, TWIMS, FAIMS, cIMS, and TIMS for various proteomic applications have been extensively detailed in a recent review [10].

7. Conclusion

IM-MS combines structural differentiation and mass analysis, improving peak capacity, resolution, sensitivity, selectivity, and isomer separation. When coupled with chromatographic separation techniques, for instance, LC-IM-MS/MS, compound

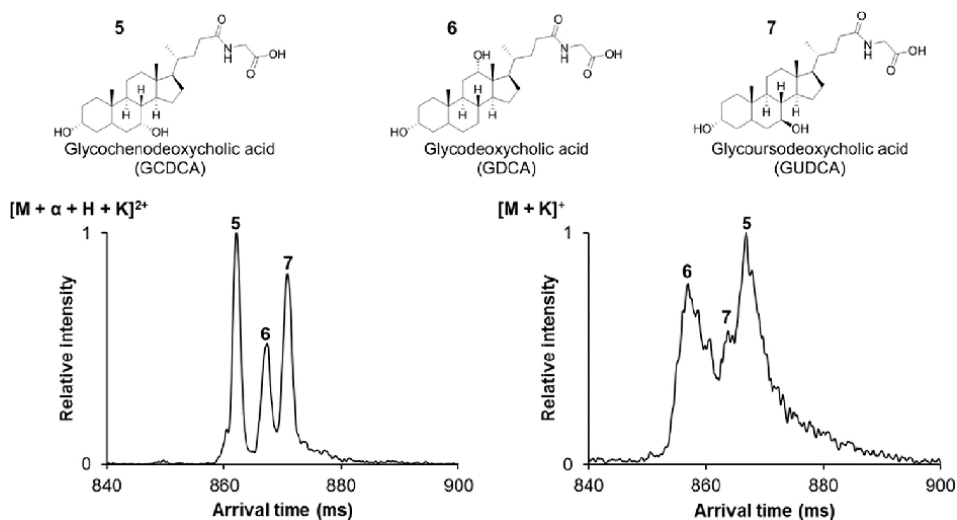


Figure 4. SLIM SUPER IM separation of three glycol-BA isomers. 72 m SLIM SUPER IM separation as $[M + \alpha + H + K]^{2+}$ ions (left) and 85.5 m SLIM SUPER IM separation as $[M + K]^+$ ions (right), where M is the BA and α is the cyclodextrin. (Adapted with permission from Ref. [114], Copyright (2018) American Chemical Society).

identification in targeted and untargeted omics analysis is improved using the four-dimensional data (i.e., RT, CCS, m/z , MS/MS). The IM separation mechanisms, resolution, duty cycle, and applications are thoroughly discussed for the comprehension of researchers in the selection of IM instruments suitable for their experiments in this chapter.

Low resolution in IM-MS instruments is the major restriction for isomer separation. For instance, the CCS difference between stereoisomers and enantiomers is less than 1% and 0.1% respectively. IM-MS instruments like DTIMS and TWIMS have resolutions of 40–60 and can only distinguish isomers with CCS differences in the range of 1.5–3%. The development of high-resolution IM-MS instruments including SLIM and cIMS with resolving power above 400 has made it possible to separate isomers with CCS difference less than 1% and can improve the development of portable ion mobility devices, especially for on-site analysis. Experimental CCS values are needed by machine learning models to accurately predict CCS; hence the use of high-resolution IM instruments would improve the accuracy of CCS prediction since challenging isomers would be separated and their CCS would be measured accordingly. This would greatly promote the application of IM-MS in the identification of unknown compounds. Improvements in IMS resolution, standardization of instrument calibration (preferred calibrant ions, etc.), enhancement of CCS database, development of CCS processing software, and coupling with other separation and MS analysis strategies are all important factors that continuously need improvement for the advancement of IM-MS and applications in all-omics studies.

Acknowledgements


Financial support for this work was provided by funds provided by Auburn University and the NIH grant 1R35GM147225.

Author details

Orobola E. Olajide, Kimberly Y. Kartowikromo and Ahmed M. Hamid*
Department of Chemistry and Biochemistry, Auburn University, Auburn, AL,
United States

*Address all correspondence to: amh0218@auburn.edu

IntechOpen

© 2023 The Author(s). Licensee IntechOpen. This chapter is distributed under the terms of the Creative Commons Attribution License (<http://creativecommons.org/licenses/by/3.0>), which permits unrestricted use, distribution, and reproduction in any medium, provided the original work is properly cited. 

References

- [1] Wu Q, Wang J-Y, Han D-Q, Yao Z-P. Recent advances in differentiation of isomers by ion mobility mass spectrometry. *TrAC Trends in Analytical Chemistry*. 2020;**124**:115801
- [2] Hollerbach AL, Norheim RV, Kwantwi-Barima P, Smith RD, Ibrahim YM. A miniature multilevel structures for lossless ion manipulations ion mobility spectrometer with wide mobility range separation capabilities. *Analytical Chemistry*. 2021;**94**(4):2180-2188
- [3] Liu L, Wang Z, Zhang Q, Mei Y, Li L, Liu H, et al. Ion mobility mass spectrometry for the separation and characterization of small molecules. *Analytical Chemistry*. 2023;**95**(1):134-151
- [4] Olajide OE, Yi Y, Zheng J, Hamid AM. Strain-level discrimination of bacteria by liquid chromatography and paper spray ion mobility mass spectrometry. *Journal of the American Society for Mass Spectrometry*. 2023;**34**(6):1125-1135
- [5] Dodds JN, Baker ES. Ion mobility spectrometry: Fundamental concepts, instrumentation, applications, and the road ahead. *Journal of the American Society for Mass Spectrometry*. 2019;**30**(11):2185-2195
- [6] Rister AL, Dodds ED. Liquid chromatography-ion mobility spectrometry-mass spectrometry analysis of multiple classes of steroid hormone isomers in a mixture. *Journal of Chromatography B*. 2020;**1137**:121941
- [7] Li T, Yin Y, Zhou Z, Qiu J, Liu W, Zhang X, et al. Ion mobility-based sterolomics reveals spatially and temporally distinctive sterol lipids in the mouse brain. *Nature Communications*. 2021;**12**(1):4343
- [8] Kliman M, May JC, McLean JA. Lipid analysis and lipidomics by structurally selective ion mobility-mass spectrometry. *Biochimica et Biophysica Acta (BBA)-Molecular and Cell Biology of Lipids*. 2011;**1811**(11):935-945
- [9] Groessl M, Graf S, Knochenmuss R. High resolution ion mobility-mass spectrometry for separation and identification of isomeric lipids. *The Analyst*. 2015;**140**(20):6904-6911
- [10] Delafield DG, Lu G, Kaminsky CJ, Li L. High-end ion mobility mass spectrometry: A current review of analytical capacity in omics applications and structural investigations. *TrAC Trends in Analytical Chemistry*. 2022;**157**:116761
- [11] Allen SJ, Bush MF. Radio-frequency (rf) confinement in ion mobility spectrometry: Apparent mobilities and effective temperatures. *Journal of The American Society for Mass Spectrometry*. 2016;**27**(12):2054-2063
- [12] Stow SM, Causon TJ, Zheng X, Kurulugama RT, Mairinger T, May JC, et al. An interlaboratory evaluation of drift tube ion mobility-mass spectrometry collision cross section measurements. *Analytical Chemistry*. 2017;**89**(17):9048-9055
- [13] Ahmed A, Cho YJ, No M-h, Koh J, Tomczyk N, Giles K, et al. Application of the Mason–Schamp equation and ion mobility mass spectrometry to identify structurally related compounds in crude oil. *Analytical Chemistry*. 2011;**83**(1):77-83

- [14] Delvaux A, Rathahao-Paris E, Alves S. Different ion mobility-mass spectrometry coupling techniques to promote metabolomics. *Mass Spectrometry Reviews*. 2022;**41**(5):695-721
- [15] Steiner WE, Clowers BH, Haigh PE, Hill HH. Secondary ionization of chemical warfare agent simulants: Atmospheric pressure ion mobility time-of-flight mass spectrometry. *Analytical Chemistry*. 2003;**75**(22):6068-6076
- [16] Tang K, Shvartsburg AA, Lee H-N, Prior DC, Buschbach MA, Li F, et al. High-sensitivity ion mobility spectrometry/mass spectrometry using electrodynamic ion funnel interfaces. *Analytical Chemistry*. 2005;**77**(10):3330-3339
- [17] Kwasnik M, Caramore J, Fernandez FM. Digitally-multiplexed nanoelectrospray ionization atmospheric pressure drift tube ion mobility spectrometry. *Analytical Chemistry*. 2009;**81**(4):1587-1594
- [18] Clowers BH, Siems WF, Hill HH, Massick SM. Hadamard transform ion mobility spectrometry. *Analytical Chemistry*. 2006;**78**(1):44-51
- [19] May JC, Knochenmuss R, Fjeldsted JC, McLean JA. Resolution of isomeric mixtures in ion mobility using a combined demultiplexing and peak deconvolution technique. *Analytical Chemistry*. 2020;**92**(14):9482-9492
- [20] Olajide OE, Yi Y, Zheng J, Hamid AM. Species-level discrimination of microorganisms by high-resolution paper spray-Ion mobility-Mass spectrometry. *International Journal of Mass Spectrometry*. 2022;**478**:116871
- [21] Jiang W, Robinson RA. Ion mobility-mass spectrometry. In: Meyers RA, editor. *Encyclopedia of Analytical Chemistry: Applications, Theory and Instrumentation*. New Jersey, United States of America: John Wiley & Sons, Ltd; 2013
- [22] Kemper PR, Dupuis NF, Bowers MT. A new, higher resolution, ion mobility mass spectrometer. *International Journal of Mass Spectrometry*. 2009;**287**(1-3):46-57
- [23] Merenbloom SI, Koeniger SL, Valentine SJ, Plasencia MD, Clemmer DE. IMS– IMS and IMS– IMS– IMS/MS for separating peptide and protein fragment ions. *Analytical Chemistry*. 2006;**78**(8):2802-2809
- [24] Feuerstein ML, Hernández-Mesa M, Valadbeigi Y, Le Bizec B, Hann S, Dervilly G, et al. Critical evaluation of the role of external calibration strategies for IM-MS. *Analytical and Bioanalytical Chemistry*. 2022;**414**(25):7483-7493
- [25] Giles K, Ujma J, Wildgoose J, Pringle S, Richardson K, Langridge D, et al. A cyclic ion mobility-mass spectrometry system. *Analytical Chemistry*. 2019;**91**(13):8564-8573
- [26] Deng L, Webb IK, Garimella SV, Hamid AM, Zheng X, Norheim RV, et al. Serpentine ultralong path with extended routing (SUPER) high resolution traveling wave ion mobility-MS using structures for lossless ion manipulations. *Analytical Chemistry*. 2017;**89**(8):4628-4634
- [27] Gabelica V. Ion mobility-mass spectrometry: An overview. London, United Kingdom: Royal Society of Chemistry; 2021
- [28] Ibrahim YM, Garimella SV, Prost SA, Wojcik R, Norheim RV, Baker ES, et al. Development of an ion mobility spectrometry-orbitrap mass spectrometer platform. *Analytical Chemistry*. 2016;**88**(24):12152-12160

- [29] Pacini T, Fu W, Gudmundsson S, Chiaravalle AE, Brynjolfsson S, Palsson BO, et al. Multidimensional analytical approach based on UHPLC-UV-ion mobility-MS for the screening of natural pigments. *Analytical Chemistry*. 2015;**87**(5):2593-2599
- [30] Baglai A, Gargano AF, Jordens J, Mengerink Y, Honing M, van der Wal S, et al. Comprehensive lipidomic analysis of human plasma using multidimensional liquid-and gas-phase separations: Two-dimensional liquid chromatography-mass spectrometry vs. liquid chromatography-trapped-ion-mobility-mass spectrometry. *Journal of Chromatography A*. 2017;**1530**:90-103
- [31] Paglia G, Stocchero M, Cacciatore S, Lai S, Angel P, Alam MT, et al. Unbiased metabolomic investigation of Alzheimer's disease brain points to dysregulation of mitochondrial aspartate metabolism. *Journal of Proteome Research*. 2016;**15**(2):608-618
- [32] Tian H, Li S, Wen H, Zhang X, Li J. Volatile organic compounds fingerprinting in faeces and urine of Alzheimer's disease model SAMP8 mice by headspace-gas chromatography-ion mobility spectrometry and headspace-solid phase microextraction-gas chromatography-mass spectrometry. *Journal of Chromatography A*. 2020;**1614**:460717
- [33] Lipok C, Hippler J, Schmitz OJ. A four dimensional separation method based on continuous heart-cutting gas chromatography with ion mobility and high resolution mass spectrometry. *Journal of Chromatography A*. 2018;**1536**:50-57
- [34] Zhong X, Chen Z, Snovida S, Liu Y, Rogers JC, Li L. Capillary electrophoresis-electrospray ionization-mass spectrometry for quantitative analysis of glycans labeled with multiplex carbonyl-reactive tandem mass tags. *Analytical Chemistry*. 2015;**87**(13):6527-6534
- [35] Zhang X, Romm M, Zheng X, Zink EM, Kim Y-M, Burnum-Johnson KE, et al. SPE-IMS-MS: An automated platform for sub-sixty second surveillance of endogenous metabolites and xenobiotics in biofluids. *Clinical Mass Spectrometry*. 2016;**2**:1-10
- [36] Chen H, Gamez G, Zenobi R. What can we learn from ambient ionization techniques? *Journal of the American Society for Mass Spectrometry*. 2011;**20**(11):1947-1963
- [37] Feider CL, Krieger A, DeHoog RJ, Eberlin LS. Ambient ionization mass spectrometry: Recent developments and applications. *Analytical Chemistry*. 2019;**91**(7):4266-4290
- [38] Rankin-Turner S, Reynolds JC, Turner MA, Heaney LM. Applications of ambient ionization mass spectrometry in 2021: An annual review. *Analytical Science Advances*. 2022;**3**(3-4):67-89
- [39] Olajide OE, Donkor B, Hamid AM. Systematic optimization of ambient ionization ion mobility mass spectrometry for rapid separation of isomers. *Journal of the American Society for Mass Spectrometry*. 2021;**33**(1):160-171
- [40] Myung S, Wiseman JM, Valentine SJ, Takats Z, Cooks RG, Clemmer DE. Coupling desorption electrospray ionization with ion mobility/mass spectrometry for analysis of protein structure: Evidence for desorption of folded and denatured states. *The Journal of Physical Chemistry B*. 2006;**110**(10):5045-5051
- [41] Bennett RV, Gamage CM, Galhena AS, Fernández FM.

Contrast-enhanced differential mobility-desorption electrospray ionization-mass spectrometry imaging of biological tissues. *Analytical Chemistry*. 2014;**86**(8):3756-3763

[42] Roscioli KM, Tufariello JA, Zhang X, Li SX, Goetz GH, Cheng G, et al. Desorption electrospray ionization (DESI) with atmospheric pressure ion mobility spectrometry for drug detection. *The Analyst*. 2014;**139**(7):1740-1750

[43] Räsänen RM, Dwivedi P, Fernández FM, Kauppila TJ. Desorption atmospheric pressure photoionization and direct analysis in real time coupled with travelling wave ion mobility mass spectrometry. *Rapid Communications in Mass Spectrometry*. 2014;**28**(21):2325-2336

[44] Sarsby J, Griffiths RL, Race AM, Bunch J, Randall EC, Creese AJ, et al. Liquid extraction surface analysis mass spectrometry coupled with field asymmetric waveform ion mobility spectrometry for analysis of intact proteins from biological substrates. *Analytical Chemistry*. 2015;**87**(13):6794-6800

[45] Huang Y-C, Chung H-H, Dutkiewicz EP, Chen C-L, Hsieh H-Y, Chen B-R, et al. Predicting breast cancer by paper spray ion mobility spectrometry mass spectrometry and machine learning. *Analytical Chemistry*. 2019;**92**(2):1653-1657

[46] Zhang X, Ibrahim YM, Chen T-C, Kyle JE, Norheim RV, Monroe ME, et al. Enhancing biological analyses with three dimensional field asymmetric ion mobility, low field drift tube ion mobility and mass spectrometry (μ FAIMS/IMS-MS) separations. *The Analyst*. 2015;**140**(20):6955-6963

[47] Koeniger SL, Merenbloom SI, Valentine SJ, Jarrold MF, Udseth HR,

Smith RD, et al. An IMS–IMS Analogue of MS–MS. *Analytical Chemistry*. 2006;**78**(12):4161-4174

[48] Liu FC, Ridgeway ME, Park MA, Bleiholder C. Tandem trapped ion mobility spectrometry. *The Analyst*. 2018;**143**(10):2249-2258

[49] Merenbloom SI, Bohrer BC, Koeniger SL, Clemmer DE. Assessing the peak capacity of IMS–IMS separations of tryptic peptide ions in He at 300 K. *Analytical Chemistry*. 2007;**79**(2):515-522

[50] Eldrid C, Thalassinou K. Developments in tandem ion mobility mass spectrometry. *Biochemical Society Transactions*. 2020;**48**(6):2457-2466

[51] Kartowikromo KY, Olajide OE, Hamid AM. Collision cross section (CCS) measurement and prediction methods in omics. *Journal of Mass Spectrometry*. 2023. DOI: 10.1002/jms.4973

[52] Garimella SV, Ibrahim YM, Webb IK, Tolmachev AV, Zhang X, Prost SA, et al. Simulation of electric potentials and ion motion in planar electrode structures for lossless ion manipulations (SLIM). *Journal of The American Society for Mass Spectrometry*. 2014;**25**(11):1890-1896

[53] Kenderdine T, Nemati R, Baker A, Palmer M, Ujma J, FitzGibbon M, et al. High-resolution ion mobility spectrometry-mass spectrometry of isomeric/isobaric ribonucleotide variants. *Journal of Mass Spectrometry: JMS*. 2020;**55**(2):e4465

[54] Sisley EK, Ujma J, Palmer M, Giles K, Fernandez-Lima FA, Cooper HJ. LESA cyclic ion mobility mass spectrometry of intact proteins from thin tissue sections. *Analytical Chemistry*. 2020;**92**(9):6321-6326

- [55] Harrison JA, Pruska A, Bittner P, Muck A, Cooper-Shepherd DA, Zenobi R. Advancing cyclic ion mobility mass spectrometry methods for studying biomolecules: Toward the conformational dynamics of mega Dalton protein aggregates. *Analytical Chemistry*. 2022;**94**(36):12435-12443
- [56] Williamson DL, Nagy G. Isomer and conformer-specific mass distribution-based isotopic shifts in high-resolution cyclic ion mobility separations. *Analytical Chemistry*. 2022;**94**(37):12890-12898
- [57] Ibrahim YM, Hamid AM, Deng L, Garimella SV, Webb IK, Baker ES, et al. New frontiers for mass spectrometry based upon structures for lossless ion manipulations. *The Analyst*. 2017;**142**(7):1010-1021
- [58] Tolmachev AV, Webb IK, Ibrahim YM, Garimella SV, Zhang X, Anderson GA, et al. Characterization of ion dynamics in structures for lossless ion manipulations. *Analytical Chemistry*. 2014;**86**(18):9162-9168
- [59] Hamid AM, Prabhakaran A, Garimella SV, Ibrahim YM, Smith RD. Characterization of applied fields for ion mobility separations in traveling wave based structures for lossless ion manipulations (SLIM). *International Journal of Mass Spectrometry*. 2018;**430**:8-13
- [60] Hamid AM, Ibrahim YM, Garimella SV, Webb IK, Deng L, Chen T-C, et al. Characterization of traveling wave ion mobility separations in structures for lossless ion manipulations. *Analytical Chemistry*. 2015;**87**(22):11301-11308
- [61] Hamid AM, Garimella SVB, Ibrahim YM, Deng L, Zheng X, Webb IK, et al. Achieving high resolution ion mobility separations using traveling waves in compact multiturn structures for lossless ion manipulations. *Analytical Chemistry*. 2016;**88**(18):8949-8956
- [62] Ibrahim YM, Hamid AM, Cox JT, Garimella SV, Smith RD. Ion elevators and escalators in multilevel structures for lossless ion manipulations. *Analytical Chemistry*. 2017;**89**(3):1972-1977
- [63] Hollerbach AL, Li A, Prabhakaran A, Nagy G, Harrilal CP, Conant CR, et al. Ultra-high-resolution ion mobility separations over extended path lengths and mobility ranges achieved using a multilevel structures for lossless ion manipulations module. *Analytical Chemistry*. 2020;**92**(11):7972-7979
- [64] Huntley AP, Hollerbach AL, Prabhakaran A, Garimella SV, Giberson CM, Norheim RV, et al. Development of a structure for lossless ion manipulations (SLIM) high charge capacity array of traps. *Analytical Chemistry*. 2023;**95**(9):4446-4453
- [65] Kinlein ZR, Anderson GA, Clowers BH. Accelerating prototyping experiments for traveling wave structures for lossless ion manipulations. *Talanta*. 2022;**244**:123446
- [66] Eaton RM, Zercher BP, Wageman A, Bush MF. A flexible, modular platform for multidimensional ion mobility of native-like ions. *Journal of the American Society for Mass Spectrometry*. 2023;**34**(6):1175-1185
- [67] Hollerbach AL, Conant CR, Nagy G, Monroe ME, Gupta K, Donor M, et al. Dynamic time-warping correction for shifts in ultrahigh resolving power ion mobility spectrometry and structures for lossless ion manipulations. *Journal of the American Society for Mass Spectrometry*. 2021;**32**(4):996-1007
- [68] Laphorn C, Pullen F, Chowdhry B. Ion mobility spectrometry mass

spectrometry of small molecules: Separating and assigning structures to ions. *Mass Spectrometry Reviews*. 2013;**32**(1):43-71

[69] Zhou Z, Tu J, Zhu Z-J. Advancing the large-scale CCS database for metabolomics and lipidomics at the machine-learning era. *Current Opinion in Chemical Biology*. 2018;**42**:34-41

[70] Larriba C, Hogan CJ Jr. Ion mobilities in diatomic gases: Measurement versus prediction with non-specular scattering models. *The Journal of Physical Chemistry A*. 2013;**117**(19):3887-3901

[71] Larriba C, Hogan CJ Jr. Free molecular collision cross section calculation methods for nanoparticles and complex ions with energy accommodation. *Journal of Computational Physics*. 2013;**251**:344-363

[72] Larriba-Andaluz C, Fernandez-Garcia J, Ewing MA, Hogan CJ, Clemmer DE. Gas molecule scattering & ion mobility measurements for organic macro-ions in He versus N₂ environments. *Physical Chemistry Chemical Physics*. 2015;**17**(22):15019-15029

[73] Mesleh MF, Hunter J, Shvartsburg A, Schatz GC, Jarrold M. Structural information from ion mobility measurements: Effects of the long-range potential. *The Journal of Physical Chemistry*. 1996;**100**(40):16082-16086

[74] Shvartsburg AA, Jarrold MF. An exact hard-spheres scattering model for the mobilities of polyatomic ions. *Chemical Physics Letters*. 1996;**261**(1-2):86-91

[75] Wytenbach T, von Helden G, Batka JJ Jr, Carlat D, Bowers MT. Effect of the long-range potential on ion mobility measurements. *Journal of the American Society for Mass Spectrometry*. 1997;**8**(3):275-282

[76] Turzo SB, Seffernick J, Lyskov S, Lindert S. Predicting ion mobility collision cross sections using projection approximation with ROSIE-PARCS webserver. *Briefings in Bioinformatics*. Oxford, United Kingdom: Oxford University Press; 2023. DOI: 10.1093/bib/bbad308

[77] Paizs B. A divide-and-conquer approach to compute collision cross sections in the projection approximation method. *International Journal of Mass Spectrometry*. 2015;**378**:360-363

[78] Ewing SA, Donor MT, Wilson JW, Prell JS. Collidoscope: An improved tool for computing collisional cross-sections with the trajectory method. *Journal of The American Society for Mass Spectrometry*. 2017;**28**(4):587-596

[79] von Helden G, Hsu MT, Gotts N, Bowers MT. Carbon cluster cations with up to 84 atoms: Structures, formation mechanism, and reactivity. *The Journal of Physical Chemistry*. 1993;**97**(31):8182-8192

[80] Bleiholder C, Wytenbach T, Bowers MT. A novel projection approximation algorithm for the fast and accurate computation of molecular collision cross sections (I) method. *International Journal of Mass Spectrometry*. 2011;**308**(1):1-10

[81] Paglia G, Kliman M, Claude E, Geromanos S, Astarita G. Applications of ion-mobility mass spectrometry for lipid analysis. *Analytical and Bioanalytical Chemistry*. 2015;**407**:4995-5007

[82] Li X, Wang H, Jiang M, Ding M, Xu X, Xu B, et al. Collision cross section prediction based on machine learning. *Molecules*. 2023;**28**(10):4050

[83] Ross DH, Cho JH, Xu L. Breaking down structural diversity for comprehensive prediction of ion-neutral

collision cross sections. *Analytical Chemistry*. 2020;**92**(6):4548-4557

[84] Zhou Z, Xiong X, Zhu Z-J. MetCCS predictor: A web server for predicting collision cross-section values of metabolites in ion mobility-mass spectrometry based metabolomics. *Bioinformatics*. 2017;**33**(14):2235-2237

[85] Zhou Z, Tu J, Xiong X, Shen X, Zhu Z-J. LipidCCS: Prediction of collision cross-section values for lipids with high precision to support ion mobility-mass spectrometry-based lipidomics. *Analytical Chemistry*. 2017;**89**(17):9559-9566

[86] Bijlsma L, Bade R, Celma A, Mullin L, Cleland G, Stead S, et al. Prediction of collision cross-section values for small molecules: Application to pesticide residue analysis. *Analytical Chemistry*. 2017;**89**(12):6583-6589

[87] Plante P-L, Francovic-Fontaine É, May JC, McLean JA, Baker ES, Laviolette F, et al. Predicting ion mobility collision cross-sections using a deep neural network: DeepCCS. *Analytical Chemistry*. 2019;**91**(8):5191-5199

[88] Colby SM, Nuñez JR, Hodas NO, Corley CD, Renslow RR. Deep learning to generate in silico chemical property libraries and candidate molecules for small molecule identification in complex samples. *Analytical Chemistry*. 2019;**92**(2):1720-1729

[89] Zeng W-F, Zhou X-X, Willems S, Ammar C, Wahle M, Bludau I, et al. AlphaPeptDeep: A modular deep learning framework to predict peptide properties for proteomics. *Nature Communications*. 2022;**13**(1):7238

[90] Tu J, Zhou Z, Li T, Zhu Z-J. The emerging role of ion mobility-mass spectrometry in lipidomics to facilitate lipid separation and identification.

TrAC Trends in Analytical Chemistry. 2019;**116**:332-339

[91] Kyle JE, Zhang X, Weitz KK, Monroe ME, Ibrahim YM, Moore RJ, et al. Uncovering biologically significant lipid isomers with liquid chromatography, ion mobility spectrometry and mass spectrometry. *The Analyst*. 2016;**141**(5):1649-1659

[92] Dong L, Shion H, Davis RG, Terry-Penak B, Castro-Perez J, van Breemen RB. Collision cross-section determination and tandem mass spectrometric analysis of isomeric carotenoids using electrospray ion mobility time-of-flight mass spectrometry. *Analytical Chemistry*. 2010;**82**:9014-9021, 9021

[93] Wojcik R, Webb IK, Deng L, Garimella SV, Prost SA, Ibrahim YM, et al. Lipid and glycolipid isomer analyses using ultra-high resolution ion mobility spectrometry separations. *International Journal of Molecular Sciences*. 2017;**18**(1):183

[94] Jeanne Dit Fouque K, Ramirez CE, Lewis RL, Koelmel JP, Garrett TJ, Yost RA, et al. Effective liquid chromatography-trapped ion mobility spectrometry-mass spectrometry separation of isomeric lipid species. *Analytical Chemistry*. 2019;**91**(8):5021-5027

[95] Bowman AP, Abzalimov RR, Shvartsburg AA. Broad separation of isomeric lipids by high-resolution differential ion mobility spectrometry with tandem mass spectrometry. *Journal of the American Society for Mass Spectrometry*. 2017;**28**(8):1552-1561

[96] May JC, Goodwin CR, Lareau NM, Leaptrot KL, Morris CB, Kurulugama RT, et al. Conformational ordering of biomolecules in the gas phase: Nitrogen

collision cross sections measured on a prototype high resolution drift tube ion mobility-mass spectrometer. *Analytical Chemistry*. 2014;**86**(4):2107-2116

[97] Picache JA, Rose BS, Balinski A, Leaptrot KL, Sherrod SD, May JC, et al. Collision cross section compendium to annotate and predict multi-omic compound identities. *Chemical Science*. 2019;**10**(4):983-993

[98] Paglia G, Williams JP, Menikarachchi L, Thompson JW, Tyldesley-Worster R, Halldórsson S, et al. Ion mobility derived collision cross sections to support metabolomics applications. *Analytical Chemistry*. 2014;**86**(8):3985-3993

[99] Hines KM, Herron J, Xu L. Assessment of altered lipid homeostasis by HILIC-ion mobility-mass spectrometry-based lipidomics. *Journal of Lipid Research*. 2017;**58**(4):809-819

[100] Hernández-Mesa M, Le Bizec B, Monteau F, García-Campaña AM, Dervilly-Pinel G. Collision cross section (CCS) database: An additional measure to characterize steroids. *Analytical Chemistry*. 2018;**90**(7):4616-4625

[101] Hines KM, Ross DH, Davidson KL, Bush MF, Xu L. Large-scale structural characterization of drug and drug-like compounds by high-throughput ion mobility-mass spectrometry. *Analytical Chemistry*. 2017;**89**(17):9023-9030

[102] Davis DE Jr, Leaptrot KL, Koomen DC, May JC, Cavalcanti GA, Padilha MC, et al. Multidimensional separations of intact phase II steroid metabolites utilizing LC-ion mobility-HRMS. *Analytical Chemistry*. 2021;**93**(31):10990-10998

[103] Zheng X, Smith FB, Aly NA, Cai J, Smith RD, Patterson AD, et al. Evaluating the structural complexity of isomeric bile acids with ion mobility spectrometry.

Analytical and Bioanalytical Chemistry. 2019;**411**:4673-4682

[104] Dodds JN, Baker ES. Improving the speed and selectivity of newborn screening using ion mobility spectrometry-mass spectrometry. *Analytical Chemistry*. 2021;**93**(51):17094-17102

[105] Zhou Z, Luo M, Chen X, Yin Y, Xiong X, Wang R, et al. Ion mobility collision cross-section atlas for known and unknown metabolite annotation in untargeted metabolomics. *Nature Communications*. 2020;**11**(1):4334

[106] Belova L, Caballero-Casero N, van Nuijs AL, Covaci A. Ion mobility-high-resolution mass spectrometry (IM-HRMS) for the analysis of contaminants of emerging concern (CECs): Database compilation and application to urine samples. *Analytical Chemistry*. 2021;**93**(16):6428-6436

[107] Bilbao A, Gibbons BC, Stow SM, Kyle JE, Bloodsworth KJ, Payne SH, et al. A preprocessing tool for enhanced ion mobility-mass spectrometry-based omics workflows. *Journal of Proteome Research*. 2021;**21**(3):798-807

[108] Causon TJ, Si-Hung L, Newton K, Kurulugama RT, Fjeldsted J, Hann S. Fundamental study of ion trapping and multiplexing using drift tube-ion mobility time-of-flight mass spectrometry for non-targeted metabolomics. *Analytical and Bioanalytical Chemistry*. 2019;**411**:6265-6274

[109] Adams KJ, Ramirez CE, Smith NF, Muñoz-Muñoz AC, Andrade L, Fernandez-Lima F. Analysis of isomeric opioids in urine using LC-TIMS-TOF MS. *Talanta*. 2018;**183**:177-183

[110] Zhang W, Lin L, Xia L, Cai W, Dai W, Zou C, et al. Multi-omics analyses

of human colorectal cancer revealed three mitochondrial genes potentially associated with poor outcomes of patients. *Journal of Translational Medicine*. 2021;**19**(1):273

[111] Cooper-Shepherd DA, Olivos HJ, Wu Z, Palmer ME. Exploiting self-association to evaluate enantiomeric composition by cyclic ion mobility–mass spectrometry. *Analytical Chemistry*. 2022;**94**(23):8441-8448

[112] McCullagh M, Giles K, Richardson K, Stead S, Palmer M. Investigations into the performance of travelling wave enabled conventional and cyclic ion mobility systems to characterise protomers of fluoroquinolone antibiotic residues. *Rapid Communications in Mass Spectrometry*. 2019;**33**:11-21

[113] Higton D, Palmer ME, Vissers JP, Mullin LG, Plumb RS, Wilson ID. Use of cyclic ion mobility spectrometry (cIM)-mass spectrometry to study the intramolecular transacylation of diclofenac acyl glucuronide. *Analytical Chemistry*. 2021;**93**(20):7413-7421

[114] Chouinard CD, Nagy G, Webb IK, Garimella SVB, Baker ES, Ibrahim YM, et al. Rapid Ion mobility separations of bile acid isomers using cyclodextrin adducts and structures for lossless ion manipulations. *Analytical Chemistry*. 2018;**90**(18):11086-11091

[115] Silveira JA, Ridgeway ME, Park MA. High resolution trapped ion mobility spectrometry of peptides. *Analytical Chemistry*. 2014;**86**(12):5624-5627

[116] May JC, Jurneczko E, Stow SM, Kratochvil I, Kalkhof S, McLean JA. Conformational landscapes of ubiquitin, cytochrome c, and myoglobin: Uniform field ion mobility measurements in helium and nitrogen drift gas.

International Journal of Mass Spectrometry. 2018;**427**:79-90

[117] Eldrid C, Ujma J, Kalfas S, Tomczyk N, Giles K, Morris M, et al. Gas phase stability of protein ions in a cyclic ion mobility spectrometry traveling wave device. *Analytical Chemistry*. 2019;**91**(12):7554-7561

Section 2

Characterization and Analysis of Samples

Characterization and Enumeration of Platelet Microvesicles in Human Platelet Concentrates by Using Transmission Electron Microscopy Including Electron Tomography

Josef Neumüller, Christof Jungbauer and Thomas Wagner

Abstract

Platelet microvesicles (PMV) carry receptors and contain genetic information. They are delivered from platelets by budding or by exocytosis of α -granules and are able to activate leukocytes and endothelial cells, resulting in inflammatory reactions. Therefore, the ultrastructural investigation and counting of PMV in platelet concentrates (PC) produced by apheresis or pooled buffy coats were investigated. High numbers of PMV in PC can occasionally provoke severe transfusion reactions in recipients suffering from thrombocytopenia caused by different diseases or therapeutic interventions. The ultrastructural investigation of PMV in PC, produced by different manufacturing methods, can significantly contribute to their quality evaluation. PMV was investigated and enumerated using transmission electron microscopy (TEM) on filmed grids by the negative contrasting method and a special photomontage option integrated with TEM. Image aspects of four areas of about $8,500 \times 8,500$ nm could be sifted through. Using reference gold particles with a known concentration, added to the sample of the PC preparation, and applied to the grid, the number of PMV/ μ l of the sample could be calculated. Using morphometry, their distribution in terms of area was determined. Visualization of single PMV in ultracentrifuged or alginate-embedded PC samples was enabled by using electron tomography (ET).

Keywords: number of platelet microvesicles, platelet concentrates, apheresis versus pooled PC electron tomography, negative contrast, embedding in alginate

1. Introduction

Platelet microvesicles (PMV) or platelet microparticles are able to address signals to leukocytes and endothelial cells. For this purpose, they are equipped with receptors for docking to these target cells but also contain genetic information in the form of small chain RNA, able to change the function of the respective target cells [1]. PMV can provide changes in coagulation and clot formation in platelet concentrates (PC) [2–4].

High numbers of PMV can induce adverse transfusion reaction by binding to the surface receptor PSGL, present on leucocytes, via the platelet activation molecule CD62P, leading to PLT activation and to a liberation of inflammatory enzymes [5, 6]. A high expression of CD40L by PMV can also be involved in the occurrence of transfusion-related acute lung injury (TRALI) [7]. PMV are also involved in several diseases such as rheumatoid arthritis, systemic lupus erythematosus, cancers, cardiovascular diseases, and infections [4].

Most PMVs exhibit a wide variety of sizes. Depending on the size and subcellular origin, they were characterized by different terms such as platelet microparticles, microvesicles, exosomes, or ectosomes. In general, two kinds of PMV can be distinguished: exosomes, originating from α -granules with a size range of 50–150 nm, and ectosomes, delivered by budding with a size of 100–1000 nm [8]. Routinely, PMV can be enumerated by using flow cytometry [9–11], but there is a detection limit concerning PMV $> 1 \mu\text{m}$ and those $< 0.5 \mu\text{m}$ [12]. Nevertheless, the use of advanced flow cytometers allows measuring smaller particles under a threshold of $0.2 \mu\text{m}$, but a clear discrimination between exosomes and ectosomes is not possible. Stoner et al. [13] recently developed a highly sensitive flow cytometer for the enumeration of PMV, to estimate size, and to demonstrate molecular characteristics of individual extracellular vesicles [14].

Therefore, the aim of our study was to count and discriminate PMV in PC derived from healthy human donors on the ultrastructural level by transmission electron microscopy (TEM) including morphometric methods. The focus of this study was not only the enumeration but also above all, the visualization of PMV at the ultrastructural level. For this purpose, we used the negative staining method on formvar/carbon-coated EM-grids. In addition, we characterized PMV, encapsulated in alginate, by ET. Furthermore, different PC manufacturing methods such as apheresis-derived versus buffy coat-pooled PC were compared.

2. Platelet concentrates

Our investigations are focused on PLT in PC. PC belongs to biogenic drugs, which are administered in order to treat severe bleeding disorders (thrombocytopenia). The presence of thrombocytopenia is, according to the definition, if the PLT number in the blood falls below $150.000/\mu\text{l}$. Health problems for a patient occur if the PLT count is lower than $50.000/\mu\text{l}$, such as in hemorrhagic diathesis, thrombocytopenic purpura, or petechiae. Dramatic bleeding episodes appear about PLT counts under $10.000/\mu\text{l}$. In this situation, a transfusion of a PC is indicated [15, 16].

There are several reasons causing thrombocytopenia:

- Failure in the development of PLT in the bone marrow
- PLT dysfunction is associated with chronic liver failure [17]
- Inherited disorders of PLT production or function such as Glanzmann–Thrombasthenia, Bernard–Soulier Syndrome, Gray Platelet Syndrome, Storage Pool Disease, and Scott Syndrome [18]
- Disseminated Intravascular Coagulation [19]

- Impaired thrombopoiesis due to tumor genesis but also after antibacterial or antitumor chemotherapy or irradiation [20]
- Increased degradation of PLT as a consequence of bacterial and viral infections [21]

For reviews, refer to [22, 23].

Platelet concentrates are produced either by apheresis or by collecting buffy coats from four donors. In this study, only pathogen-inactivated PCs were investigated. This implies that the receptors at the surface of the PMV remain generally intact while the nucleic acids inside of the particles are inactivated. Therefore, the communication of PMV with target cells such as leucocytes and endothelial cells is certainly reduced.

Apheresis requires apheresis machines that work on the principle of zonal centrifugation. In our studies, a Fenwal Baxter Amicus™ (Baxter Healthcare Corporation, Fenwal Division, Round Lake, USA) or a Haemonetics MCS® + 9000 Mobile Platelet Collection System, Haemonetics Austria GmbH were used. In the Fenwal Baxter Amicus system, plasma containing PLT is continuously separated during centrifugation in a collection chamber while the other blood components are reinfused to the donor. The advantage of this technique is a high yield of PLT and a relatively short apheresis duration, which is less stressful for the donor. The disadvantage of this method is the fact that the PLT remains in the collection chamber during the whole centrifugation time, which implies a higher shear stress. With respect to the Haemonetics MCS device, whole blood is continuously processed, but the system changes in definite time intervals between blood collection and reinfusion of the PLT-extracted blood components. PLT is collected in a storage chamber, which is not subjected to centrifugation. Therefore, this processing method is milder since the PLT are less subjected to centrifugation forces, but the apheresis duration with the Haemonetics MCS system is significantly longer compared with the apheresis time using the Fenwal Baxter machine, which is more stressful for the donor. Buffy coat-derived PC is prepared in a two-step centrifugation process. In the first step, whole blood is collected into triple bags containing a citrate buffer solution (CPD) and centrifuged at $4000 \times g$ for 10 min. Red blood cells and plasma are separated from the buffy coat fraction and transferred into satellite containers. Subsequently, buffy coats from four different donors and one bag containing either 300 ml plasma from one of the four donors or PLT additive solution are connected by using a sterile connection device and are pooled in one container. Subsequently, a 1 l polyolefin bag and a leukocyte reduction filter are connected. This pool is then centrifuged at $500 \times g$ for 8 min at 22°C. The supernatant is squeezed out immediately into the storage bag by means of a plasma extractor.

PC are stored in gas-permeable plastic bags for five to seven days. In our experience, all manufacturing processes induced a slight PLT activation, which was partially reversible. With lasting storage time, dead PLT caused by necrosis and apoptosis occurs. In our experiments, the effect of storage time on the number of PMVs was investigated. Not only PLT but also PMV were damaged, leading to single or aggregated membrane fragments. There is no technique available other than transmission electron microscopy using high magnification in combination with negative contrast staining in order to visualize the real condition of a PC preparation.

All these manufacturing methods also lead to a deliberation of PMV, which is increased at higher shear stress, e.g., due to centrifugation forces. As mentioned above, high numbers of PMV may be harmful for the recipient, who is usually in a

bad health condition. Using electron microscopical methods, the goal of our study was to count and visualize PMV in PC, comparing different manufacturing methods.

3. Experimental design

3.1 PLT donors

PC, separated from whole blood, was obtained from healthy volunteer donors. In order to investigate the release of PMV at the Austrian Red Cross Blood Donation Center for Vienna, Lower Austria, and Burgenland according to the Austrian regulations for blood donation and after informed consent, the donors were carefully selected and held under health surveillance. The study comprises 14 apheresis PC and 16 pooled buffy coat PC.

As mentioned above, apheresis samples were obtained using a Fenwal Baxter Amicus cell separator (Baxter Healthcare Corporation, Fenwal Division, Round Lake, USA), as previously described [24] or from a Haemonetics MCS® + 9000 Mobile Platelet Collection System, Haemonetics Austria GmbH. For a detailed description, see the user manual “Working with the Haemonetics MCS® + Operation Manual” [25].

Preparation of buffy coat-derived PC was carried out as previously described [26].

Pathogen inactivation was carried out using the Intercept™ blood system (Cerus Europe BV, Amersfoort, The Netherlands). This inactivation system uses the psoralen-compound Amotosalen-HCl ($C_{17}H_{20}ClNO_4$) that penetrates cell and nucleus membranes and exhibits a high affinity to nucleic acids. Subsequently, Amotosalen-HCl binds covalently to the pyrimidine bases of nucleic acids, which were crosslinked using UV irradiation. The inactivation capacity concerns viruses, bacteria fungi and protozoa [27].

Samples stored in PAS2 additive solution were prepared for TEM analysis on different days over a period of ten days. The PAS2-PLT storage solution represents a modified Thyrode buffer providing the full functionality of PLT in PC [28].

3.2 Sample preparation

10 ml of a PC were centrifuged at $800 \times g$ for 15 min at $20^\circ C$ using a centrifuge with a swing bucket support ring rotor (Haereus Varifuge CL, Haereus Christ, Hanau, Germany). The PLT pellet was fixed in 0.2 M cacodylate buffer, pH 7.2, containing 2.5% glutaraldehyde (Fluka, Vienna, Austria) for 90 min at $20^\circ C$. After fixation, PLT were washed twice by centrifugation at $800 \times g$ for 10 min at $4^\circ C$ and transferred to 2 ml Eppendorf vials (Eppendorf AG, Hamburg, Germany) 5 ml of the supernatant, containing the PMV, was discarded and fixed for 5 min by adding of 20 μl glutaraldehyde (2.5%). This solution was transferred to dialysis tubes (Spectrum™ Spectra/Por 6 MWCO 1000kD, Fisher Scientific, Vienna, Austria) and dialyzed for 1 h against distilled water. In this study, 5 μl of the following negative contrast solution mix was applied to hexagonal formvar/carbon filmed grids (Electron Microscopy Sciences, Hatfield, Pennsylvania, USA) according to Hacker et al. [29] using an appropriate modification

- 100 μl of 15 nm reference gold particles (concentration: $1.5 \times 10^7/\mu l$), (AURION Immuno Gold Reagents & Accessories, Wageningen, The Netherlands)
- 200 μl 1% thulium acetate in 1mM HEPES buffer, Sigma-Aldrich (Vienna, Austria)

- 100 µl methyl cellulose (25 centipoises, 2% in distilled water), Sigma-Aldrich
- 1400 µl ultrapure distilled water
- 200 µl of the fixed and dialyzed PC

The drop of the applied solution was allowed to dry and provided for the ultra-structural investigation.

3.2.1 Preparation of free-floating or ultracentrifuged PMV, encapsulated in alginate beads

10 ml of free-floating PMV, present in the supernatant after centrifugation at $800 \times g$ for 5 min as described above, were centrifuged again by using an Optima XL-80K ultracentrifuge, Beckman Coulter, Inc. 250 S., Kraemer Blvd Brea, CA, USA, at $120.000 \times g$ for 2 h. Pellets were resuspended in 0.5 ml of 2% alginate (Kelco, Rahway, NJ, USA) in a Ca^{2+} and Mg^{2+} -free PBS (pH 7.4). Encapsulation was initiated by dropping the PLT-containing alginate suspension in a 0.2 M aqueous $CaCl_2$ solution. After 5 min of gelation, the alginate beads were transferred to 10 mL of 2.5% glutaraldehyde in 0.1 M cacodylate buffer (pH 7.2) and incubated for 90 min at 4°C. Alternatively, 100 µl of the PLT containing pellet were directly mixed with 900 µl alginate solution and jellified as described above. Encapsulation in alginate was performed to minimize PLT damage during preparation after fixation and to handle them like a piece of tissue. After washing with cacodylate buffer for 30 min, the beads were fixed again with an aqueous solution of 1% OsO_4 (Fluka) for 90 min. Samples were washed again, dehydrated in ethanol, and embedded in Spurr epoxy resin (Fluka). Semithin sections of 300 nm as well as ultrathin sections of 60 nm thickness were performed on an ultramicrotome (Ultracut E, Reichert-Jung, Vienna, Austria) and transferred to Hexagonal Center-Marked Grids, 90 mesh, copper grids with PELCO, Redding, CA, USA, and contrasted for 20 min with 0.2% OTE (Oolong Tea Extract, Nisshin EM Co. Ltd. Tokyo, Japan) in PBS (pH 7.4) and for 5 min with 8% alkaline lead citrate (Merck).

3.3 Electron microscopy

For this study, a Tecnai-20 transmission electron microscope (FEI Company, Eindhoven, The Netherlands) working at a maximum acceleration voltage of 200 KV and equipped with a Lanthanhexaborid (LaB_6) cathode, a eucentric goniometer (Compostage), a panorama software (PhotomontageTM) and an electron tomography acquisition software (Xplore3DTM, all from FEI company). Digital images were acquired by using a bottom-mounted Eagle 4k CCD camera; chip size: $4,096 \times 4,096$ pixels (FEI Company).

Counting of PMV on filmed grids after negative contrast preparations: using the photomontage software, four different areas on the respective grid were selected for enumeration. Digital photos were taken and computerized at $5,000\times$ magnification. At this low magnification, a raster with nine subareas was preselected, each of which was photographed successively by using an internal beam positioning device at a magnification of $14.500\times$. After complete acquisition, all images were joined together appropriately by stitching. The composed images comprised an area of approximately $18,000 \times 18,000$ pixels, corresponding to $8,500 \times 8,500$ nm. Images were analyzed using the extended version of Adobe Photoshop 56 (Adobe Systems Software, Dublin,

Ireland) using the manual point counting facility. In the first step, the 15 nm reference beads were counted, and in the second step, the negatively contrasted PMV (Figure 1). The linearity of gold particle numbers in a twofold dilution series was proofed by a calibration curve (Figure 2). The absolute number of PMV per µl was calculated according to the formula (1):

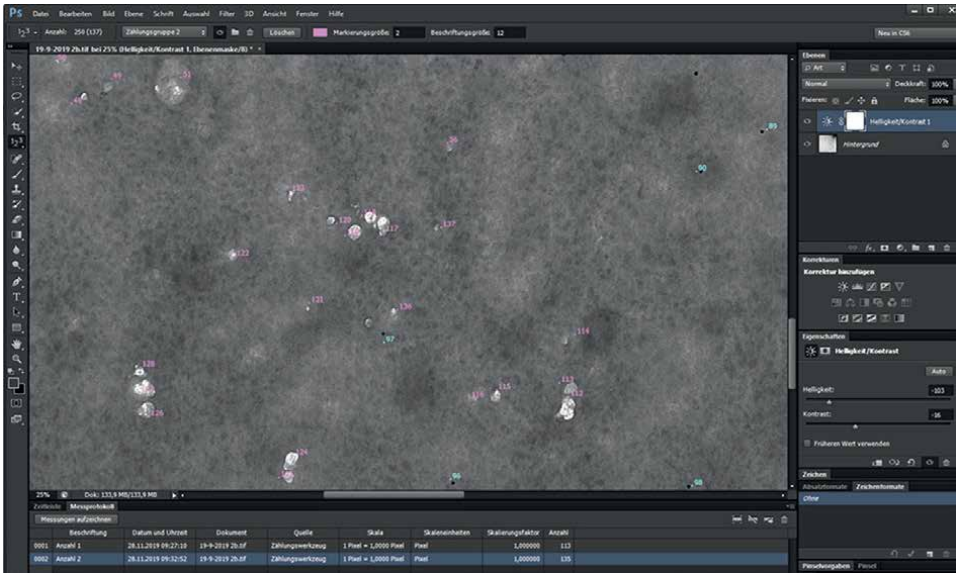


Figure 1. View of a composed image composed of nine single and stitched images generated by using the photomontage software (11780°11805 Pixel corresponding 8489°8507 nm). Counted PMV are marked in magenta, whereas counted gold reference particles are in blue.

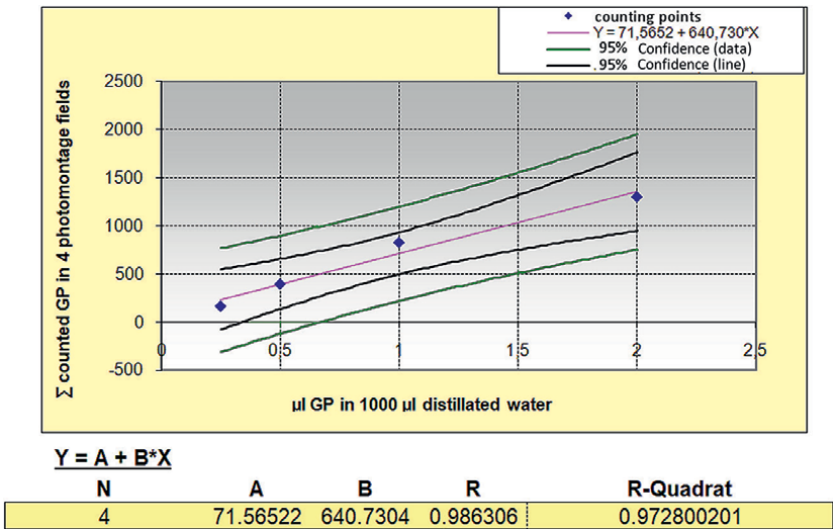


Figure 2. Graphic of the linear regression analysis of 4 measurement points from a twofold dilution series, performed according to the protocol shown in Figure 1 but without the PC sample. The graph shows a good fitting of the measurement points to the regression line (R value = 0.97).

$$\frac{\text{counted PMV} * \text{number of counted RGP}}{1,5 * 10E + 11 * 200 \mu l} \quad (1)$$

Referring to RGP as the reference gold particles, 200 μ l as the volume of the added PC sample, and $1,5 \times 10^{11}$ as the gold particles per μ l of the whole sample.

In addition, morphometric analysis was performed using the free available ImageJ software package in randomly selected apheresis versus pooled BC samples by measuring the area of PMV in the images composed by photomontage as described above, by ringing them manually using a sensitive cursor.

All data were represented and calculated by Excel worksheets. *Statistical comparison* was performed using the parameter-free Wilcoxon test with the help of the WinSTAT for Excel software package (R. Fitch Software, Bad Krotzingen, Germany). The comparison of the measurement data on different storage days was carried out by the Pearson correlation using the same statistic package.

3.4 Electron tomography (ET)

The 300 nm thick semithin was coated with 10 nm colloidal gold particles on both surfaces, functioning as fiducial markers during subsequent image alignment. Single-axis tomography was carried out by acquisition of a tilt series at a tilt range of -65° to $+65^\circ$ with an increment of 1° using a single tilt holder (FEI Company). The acquisition of the tilt series was performed using an Eagle 4k CCD camera (FEI Company). Tilt series data were digitally recorded automatically with the Xplore3D software (FEI Company), which allows compensating dislocations of the region of interest during tilting. The digital images were stored in stack files (.mrc). Tilt series were aligned using the 10 nm gold fiducial markers and reconstructed by means of the weighted back projection (WBP) algorithm with the IMOD software (Boulder Laboratory for 3D Electron Microscopy of Cells, University of Colorado, USA). For 3D modeling, the structures of interest in each slice were traced with colored contours that were subsequently merged in the Z-axis with the help of the Amira 5.3 software (Mercury Computer Systems, Merignac, Cedex, France).

4. Results and discussion

The most abundant extracellular vesicles in human blood are derived from PLT or megakaryocytes, accounting for more than half of all EVs in the peripheral blood. As mentioned above, they are able to exert positive and negative effects on human beings [4]. In respect to PC, one can therefore assume that the majority of extracellular vesicles are PMV. As summarized in [30], using cryo-immune electron microscopy, exosomes with a size of 30–100 nm bear the receptor CD63, while ectosomes, sized between 100 and 1000 nm are characterized by the expression of annexin-V at the outer leaflet of the plasma membrane, factor X and prothrombin. The intracellular origin of PMV was shown ultrastructurally by Ponomareva et al. [31]. These authors demonstrated that a fraction of PMV having an intracellular origin contains organelles, such as mitochondria, glycogen granules, and vacuoles. These two types of PMV were also shown by Hermida-Nogueira et al. [32] in Mirasol® pathogen-inactivated PC using TEM.

In randomly selected pellets of PC, different activation stages of PLT as well as apoptotic PLT, can be demonstrated (Figure 3). PMV can also be observed between

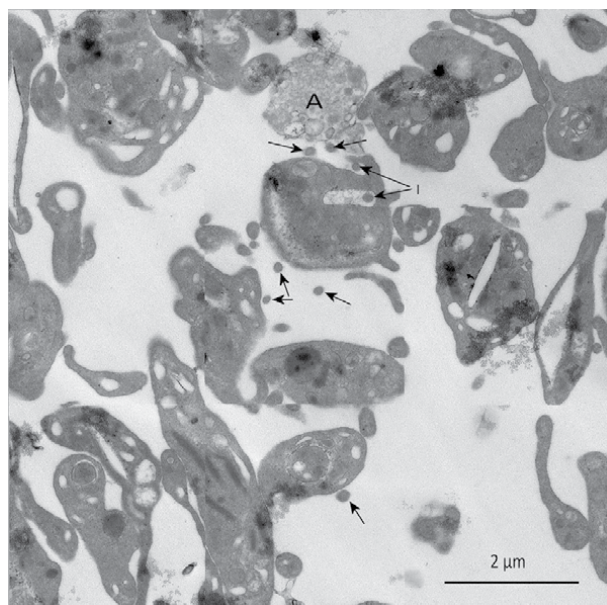


Figure 3. PLT, collected in a centrifuged PC pellet (800*g for 10 min at 20°C). The image shows that most of the PLTs are slightly activated. One PLT is apoptotic (A). Numerous PMVs are visible (arrows), and one of them (I) sticks already inside of the Open Canalicular System.

the PLT, but these are occasionally hard to distinguish from small cross-sectioned filopodia of activated PLT. It is important to note that strongly activated PLTs lose their discoid shape, become amoeboid, and release the contents of their α -granules. Slightly activated PLT remains in a resting stage and can return to its original shape.

Using negative contrast, our study revealed that several types of exosomes could be found in PC. Some of them consist of cohesive aggregates composed of up to 10 single vesicles, as shown in **Figure 4**. In this respect, we were interested in whether there is a differentiation in the distribution of ectosomes and exosomes in apheresis and BC pooled PC with the help of the morphometric measurement of the area of negatively contrasted PMV. Histograms of the two investigation groups demonstrated a prevalence of larger PMV in apheresis samples.

4.1 PMV counting

In contrast to studies using advanced flow cytometers [9–14], TEM remains the gold standard for detection, characterization, and enumeration of extracellular vesicles [33, 34]. The PMV counting in the negative contrast preparations revealed a conspicuous high concentration between $8.75 \cdot 10^7$ and $1.02 \cdot 10^9$ per μL . This high concentration certainly implicates significant stress for the recipient of a PC transfusion. As stated by Xie et al. [7], C40L-bearing apheresis-derived PMV, stored for five days, is able to initiate fMLP-activated PMN respiration burst, which might be relative to TRALI. These investigations were carried out with non-pathogen-inactivated PC. Therefore, we do not know what happens with pathogen-inactivated PC after transfusion. Comparing the PMV counts of apheresis and pool PC, no significant difference could be found using the U-test of Mann–Whitney ($p = 0.36$) as well as with the Wilcoxon test ($p = 0.22$). These data are of particular interest since a long-lasting

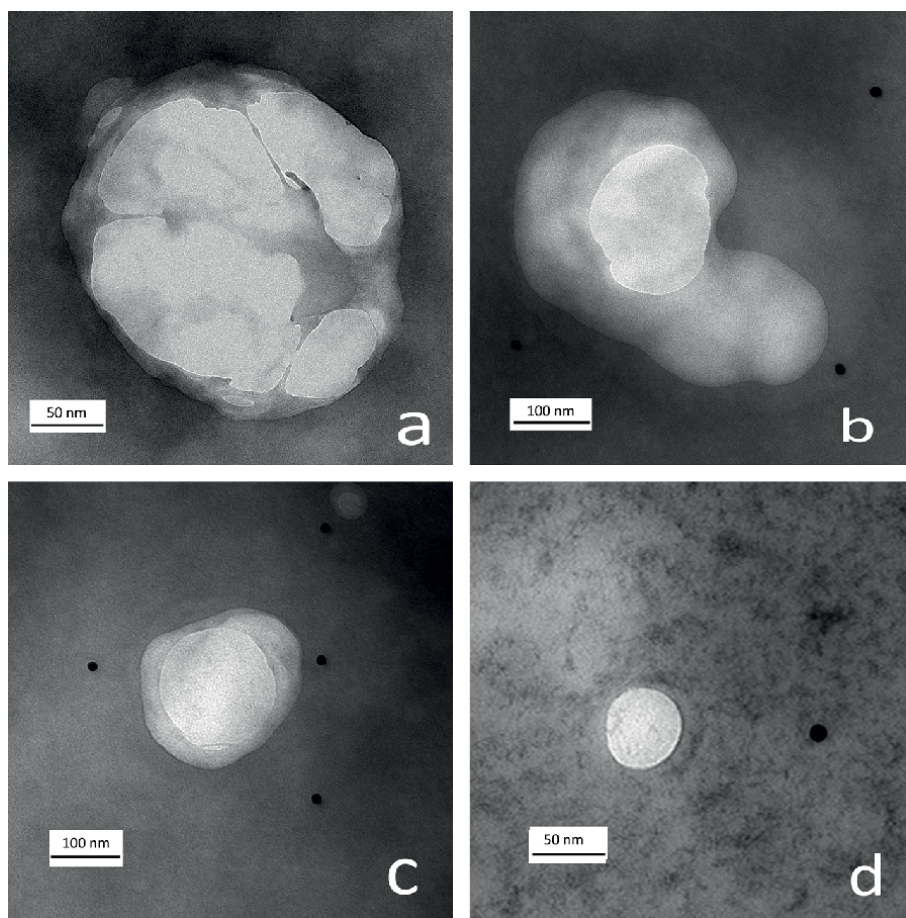


Figure 4.
 The image shows different PMVs, regarded as ectosomes (a–c), and one single PMV being an exosome. Images are taken at high magnification (50,000 \times).

discussion of possible quality differences exists between the two production methods. Apheresis PC is always produced from one donor, while pooled PC is derived from different donors, implicating a heterogenic expression of PLT surface molecules of the human platelet antigens (HPA) and the human leucocyte antigens (HLA). Therefore, only HLA- and HPA-matched apheresis PC can be used for transfusion if histocompatibility is required. Apheresis PCs are thought to be more safe and exhibit fewer adverse reactions than pooled PC [35–37].

In this study, also the effect of PC storage on PMV counts between 10 days has been investigated. In contrast to pathogen-inactivated PC that can only be stored for a maximum of 5 days, pathogen-inactivated PC allow a prolonged storage time of seven days. Storage must be performed at room temperature in order to avoid cold-induced storage lesions [38]. Regarding the influence of both kinds of PC preparations, there was a significant continuous decrease in PMV with longer storage time (Pearson correlation $p = 0.013$; **Figure 5**). This storage effect was more pronounced with respect to the PMV count in apheresis PC (Pearson correlation $p < 0.01$) (**Figure 6**). We assume that higher stress for the PLT would occur under apheresis conditions, a finding supported by the observation of a higher number of ultrastructurally visible breakdown

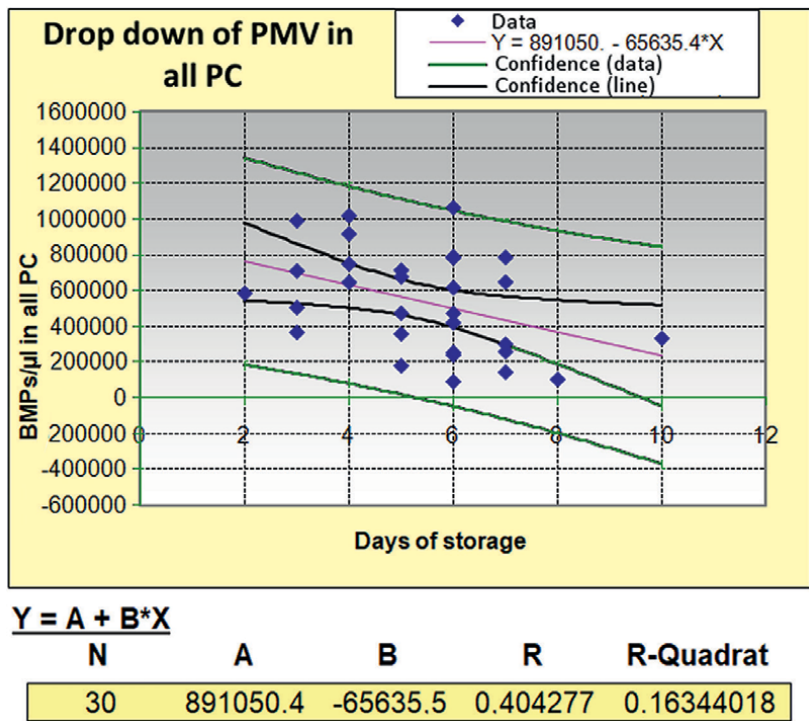


Figure 5.
Graphic of the linear regression analysis showing the drop-down of PMV numbers measured on different days during storage.

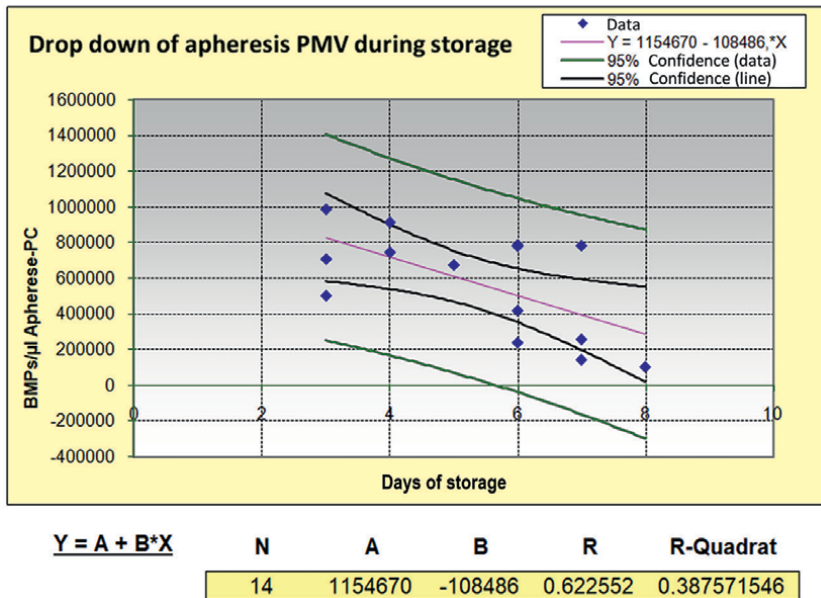


Figure 6.
Graphic of a linear regression analysis showing a more pronounced drop-down of PMV numbers measured on different storage days, respecting only apheresis PC data.

products in the preparations of prolonged stored PC preparations. This is a new result since not all of the investigations cited above found clear evidence for differences between apheresis and pooled buffy coat PC. In this respect, it is also difficult to interpret this effect concerning the recipient of a PC transfusion.

4.2 Transmission electron microscopy of PMV at high magnification and morphometric analysis

At high magnification (50.000 \times), a majority of PMV was composed of no single particles but was composed of up to eight subunits (**Figure 4**). Spot-checked morphometric measurements of the area projections of PMV in the negative contrast images showed distribution differences between apheresis and pooled buffy coat PC. Larger PMV were found in apheresis PC (**Figure 7**). One interpretation for this might be that the composed particles were more disintegrated during the processing of BC pooled PC. In earlier studies, using electron tomography, we could show the liberation of PMV by PLT in the form of sack-like protrusions filled with uniform particles [39]. It is important to note that composed PMV can only be demonstrated by electron microscopy but not flow cytometry, even if highly sensitive apparatuses are applied.

Electron tomography (ET) of alginate-encapsulated PMV pellets after ultracentrifugation as well as encapsulated free PMV, allowed the visualization of PMV in 300 nm semithin sections, which we reported already in earlier publications [40, 41]. ET volumes of both methods were compared (**Figure 8**). In ultracentrifuged pellets, not only PMV but also single granules and numerous breakdown products are less visible in the preparations of the PMV-containing supernatants where they are present

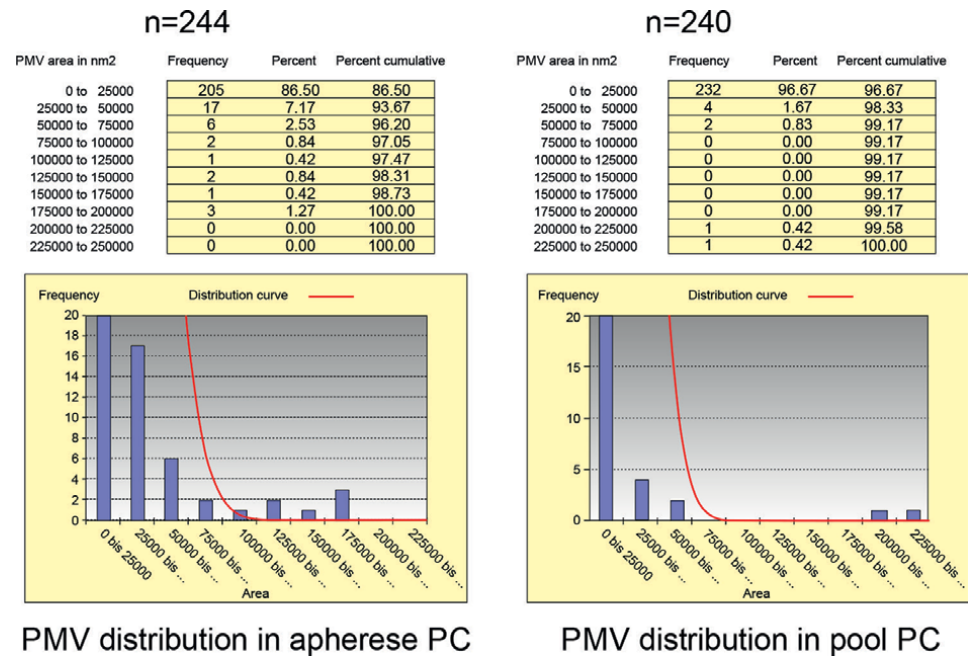


Figure 7. Morphometric analysis of the projected areas in negatively contrasted samples of apheresis (n = 244) and pooled buffy coat PC (n = 240). The measurement data are histograms showing that larger PMV predominate in apheresis PC.

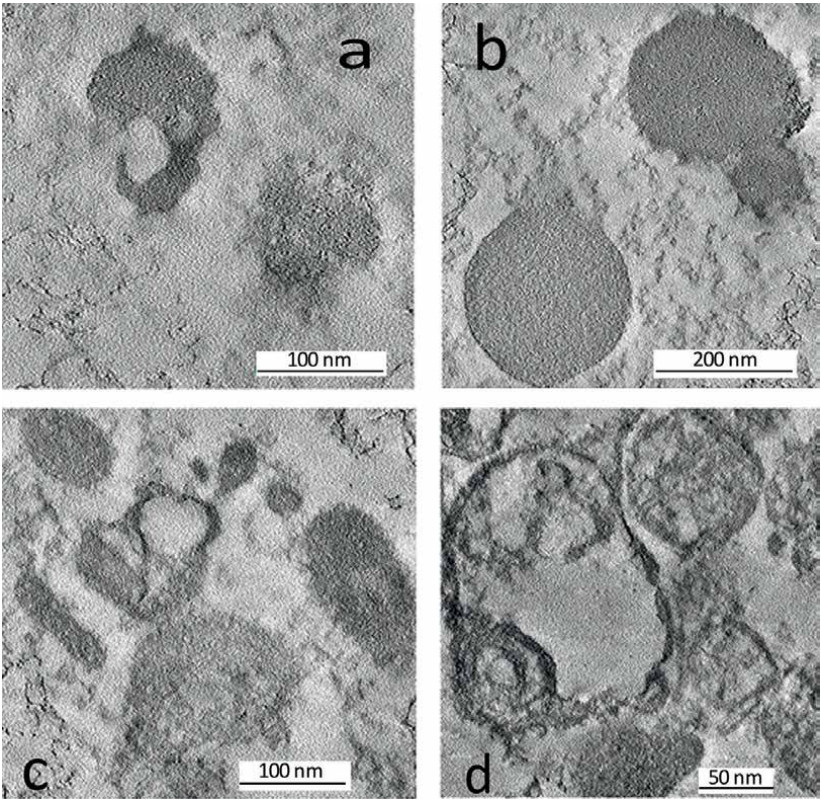


Figure 8.
Preparation of PMV in the supernatant of PC after removal of PLT using centrifugation at 800 g showing exosomes in slices of ET volumes (8a and 8b). The content of the vesicles is uniformly and fine-granulated, corresponding to their origin from PLT α -granules. 8b shows a small particle connected to a larger one. In 8c and d, slices of ET volumes of ultracentrifuged samples with composed ectosomes appear partially empty. In 8a, particles and breakdown products are visible.*

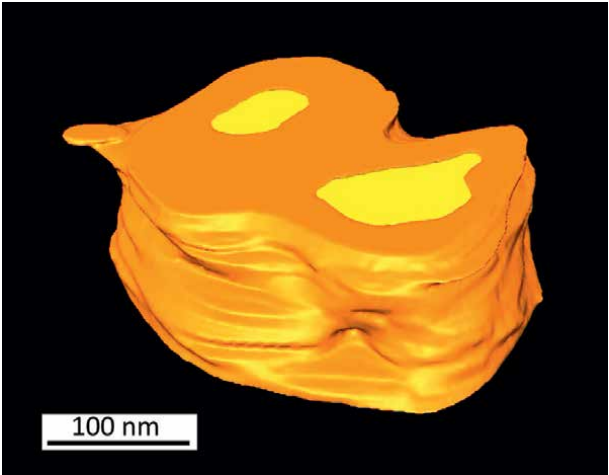


Figure 9.
Displays an ET model from an ectosome that can also watched as a movie. Video related to this figure.

in a diluted form can be found. For illustration, a single ectosome is shown as an ET model in **Figure 9** and in a related movie.

5. Conclusion

Our investigations show that transmission electron microscopy represents a powerful tool for the visualization and enumeration of PMV. Above all, technical electron microscopical devices such as photomontage and ET are very helpful in this respect. The use of negative contrast of PMV preparations on filmed grids is a relatively simple way to have an overlook of the quality of PC processing.

Nevertheless, the analysis of PMV after preparation including enumeration as well as morphometry is very time-consuming, but in contrast to flow cytometric methods, showing dot plots which are to interpret, electron microscopy allows to check “what one sees.”

The visualization of PMV by using ET allows to understand the 3D structure of PMV. In this respect, the encapsulation in alginate beads is an easy nursing preparation method.

As already mentioned in an earlier book chapter [39], TEM and ET are appropriate supplementary methods to evaluate the quality of PLT in PC obtained by different manufacturing processes.

Acknowledgements

The authors gratefully acknowledge the provision of apheresis PCs by Mrs. Renate Renz (Blood Donation Center of the Austrian Red Cross for Vienna, Lower Austria, and Burgenland), the skillful technical assistance of Mr. Ulrich Kaindl and Mr. Thomas Nardelli for their valuable help with the artwork and the 3D modeling (Center for Anatomy and Cell Biology, Department of Cell and Development Biology, Medical University of Vienna).

Conflict of interest

The authors declare no conflict of interest.

Abbreviations

BC	buffy coat
ET	electron tomography
PC	platelet concentrates
PLT	platelets
PMV	platelet microvesicles (platelet microparticles)
TEM	transmission electron microscopy
TRALI	Transfusion-associated Lung Injury
WBP	Weighted Back Projection

Author details

Josef Neumüller^{1,2}, Christof Jungbauer¹ and Thomas Wagner^{3*}


1 Blood Donation Center of the Austrian Red Cross for Vienna, Lower Austria and Burgenland, Vienna, Austria

2 Center for Anatomy and Cell Biology, Medical University of Vienna, Vienna, Austria

3 University Clinic for Blood Group Serology and Transfusion Medicine, Medical University of Graz, Graz, Austria

*Address all correspondence to: thomas.wagner@medunigraz.at

IntechOpen

© 2024 The Author(s). Licensee IntechOpen. This chapter is distributed under the terms of the Creative Commons Attribution License (<http://creativecommons.org/licenses/by/3.0>), which permits unrestricted use, distribution, and reproduction in any medium, provided the original work is properly cited. 

References

- [1] Edelstein LC. The role of platelet microvesicles in intercellular communication. *Platelets*. 2017;**28**:222-227. DOI: 10.1080/09537104.2016.1257114
- [2] Pasquet JM, Toti F, Nurden AT, Dachary-Prigent J. Procoagulant activity and active calpain in platelet-derived microparticles. *Thrombosis Research*. 1996;**82**:509-522. DOI: 10.1016/0049-3848(96)00101-6
- [3] Morel O, Morel N, Freyssinet JM, Toti F. Platelet microparticles and vascular cells interactions: A checkpoint between the haemostatic and thrombotic responses. *Platelets*. 2008;**19**:9-23. DOI: 10.1080/09537100701817232
- [4] Melki I, Tessandier N, Zufferey A, Boilard E. Platelet microvesicles in health and disease. *Platelets*. 2017;**28**:214-221. DOI: 10.1080/09537104.2016.1265924
- [5] Cognasse F, Hamzeh-Cognasse H, Laradi S, Chou ML, Seghatchian J, Burnouf T, et al. The role of microparticles in inflammation and transfusion: A concise review. *Transfusion and Apheresis Science*. 2015;**53**(2):159-167. DOI: 10.1016/j.transci.2015.10.013
- [6] Roka-Moiia Y, Ammann KR, Miller-Gutierrez S, Sheriff J, Bluestein D, Italiano JE, et al. Shear-mediated platelet microparticles demonstrate phenotypic heterogeneity as to morphology, receptor distribution, and hemostatic function. *International Journal of Molecular Science*. 2023;**24**(8):7386. DOI: 10.1101/2023.02.08.527675
- [7] Xie RF, Hu P, Li W, Ren YN, Yang J, Yang YM, et al. The effect of platelet-derived microparticles in stored apheresis platelet concentrates on polymorphonuclear leucocyte respiratory burst. *Vox Sanguinis*. 2014;**106**(3):234-241. DOI: 10.1111/vox.12092
- [8] Boilard E, Duchez AC, Brisson A. The diversity of platelet microparticles. *Current Opinion in Hematology*. 2015;**22**:437-444. DOI: 10.1097/MOH.0000000000000166
- [9] Mobarrez F, Antovic J, Egberg N, Hansson M, Jorreskog G, Hultenby K, et al. A multicolor flow cytometric assay for measurement of platelet-derived microparticles. *Thrombosis Research*. 2010;**125**:e110-e116. DOI: 10.1016/j.thromres.2009.10.006
- [10] Nielsen MH, Beck-Nielsen H, Andersen MN, Handberg A. A flow cytometric method for characterization of circulating cell-derived microparticles in plasma. *Journal of Extracellular Vesicles*. 2014;**3**:1-12. DOI: 10.3402/jev.v3.20795
- [11] Black A, Pienimaeki-Roemer A, Kenyon O, Orso E, Schmitz G. Platelet-derived extracellular vesicles in plateletpheresis concentrates as a quality control approach. *Transfusion*. 2015;**55**:2184-2196. DOI: 10.1111/trf.13128
- [12] Nolan JP, Jones JC. Detection of platelet vesicles by flow cytometry. *Platelets*. 2017;**28**:256-262. DOI: 10.1080/09537104.2017.1280602
- [13] Stoner SA, Duggan E, Condello D, Guerrero A, Turk JR, Narayanan PK, et al. High sensitivity flow cytometry of membrane vesicles. *Cytometry. Part A*. 2016;**89**:196-206. DOI: 10.1002/cyto.a.22787
- [14] Shao H, Im H, Castro CM, Breakefield X, Weissleder R, Lee H. New

- technologies for analysis of extracellular vesicles. *Chemical Reviews*. 2018;**118**(4): 1917-1950. DOI: 10.1021/acs.chemrev.7b00534
- [15] Rebulla P. Trigger for platelet transfusion. *Vox Sanguinis*. 2000;**78**(Suppl. 2):179-182
- [16] Rebulla P. Revisitation of the clinical indications for the transfusion of platelet concentrates. *Reviews in Clinical and Experimental Hematology*. 2001;**5**(3):288-310. DOI: 10.1046/j.1468-0734.2001.00042.x
- [17] Giannini EG, Peck-Radosavljevic M. Platelet dysfunction: Status of thrombopoietin in thrombocytopenia associated with chronic liver failure. *Seminars in Thrombosis and Hemostasis*. 2015;**41**(5):455-461. DOI: 10.1055/s-0035-1550432
- [18] Tsai FD, Battinelli EM. Inherited platelet disorders. *Hematology/Oncology Clinics of North America*. 2021;**35**(6):1069-1084. DOI: 10.1016/j.hoc.2021.07.003
- [19] Levi M, Sivapalaratnam S. Disseminated intravascular coagulation: an update on pathogenesis and diagnosis. *Expert Review of Hematology*. 2018;**11**(8):663-672. DOI: 10.1080/17474086.2018.1500173
- [20] Kvolik S, Jukic M, Matijevic M, Marjanovic K, Glavas-Obrovac L. An overview of coagulation disorders in cancer patients. *Surgical Oncology*. 2010;**19**(1):33-46. DOI: 10.1016/j.suronc.2009.03.008
- [21] Franchini M, Veneri D, Lippi G. Thrombocytopenia and infections. *Expert Review of Hematology*. 2017;**10**(1):99-106. DOI: 10.1080/17474086.2017.1271319
- [22] Hrachovinová I. Diagnostic strategies in disorders of hemostasis. *Vnitřní Lékařství*. 2018;**64**(5):537-544
- [23] Krishnegowda M, Rajashekaraiiah V. Platelet disorders: An overview. *Blood Coagulation & Fibrinolysis*. 2015;**26**(5):479-491. DOI: 10.1097/01.mbc.0000469521.23628.2d
- [24] Laurencet FM, Doucet A, Lydiat V, Jacquier MC, Mermillod B, Andersen S, et al. Quality evaluation of plateletpheresis using the new AMICUS (Baxter) cell separator: Evolution of CD 62 expression. *Journal of Clinical Apheresis*. 1998;**13**(2):47-55. DOI: 10.1002/(sici)1098-1101(1998)13:2<47::aid-jca1>3.0.co;2-8
- [25] Working with Haemonetics MCS®+. Operation manual [Internet]. 2006. Available from: http://www.frankshospitalworkshop.com/equipment/documents/automated_analyzer/user_manuals/Haemonetics%20MCS+%20Analyzer%20-%20User%20manual.pdf
- [26] Neumüller J, Meisslitzer-Ruppitsch C, Ellinger A, Pavelka M, Jungbauer C, Renz R, et al. Monitoring of platelet activation in platelet concentrates using transmission electron microscopy. *Transfusion Medicine and Hemotherapy*. 2013;**40**(2):101-107. DOI: 10.1159/000350034
- [27] Pelletier JP, Transue S, Snyder EL. Pathogen inactivation techniques. *Best Practice & Research. Clinical Haematology*. 2006;**19**(1):205-242. DOI: 10.1016/j.beha.2005.04.001
- [28] Azuma H, Hirayama J, Akino M, Ikeda H. Platelet additive solution – Electrolytes. *Transfusion and Apheresis Science*. 2011;**44**(3):277-281. DOI: 10.1016/j.transci.2011.03.002

- [29] Hacker C, Asadi J, Pliotas C, Ferguson S, Sherry L, Marius P, et al. Nanoparticle suspensions enclosed in methylcellulose: A new approach for quantifying nanoparticles in transmission electron microscopy. *Scientific Reports*. 2016;**4**(6):25275. DOI: 10.1038/srep25275
- [30] Brisson AR, Tan S, Linares R, Gounou C, Arraud N. Extracellular vesicles from activated platelets: a semiquantitative cryo-electron microscopy and immuno-gold labeling study. *Platelets*. 2017;**28**(3):263-271. DOI: 10.1080/09537104.2016.1268255
- [31] Ponomareva AA, Nevzorova TA, Mordakhanova ER, Andrianova IA, Rauova L, Litvinov RI, et al. Intracellular origin and ultrastructure of platelet-derived microparticles. *Journal of Thrombosis and Haemostasis*. 2017;**15**(8):1655-1667. DOI: 10.1111/jth.13745
- [32] Hermida-Nogueira L, García Á. Extracellular vesicles in the transfusion medicine field: The potential of proteomics. *Proteomics*. 2021;**21**(13-14):e2000089. DOI: 10.1002/pmic.202000089
- [33] Théry C, Amigorena S, Raposo G, Clayton A. Isolation and characterization of exosomes from cell culture supernatants and biological fluids. *Current Protocol Cell Biology*. 2006;**30**(1), UNIT 3.22: 1-29. DOI: 10.1002/0471143030.cb0322s30
- [34] Corona ML, Hurbain I, Raposo G, van Niel G. Characterization of extracellular vesicles by transmission electron microscopy and immunolabeling electron microscopy. *Methods in Molecular Biology*. 2023;**2668**:33-43. DOI: 10.1007/978-1-0716-3203-1_4
- [35] Schrezenmeier H, Seifried E. Buffy-coat-derived pooled platelet concentrates and apheresis platelet concentrates: which product type should be preferred? *Vox Sanguinis*. 2010;**99**(1):1-15. DOI: 10.1111/j.1423-0410.2009.01295.x
- [36] van der Meer PF. Platelet concentrates, from whole blood or collected by apheresis? *Transfusion and Apheresis Science*. 2013;**48**(2):129-131. DOI: 10.1016/j.transci.2013.02.004
- [37] Fiedler SA, Boller K, Junker AC, Kamp C, Hilger A, Schwarz W, et al. Evaluation of the in vitro function of platelet concentrates from pooled buffy coats or apheresis. *Transfusion Medicine and Hemotherapy*. 2020;**47**(4):314-324. DOI: 10.1159/000504917
- [38] Ng MSY, Tung JP, Fraser JF. Platelet storage lesions: What more do we know now? *Transfusion Medicine Reviews*. 2018;**17**:S0887-7963. DOI: 10.1016/j.tmr.2018.04.001
- [39] Neumüller J, Elllinger A, Wagner T. Transmission electron microscopy of platelets from apheresis and buffy-coat-derived platelet concentrates. In: Maaz K, editor. *The Transmission Electron Microscope*. London, UK, London, UK: IntechOpen Book; 2015. pp. 255-284. DOI: 10.5772/60673
- [40] Neumüller J. Electron tomography-a tool for ultrastructural 3D visualization in cell biology and histology. *Wiener Medizinische Wochenschrift* (1946). 2018;**168**(11-12):322-329. DOI: 10.1007/s10354-018-0646-y
- [41] Neumüller J, Wagner T. Electron tomography contributing to ultrastructural research in vascular biology and transfusion medicine. *Journal of Cardiology and Cardiovascular Sciences*. 2019;**3**(1):4-10. DOI: 10.29245/2578-3025/2019/1.1165

The Use of Electron Microscopy for Lithiasis Research

*Naima Mammate, Salim Belchkar, Salma Ssouni,
Ghita el Mouhri and Tarik Sqalli Houssaini*

Abstract

The purpose of this work is to highlight the significance of applying scanning electron microscopy coupled with X-ray energy dispersive (SEM–EDX) as a method of analyzing the surface of kidney stones, to assess the antilithiatic activity of extracts from medicinal plants, such as *Saussurea costus* (Falc) Lipsch. This chapter aims to showcase the substantial application and use of electron microscopy in the field of medical research, with particular emphasis on urinary lithiasis. Initially, we will present the pathology of urinary lithiasis and kidney stones. We will then examine the evaluation of kidney stones and the importance of characterizing them using various methods, including electron microscopy. Subsequently, we will provide an overview of scanning electron microscopy coupled to X-ray energy dispersive (SEM–EDX) and its implementation in antilithiatic activity using the stone dissolution test built upon our previous study.

Keywords: antilithiatic activity, kidney stones, dissolution test, scanning electron microscopy, SEM–EDX

1. Introduction

The electron microscope, a revolutionary type of microscope [1], was developed by German physicists Ernst Ruska and Max Knoll at the University of Berlin in 1931 [2]. In 1986, Ernst Ruska was awarded the Nobel Prize in Physics for his invention and development of the transmission electron microscope [3]. Electron microscope use electron beams [4] to produce images with significantly higher precision and resolution than those obtained with ordinary optical microscopes [4]. Electron microscope are limited by the wavelength of the light, while the resolution of an optical microscope is limited by the phenomenon of diffraction, with the size of the details observed becoming comparable to the wavelength of the light used, resulting in the mixing of information and blurring of fine details [5]. Electron microscopes, on the other hand, have been specially designed to overcome this resolution constraint. Instead of using visible light, they use electron beams, that is, fast electrons, as a source of radiation. One of the main benefits of electron radiation is its short wavelength, allowing for high resolution. This means that finer details can be distinguished [5], such as transmission electron microscopy, which uses fast electrons, usually around 100 to 200 keV, approximately equivalent to half the speed of light [5].

Electron microscopy offers an innovative approach thanks to various components such as an electron gun, responsible for producing the electron beam, a set of magnetic lenses, a scanning coil and an electron detection system [6].

The main types of electron microscopy include scanning electron microscopy (SEM), which has made great strides in terms of resolution and flexibility, enabling us to observe the surface of samples with nanometric resolution [7]; transmission electron microscopy (TEM), to examine the internal structure and composition of samples at atomic resolution [8]; scanning transmission electron microscopy (STEM), which combines the advantages of both techniques to provide high-resolution images of the internal structure and surface of samples [9] and finally, scanning tunnel electron microscopy (STEM), which enables the topography and surface properties of materials to be studied at the atomic scale, allowing detailed exploration of surface structure and characteristics [10]. All these different types of electron microscopy can be coupled with energy dispersive X-ray (EDX) microanalysis, which provides information on the structure and chemical composition at the atomic level of the sample being analyzed. This makes it possible to explore the composition of samples in greater detail. Electron microscopes can be used in many fields, including biology and biotechnology [11], nanotechnology in the ability to manipulate and observe the nanoscale world [12], materials chemistry, particularly for energy devices such as rechargeable batteries and fuel cells [13], the geology of mineral deposits [14] and medical research, in particular for accurate diagnostic assessment of kidney lesions in native medical kidney biopsies [15]; they are also highly accurate in the field of urinary lithiasis, making it possible to accurately determine the composition of kidney stones [16]. As medical scientific research is our field of interest, we will focus on the scientific study of urinary lithiasis pathology and its relationships using electron microscopy.

This chapter focuses on presenting the application and use of electron microscopy in the context of medical research related to urinary lithiasis, and highlights the importance of accurately determining the composition of kidney stones, as it is crucial to correctly determine the type of stone to prescribe the appropriate preventive treatment. First, we will identify and examine the pathology associated with urinary lithiasis and kidney stones. Next, we will explore the assessment of kidney stones, highlighting the importance of characterizing them using a variety of methods, including electron microscopy. We will then give an overview of the scanning electron microscope coupled to X-ray energy dispersive (SEM–EDX) and its application in the field of urinary lithiasis, focusing on the stone dissolution test. Finally, we will look at future developments in this field.

2. Pathology of urinary lithiasis and kidney stones

2.1 Pathophysiology of urinary lithiasis

The global prevalence of kidney disease is increasing, primarily due to factors that contribute to its occurrence, such as urinary stones, which have become more common in the general population in recent decades [17]. It is crucial to first understand the pathology of urinary lithiasis in this chapter, which corresponds to the formation of kidney stones in the kidneys or urinary tract, often accompanied by severe pain in most cases of lithiasis. Urolithiasis is a complex disease involving multiple factors [18]. Factors that increase the likelihood of stone formation and development include urinary pH abnormalities, such as $\text{pH} > 6.5$, which favors alkaline precipitation and

the presence of struvite [19]; nutritional factors, such as increased dietary intake of oxalate [20]; environmental factors, such as climate, which are involved in the epidemiology of urinary lithiasis [21]; age and sex in general, with a higher incidence of urolithiasis in men over 50 and women over 40 [22] and genetic factors, with urolithiasis induced by hereditary diseases being relatively rare [23].

This pathology occurs when crystals saturate the urine due to their high concentration and begin to accumulate, crystallize and agglomerate in the renal parenchyma, moving to other parts of the urinary tract where they can become trapped in the urethra or bladder, forming kidney stones [24]. These stones follow a formation process called lithogenesis, which takes place in several stages [25].

2.2 Urinary stones formation steps

2.2.1 Lithogenesis

The pathology of urinary lithiasis is the result of a urinary biochemical imbalance between inhibitors and promoters of the stone-forming process known as lithogenesis [26]. Lithogenesis is the set of processes that lead to the development and formation of a calculus in the urinary tract [27]. It comprises various stages that are represented in succession, and are eventually divided into seven distinct stages: urine supersaturation, crystal growth, crystal aggregation, crystal agglomeration, retention of crystallized particles and growth of calculus [28].

Urine supersaturation: Supersaturation occurs when the concentration of one or more molecules or atoms dissolved in urine exceeds the maximum limit, beyond which any new fraction of the added substance remains insoluble due to physiological changes and physicochemical conditions.

Crystal growth: Happens when the level of urinary supersaturation level is high enough for undissociated dissolved molecules to accumulate to form crystalline nuclei.

Crystal aggregation: This stage ensures that crystals are enlarged by the mixing of new ions or new molecules, thus converting primitive crystals of a few tens of nanometers into micrometer-sized crystals.

Crystalline agglomeration: This process results in the rapid formation of large particles, driven by electrostatic attraction forces and interactions between crystalline nuclei and urinary macromolecules. Urinary macromolecules have the ability to bind new crystals and form agglomerates.

Retention of crystallized particles: The crystalline particles formed during the various phases of crystallogenesis are likely to be retained in the kidneys or urinary tract, where they may grow to form a calculus.

Calculus growth: In the urinary tract, calculus development depends on several factors, such as the increase in promoter concentration, which allows new crystals to be attached, with highly variable calculus growth rates.

2.2.2 Promoters and inhibitors of lithogenesis

There is generally a balance between promoters and inhibitors of crystallization in urine [29]. This equilibrium can be disturbed either by an excess of promoters or by a deficit of inhibitors. The ions involved in the constitution of insoluble species are called crystallization promoters, such as calcium, urate and cystine. Numbering approximately ten, they very often combine in twos or threes to form a crystallizable substance, which can occur in several crystalline species. Lithogenesis inhibitors are

molecules that slow crystal growth. These inhibitors fall into two categories: urinary ionic molecules, such as Zn^{2+} , Fe^{3+} and Mg^{2+} , act by forming a soluble complex with crystallizable substances, thus reducing supersaturation. High molecular weight inhibitors such as uropontine and bikunine act directly on the crystals by blocking the growth sites on their surface [30].

2.3 Types of urinary calculi

The classification of urinary stones is important for medical diagnosis, as it helps identify the primary causes of their formation to be determined, thus facilitating the treatment of the disease [31]. For this, a morpho-constitutional analysis must be carried out to determine the chemical composition and crystalline form of the stones, thus revealing the specific cause of the pathology [32]. There are several types of urinary calculi, the most common of which are oxalocalcic calculi, which account for up to 80% of cases and can be divided into two forms: calcium oxalate dihydrate (wed-dellite) and calcium oxalate monohydrate (whewellite) [33]. In addition, phosphate calculi can be divided into two forms: calcium phosphates, which have a macroscopic chalky appearance, as in the case of brushite, and ammonium-magnesium phosphates, of which struvite represents 20%, which are included in the category of infectious lithiasis, because the presence of struvite necessarily attests to the intervention of a ureolytic germ (*Proteus* or *Klebsiella*), which can cause urinary alkalinity to be sufficiently high to provoke the simultaneous precipitation of ammonium and magnesium phosphates [19]. In addition, there are rare types of stones such as cystine stones, which account for 1% and are present as smooth, light-yellow and waxy-looking stones. They are caused by a genetic abnormality of the renal tubules, which leads to reduced reabsorption of cystine by the proximal tubules, resulting in increased cystine concentrations in the urine [34]. Another rare type is drug-induced calculi, which can occur in patients on long-term, high-dosage treatments, such as atazanavir [35].

All these types of stones need to be identified and defined to control patient treatment using urinary stone analysis methods. So, what are these methods?

3. Urinary stone analysis method

Characterizing urinary calculi requires a thorough understanding of their chemical composition and origin, facilitating the optimal selection of treatment and prevention strategies tailored to each individual patient. To achieve this goal, it is crucial to analyze the structure in order to comprehend the pathological conditions that lead to their formation. This assessment of urinary calculi involves evaluating both their qualitative and quantitative composition [36]. As far as qualitative characterization is concerned, several techniques are used to determine the physicochemical characteristics of urinary calculi. These include chemical laboratory approaches such as binocular loupe and scanning electron microscopy. The latter allows us to describe the topology and surface of stones, examining both superficial and internal characteristics. Various methods are used to quantitatively characterize the composition of urinary calculi, each based on a specific principle. Infrared spectrophotometry, for example, identifies the chemical composition of stones by analyzing the chemical bonds between atoms, allowing for the determination of stones types. X-ray diffraction, on the other hand, provides a chemical composition analysis that focuses on atomic proportions [37].

3.1 Quantitative composition

3.1.1 Binocular stereomicroscope

Binocular stereomicroscope utilizes fiber optics and offers 40x magnification. It is employed for morphological analysis of urinary calculi and to identify their morphological type of calculus according to Daudon's classification [34]. Its purpose is to inspect the stone optically, noting its surface characteristics. He examines the surface, including aspects such as color, texture, Randall's spots and the possible presence of umbilical cords. Then, after making a cross-section of the calculi using a scalpel, he highlights the presence of the nucleus, deep layers, middle layers and peripheral layers of the calculus. The use of this stereomicroscope is often linked to the use of the Fourier transform infrared microscope, a quantitative technique [38]. This shows that combining quantitative and qualitative techniques in the characterization of stones improves the reliability and accuracy of the results obtained.

3.1.2 Scanning electron microscopy

Scanning electron microscopy (SEM) is a powerful technique for high-resolution imaging and for characterizing texture and local chemical composition, in other words determining the predominant elements on the surface of massive materials, as is the case when examining the surface structure of calculi at nanometric resolution. In this context, the imaging of pathological calcifications plays a crucial role, in whether they manifest themselves as mesoscopic-sized calculi [38]. The capabilities of scanning electron microscopy go far beyond the precise visualization of the topology of these calcifications on a submicron scale. Indeed, scanning electron microscopy accurately visualizes not only the topology of these submicron calcifications but also maps them chemically, thanks to coupling with energy-dispersive X-ray spectroscopy (EDS) [39].

3.2 Qualitative composition

3.2.1 Fourier-transform infrared spectroscopy

The spectrophotometer is a physical technique for molecular analysis. It has undergone a major evolution with the advent of Fourier transform spectrophotometers (FTIR). This method is frequently utilized in nephrology departments to identify the composition of stones by analyzing the distinct bands that indicate the bonding types between the atoms forming the molecules of the calculus. This information can be used to guide the patient's diet or treatment. The operating principle is based on the use of an infrared beam that induces a specific vibration for each molecule exposed. These vibrations produce a spectrum whose absorption bands correspond to the specific presence of one or more molecular bonds [40].

3.2.2 X-ray diffraction

X-ray diffraction (XRD) is a technique for characterizing crystallized materials and is used to determine the phase composition of all urinary calculi. This technique makes it possible to identify the crystals, in other words, just the minerals present in the stones which is essential for classifying the type of stone [16]. X-ray diffraction

measurements are a simple means of phase recognition. Once the diagram has been obtained, the positions and intensities of the observed peaks are compared with those in the database. This enables rapid verification of a synthesis result (correct crystal phase, presence of impurities, etc.) or confirmation that a new compound has been obtained. This technique then provides a product identity card by comparison with a database. X-ray diffraction can also be utilized to determine the chemical composition, as long as the phase is crystallized, and it also indicates the size of the crystal [41].

4. Overview of MEB-EDX

4.1 Principle of scanning electron microscopy

Scanning electron microscopy (SEM) has marked a significant advance in scientific research, proving to be a powerful tool for both textural and local chemical characterization of massive materials. Based on the interaction between electrons and matter, the term “electron” reflects the use of electrons as probe particles. Similarly, the use of the term “scanning” recalls that the image of the sample surface is formed as the electron beam moves along its surface, and this image is then displayed on a viewing screen [42]. SEM merges high-resolution imaging with an extended depth of field, taking advantage of electrons’ short wavelengths and their ability to be focused by electrostatic and electromagnetic lenses [2].

Scanning electron microscopy is based on the principles of electron-sample interaction. Samples are observed by bombarding their surface with an electron beam generated in an electron gun. In this gun, electrons are emitted from a Joule-heated lanthanum hexaboride filament. They are then accelerated by a potential difference created between a cathode and an anode positioned at the center of the gun, allowing the beam to pass through. The beam thus formed passes through several elements of the optical column. Multiple holes are present throughout this column, and electromagnetic lenses (condensers) enable the beam size to be adjusted and modified. By controlling the current (in a range from 10^{11} to 10^{17} electrons per second), it becomes possible to regulate the beam size. The lower the current is, the finer the beam size. The interaction between the electrons in the beam and the sample occurs at a precise point, usually less than 100 nm away. This means that certain areas of the sample can only be analyzed by scanning with the beam. To this end, two scanning lenses (one for each plane direction) are positioned close to a condensing lens. These scanning lenses guide the beam in both directions, allowing for the sample’s surface to be scanned line by line. When this scan is combined with a CRT screen, it produces an image of the sample surface [3, 43].

4.2 Energy-dispersive X-ray spectroscopy

X-rays are photons with energies ranging from 10 eV to 100 KeV, and the control of these X-rays depends on the precision of a target with a medium-energy electron. The energy-dispersive X-ray detector was developed in the 1960s, primarily for nuclear purposes, but its adaptation to SEM analysis around 1970 was extremely effective and has since become an essential tool in various applications, from production environments to cutting-edge research laboratories. Energy- and wavelength-dispersive X-ray spectroscopy involves the emission of X-rays and their interaction with the sample, to analyze the chemical elemental properties of the sample, whether organic or inorganic, as a function of the energy and wavelength of the dispersed X-rays [44, 45].

Scanning electron microscopy (SEM) was used to examine the surface of the stone and energy dispersive X-ray (EDX) spectroscopy was used to identify all the sample atomic elements. However, one approach is to merge these two methods to characterize urinary calculi, particularly in the context of lithiasis research. This approach focuses on studying the anti-lithiasis properties of medicinal plants. Scanning electron microscopy (SEM) coupled with energy dispersive X-ray spectroscopy (EDS) was used to study compositional mapping. This means they examined the distribution of chemical elements in kidney stone samples. This technique makes it possible to visualize the distribution of different elements in stones, which can help to identify the type of stone based on its chemical composition. The combination of scanning electron microscopy (SEM) and energy dispersive X-ray spectroscopy (EDS) appears to be a relevant method for exploring the field of urinary lithiasis [16].

So, how is the SEM–EDS technique used in the context of anti-lithiasis activity?

5. Anti-lithiasis activity by dissolution test and use of SEM-EDS

5.1 General description

As mentioned earlier in this chapter, urinary lithiasis is a disease resulting from the formation of stones in the kidneys or urinary tract, caused by a variety of factors, including anatomical, genetic and metabolic factors. Conventional treatment of urinary lithiasis, involving a range of techniques and medications, can be complex and have significant side effects. It is in this context that the use of medicinal plants, or phytotherapy, has emerged as a promising alternative [33].

The world's plant diversity offers a vast heritage, including medicinal plants that have long been used in the traditional treatment of various pathologies, including urinary lithiasis. These include *Saussurea costus* (Falc) Lipsch [46], *Herniaria hirsuta* L [47] and many others. Nevertheless, the importance of scientific research in the renal field lies in its ability to corroborate the beneficial effects of these plants in the treatment of lithiasis. This involves identifying and characterizing the active ingredients responsible for the therapeutic effect, determining nontoxic doses and so on.

In this context, other work involves assessing the anti-lithiasis activity of medicinal plant extracts, such as the urinary stone dissolution test, which consists of monitoring the variation in stone mass (of all types) and structural modifications before and after treatment with plants, by observing the stones using an energy-disappearing X-ray scanning electron microscope (SEM–EDS).

5.2 Dissolution test

5.2.1 Anti-Lithiasis exploration

Once the medicinal plant has been selected according to a logical scientific approach based on ethnobotanical surveys, and extracted using extraction techniques such as maceration, sohxhlet and decoction, depending on the solvent involved (water, ethanol, hexane, apolar affinity, etc.), the active ingredients are chemically characterized using techniques such as gas chromatography coupled with mass spectrometry (GC–MS) and high-performance liquid chromatography coupled with mass spectrometry (HPLC–MS). Once the active ingredients have been chemically

characterized, the transition to *in vitro* testing is valid and favorable for studying antilithiasis activity, which involves the dissolution of urinary calculi.

5.2.2 Evaluation of the effect of plants on urinary calculi

The aim of the stone dissolution test is to evaluate the effect of herbal extracts on the loss of urinary stone mass over a given period, under optimized physiological conditions. To start the test, the initial step involves gathering urinary stones. Then, the chemical composition of these stones was determined using Fourier transform infrared spectroscopy (FTIR) as a qualitative method. These findings were subsequently validated by scanning electron microscopy coupled with energy dispersive spectrometry (SEM-EDS) [33].

5.2.3 Protocols for dissolving urinary calculi

Setting up a dissolution protocol depends on the choice of plants and urinary stones. For example, in our recent study, we chose aqueous and ethanolic extracts of the plant *Saussurea costus* (Falc) Lipsch to target cystine-type calculi. In this study, plant extracts at a concentration of 0.5% each were prepared in 50 ml of physiological solution (9 g/l NaCl).

NaCl solution was used as a negative control to monitor variations in stone mass and structure, while potassium citrate was used as a positive control. The stones were then immersed in Erlenmeyer flasks, each containing one extract, and maintained at a temperature of 37°C. Each sample was subjected to constant magnetic agitation at 130 rpm for 6 weeks. Throughout the experiment, the pH of the solution was measured every 7 days using a pH meter. In addition, the loss of mass of the kidney stones was assessed by measuring their weight after drying in an oven at 40°C for 18 hours. For further analysis, the surface of the stones was examined before and after the experiment using scanning electron microscopy (SEM) in conjunction with energy dispersive spectrometry (EDX). This made it possible to characterize the chemical elements present in the stones and corroborate the results previously obtained by infrared spectroscopy, thus confirming the composition of these cystine stones [33].

5.2.4 Dissolution test results

The results obtained from this protocol involve the use of scanning electron microscopy coupled to energy dispersive spectrometry (SEM-EDS), and are of great importance in the context of this chapter. The results of our recent study significantly highlight the effect of the plant extracts studied on the dissolution of cystine kidney stones. To confirm the interactions between plant extracts and cystine stones, changes in crystallite morphology were monitored (**Figure 1**).

Data from this study revealed that, prior to treatment, the composition of cystine stones consisted mainly of carbon (C), nitrogen (N), oxygen (O) and sulfur (S), an analysis corroborated by infrared spectra. However, after treatment with plant extracts (aqueous and ethanolic), a new composition emerged, including elements such as oxygen (O), nitrogen (N), sulfur (S) and chlorine (Cl), in addition to those initially present. Similar changes were observed in *Saussurea costus* extracts, where constituents shifted from carbon (C) to oxygen (O), sodium (Na), sulfur (S) and chlorine (Cl). In the case of citrate, only carbon (C) and sulfur (S) were detectable [33].

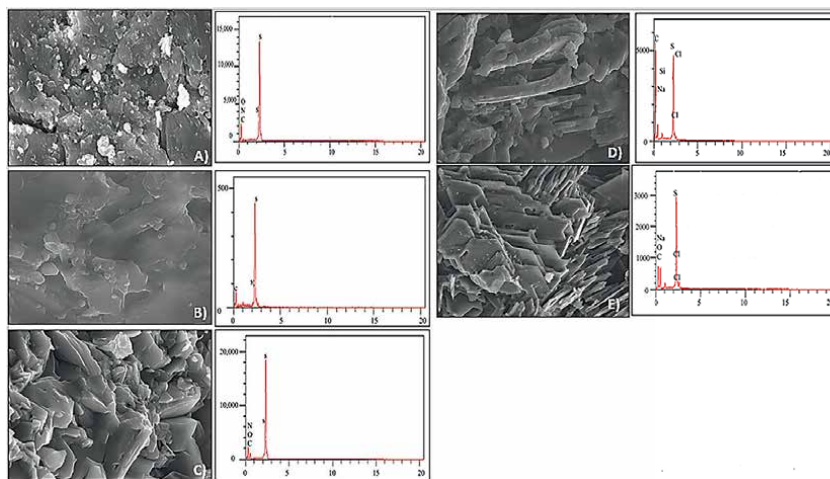


Figure 1.
 A) Crystal surface visualized by SEM coupled to EDX before any treatment, B) crystal surface visualized by SEM coupled to EDX after treatment with citrate, C) crystal surface visualized by SEM coupled to EDX after treatment with aqueous NaCl solution, D) the surface of crystals visualized by SEM that is coupled to EDX after treatment with the solution containing the ethanolic extract of *Saussurea costus* (Falc) Lipsch and E) the surface of crystals visualized by SEM that is coupled to EDX after treatment with the solution containing the aqueous extract of *Saussurea costus* (Falc) Lipsch [33].

The application of scanning electron microscopy in conjunction with energy dispersive spectrometry analysis fully confirmed the changes in the ultrastructural characteristics and elemental composition of the cystine stones before and after treatment. These results suggest the possibility of a curative effect induced by the plant in question, probably thanks to the presence of various compounds acting as active principles in the plant extracts studied, although we did not observe any significant change in mass levels in comparison with the other plant extracts used in Hannache's experiment [42], which showed a high dissolution percentage for the cystine stones, indicating that our plant does indeed have a slight effect for this type of stone, but is probably effective for another type.

6. Conclusion

In conclusion, this chapter demonstrates the significance of electron microscopy in scientific research within the medical field. It allows for the exploration of the effects of *Saussurea costus* plant extracts on urinary lithiasis and the dissolution of cystine-type urinary calculi. This is achieved through the use of scanning electron microscopy coupled with X-ray energy dispersive spectrometry (SEM-EDS). The observations of variations in the surface of the stones and their composition lead to the conclusion that there is an interaction between the extracts containing the active ingredients and the stones.

Furthermore, scanning electron microscopy coupled with X-ray energy dispersive spectrometry (SEM-EDS), as a qualitative and quantitative technique, has a high potential for studying and detecting surface changes, as well as for determining the chemical elements present in the structure of stone crystals. This technique confirms the results of Fourier transform infrared spectroscopy as a quantitative approach.

In brief, this technology has the potential to equal or even exceed infrared technology in the chemical analysis of patient stones.

Conflict of interest

The authors declare no conflicts of interest.

Author details

Naima Mammate^{1*}, Salim Belchkar¹, Salma Ssouni^{1,2}, Ghita el Mouhri^{2,3}
and Tarik Sqalli Houssaini^{1,4}

1 Faculty of Medicine, Laboratory of Epidemiology and Research in Health Sciences, Pharmacy, and Dental Medicine, Sidi Mohammed Ben Abdellah University of Fez, Morocco


2 Faculty of Medicine, Laboratory of Biochemistry, Pharmacy and Dental Medicine, University Sidi Mohamed Ben Abdellah, Fez, Morocco

3 Higher Institute of Nursing Professions and Health Techniques of Fez/Taza, Ministry of Health and Social Protection, Taza, Morocco

4 Department of Nephrology, Dialysis, and Transplantation, Hassan II University Hospital, Fez, Morocco

*Address all correspondence to: naima.mammate@usmba.ac.ma

IntechOpen

© 2024 The Author(s). Licensee IntechOpen. This chapter is distributed under the terms of the Creative Commons Attribution License (<http://creativecommons.org/licenses/by/3.0>), which permits unrestricted use, distribution, and reproduction in any medium, provided the original work is properly cited. 

References

- [1] Sandberg PA, Hay WW. Study of Microfossils by Means of the Scanning Electron Microscope. Tulsa, Oklahoma: SEPM Society for Sedimentary Geology; 2023
- [2] Freundlich MM. Origin of the electron microscope. *Science*. 1963;**142**(3589):185-188. DOI: 10.1126/science.142.3589.185
- [3] Mestres Ventura PJ. The electron microscope on the eve of its first centenary. *EJA*. 2023;**27**:111-127. DOI: 10.1126/science.142.3589.185. Available from: <https://eurjanat.com/articles/the-electron-microscope-on-the-eve-of-its-first-centenary>
- [4] Masters BR. History of the Electron Microscope in Cell Biology. 1st ed. John Wiley & Sons, Ltd; 2009 [cited 2023 Sep 4]. Available from: <https://onlinelibrary.wiley.com/doi/10.1002/9780470015902.a0021539>
- [5] Kociak M. Introduction à la microscopie électronique. *JDN*. 2007;**12**:61-74. Available from: <http://www.neutron-sciences.org/10.1051/sfn:2007006>
- [6] López De La Rosa F, Sánchez-Reolid R, Gómez-Sirvent JL, Morales R, Fernández-Caballero A. A review on machine and deep learning for semiconductor defect classification in scanning electron microscope images. *Applied Sciences*. 2021;**11**(20):9508. Available from: <https://www.mdpi.com/2076-3417/11/20/9508>
- [7] Roussel LY, Stokes DJ, Gestmann I, Darus M, Young RJ. In: Postek MT, Newbury DE, Platek SF, Joy DC, editors. Extreme High Resolution Scanning electron Microscopy (XHR SEM) and beyond. Monterey, CA; 2009. p. 73780W. Available from: <http://proceedings.spiedigitallibrary.org/proceeding.aspx?doi=10.1117/12.821826>
- [8] Ross FM. Opportunities and challenges in liquid cell electron microscopy. *Sciences*. 2015;**350**(6267):aaa9886. Available from: <https://www.science.org/doi/10.1126/science.aaa9886>
- [9] Ge B. Scanning transmission electron microscopy (STEM). In: Wang R, Wang C, Zhang H, Tao J, Bai X, editors. Progress in Nanoscale Characterization and Manipulation. Singapore: Springer; 2018. pp. 205-254. (Springer Tracts in Modern Physics; vol. 272). Available from: http://link.springer.com/10.1007/978-981-13-0454-5_4
- [10] Binnig G, Rohrer H. Scanning tunneling microscopy. *Surface Science* (North-Holland Publishing Company). 1983;**126**:236-244
- [11] Smith D, Starborg T. Serial block face scanning electron microscopy in cell biology: Applications and technology. *Tissue and Cell*. 2019;**57**:111-122. Available from: <https://linkinghub.elsevier.com/retrieve/pii/S004081661830212X>
- [12] Schaming D, Remita H. Nanotechnology: From the ancient time to nowadays. *Foundational Chemistry*. 2015;**17**(3):187-205. Available from: <http://link.springer.com/10.1007/s10698-015-9235-y>
- [13] Fan Z, Zhang L, Baumann D, Mei L, Yao Y, Duan X, et al. In situ transmission electron microscopy for energy materials and devices. *Advanced Materials*. 2019;**31**(33):1900608. Available from: <https://onlinelibrary.wiley.com/doi/10.1002/adma.201900608>

- [14] Frelinger SN, Ledvina MD, Kyle JR, Zhao D. Scanning electron microscopy cathodoluminescence of quartz: Principles, techniques and applications in ore geology. *Ore Geology Reviews*. 2015;**65**:840-852. Available from: <https://linkinghub.elsevier.com/retrieve/pii/S0169136814002595>
- [15] Yamashita M, Lin MY, Hou J, Ren KYM, Haas M. The continuing need for electron microscopy in examination of medical renal biopsies: Examples in practice. *Glomerular Diseases*. 2021;**1**(3):145-159. Available from: <https://www.karger.com/Article/FullText/516831>
- [16] (Porikli) Durdađi S, AHH A-J, Yalçın P, Bozkurt AS, Salcan S. Morphological characterization and phase determination of kidney stones using X-ray diffractometer and scanning electron microscopy. *Chinese Journal of Physics*. 2023;**83**:379-388. Available from: <https://linkinghub.elsevier.com/retrieve/pii/S0577907322002258>
- [17] Siener R. Nutrition and kidney stone disease. *Nutrients*. 2021;**13**(6):1917. Available from: <https://www.mdpi.com/2072-6643/13/6/1917>
- [18] Grases F, Costa-Bauza A, Prieto RM. Renal lithiasis and nutrition. *Nutrition Journal*. 2006;**5**(1):23. Available from: <http://nutritionj.biomedcentral.com/articles/10.1186/1475-2891-5-23>
- [19] Mammate N, El Oumari FE, Imtara H, Belchkar S, Benjelloun Touimi G, Al-Zharani M, et al. Anti-struvite, antimicrobial, and anti-inflammatory activities of aqueous and ethanolic extracts of *Saussurea costus* (Falc) Lipsch Asteraceae. *Molecules*. 2023;**28**(2):6673. Available from: <https://www.mdpi.com/1420-3049/28/2/667>
- [20] Dako E, Retta N, Desse G. Comparison of Three Sweet Potato (*Ipomoea batatas* (L.) Lam) Varieties on Nutritional and Anti-Nutritional Factors. USA; 2016
- [21] Wróbel G, Kuder T. The role of selected environmental factors and the type of work performed on the development of urolithiasis – A review paper. *International Journal of Occupational Medical and Environmental Health* 2019 **32**(6):761-775. Available from: <http://www.journalssystem.com/ijomeh/The-role-of-selected-environmental-factors-and-the-type-of-work-performed-on-the,111685,0,2.html>
- [22] Temporal trends in the incidence of kidney stone disease. *Kidney International*. 2013;**83**(1):146-152. Available from: <https://www.sciencedirect.com/science/article/pii/S008525385556949>
- [23] Dalibon P. La lithiase urinaire, une affection sous surveillance. *Actualités Pharmaceutiques*. 2015;**54**(542):23-29. Available from: <https://linkinghub.elsevier.com/retrieve/pii/S0515370014004303>
- [24] Thakore P, Liang TH. Urolithiasis. *StatPearls*. Treasure Island, FL; 2023. Available from: <https://www.ncbi.nlm.nih.gov/books/NBK559101.pdf>
- [25] Srivastava A, Swain KK, Chahar V, Bhardwaj S, Ajith N, Mete U, et al. Role of diet and trace elements in lithogenesis of renal calculi. *Journal of Radioanalytical Nuclear Chemistry*. 2019;**319**(1):271-278. Available from: <http://link.springer.com/10.1007/s10967-018-6335-x>
- [26] Singh P, Harris PC, Sas DJ, Lieske JC. The genetics of kidney stone disease and nephrocalcinosis. *Nature Reviews Nephrology*. 2022;**18**(4):224-240. DOI: 10.1038/s41581-021-00513-4

- [27] Wang M, Chiu Y, Flahaut D, Jones IP, Zhang Z. Secondary phase area fraction determination using SEM-EDS quantitative mapping. *Materials Characterization*. 2020;**167**:110506. Available from: <https://linkinghub.elsevier.com/retrieve/pii/S104458032031977X>
- [28] Miller NL, Evan AP, Lingeman JE. Pathogenesis of renal calculi. *Urologic Clinics of North America*. 2007;**34**(3):295-313. Available from: <https://linkinghub.elsevier.com/retrieve/pii/S0094014307000468>
- [29] Cochat P, Bacchetta J, Sabot JF, Bertholet-Thomas A, Demède D. Lithiase urinaire de l'enfant. *Journal de Pédiatrie et de Puériculture*. 2012;**25**(5):255-268. Available from: <https://linkinghub.elsevier.com/retrieve/pii/S0987798312001065>
- [30] Daudon M, Traxer O, Lechevallier E, Saussine C. La lithogénèse. *Progrès en Urologie*. 2008;**18**(12):815-827. Available from: <https://linkinghub.elsevier.com/retrieve/pii/S1166708708003904>
- [31] Bazin D, Daudon M, Chevallier P, Rouzière S, Elkaim E, Thiaudière D, et al. Les techniques de rayonnement synchrotron au service de la caractérisation d'objets biologiques : un exemple d'application, les calculs rénaux. *Annales de Biologie Clinique*. 2006;**2006**:64
- [32] El Habbani R, Chaqroune A, Sqalli Houssaini T, Arrayhani M, El Ammari J, Dami F, et al. Étude épidémiologique sur les calculs urinaires dans la région de Fès et sur le risque de récurrence. *Progrès en Urologie*. 2016;**26**(5):287-294. Available from: <https://linkinghub.elsevier.com/retrieve/pii/S1166708716000294>
- [33] Mammate N, El Oumari FE, Imtara H, Belchkar S, Lahrichi A, Alqahtani AS, et al. Antioxidant and anti-urolithiatic activity of aqueous and ethanolic extracts from *Saussurea costus* (Falc) Lispich using scanning electron microscopy. *Life*. 2022;**12**(7):1026. Available from: <https://www.mdpi.com/2075-1729/12/7/1026>
- [34] Daudon M, Jungers P, Traxer O. *Lithiase Urinaire*. Paris: Lavoisier; 2012
- [35] Plawecki M, Bistoquet M, Grillet PE, Abdo N, Souweine JS, Cristol JP. Drug-induced urinary stone of atazanavir incidentally found in an asymptomatic patient: A case report. *Case Reports in Urology*. 2023;**2023**:4. Article ID 4890711. Available from: <https://www.hindawi.com/journals/criu/2023/4890711/>
- [36] Singh VK, Rai PK. Kidney stone analysis techniques and the role of major and trace elements on their pathogenesis: A review. *Biophysical Reviews*. 2014;**6**(3-4):291-310. DOI: 10.1007/s12551-014-0144-4
- [37] Tcheka C, Moubarik A, Outzourhit A, Mbarki M, Benguellah BL, Mbadcam JK, et al. Epidemiological exploration of urinary stones. *Physical and Chemical News*. 2011;**61**:120-127
- [38] Hannache B. La lithiase urinaire : épidémiologie, rôle des éléments traces et des plantes médicinales [Internet] [thesis]. Paris 11; 2014. Available from: <http://www.theses.fr/2014PA114804>
- [39] Bougouma M, Keraghel F, Sawadogo J, Adama K, Buess-Herman C, Doneux T. Caractérisation physico-chimique et électrochimique de monocristaux de MoO₃, W₂O₅, Se₂ obtenus par croissance cristalline. 2020
- [40] Paramita C, Arup C, Mukherjee AK. Phase composition and morphological characterization of human kidney stones using IR spectroscopy, scanning electron microscopy and X-ray Rietveld analysis.

Spectrochimica Acta Part A: Molecular and Biomolecular Spectroscopy. 2018;**200**:33-42. Available from: <https://www.sciencedirect.com/science/article/pii/S1386142518303044>

[41] Guinebretière R. La diffraction des rayons X sur des échantillons polycristallins- l'actualité chimique - juil.-août-sept.-oct. 2014 - n° 387-388-389

[42] Hannache B. La lithiase urinaire : épidémiologie, rôle des éléments traces et des plantes médicinales [These de doctorat]. Paris 11; 2014 [cited 2023]. Available from: <https://www.theses.fr/2014PA114804>

[43] Doumalin P. Microextensométrie locale par corrélation d'images numériques. Application aux études micromécaniques par microscopie électronique à balayage. Thèse de doctorat en Sciences de l'ingénieur [physique]. Ecole Polytechnique X, 2000. En français. Numéro de thèse: 2000EPXX0027. Identifiant pastel: pastel-00001162

[44] Bell DC, Garratt-Reed AJ. Energy dispersive X-ray analysis in the electron microscope. Garland Science. 2003;**2003**:163

[45] Technique (ANRT) AN de la R. Electron-probe microanalysis: x-ray spectroscopy. Association Nationale de la Recherche Technique (ANRT); 1987 [cited 2023 Sep 10]. Report No.: FRNC-R--274. Available from: http://inis.iaea.org/Search/search.aspx?orig_q=RN:21052160

[46] Taïbi K, Aït Abderrahim L, Boussaid M, Taïbi F, Achir M, Souana K, et al. Unraveling the ethnopharmacological potential of medicinal plants used in Algerian traditional medicine for urinary diseases.

European Journal of Integrative Medicine [Internet]. 2021;**44**:101339. Available from: <https://linkinghub.elsevier.com/retrieve/pii/S1876382021000573>

[47] Idmhand E, Msanda F, Cherifi K. Étude ethnobotanique des plantes médicinales utilisées dans le traitement de la lithiase urinaire dans la province de Tarfaya (Maroc). International Journal of Innovation and Applied Studies. Jun 2019;**26**(3):711-719. ISSN: 2028-9324

Mass Spectrometry Analysis Using Formalin-Fixed Paraffin-Embedded Pathological Samples

Takuya Hiratsuka and Tatsuki Tsuruyama

Abstract

Biomarker discovery using mass spectrometry (MS) plays a significant role in clinical medical research. However, proteomic analysis of formalin-fixed paraffin-embedded (FFPE) specimens using MS has been challenging because of the reduced solubility caused by fixation, leading to crosslinking reactions among amino acid side chains in proteins. This review presents the techniques employed for omics analysis of FFPE specimens to identify disease-specific biomarkers.

Keywords: biomarker, pathology, formalin-fixed paraffin-embedded (FFPE), liquid chromatography (LC), mass spectrometry imaging (MSI)

1. Introduction

1.1 Mass spectrometry (MS)

MS is a technique used to ionize molecules for measurement and determine their mass-to-charge ratios (m/z). Metabolites, such as nucleic acids, lipids, and small molecules, have been identified as biomarkers. However, there are challenges in treating them as biomarkers, including difficulties in interpreting the amount of change. By contrast, proteins directly reflect biomedical phenomena. For instance, increased levels of pro-inflammatory cytokines indicate local inflammation, whereas elevated levels of specific proteins, such as tumor markers, provide essential information about cancer progression. Changes in the protein levels of these pathologies are diagnostically significant and offer valuable insights into disease monitoring, follow-up, and relapse prevention.

Furthermore, the ongoing development of antibody drugs targeting specific proteins has significant implications for diagnosis and treatment selection. In recent years, advancements in analyzer accuracy and data analysis technology have enabled the comprehensive analysis of proteins (proteome analysis). Liquid chromatography-tandem mass spectrometry (LC-MS/MS) is widely used for protein identification based on spectra. In addition, mass spectrometry imaging (MSI) has recently been developed to identify in situ proteins in pathological lesions. In the field of clinical MS, it is necessary to understand the methods of protein extraction, ion generation, mass analysis algorithms, interpretation of mass spectra, pathological analysis, and clinical data evaluation (**Figure 1**).

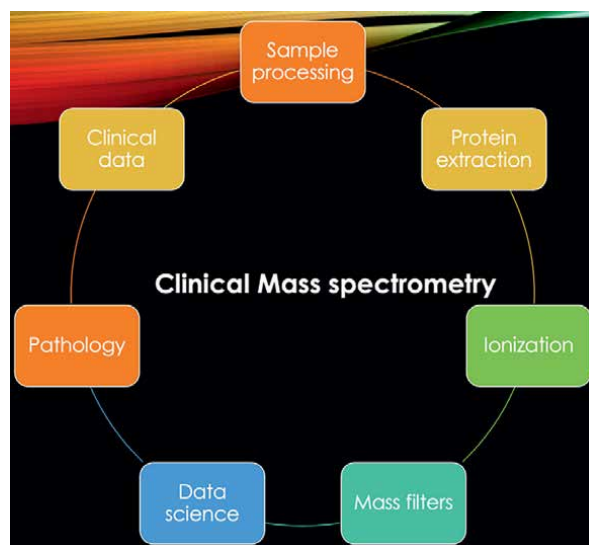


Figure 1.
Multifaceted mass spectrometry (MS) and the interconnected steps contributing to clinical MS.

1.2 Formalin-fixed paraffin-embedded (FFPE) proteomics

Protein datasets contain large amounts of information. Therefore, it is necessary to efficiently use analytical tools to discriminate protein functions by ontology analysis and determine whether they are metabolic enzymes, structural proteins, chaperones or stress response, and apoptotic or proliferative proteins for data interpretation. Network analysis of proteins and cell biological functional data will provide insights into pathogenesis and disease development. In addition, a collection with pathological tissue findings is beginning. Pathological conditions, such as hemorrhagic necrosis, changes in cell distribution during inflammation and immune responses, cell invasion, tumor growth, and infection, lead to changes in the concentration and distribution of proteins in tissues. Protein distribution and location information in pathological samples are expected to be useful biomarkers by correlating them with histopathological findings associated with clinical findings. We have previously reported its use in colon cancer [1], acute myocardial infarction [2–5], glioblastoma and metastatic lung cancer [6], systemic lupus erythematosus (SLE) and its associated diseases [7–9], and malignant mesothelioma [10]. FFPE-based proteomics is a promising method for identifying disease biomarkers.

2. Liquid chromatography-Tandem mass spectrometry (LC-MS/MS) of formalin-fixed paraffin-embedded (FFPE) specimens

2.1 Liquid chromatography-Tandem mass spectrometry (LC-MS/MS)

LC-MS/MS combines the physical separation capabilities of liquid chromatography (LC) with the two-stage mass analysis capabilities of MS. It is a powerful tool for analyzing proteins, allowing for the precise and sensitive detection of proteins and peptides in FFPE samples.

2.2 Sample preparation: Laser microdissection and proteomics

Laser microdissection (LMD) is used to precisely separate and extract specific cells from tissue sections, allowing for the accurate isolation of lesions. LMD is currently employed as a clinical test for cancer mutation analysis. However, this method has limitations in obtaining sufficient amounts and quality of proteins because proteins cannot be amplified unlike DNA. When working with specimens other than cancer cell tissues, extracting the minimum required amount while avoiding contamination from surrounding tissue components and the working environment becomes challenging. For instance, if a specific stain is used to identify lesions, it may interfere with subsequent analyses, requiring careful selection.

The quality of the samples and preprocessing significantly affected the reliability of MS omics data. Preprocessing involves extraction, purification, and digestion. In using the serum samples, identifying low-abundance proteins (especially potential disease biomarkers) is challenging in the presence of nonspecific, high-abundance proteins, such as albumin [2–5]. Therefore, adequate purification using affinity columns is necessary in some cases.

2.3 Chemistry of fixation

Formaldehyde-fixed cells and tissues become resistant to degradation, maintaining their morphology during subsequent procedures, such as staining. Formaldehyde is a simple aldehyde that can potentially interact with biological molecules, especially proteins, through its highly reactive carbonyl group. This reactivity primarily results from the partial positive charge on the carbonyl carbon, which attracts electron-rich nucleophiles.

A detailed reaction mechanism between formaldehyde and amino acids is as follows:

Step 1: Nucleophilic addition. The primary amine group in lysine ($-\text{NH}_2$) acts as a nucleophile. It approaches the electrophilic carbon in the carbonyl group of formaldehyde. The nucleophilic attack forms a tetrahedral intermediate.

Step 2: Elimination of water. This intermediate then undergoes a rearrangement, leading to the elimination of a water molecule and forming an imine linkage as follows: $\text{Lys-NH-CH(OH)-H} \rightarrow \text{Lys} = \text{NCH}_2 + \text{H}_2\text{O}$.

Step 3: A further reaction with another amino group. This imine is reactive and can undergo further reactions. A nucleophilic attack occurs when this imine comes into proximity with an amino group from another lysine. The nucleophilic NH_2 group of the second lysine attacks the imine carbon, leading to the formation of a methylene bridge ($-\text{CH}_2-$) between the two lysine residues as follows: $\text{Lys} = \text{NCH}_2 + \text{H}_2\text{N-Lys} \rightarrow \text{Lys-N-CH}_2\text{-NH-Lys}$.

Recent MS studies have shown that although most of the FA crosslinks occur between lysine or arginine residues, a significant portion of the crosslinks also includes asparagine, histidine, aspartic acid, tyrosine, and glutamine residues [11, 12]. This methylene bridging reaction results in an increase in molecular weight of 12 Da. However, in MS analyses, there are instances wherein an increase of 24 Da is observed. This suggests that a complex state may be formed wherein dimerization occurs among imine groups; however, the details remain unclear [11].

This methylene bridging results in covalent crosslinks among protein molecules or within the same protein molecule, stabilizing the tertiary and quaternary structures of the protein. These crosslinks are the primary reason formaldehyde is an effective

fixative, preserving the structural integrity of biological specimens. The methylene bridge reaction aggregates proteins within the sample into a large cohesive mass, creating a hydrophobic environment. Therefore, it inhibits proteolytic reactions that require water, thereby stabilizing the bulk protein mass. Crosslinking helps preserve cellular structures by “fixing” them, making it easier for pathologists to observe tissues under microscopes. However, this aggregation poses challenges in identifying individual protein components within the bulk, and fixed proteins can become protease-digestion resistant, such as trypsin-digestion resistant. The specific cleavage sites of trypsin, particularly those near lysine and arginine residues, may be rendered spatially inaccessible because of methylene crosslinking using formaldehyde. Therefore, preprocessing to enhance the digestion reaction is necessary.

2.4 Protein extraction and digestion

Trypsinization and fragmentation of this fixed protein mass necessitate a suitable hydrophilizing and swelling process. Repeated heating and cooling cycles help break the methylene or nonspecific bonds, diminishing the forces among structural proteins, such as collagen, and facilitating digestive reactions.

The most crucial process in FFPE protein extraction is the fragmentation of the bulk protein through sufficient physical crushing before digestion [1, 3, 11]. **Figure 2** shows an example of the extraction protocol. Each microdissected sample was suspended and crashed using an ultrasonic homogenizer in 0.1 mol/L NH_4HCO_3 containing 30% (v/v) CH_3CN (Buffer A). The sample tubes were heated at 95°C for 90 min with shaking every 30 min. The samples were centrifuged at 10,000 g for 1 min and cooled on ice. Trypsin and lysyl-endopeptidase were added for digestion, and samples were incubated at 37°C overnight for tissue swelling. Then, samples were heated at 95°C for a few minutes to deactivate trypsin. After drying, the samples were resuspended in trifluoroacetic acid containing 2% CH_3CN [1, 3]. Optionally, following trypsin digestion, peptides are often purified to remove nonpeptide components that could interfere with downstream analysis. This purification process involves various techniques, including desalting, solid-phase extraction, and spin column chromatography. However, the purification process may be omitted when the proteins extracted from the FFPE sample are present in trace amounts [13].

2.5 Liquid chromatography (LC) and ionization

The peptide mixture was loaded onto an LC column. The peptides interacted differently with the column material and were eluted at different times. The solvent (mobile phase) was pumped through a column containing a stationary phase. The components in the sample interact differently with the stationary phase, causing them to flow through the column at different rates to separate the mixture into individual components based on their chemical properties.

As the separated components exit the LC column, they are introduced into the mass spectrometer and ionized through electrospray ionization (ESI) to charge the molecules so that they can be manipulated by electric fields within the mass spectrometer.

2.6 First mass filter (MS1)

The ions were then passed through the MS1, which separated them based on their m/z values. The most common mass analyzers in LC-MS/MS are quadrupoles,

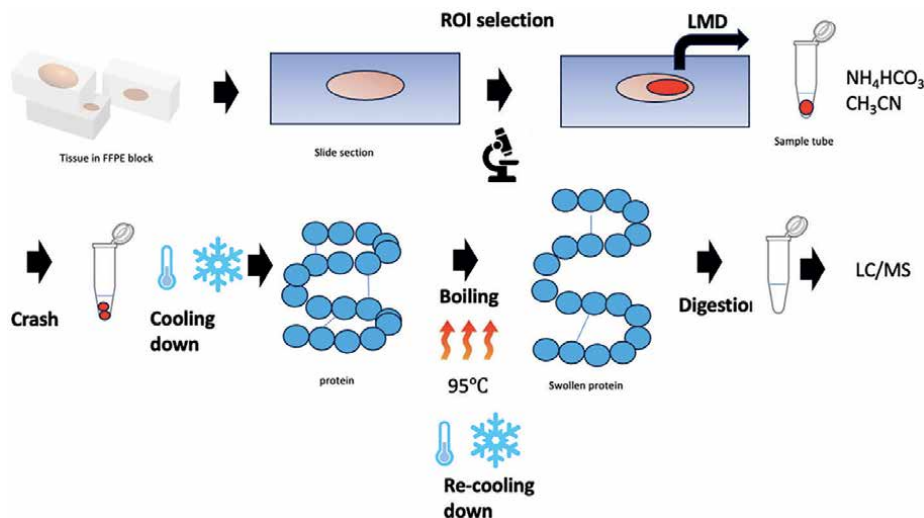


Figure 2.
 Sample preparation scheme for liquid chromatography–mass spectrometry (LC–MS).

ion traps, and time-of-flight (TOF) analyzers. In the quadrupole MS, four cylindrical metal rods were arranged in a vacuum chamber at equal intervals. By applying a DC voltage (V_d) and a high-frequency AC voltage ($V_i \cos \omega t$; where ω is the high frequency), a rapidly changing electric field was generated in the quadrupole. The parameters U , V , and ω were adjusted so that ions within a specific range of m/z entered a stable oscillation state, passed through the quadrupole, and reached the detector. The ions of interest passed through the quadrupole field, whereas the others were expelled. An ion trap system based on the quadrupole principle was recently adopted.

The ions generated in the ionization section are accelerated by a high acceleration voltage (10–30 kV) and fly at a constant speed through a drift region without an electric field. As the ions reached a constant flight distance, ions with lower m/z values arrived at the detector earlier, whereas ions with higher m/z values arrived later. This time difference can be converted into a mass difference, allowing the generation of a mass spectrum.

2.7 Collision-induced dissociation (CID)

The ions selected by the first mass analyzer were fragmented into smaller ions through CID in the collision cell. This process involves accelerating the ions and colliding them with an inert gas. The resulting fragment ions varied depending on the cleavage of the peptide bonds among the amino acids constituting the protein. Fragment ions were named based on the position of the cleavage bond, with those containing the N-terminus referred to as a, b, and c ions. Those containing the C-terminus were referred to as x, y, and z ions (see the below chemical structure formula in **Figure 3**; R_1 , R_2 , and R_3 indicate alkyl groups). Because the spectrum contains a variety of fragment ions, it is crucial to accurately distinguish these ions and determine the amino acid sequence based on the mass differences among adjacent homoserine ions.

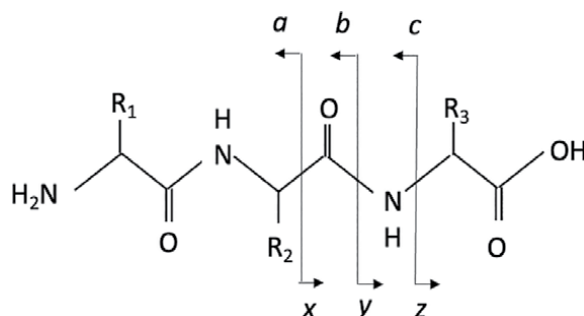


Figure 3.
Type of ions due to fragmentation by the collision.

2.8 Second mass filter (MS2)

The resulting fragment ions were passed into a second mass analyzer to separate the ions based on their m/z values. The second stage of MS was used to analyze the fragments. The resulting spectra provided information on the amino acid sequence of the peptide. Each step of the mass filtering, coupled with an identification method involving two stages of mass filtering after LC, is referred to as LC-MS/MS.

2.9 Detection

Finally, the ions are detected, usually using an electron multiplier, and their abundance is measured. This information was used to create a mass spectrum for analysis. Peptide sequences were identified from the MS/MS spectral information and matched against an amino acid sequence database. Proteins were deduced based on the protein sequences to which the peptide sequences were assigned.

3. Data preprocessing

The false discovery rate (FDR) is often calculated and evaluated to assess the reliability of an analysis. In this method, reverse sequences (decoy sequences) with reversed amino acid sequences were intentionally included in the protein database for identification, allowing for the determination of the number of incorrectly identified decoy sequences. FDR is calculated as $[(\text{the number of identified decoy sequences} \times 2) \div (\text{the total number of identified sequences})]$. The desired FDR discovery rate was $<1\%$.

In MS, “shared peptide” refers to peptides shared among different proteins. Different proteins may possess similar peptide sequences. Shared peptides are typically excluded from omics data to prevent false positive results. Furthermore, potential contaminants, such as tryptic autolysates, and worker-derived proteins, such as keratin, may be excluded.

Additionally, a correlation analysis between samples using protein profiles obtained from simultaneous extractions is necessary to confirm whether protein extraction was conducted correctly according to the protocol. This analysis is crucial because protein extraction involves multiple steps that can influence experimental conditions. If the correlation coefficient is 0.6 or lower, it indicates a questionable result, which might make proper comparisons among challenging samples.

Our previous studies [3, 11] suggest that the number of identifiable proteins in tissues is approximately 2.0×10^3 . Typically, seven to eight peptide fragments estimate the entire protein. However, to ensure statistical reliability, some proteins may only be identified from a single fragment and were excluded from the identified proteins. Moreover, because these proteins are initially present in low quantities when they emerge as biomarker candidates, they should not be ignored but rather reanalyzed or confirmed using other methods.

Many proteins identified using FFPE samples are metabolic enzymes, chaperones, heat shock proteins, ribosomal components, and immunoglobulins. Tissue-specific collagen and other proteins are also included. Because of the high abundance of these proteins, they should be excluded when considering biomarkers. Various measures are required to prevent contamination. The inclusion of known biomarkers is essential for validating proteomic analyses. In previous reports of myocardial infarction, biomarkers, such as troponin, were required. Confirmation of existing biomarkers is beneficial for validating proteomic analysis. The amount of the analyzed proteins that can be stably and simultaneously extracted include glyceraldehyde 3-phosphate dehydrogenase (GAPDH), commonly used as a control in western blotting. Alternatively, tissue-specific signature proteins could be used as baselines.

3.1 Data visualization

Statistical techniques are generally used to explore biomarkers when the fold change in abundance exceeds a reference value (e.g., 1.5 times) compared with the control group. In the case of clinical samples, wherein abundance does not follow a normal distribution, a volcano plot can be used with a p-value < 0.05 from the non-parametric test on the vertical axis. If a plot corresponding to one protein is far from the others, it may be a candidate biomarker.

When separating the research subject group and the control group, it is possible to reduce dimensionality through principal component analysis (PCA). If the number of cases is small, this analysis can visually confirm how much the two groups are differentiated [11]. After using PCA for dimensionality reduction of the data, a common approach is to apply another method, such as logistic regression or support vector machines, for classification using the principal components. In doing so, the increasing or decreasing trend of each protein must be clear among groups. If a protein consistently shows a decrease in the subject group and an increase in the control group, and there is a significant difference between the two groups, then that protein could be considered a potential biomarker. This can be confirmed using methods, such as immunostaining, for the identified candidates using many cases, such as tissue microarray, which increases the probability that the observation is accurate.

Additionally, by performing network analysis on large-scale protein data, it is possible to conceive the formation of pathological conditions because of the interactions between these proteins. One method for analyzing protein networks is using a STRING program (<https://string-db.org/>), which has been recently utilized. When a robust network is formed, it can provide insights into disease pathology. For example, apoptotic inhibitor proteins may form interconnected networks in the context of the proteins involved in cancer growth. Similarly, networks can also arise among proteins involved in stress responses. Further analysis of these diverse networks will facilitate a deeper understanding of disease pathogenesis. Unlike in genomic analysis, the interactions among expressed proteins are straightforward, allowing for such interpretations.

4. Biomarker search

Biomarker proteins are expected to be released into the blood for testing, have sufficient sensitivity and specificity, and their dynamics must be understood. For example, creatine kinase and troponin are well-known markers of myocardial infarction; these biomarkers are degraded within 24–48 hours and rarely retained for long periods. Information on the localization of the candidate proteins is essential to identify a new biomarker. Examples of localization information include whether it is on the plasma membrane or exists in intracellular organelles, the cytoplasm, the nucleus, or the extracellular matrix. In addition, protein solubility should be determined by the amino acid composition. This includes whether the protein is hydrophilic or hydrophobic and the pH at which the overall charge of a solute or particle is zero (isoelectric point). Finally, the analysis and interpretation of the whole protein obtained, that is, proteomic data, are essential.

Additionally, the discovery of biomarkers related to the physical functions of proteins in pathological tissues, such as the heart, is expected to play a significant role in histopathological diagnosis. Combining proteomics data with immunostaining and phosphotungstic acid-haematoxylin staining has made it possible to obtain diagnostic information with the expertise of pathologists in understanding pathology and capturing morphological changes. The use of FFPE is a powerful approach to the identification of protein biomarkers. However, the protocol for such an analysis has yet to be completely standardized, and although it is feasible, further research is needed. Nonetheless, techniques such as MSI have become possible and hold promise for future advancements in this field.

5. Application of mass spectrometry imaging (MSI) based on time-of-flight mass spectrometry (TOF-MS)

MSI involves sectioning, mounting on a slide glass, dehydrating, and direct matrix deposition on tissue surfaces to promote the ionizing of peptides in tissues, that is, matrix-assisted laser desorption/ionization (MALDI). When a laser irradiates the surface and measures the mass spectrum at each point of the tissue, ions are generated from the sample. Based on the obtained mass spectrum data, the spatial distribution of various molecules can be visualized as a two-dimensional (2D) image (**Figure 3**).

5.1 Matrix chemistry

A matrix is a small molecule with aromatic rings (**Figure 4**). The reasons why structures with aromatic rings are favored as matrices include the following:

1. Crystallization: Matrices with aromatic rings tend to form homogeneous crystals with high reproducibility, enhancing the reproducibility and resolution in MS.
2. Strong ultraviolet (UV) absorption: Aromatic rings demonstrate strong UV absorption because of π - π^* transitions. DHB (2,5-dihydroxybenzoic acid) primarily absorbs in the 337 nm UV range, corresponding to the emission of nitrogen lasers.
3. Rapid energy transfer: The matrix efficiently absorbs the laser energy and rapidly transfers this energy to the analyte molecules. During this process, the energy levels of the peptides increase, and the activation energy for ionization reactions

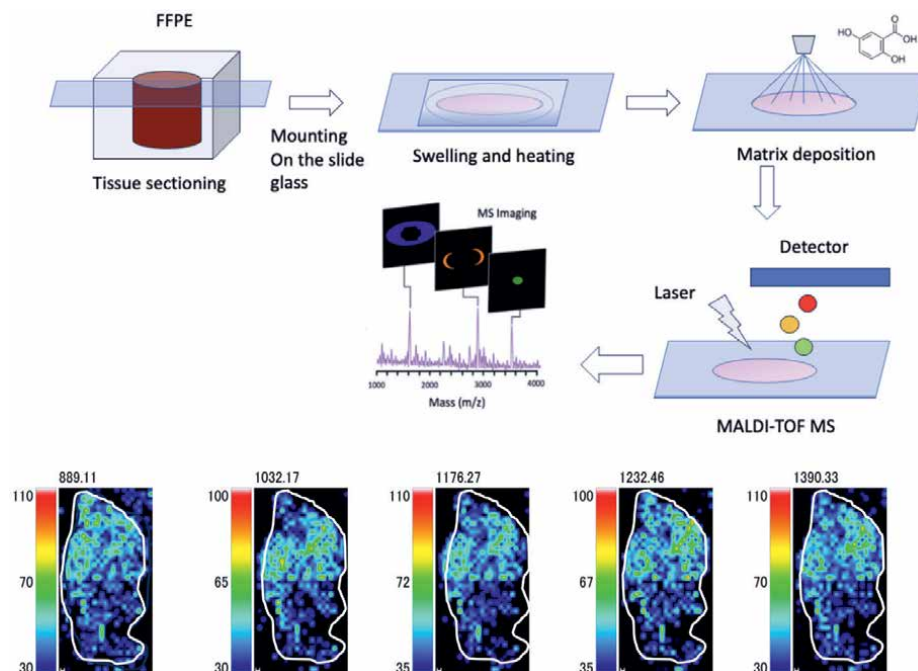


Figure 4.

Scheme of matrix-assisted laser desorption/ionization time-of-flight (MALDI-TOF) mass spectrometry imaging (MSI). Following the deposition of the matrix (DHB: 2,5-dihydroxybenzoic acid), a laser was used to ionize the peptides, and an electric field was applied until they reached the detector. The ionized peptides were separated based on mass-to-charge ratio (m/z) values, and the spectrum revealed a two-dimensional (2D) distribution of the peptides within the tissues. For each laser shot, a full mass spectrum is recorded. Thus, there is a corresponding mass spectrum for each pixel position on the tissue. The laser in the instrument systematically raster scans the entire tissue section. At each raster position (pixel), the laser desorbs and ionizes the molecules, which are then detected by the time-of-flight (TOF) mass analyzer. The photos in **Figure 4** depict the MSI of the neuron-related nestin protein in glioblastoma tissue [6]. The number above each image represents the m/z values corresponding to the protein. The outline demarcates the margin of the tissue, and the color heatmap indicates the signal intensity of the MSI. In these images, the upper portion of the tissue shows a higher intensity, corresponding to a greater abundance in areas with a higher tumor cell density.

decreases. The role of the matrix is to function as an energy bridge, aiding in the ionization of the peptides. Therefore, the matrix facilitates the protonation (in positive ion mode) or the deprotonation (in negative ion mode) of the peptide.

4. Sample protection: Matrices with aromatic rings protect the analyte molecules from direct laser irradiation. This helps prevent the thermal decomposition of biological molecules, such as proteins and peptides.
5. Ionization assistance: Some matrices are known to have their conjugated aromatic systems involved in the ionization mechanism. For instance, they can assist in ionization via proton transfer (**Figures 5 and 6**).

5.2 Preprocessing of tissue sample

A method was developed for preprocessing tissue samples. This method involves heating the sample in acetone in an acetonitrile aqueous solution (Buffer

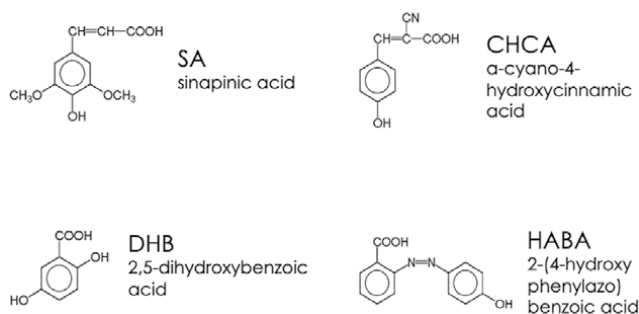


Figure 5.

Representative matrices. The matrix effectively absorbs laser light of a specific wavelength. Most matrices have a chromophore, such as in aromatic rings, which allows the matrix to be electronically excited because of this chemical property.

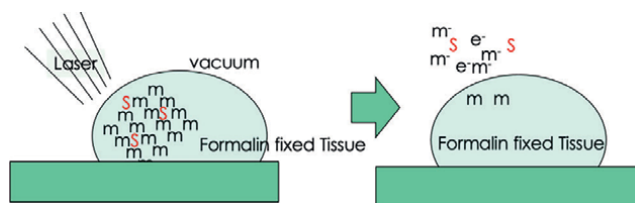


Figure 6.

Matrix-assisted laser desorption/ionization (MALDI). This ionization method utilizes a matrix that absorbs laser energy to generate peptide ions. In MALDI, the matrix and proteins present in the tissue are cocrystallized. Subsequently, during the ionization process, when the matrix is ionized and sublimated, energy is transferred from the matrix to the coexisting peptides, resulting in their ionization.

A, containing acetonitrile and NH_4HCO_3 ; **Figure 7**) and immersing it at 37°C for an extended period to induce swelling and allow the molecules within the solid tissue to move to the surface. This process facilitates efficient interactions between the matrix and laser desorption/ionization, resulting in enhanced sensitivity for MSI. Acquiring such data requires knowledge and techniques of solid-phase surface chemistry rather

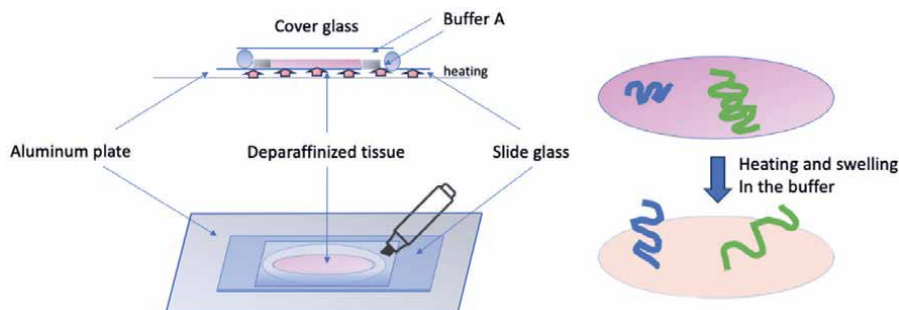


Figure 7.

A PAP pen was used to encircle the tissue on the slide glass. After applying resin around the tissue, the slide was immersed in buffer a. a cover glass was placed on top and secured with a bond. The slide glass was placed on an aluminum plate and heated briefly with enough intensity to produce bubbles, ensuring buffer a to not evaporate from the bottom. The steric structure of proteins becomes loose and fluctuates with heat fluctuations [1].

than those of liquid-phase solutes. Evaporators of the matrix help generate homogeneous “mixed crystals” containing the matrix and peptides on tissue surfaces.

5.3 Matrix application

The matrix is applied to the tissue in order to assist in desorption/ionization. The “co-crystal” of peptides and matrix is a physical state wherein the crystal lattice of the matrix surrounds the proteins and peptides rather than a result of chemical interactions. However, the specifics of this interaction are still not fully understood. The shape and size of the crystal vary depending on factors such as the evaporation rate of the matrix solvent, the type and concentration of the matrix used, the concentration of the peptide, and the condition of the sample surface (which can be assessed by the wetting angle of the matrix solution, i.e., a large angle indicates that the solvent is repelled by the surface, suggesting low wettability or hydrophobicity of the surface). If the sample contains connective fiber components, it may repel the matrix solution, further influencing the outcome. This highlights the importance of the preprocessing step for higher hydrophilicity.

Furthermore, the co-crystals must be more uniform. Techniques such as using iMLayer (by Shimadzu Corporation, Kyoto, Japan) can achieve this. This is where the matrix is heated in a vacuum to sublime and deposited using an automatic deposition device.

5.4 Sample ionization

The peptide in the sample is then irradiated by a laser, leading to desorption and ionization of molecules. An electric field accelerates the ionized molecules into a flight tube. Larger ions take longer to travel through the tube than smaller ions. The time difference between ions is measured and used to determine the m/z values of the ions. In a MALDI device, the sample stage can be designed to move relative to the terminal, ensuring as uniform laser ionization as possible on the sample wherein mixed crystals have formed on the surface. Electrons (e^-), positive matrix ions (M^+), hydrogen atoms (H), and peptide radical species (P) are generated during the initial stages of MALDI when using UV lasers (e.g., nitrogen lasers). The wavelength of the nitrogen laser (337 nm) corresponds to an energy of 3.7 eV per photon. The ionization energy of a single molecule of DHB is 8.0 eV, requiring the absorption of at least three photons.

However, when DHB forms crystals, stacking or clustering occurs, allowing the absorption of just two photons to cover the activation energy. Following the energy absorption, DHB is ionized on the crystal surface. Increasing the irradiation amount of the laser causes more vaporization of the DHB ions with cluster forms. Proton transfer reactions from the ionized DHB to non-ionized DHB occur within this cluster. It is crucial to note that the proton is provided not from the carboxyl group of the DHB side chain but from the hydroxyl group at the 5'-position (**Figure 7**) [14].

The sublimation of the DHB from the solid phase to the gas phase by photon energy and the ionization of the peptide by proton transfer from the DHB in the gas phase in DHB and peptide interactions are represented in **Figure 8**. There is a debate as to whether the peptide is already ionized in the solid phase mixed crystal. As aforementioned, it seems energetically favorable for ionization to occur in the solid phase when DHB clusters accompany the peptide. However, for the ionized peptide to begin flying to the detector, it must not react with surrounding anions and simultaneously be released from the sublimated DHB clusters, requiring a multistep process.

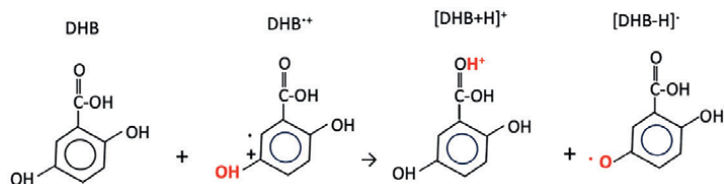


Figure 8.
Matrix ionization. The proton transfer is highlighted in red.

Therefore, ionization is expected to occur at a very low probability; the ion yield in MALDI is estimated to be approximately 10^{-9} to 10^{-8} in terms of the ion/neutral ratio [15].

Another model does not assume pre-ionization of the peptide and accepts a proton from the ionized DHB in the gas phase to ionize. Both mechanisms might occur simultaneously. There is a debate on which mechanism is more dominant [16].

5.5 Image creation

The mass spectra from each discrete location are combined to create an image showing the distribution of specific molecules. Functionally or in pathological conditions, related proteins are expected to have spatial distributions that correlate.

5.6 Resolution

Current MSI techniques have inherent resolution limitations that restrict detailed analysis, particularly at the microtissue or cellular level. Resolutions on the order of 10 microns have been achieved thus far, which is approximately the size of large cells, enabling signal acquisition on a cell-by-cell basis. Ten microns corresponds to the diameter of large epithelial cells and monocytes, and the resolution is sufficient for histological evaluation at the tissue level, for example, cancer invasion range.

5.7 Region of interest (ROI) analysis in mass spectrometry imaging (MSI)

In pathology, immunohistochemistry is the only method to detect protein localization within FFPE pathological specimens. This method confirms known proteins but does not provide data on unknown proteins. In contrast, MSI possesses the potential to comprehensively analyze proteins within tissues, paving its way as an indispensable tool for future pathological research. Furthermore, advancements in artificial intelligence (AI) have enabled the analysis of segmentation impressions on histopathological specimens stained with hematoxylin and eosin, yielding findings consistent with lesions. In pathology, by defining an ROI on images, areas, such as the entire tumor, its background, regions with specific histological characteristics, or around blood vessels, can be predetermined [6]. Direct comparative correlation analysis of signal intensity between the ROI and other regions using MSI has become feasible. This approach has realized the identification of peptide proteins specific to lesions. Nowadays, acquiring images using virtual slides is commonplace, and various image analysis software tools, such as HALO-AI (<https://indicalab.com/halo-ai/>), come equipped with histological analysis functionalities for lesion segmentation and correlation analysis of 2D data within image plots.

6. Hierarchical cluster analysis in MSI

MSI provides detailed image data that reflect the abundance of each m/z at specific coordinates on tissue samples. Essentially, this data can be represented as a mathematical matrix, enabling the computation of signal distribution distances using matrix operations.

One powerful analytical technique applied to this data is hierarchical cluster analysis. This method groups observations within a dataset into a tree-like structure called a dendrogram (**Figure 9**). Observations or proteins that showcase similar 2D distribution patterns on this dendrogram are positioned close to each other. This closeness suggests potential functional and pathological relationships between these proteins.

Among the techniques for hierarchical cluster analysis, Ward's method stands out. It initially views the signal intensity value of each pixel in an image for a single m/z as a distinct cluster. As the clustering progresses, it combines clusters to minimize the increase in variance stemming from this integration. The primary objective is to ensure strong cohesion within each cluster while maintaining clear distinctions between different clusters.

When hierarchical cluster analysis is performed on the 2D plot distribution pattern from MSI data, it is possible to identify proteins with similar spatial distributions. A noteworthy application of this was showcased by Hiratsuka et al., who found a correlation between the signal distribution patterns of glial fibrillary acidic protein (GFAP) and those of tubulin/histones in glioma [6]. GFAP, an intermediate filament protein, is predominantly found in astrocytes, a specific type of glial cell in the central nervous system. It is used in neuropathology as a diagnostic marker to identify astrocytic cells and differentiate astrocytic tumors from other brain tumor types. The identified correlation between GFAP and tubulin/histones points to the possible roles these proteins play in brain tumor pathology and development.

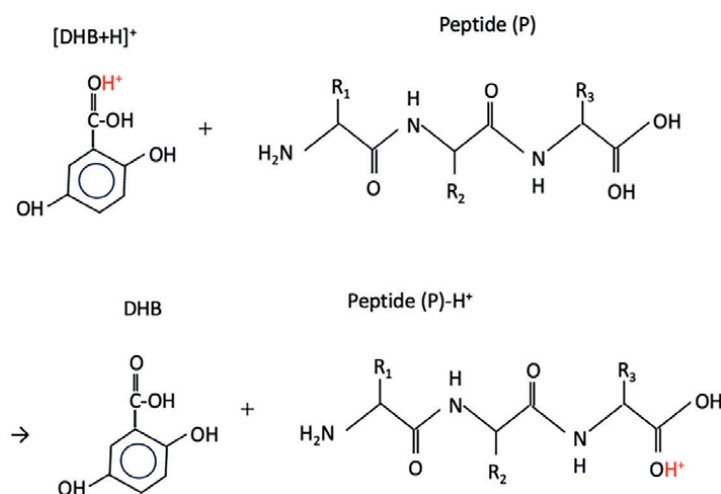


Figure 9.
Peptide ionization by the transfer of a proton ion from ionized 2,5-dihydroxybenzoic acid (DHB).

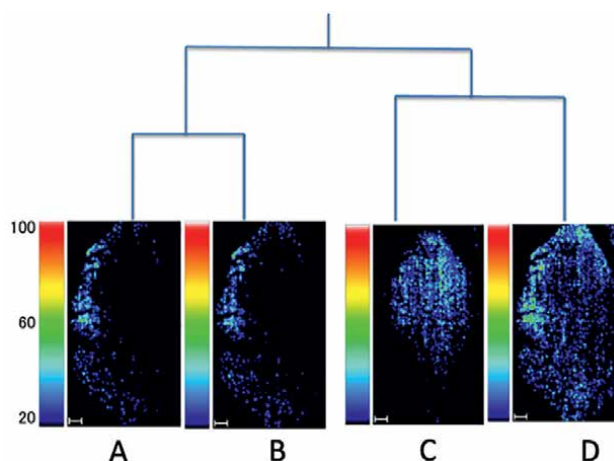


Figure 10.

Dendrogram illustrating hierarchical clustering based on matrix-assisted laser desorption ionization time-of-flight (MALDI-TOF) mass spectrometry imaging patterns, facilitating histopathological correlation analysis among proteins. The height at which two branches merge in the dendrogram represents the distance between two data points or clusters. The similarity in the distribution pattern between A and B is greater than that between C and D, indicating that A and B cooperate more closely in function than C and D.

Furthermore, glioblastomas exhibit frequent hemorrhaging. Research suggests that the spatial distribution of hemoglobin subunits is closely associated with this characteristic. This observation underscores the value of MSI data, providing invaluable insights into the pathological conditions and characteristics of various diseases, such as glioblastomas (Figure 10) [6].

7. Conclusions and future perspective

MS studies of FFPE pathological specimens are expected to be powerful tools for analyzing pathophysiology. Correlative analysis of proteins using general LC-MS and protein abundance using MSI and histological findings can provide valuable insights.

MSI of FFPE specimens can be combined with spatial biology methods, such as analyzing the spatial distribution of mRNA in gene expression, enabling more detailed pathological analysis. This approach integrates multiple data sources to build a multimodal database that facilitates statistical analysis. Therefore, MS is expected to become an increasingly powerful tool for identifying biomarkers.

Acknowledgements

We thank Takushi Yamamoto and Hideshi Fujiwake of the Shimadzu Corporation for their advice.

Conflict of interest

The authors declare no conflict of interest.

Acronyms and abbreviations


DHB	2,5-dihydroxybenzoic acid
ESI	Electrospray ionization
FFPE	Formalin-fixed paraffin-embedded
LC	Liquid chromatography
LC-MS/MS	Liquid chromatography-tandem mass spectrometry
MALDI-TOF	Matrix-assisted laser desorption ionization time-of-flight
MS	Mass spectrometry
MSI	Mass spectrometry imaging

Author details

Takuya Hiratsuka and Tatsuaki Tsuruyama*
Department of Drug Discovery Medicine, Medical Innovation Center, Kyoto
University Graduate School of Medicine, Kyoto, Japan

*Address all correspondence to: tsuruyam@kuhp.kyoto-u.ac.jp

IntechOpen

© 2024 The Author(s). Licensee IntechOpen. This chapter is distributed under the terms of the Creative Commons Attribution License (<http://creativecommons.org/licenses/by/3.0>), which permits unrestricted use, distribution, and reproduction in any medium, provided the original work is properly cited. 

References

- [1] Kakimoto Y, Tsuruyama T, Yamamoto T, Furuta M, Kotani H, Ozeki M, et al. Novel in situ pretreatment method for significantly enhancing the signal in MALDI-TOF MS of formalin-fixed paraffin-embedded tissue sections. *PLoS One*. 2012;**7**(8):e41607. DOI: 10.1371/journal.pone.0041607
- [2] Yajima Y, Hiratsuka T, Kakimoto Y, Ogawa S, Shima K, Yamazaki Y, et al. Region of interest analysis using mass spectrometry imaging of mitochondrial and sarcomeric proteins in acute cardiac infarction tissue. *Scientific Reports*. 2018;**8**(1):7493. DOI: 10.1038/s41598-018-25817-7
- [3] Kakimoto Y, Ito S, Abiru H, Kotani H, Ozeki M, Tamaki K, et al. Sorbin and SH3 domain-containing protein 2 is released from infarcted heart in the very early phase: Proteomic analysis of cardiac tissues from patients. *Journal of the American Heart Association*. 2013;**2**(6):e000565
- [4] Kakimoto Y, Tsuruyama T, Miyao M, Abiru H, Sumiyoshi S, Kotani H, et al. The effectiveness and limitations of triphenyltetrazolium chloride to detect acute myocardial infarction at forensic autopsy. *The American Journal of Forensic Medicine and Pathology*. 2013;**34**(3):242-247. DOI: 10.1097/PAF.0b013e31828879cd
- [5] Tsuruyama T, Kakimoto Y. Forensic diagnosis of acute myocardial infarction: Application of mass spectrometry. *International Journal of Forensic Science & Pathology*. 2014;**2**(8):1-5. DOI: 10.19070/2332-287X-1400018
- [6] Hiratsuka T, Arakawa Y, Yajima Y, Kakimoto Y, Shima K, Yamazaki Y, et al. Hierarchical cluster and region of interest analyses based on mass spectrometry imaging of human brain tumours. *Scientific Reports*. 2020;**10**(1):5757. DOI: 10.1038/s41598-020-62176-8
- [7] Kiso K, Yoshifuji H, Oku T, Hikida M, Kitagori K, Hirayama Y, et al. Transgelin-2 is upregulated on activated B-cells and expressed in hyperplastic follicles in lupus erythematosus patients. *PLoS One*. 2017;**12**(9):e0184738. DOI: 10.1371/journal.pone.0184738
- [8] Miyagawa-Hayashino A, Yoshifuji H, Kitagori K, Ito S, Oku T, Hirayama Y, et al. Increase of MZB1 in B cells in systemic lupus erythematosus: Proteomic analysis of biopsied lymph nodes. *Arthritis Research & Therapy*. 2018;**20**(1):13. DOI: 10.1186/s13075-018-1511-5
- [9] Salah A, Yoshifuji H, Ito S, Kitagori K, Kiso K, Yamada N, et al. High expression of galectin-3 in patients with IgG4-related disease: A proteomic approach. *Pathology Research International*. 2017;**2017**:9312142. Epub 2017/06/09. DOI: 10.1155/2017/9312142
- [10] Hiratsuka T, Yamamoto T, Yoshizawa A, Toyokuni S, Tsuruyama T. RhoA and vigin are candidates for immunohistochemical markers for epithelioid malignant mesothelioma. *Scientific Reports*. 2022;**12**(1):18519. DOI: 10.1038/s41598-020-62176-8
- [11] Tayri-Wilk T, Slavin M, Zamel J, Blass A, Cohen S, Motzik A, et al. Mass spectrometry reveals the chemistry of formaldehyde cross-linking in structured proteins. *Nature Communications*. 2020;**11**(1):3128. DOI: 10.1038/s41467-020-16935-w
- [12] Ramos-Vara JA, Miller MA. When tissue antigens and antibodies get

along: Revisiting the technical aspects of immunohistochemistry—The red, brown, and blue technique. *Veterinary Pathology*. 2014;**51**(1):42-87. DOI: 10.1177/0300985813505879

[13] Hiratsuka T, Sakai IS, Yokose T, Endo T, Daigo Y, Miyagi Y, et al. Proteome analysis of CD5-positive diffuse large B cell lymphoma FFPE tissue reveals downregulation of DDX3X, DNAB1, and B cell receptor signaling pathway proteins including BTK and immunoglobulins. *Clinical Proteomics*. 2023 [In press]

[14] Knochenmuss R. The coupled chemical and physical dynamics model of MALDI. *Annual Review of Analytical Chemistry* (Palo Alto Calif). 2016;**9**(1):365-385. DOI: 10.1146/annurev-anchem-071015-041750

[15] Lu IC, Chu KY, Lin CY, Wu SY, Dyakov YA, Chen JL, et al. Ion-to-neutral ratios and thermal proton transfer in matrix-assisted laser desorption/ionization. *Journal of the American Society for Mass Spectrometry*. 2015;**26**(7):1242-1251. DOI: 10.1007/s13361-015-1112-3

[16] Takayama M. Understanding of the mechanism of matrix-assisted laser desorption/ionization. *Journal of the Mass Spectrometry Society of Japan* (In Japanese). 2016;**64**(5):1-5. DOI: 10.11477/mf.2425101590

Section 3

Applications

Harnessing Electron Microscope for Trace Evidence Analysis

Niha Ansari, Jeet Dasgupta, Shweta Umre and Priya Rajput

Abstract

Trace evidence analysis is essential in criminal investigations as it provides vital information for establishing connections between suspects and scenes. Minute or complicated trace evidence is sometimes difficult for traditional microscopic techniques to handle. At micro- and nanoscale, electron microscopy (EM) shows great promise as a potent technique for characterization and visualization. Scanning electron microscopy (SEM) and transmission electron microscopy (TEM) offer valuable insights into morphology, chemical composition, and crystalline structure of trace evidence, enabling the identification and differentiation of similar materials. TEM allows high-resolution examination of paint components, dirt particles, gunshot residues (GSR), fibers, hair structures, glass shards, nano-particles, explosive materials, etc. In forensic investigations, SEM is a crucial instrument, especially when it comes to GSR analysis, which uses SEM to correlate bullets to firearms more successfully than visual approaches. Additionally, SEM plays a major role in the examination of gemstones and jewelry by identifying manufactured and natural gems, analyzing surface imperfections, and determining elemental compositions. SEM also improves forensic inspection in non-conductive material analysis, paint and fiber analysis, filament bulb investigations, handwriting analysis, and counterfeit detection. The adoption of EM in forensic trace evidence analysis has potential to revolutionize the field, offering valuable insights that were previously unattainable.

Keywords: forensic trace evidence, criminal investigations, electron microscopy (EM), transmission electron microscopy (TEM), scanning electron microscopy (SEM)

1. Introduction

Throughout human history, crime has been a persistent aspect of society, harming people, animals, and entire communities. It is interesting to note that great minds focused on this mystery in the late nineteenth century, which is when the scientific study of criminal phenomena started to gain traction. This led to the creation of the field of forensic science, an applied discipline that is seamlessly incorporated into a society's legal framework and serves the dual purposes of providing justice to victims of crime and understanding the motivations behind the actions of those who commit it to discourage such evil deeds within the community. In the wake of the renowned forensic scientist Sir Edmond Locard, who famously declared that "every contact leaves a trace," a crucial advancement in forensic science arose: the identification and

application of trace evidence. This type of evidence plays a crucial role in forensic analysis because it provides important information about the presence or absence of people and things at crime scenes, illuminating the complex network of relationships that connects the criminal act to its surroundings.

Every contact contains trace evidence, and the crucial question is how much our scientific knowledge can identify and track these minute remnants. What is just as important is the competence of the people using the technology; they need to be able to predict the kinds of traces that could be found.

Scientific progress, combined with the use of a wide range of instrumental methods, has greatly improved the ability to perform in-depth analyses of traces of evidence. Notably, in this dynamic environment, electron microscopy technology arises as a revolutionary instrument, providing hitherto unseen accuracy and understanding into the micro-scale realm of trace evidence.

The first electron microscope was invented in 1931 by Ernst Ruska and Max Knoll, two University of Berlin physicists and electrical engineers, respectively. This prototype was the first to demonstrate what could be done with electron microscopy, producing a 400-power magnification [1].

Ten years later, Ruska developed a comparable but distinct method that delivered information about the topography and composition of a sample by scanning its surface in a rectangular pattern with a focused electron beam. In contrast to TEM, the new scanning electron microscope's (SEM) image was produced after the instrument gathered and tallied the dispersed electrons.

Many believe that the introduction of the digital microscope by Japanese scientists in 1986 transformed the field of microscopy. They devised a method for moving the image from the microscope to a computer so that it could be examined right away. These days, high-resolution monitors are integrated into microscopes, so viewing images does not require an extra computer [2].

Fibers, hairs, glass shards, paint chips, soil particles, plants, insects, gunshot residue, and more can be included in this category. By connecting these items to certain sources or people, trace evidence analysis seeks to provide important details for criminal investigations [3]. With its unmatched resolution and extraordinarily high magnification powers, electron microscopy is a technological marvel when it comes to trace evidence examination. This sophisticated technique, in contrast to traditional optical microscopy, reduces material distortion commonly associated with sample preparation, maintaining the integrity and fidelity of the materials under examination. Furthermore, the use of electron microscopy makes it possible to examine specimens at different strata and to investigate a wider depth of field. This function plays a crucial role in revealing minute details and nuanced aspects within the trace evidence, offering priceless insights for forensic analyses and contributing to a thorough comprehension of the evidentiary landscape [4].

The minute number and exquisite structure of these evidential elements present a major difficulty for laboratory analysis and research employing trace evidence. It is now essential to use electron microscopes to address this problem. Because of the incredibly small size and complex structure of these materials, conventional methods may not be able to reach the precise visualization and analysis that this sophisticated equipment enables when examining trace evidence at the micro- and nanoscales.

The study of trace evidence presents difficulties because the evidence is complex and does not lend itself to standard microscopic procedures. These difficulties include low resolution, complicated evidence (e.g., nanoparticles or intricate fiber structures), and the incapacity to identify minute characteristics that are essential

for differentiating between materials and connecting evidence to crime scenes. Nevertheless, electron microscopy (EM), particularly scanning electron microscopy (SEM) and transmission electron microscopy (TEM), skillfully handles these difficulties. Excellent high-resolution imaging capabilities provided by EM methods allow the viewing of minuscule details, even at the nanoscale. Furthermore, EM enables thorough characterization of traces, supporting material analysis, identification, and differentiation according to elemental composition, morphology, and structure. By facilitating the identification of minute details and minute variations between materials, the improved discriminating power of EM considerably advances forensic investigation by offering crucial insights into the nature and provenance of trace evidence.

In this chapter, we examine a number of situations in which the application of electron microscopes to the examination of trace evidence provides not only improved structural analysis but also special chances to examine characteristics that are not accessible through conventional microscopy techniques. The utilization of electron microscopes facilitates a comprehensive analysis at the micro- and nanoscales, offering unmatched clarity and permitting the discovery of minuscule structural subtleties and more minute details that were previously unobservable by traditional microscopic methods.

The first section of the chapter covers the definitions of electron microscopes (EM) and the essential structural elements that are present in transmission electron microscopes (TEM) and scanning electron microscopes (SEM). From the second section, a methodical investigation into the various domains in which TEM finds application is then undertaken. The second section carefully explains the use of TEM in paint analysis, soil analysis, gunshot residue (GSR) characterization, fiber and hair structure clarification, glass analysis, and nanoparticle scrutiny. After that, in the third section, the story shifts to a detailed examination of SEM applications. In particular, thorough research is conducted into the critical role that SEM plays in GSR analysis, firearm identification, gemstone investigation, paint and fiber analysis, and filament bulb scrutiny. The final and last section of the chapters deals with a through summery of the key learning.

This chapter delves into the complex and subtle uses of TEM and SEM in several fields of trace evidence analysis using a thorough scientific methodology.

1.1 Electron microscope

Currently, one of the most important tools for evaluating the surface or internal structure is electron microscopy (EM), which has a greater resolution than light microscopy (LM) since it creates images using an accelerated electron beam rather than photons. Electron beams can identify tiny structures because their wavelengths are smaller than those of visible light. To reduce electron beam scatter, conventional electron microscopy operates at high vacuum (10^{-5} – 10^{-7} Pa).

Two primary types of electron microscopy techniques are employed: scanning electron microscopy (SEM) and transmitted electron microscopy (TEM). SEM and TEM have different principles and resolutions, and the information obtained by both methodologies complements each other [5].

1.2 Scanning electron microscope (SEM)

Using a thermal electron source, the scanning electron microscope (SEM) (**Figure 1**) projects a high-energy electron beam (100–30,000 eV) onto an object. Through the use of lenses, the spot size is reduced to less than 10 nm to accomplish fine

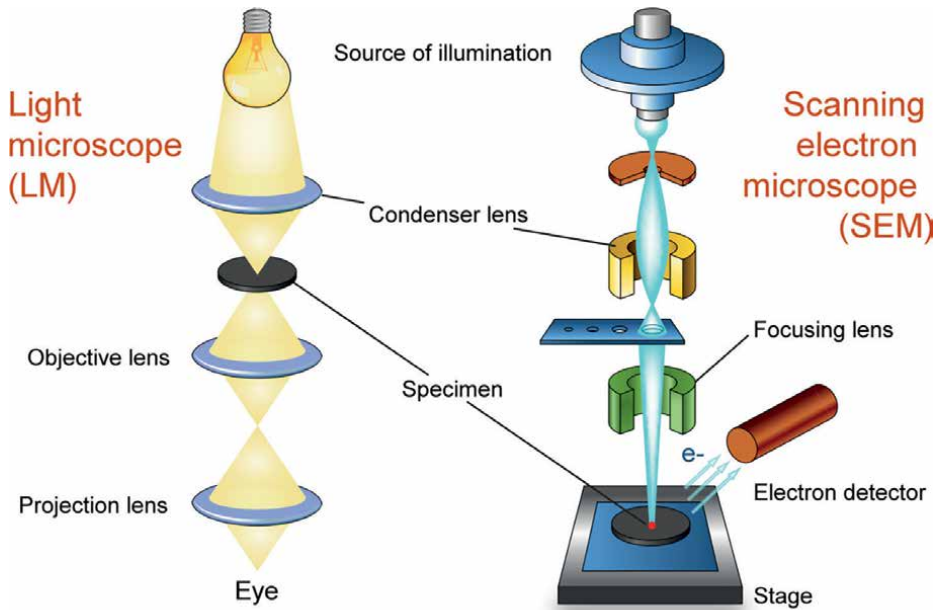


Figure 1.
Parts of scanning electron microscope [6].

imaging. Electrons generate signals for picture creation by penetrating the specimen up to 1 μm . Using scan coil movements that change depending on the necessary magnification, the SEM creates an image point by point. Signals generated by electrons are detected by electron detectors; backscattered electrons (BSE) and secondary electrons (SE) are employed in imaging. The degree of surface or inner sample features is determined by the electron voltage mode; greater voltages penetrate deeper and reveal more surface information. The SEM offers a three-dimensional picture that highlights the topography of the sample, which is influenced by the surface's degree of inclination [7].

1.3 Transmission electron microscope (TEM)

In materials research, transmission electron microscopy (TEM) (**Figure 2**) is a useful instrument. It employs thermionic or field emission to release electrons from an electron source, such as a tungsten filament or lanthanum hexaboride (LaB6), that is linked to a high-voltage source. Upper TEM lenses shape the released electrons into an electron probe, and they can be manipulated by applying magnetic and electrostatic fields. Condenser lenses, objective lenses, and projector lenses make up TEM optics, which allow for variations in magnification through the manipulation of current flow. To display images, one uses an imaging device, such as a phosphor screen. TEM works in a low-pressure setting to improve the clarity of the electron path. Sample grids are supported by specimen stages, while electron beams are produced and managed by electron cannons. Electromagnetic coils are used in electron lenses for electron path correction and focus. Electron beams are selectively filtered by apertures to enhance imaging quality. The methods used for sample preparation—which include grid deposition and fixation for biological samples—depend on the materials and data needed [9].

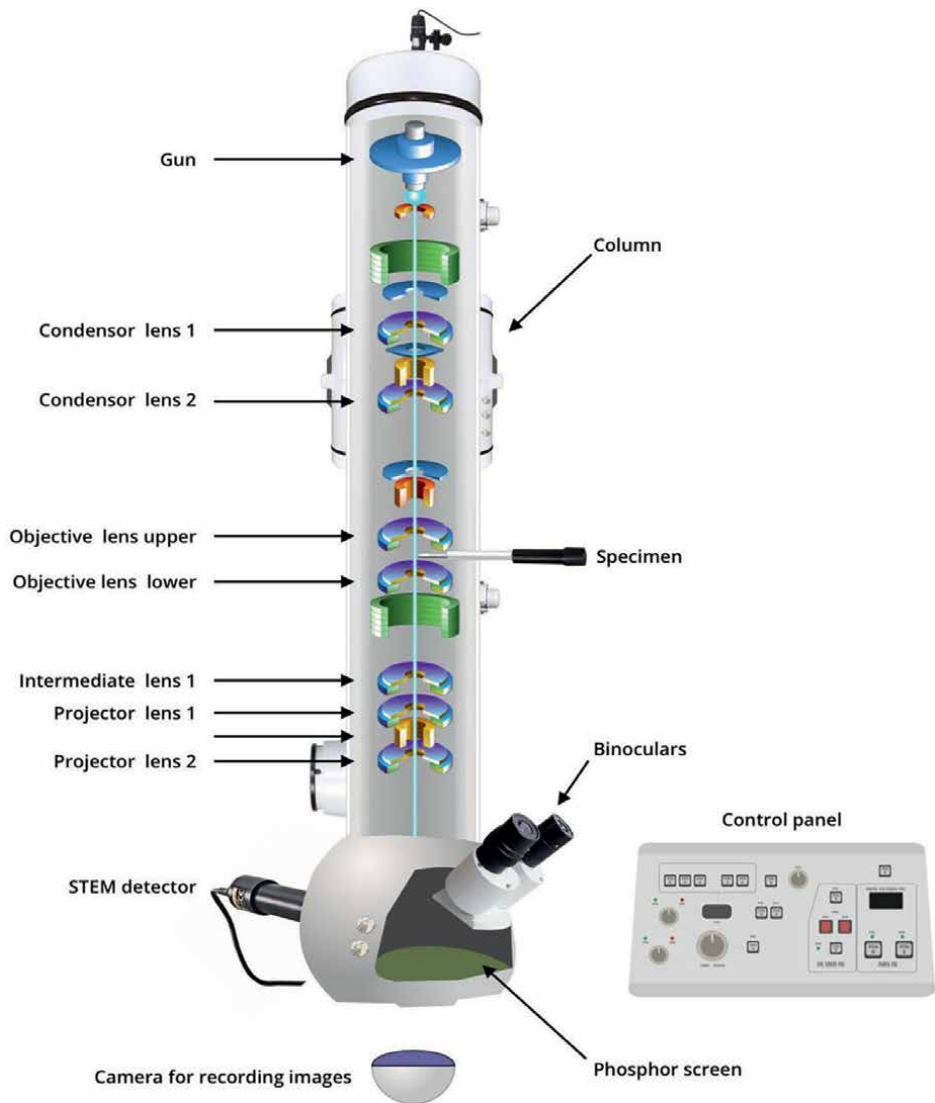


Figure 2.
Parts of transmission electron microscope [8].

2. Sample preparations

2.1 Transmission electron microscope (TEM)

2.1.1 General preparation

Preparing the specimen for TEM visualization: In order to facilitate visualization and produce a crisp image, the specimen to be examined under the TEM needs to go through a certain preparation process.

- On solid materials, electrons are readily absorbed and dispersed, resulting in poor visibility for thick specimens. For accurate and clear vision that also forms a

crisp image, very thin specimens are used. The specimen should have a diameter of 0.025–0.1 nm and a thickness of roughly 20–100 nm, or as small as a bacterial cell. Thin specimens are able to preserve their inherent structure while interacting with electrons in a vacuum.

- The specimen is initially fixed on a plastic surface using glutaraldehyde or osmium tetroxide in order to obtain thin-slice specimens. These chemical substances preserve the cell's uniqueness while stabilizing its structure. When an organic solvent, such as alcohol, is added, since ethanol will totally dry out the cell, it is necessary to embed the specimen in the plastics.
- After that, the specimen is permeated with unpolymerized liquid epoxy plastic, which solidifies it into a block. This is the area where thin sections are cut with a glass knife and an ultramicrotome, a piece of specialized equipment.
- Subsequently, the material is suitably dyed (using the suitable stain) to ensure consistent electron dispersion. After that, the thin sections are immersed in heavy metallic substances such as uranyl acetate and lead citrate, which enable the lead and aluminum ions to bond to the arrangements of cells. To improve contrast, this creates an opaque coating to block the electrons on the cell structures.
- After staining, the thin pieces are put on copper grids so they can be seen. Negative staining combined with a strong metallic element coating is the main staining approach used for TEM viewing. The study of bacterial and viral cell morphologies and structures is facilitated by the metallic coating's ability to scatter electrons, which show up on the photographic film in uncoated portions.

2.1.2 Freeze-itching treatment

- Unlike chemical fixation, dehydration, and embedding, freeze-itching is specifically employed for the treatment of microbial cells in order to minimize the potential risks of artifacts.
- Microbial cell organelles receive a unique treatment called freeze-itching, where the specimens are prepped with liquid nitrogen and subsequently heated at -100°C in a vacuum chamber. This is the process when the majority of specimens become contaminated.
- The parts are then cut in liquid nitrogen at -196°C using a knife that has been precooled. The sectioned specimen can be covered with platinum and carbon layer-forming replicas after being heated in a high vacuum for roughly 2 minutes.
- These can then be examined under a TEM, which shows the cell's inside architecture in greater detail in three dimensions. This phase of liquid nitrogen therapy is referred to as "freeze-itching."

2.2 Scanning electron microscope

2.2.1 Scrubbing the specimen's surface

It is critical to thoroughly clean the sample's surface because it may include a range of undesirable deposits, such as silt, dust, detritus, media elements, or other pollutants, contingent upon the origin of the biological material and any experiment that might have been carried out before the fabrication of the SEM specimen.

2.2.2 Maintaining the specimen's stability

Fixatives are usually used for stabilization. Fixation can be accomplished through perfusion, for instance, by employing a variety of fixatives, such as aldehydes, osmium tetroxide, tannic acid, or thiocarbohydrazide, *via* microinjection, immersions, or vapors.

Rinsing the specimen: Following the fixation phase, samples need to be rinsed to get rid of extra fixative.

2.2.3 Dehydration the specimen

It is imperative that a biological sample be dehydrated with extreme caution. Either a graded series of acetone or ethanol is usually used for it.

2.2.4 Mounting the specimen

The samples need to be mounted on a holder that can be placed inside the scanning electron microscope once they have been cleaned, fixed, washed, dehydrated, and dried according to the proper technique. Usually, the double-stick tape is used to mount samples on metallic (aluminum) stubs. Prior to attaching the specimen, the investigator must determine the optimal orientation for it on the mounting stub. Reorienting the sample proves to be challenging and may cause serious harm.

2.2.5 Coating the specimen

By transporting the charge to the ground, the coating increases the specimen's conductivity under the scanning electron microscope and inhibits the accumulation of high-voltage charges on it. Usually, specimens have a thin layer of conductive metal (such as platinum, gold-palladium, or gold) covering them, ranging from 20 to 30 nm. Since they are all conductive, metals can be used without any prior treatment. A small layer of conductive material must be applied to the sample in order to make all non-metals conductive. The tool used to accomplish this is known as a "sputter coater." Argon gas and an electric field are used by the sputter coater. The sample is put in a tiny vacuum-shielded chamber.

The atoms become positively charged when argon gas and an electric field remove one of the atoms' electrons.

A negatively charged gold foil then attracts the argon ions. Gold atoms are removed from the gold foil's surface by the argon ions. A thin layer of gold is created on the sample's surface as a result of these gold atoms falling and settling there.

3. Applications of electron microscopy for trace evidence analysis

3.1 Application of transmission electron microscope

The investigation of trace evidence is greatly aided by transmission electron microscopy (TEM), which provides in-depth information at the nanoscale, leading to recognize and describe minuscule particles such as paint bits, fibers, and gunshot residue. The great resolution of TEM makes it possible to determine the chemical and elemental makeup of materials, which facilitates source identification. When it comes to examining fibers, this technique is quite helpful as it provides crucial information that helps connect items to crime scenes. Furthermore, TEM offers tiny details that conventional techniques would overlook, greatly assisting forensic investigations in the evaluation of biological trace evidence, tool marks, and counterfeit materials.

3.1.1 Paint

Forensic investigations in particular heavily rely on transmission electron microscopy (TEM) for paint chip examination. With the ability to give high-resolution images of tiny paint fragments and fine-grained compositional data, TEM can help identify pigments, binders, and layer structures, as shown in **Figure 3**, as well as facilitate material characterization. This analytical method is essential for investigating trace evidence discovered at crime scenes because it provides a way to identify the paint materials' inorganic components with remarkable precision and clarity.

The adhesive factor of paints is an important aspect for its application on any surface, especially automobile surfaces, which are exposed to a lot of environmental factors. In such cases, thermoplastic polyolefins (TPO) are mostly used as an adhesive, but they have poor adhesive properties; to compensate for this, we use chlorinated polyolefins, an extra layer over the TPO layer, and through observation in injection-molded TPO samples, a rich layer of polypropylene (PP layer) is present [10], which can be seen in **Figure 4**.

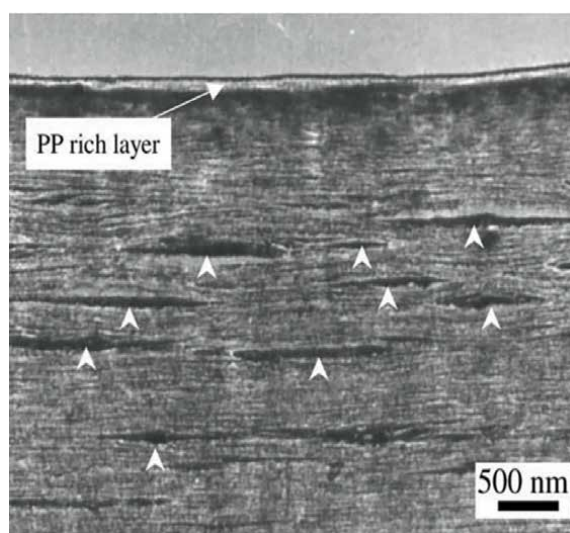


Figure 3.
Three layers of paint [10].

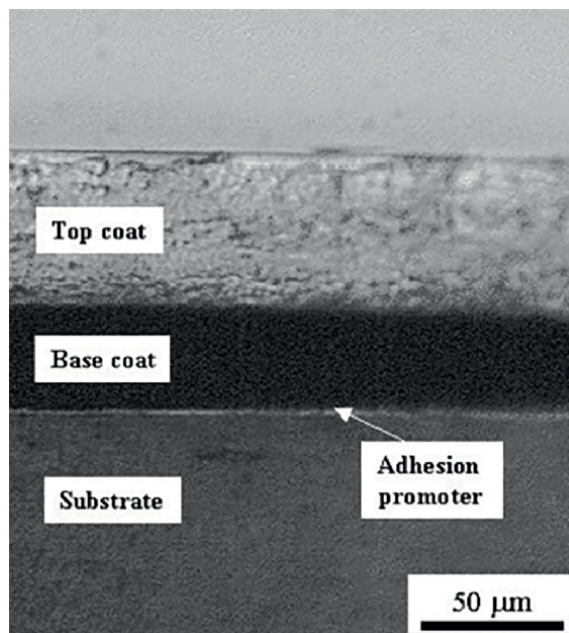


Figure 4.
Polypropylene homo-polymer seen in paint layer under TEM [10].

A study examining paintings from the fourteenth century serves as an example of the usefulness of TEM in analyzing the authenticity of antique paintings. In this instance, the original layer arrangement was preserved, while TEM was used to examine the makeup and structure of paint and base layers. Meticulously manufactured thin micro-samples showed a vivid red paint coat and underlying layers. Major and minor components within these layers were identified by examining individual particles using electron diffraction. The findings showed that gypsum made up the majority of the basal layer, with small amounts of calcite and dolomite. Notably, it was discovered that the paint layer was made entirely of vermilion [11]. But we encounter paint samples mostly in case of car accidents. A lot of work has gone into identifying special characteristics, especially for primers and fillers. TEM is crucial for the assessment of their micromorphology because of its remarkable capacity to reveal minute features. Furthermore, pearl luster pigments such as Iridin and Afflair, which are mostly found in cars manufactured in the United States and Europe, can also be examined using TEM in paint analysis [12].

Additionally, when paint samples are generated with focused ion beam technology, TEM provides useful capabilities for imaging and identifying nanometer-sized particles scattered throughout the surface zone of the samples. This cutting-edge method makes it possible to see and identify particular components, such as lead-rich particles, on a 0.5-micrometer surface area. For tasks that conventional scanning electron microscopy (SEM) and electron probe microanalysis (EPMA) cannot do, TEM's high resolution and specificity make it an invaluable tool [13].

3.1.2 Soil

Soil, being a complex and dynamic material, is an essential trace evidence in criminal investigations. Most soil particles are of a variety of sizes, ranging from

several nanometers to several centimeters. Soil mostly acts as associative evidence in criminal investigation helping us in determining the place from where our person of interest has arrived or where he went. Transmission electron microscopy (TEM) is an indispensable tool for the accurate characterization of tiny soil particles, particularly those with a size between a few nanometers and a few micrometers.

The investigation of crystallographic alterations in terrestrial particles under physicochemical and environmental factors is made easier by TEM. It is essential to comprehend how living things, such as fungi and bacteria, alter the makeup of soil, including the transformation of its elemental chemical forms. Current studies highlight the usefulness of TEM in examining micrometer-scale micro aggregates, offering insights into the impact of microbes on soil function. Soil near the mining area contains a characteristic amount of the mineral present in the soil as nanoparticles, and even in other soil profiles, trace minerals can be found in the soil, which can generate a unique profile for the soil and point us toward the probable source.

TEM makes it possible to qualitatively evaluate the interactions that take place between bacteria and fungus in organo-mineral connections, which include biogenic structures such as bulk soil, the soil-root interface, and casts. This information takes into account the inherent diversity of soil and aids in assessing the state of these microorganisms at the time of sample collection [14, 15], as shown in **Figure 5**.

For a thorough analysis of soil particles magnified more than 100,000 times, transmission electron microscopy (TEM) and scanning electron microscopy (SEM) are also used. TEM and SEM make it possible to use methods like energy-dispersive X-ray spectroscopy to investigate the morphology and chemical composition of particles. These high-resolution techniques are very helpful for analysis and discrimination, greatly advancing our knowledge of pollen spores, minerals found in soil, and fossils—all of which are pertinent to forensic soil study [17].

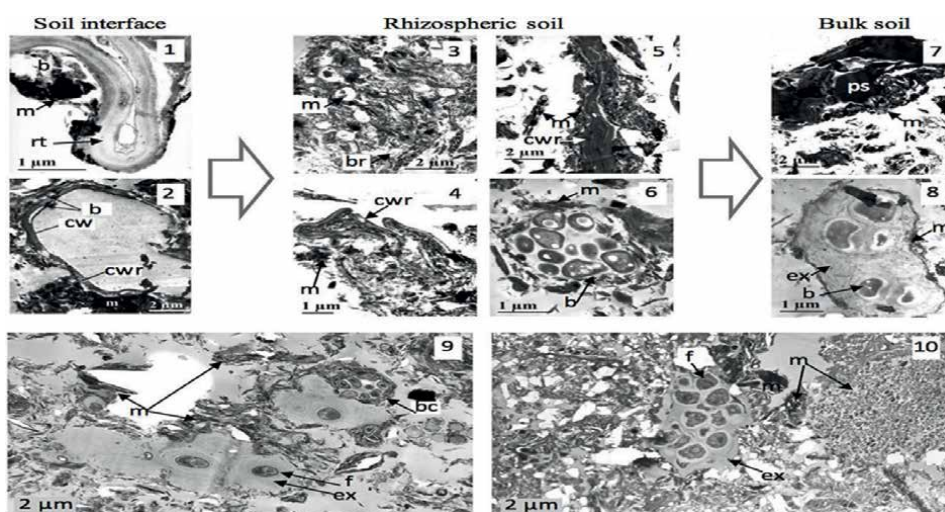


Figure 5. Soil-microorganism interactions at hotspots of biological activity. TEM views (1–8) (soil 4): Micro-aggregation from maize root-soil interface (1, 2) to rhizospheric soil (3–6) and to bulk soil (7, 8) [16].

3.1.3 Gun shot residue (GSR)

Particles created when a firearm is discharged are referred to as gunshot residue, cartridge discharge residue (CDR), or firearms discharge residue. The primer and propellant combustion products will be emitted simultaneously when a cartridge round is shot in a weapon [18]. Gunshot residues are made up of partially and unburned materials, smoke, propellant powder, bullet primer fragments, metals, grease, and lubricants from the cartridge in addition to the actual weapon [19].

According to a scientific study, depending on the type of ammunition, gunshots release sub-micrometer nanoparticles into the environment. About 80 to 94% of the samples were in the nanometer size range, as shown in **Figure 6**.

These tiny particles—particularly gunshot residue (GSR) nanoparticles—could linger in suspension in the atmosphere for as long as 12 hours. GSR nanoparticles are especially significant in forensic investigations because they are more common and persistent than bigger particles. The elemental analysis and high-resolution imaging capabilities of transmission electron microscopy with energy-dispersive X-ray spectroscopy (TEM-EDS) make it an invaluable tool for the analysis of GSR nanoparticles. Future forensic analyses depend on the detection of GSR nanoparticles [21].

TEM can recognize distinctive components that are particular to producers or geographical areas. Gunshot residue (GSR) examination using ammunition manufactured in Brazil revealed that TEM provided a better comprehension of nanoscale particles than SEM [22].

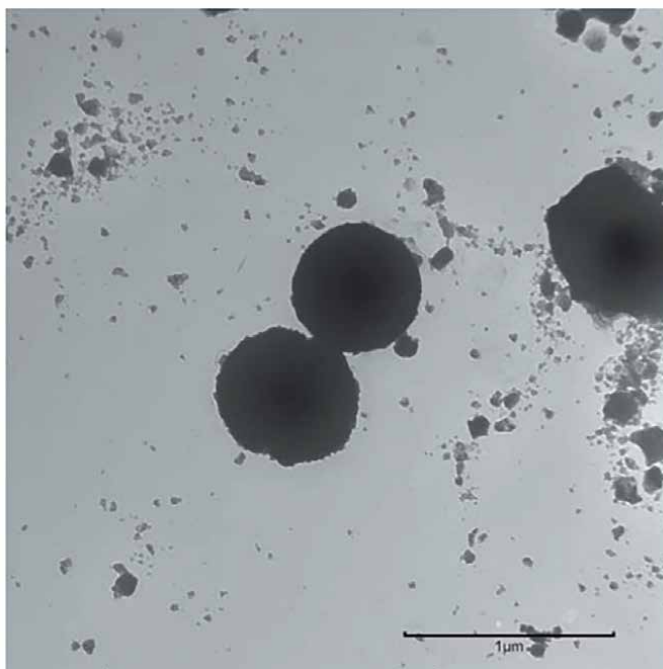


Figure 6.
TEM image of particles collected on the filter during the discharge of one round of S&B ammunition. Scale bar = 1 μm. [20].

3.1.4 Fiber

Another type of trace evidence is fiber, which includes compounds derived from synthetic materials such as rayon and nylon as well as natural sources such as cotton and silk. These fibers often have a major impact on assault and burglary cases. They are useful associative evidence, and it is frequently necessary to examine their distinctive architecture to determine their origins. Although scanning electron microscopy (SEM) is the most commonly used technique for fiber analysis, transmission electron microscopy (TEM) has also shown value in some situations.

It has been found useful where it was found that analytical TEM can be of great application for finding mineral fibers and residues in the lung tissue of the dead, which can be found due to occupational hazards and death due to working in poor health-sanctioned paces [23].

Asbestos fiber has caused some major health issues over the decades, namely asbestosis, carcinoma of the lung (LC), pleural plaques, and malignant mesothelioma (MM). TEM has been useful in identifying it in tissue samples from lungs, which can be useful in case of death due to this reason [23]; it is useful in the study of the orientation of microfibrils present in wooden fiber and other forms of fibers, as shown in **Figure 7**.

3.1.5 Hair

In forensic science, hair follicles are mostly used to get DNA samples, which allows for individualization. Still, these follicles conceal a more profound mystery concerning the coordinated actions of neighboring cells and their complex interaction with our nervous system. The application of the transmission electron microscope's (TEM) potent imaging capabilities becomes essential to revealing this hidden knowledge. Morioka used TEM images in a noteworthy work to interpret the complex cellular structure around hair follicles. This study adds to our understanding of this intricate

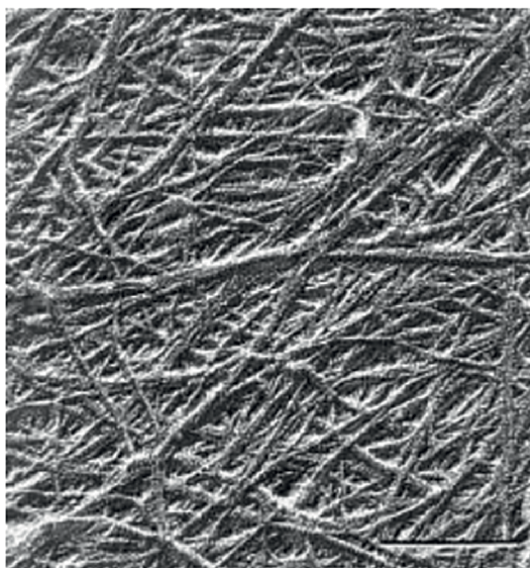


Figure 7.
TEM image of a spruce Kraft pulp fiber surface replica showing the microfibril orientation [24].

biological system by illuminating the previously unknown relationships and dynamics within this milieu [25].

With scanning electron microscopy, the hair shaft is easily visible (SEM). But hair coloring and hair treatments have become common in modern society, which means that these procedures could be sources of personal traits. Such chemical treatments leave the hair structure with characteristic damage patterns and markings. Transmission electron microscopy (TEM) can be a useful tool for studying and characterizing these effects [26]. This bleaching and coloring of hairs are very particular to a trend in certain communities, creating a mass effect and, hence, sometimes can also be used for racial identification, as shown in **Figure 8**.

As bleaching became more severe, leached proteins showed progressive oxidation. Bleached fibers exhibited significant damage to both cuticle layers and the cortex. Even mild bleach treatments led to extensive melanin granule degradation. Protein oxidation primarily affected cortical intermediate filaments, rich in sulfur-containing amino acids, notably the conversion of cystine disulfide bonds to cysteic acid. This data reveals the detrimental impact of bleach on hair structure and proteins, particularly in the cortex [28].

3.1.6 Glass

Glass is an amorphous solid used in various places of our day-to-day life, which includes including building materials from windows to table tops, used in scientific laboratories to our car windshields, and lastly, in our smartphones, glass has become a very common form of trace evidence found on a crime scene.

Glass examination by a forensic scientist may be requested to reconstruct events (e.g., to ascertain whether an exterior or interior window break occurred) or to link an individual or item to the crime scene or a victim. The type of glass involved, whether it is uncommon or common, how accurately it is described, and the

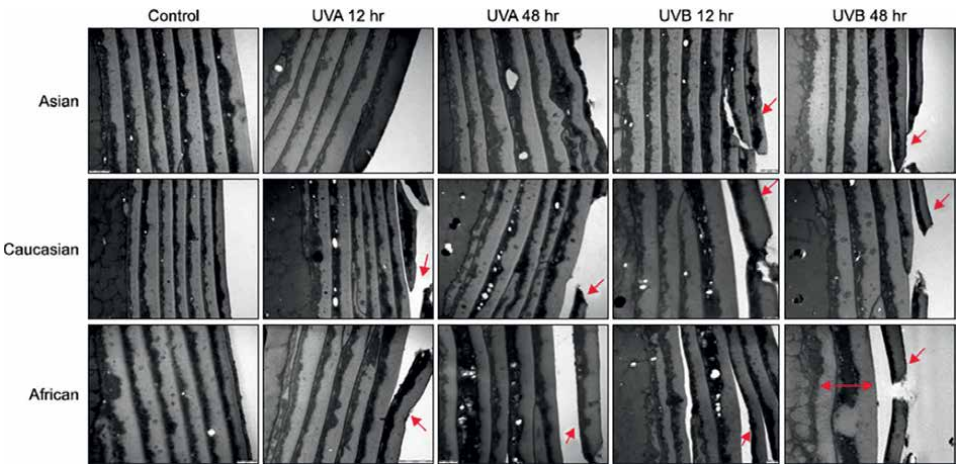


Figure 8. Conventional transmission electron microscopy findings for all hair samples. Ultraviolet B (UVB) irradiation resulted in more damage than UVA irradiation (red arrow). All three groups exhibited similar patterns of damage. However, the African hair exhibited weaker resistance to UV irradiation than the other groups, and the African hair also exhibited a decreased number of cuticle layers than the other groups (red two-way arrow) [27].

background information and comparisons utilized all affect how strong the forensic scientist's view is [29].

Glass samples' interior microstructure, including imperfections, inclusions, and cracks, can be seen *via* TEM. This data is particularly useful in identifying the origin of glass fragments from shootings or hit-and-run incidents. To ascertain the glass's elemental composition, TEM can be used with energy-dispersive X-ray spectroscopy (EDS). Through glass composition analysis, forensic investigators can establish a connection between glass shards discovered at a crime scene and a specific source, like a certain kind of window or bottle. It can also be used to study the delamination of glass bottles, which is a reaction to storing chemicals in them, as shown in **Figure 9**. Using TEM in conjunction with focused ion beam (FIB) milling, forensic scientists can do depth profiling to determine how glass layers were deposited or modified. This can help us learn about the origins and history of a glass sample.

3.1.7 Nanoparticles

The use of nanoparticles as trace evidence in forensic sciences has grown in recent years as a result of improvements in analytical methods and nanotechnology. In forensic science, nanoparticles are used as trace evidence in the following ways:

Characterization of nanoparticles: Other nanoparticles discovered at crime scenes can be identified and characterized using reference materials. Nanoparticles are inspected and categorized according to size, shape, and composition using methods such as transmission electron microscopy (TEM) [31], as shown with silver and gold nanoparticles in **Figure 10**.

The manufacturing and utilization of nanoparticles are both steadily rising. Thus, the characterization of these particles is crucial for investigating their influence on trace evidence analysis, creating a particle database with TEM that offers a reference atlas of the different kinds of particles that might be found during trace evidence investigations in the future. The database, which is continuously updated, includes an image, a selected area electron diffraction (SAED) pattern, and an EDS of several

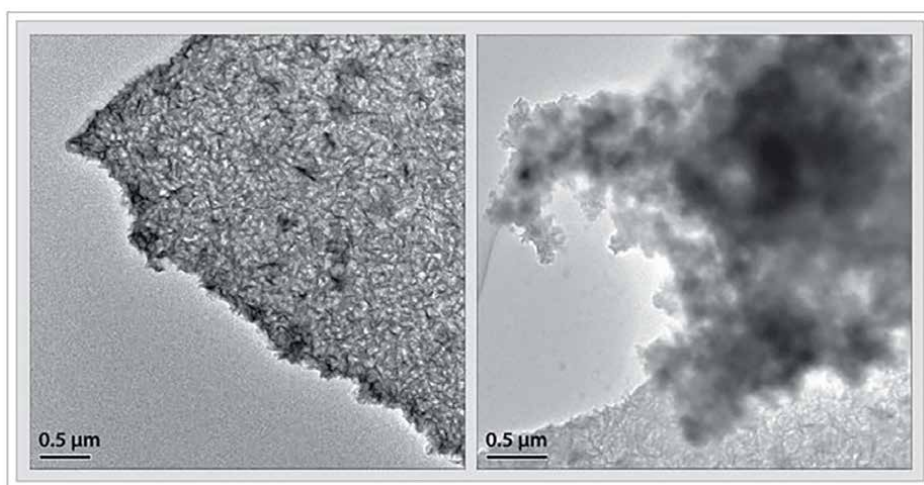


Figure 9.
TEM images of delamination particles filtered from the same vial [30].

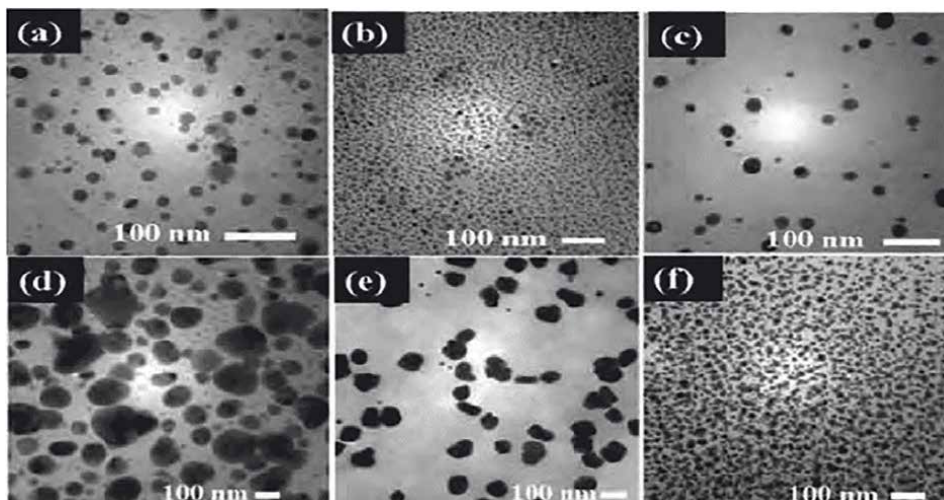


Figure 10.
Transmission electron microscopy (TEM) image of silver nanoparticles [32].

particles from different origins. TEM is a useful tool in forensic science trace evidence studies since it may provide morphological, elemental, and internal structural information on very minute particles that may be missed or difficult to analyze with other microscopical techniques. This information can be used to supplement other analytical investigations [33].

3.1.8 Explosives

Explosives are a broad category that includes both high and low explosives. They have become powerful weapons of mass devastation that are frequently used to cover up illicit activity by feigning unintentional explosions. Pre- and post-blast analysis is a two-pronged strategy used by the field of forensic investigation in handling explosion-related situations. Because samples that are thought to be explosives are readily available, pre-blast analysis can be done rather easily. This makes it possible to apply different chemical and analytical tests to ascertain their properties and makeup. On the other hand, post-blast analysis poses a unique set of difficulties. In this case, forensic specialists have the difficult duty of looking through explosion leftovers and wreckage.

Small amounts of the explosive material, frequently in the nanoscale range, are usually present in these residues. Because these traces are so small and scattered throughout the debris, it is a challenging task to analyze them. In a post-blast analysis, the use of TEM-EDX has been found successful in which shot from the air after the blast was studied, and the type of explosive used was identified [34].

Transmission electron microscopy (TEM) has become an important tool to overcome these obstacles. TEM has the extraordinary capacity to examine a material's crystalline structure at the nanoscale. This characteristic is essential for analyzing the post-blast residue because it allows for a thorough analysis of the structural characteristics of the explosive, which makes it easier to identify and connect it to the explosion. It also helps in the study of quantum dots, which are nowadays used to identify some common nitro base explosives [35].

3.2 Application of scanning electron microscope

The scanning electron microscope (SEM), which provides high-resolution, three-dimensional surface imaging, is an essential instrument in the investigation of trace evidence. SEM is utilized in forensic applications to examine the topography and morphology of trace materials. By offering fine-grained surface pictures, it facilitates the detection of various particles such as paint fragments, dirt, and gunshot residue. SEM is very useful for fiber analysis since it may be used to differentiate between various fiber types depending on surface features. Highlighting minute details on surfaces and connecting tools to particular markings helps with toolmark analysis. SEM is also used for surface imaging of different materials, paint study, hair morphology research, and tire tread analysis, all of which provide crucial information for forensic investigations.

3.2.1 GSR

Gunshot residue (GSR) or firearm discharge residue (FDR) comprises particulate matter generated during the act of discharging a firearm. These residues are commonly linked to components such as the primer, primer cup, propellant, projectile (slug/shot), projectile jacket and lubricant, cartridge case, and firearm barrel.

Anand et al. [36] showed gunshot residue (GSR) constitutes a heterogeneous assemblage of vapors emanating from the explosive components housed within the cartridge. When a firearm is involved in a criminal incident, the dissemination of gunshot residue (GSR) particles occurs not only through the muzzle but also through the cylindrical apertures, ejection ports, and other orifices within the firearm structure. These particles serve as crucial forensic evidence, prompting the need for their meticulous examination. Utilizing scanning electron microscopy coupled with energy-dispersive spectroscopy (SEM/EDX) is a conventional method for the comprehensive imaging and elemental analysis of gunshot residue (GSR) particles extracted from the specimens. Regrettably, a limited scholarly inquiry has explored the detection of GSR particles at extended distances employing SEM. Therefore, this current research introduces a novel methodology designed to identify GSR particles resulting from long-range firing. The approach involves an assessment of lead (Pb), barium (Ba), antimony (Sb), and other trace elements on the target material *via* SEM analysis. In the results, it was established that the novel method employing SEM and EDX has facilitated the examination of specific samples spanning a range from close contact to a considerable distance from the shooter. The results reveal the persistence of gunshot residue (GSR) particles at extended distances, a phenomenon that traditional chemical and elemental techniques typically fail to detect. Conclusively, the application of this method represents a significant advancement in forensic investigations, enabling the estimation of the firing range between the target and the shooter over substantial distances. Such an approach holds promise for enhancing the capabilities of the forensic community and investigative agencies in resolving crimes occurring at significant distances.

Brožek-Mucha et al. [37] state that gunshot residues stemming from six distinct pistol ammunitions were the subject of investigation. Six individuals with no habitual firearm exposure discharged three rounds, each using a different pistol. Samples of the resulting gunshot residues were obtained from the shooters' hands employing aluminum stubs affixed with black carbon adhesive tabs. These samples were subsequently subjected to morphological and elemental analyses through an automated process utilizing a scanning electron microscope integrated with an energy-dispersive X-ray spectrometer.

In the comparative analysis, focus was solely placed on the examination of primer residues. The percentage of particles representing specific chemical categories relative to the total count of detected particles was computed to determine their occurrence frequency. Varied relationships were observed between the frequencies of particular chemical residue occurrences for most of the studied ammunition types, as discerned through both non-statistical and non-parametric statistical methodologies (R-Spearman and τ -Kendall correlation coefficients). These statistical techniques facilitated the differentiation of one ammunition type from each of the other examined types. The analyses conducted unveiled discernible dissimilarities in the occurrence frequency defines that how many times the same component appeared in a samples under the study. Here it is define that which chemical component appeared to be present in various primer under study hence their occurrence frequency was determined.

Reyes et al. [38] showed that upon discharge of a firearm, a rapid release of a gaseous cloud containing distinct particles of gunshot residue (GSR) occurs, disseminating both forward and backward. These particles are deposited on various surfaces, including clothing, hands, face, and hair. Furthermore, they are also inhaled, leading to retention within the nostrils of the individual who discharged the weapon. GSRs, characterized by specific sizes and morphologies, comprise a composite of lead, antimony, barium, and other elemental components. Although scanning electron microscopy with energy-dispersive X-ray spectroscopy (SEM-EDS) represents a widely accepted technique for GSR analysis, limited research has addressed samples obtained from the suspect's nostrils. While the analysis of residues found on the hands has been more commonplace, this study introduces a non-invasive collection device (Nasal Stub) designed for the retrieval of GSR particles from the nostrils. Additionally, a corresponding platform compatible with SEM-EDS has been developed. The efficacy of the Nasal Stub in collecting GSR particles from nasal hairs was evaluated using four different-caliber firearms. Nasal samples were collected at specific intervals (0, 2, 4, 6, 8, and 20 hours) post-firing. The findings indicate that the Nasal Stub successfully retrieved GSR particles from nasal hairs associated with all utilized firearms, even after a duration exceeding 20 hours in some instances. Consequently, it was determined that the proposed Nasal Stub **Figure 11**, in conjunction with the methodology for the analysis of nasal GSR from nose hairs *via* SEM-EDS, proved effective. Moreover, it was emphasized that this approach could complement conventional GSR particle analyses, thereby reinforcing the forensic evidence presented in legal settings, such as tribunals or courts.

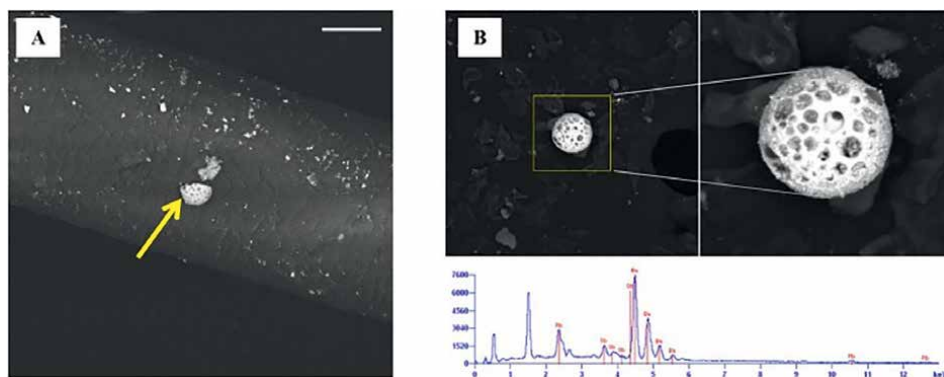


Figure 11.
GSR in nasal swab [39].

Kara et al. [39] mention that an investigation was focused on examining variations in the quantities of gunshot residues (GSR) collected from the shooter's right hand using the "swab" method. Scanning electron microscope/energy-dispersive spectroscopy (SEM-EDS) was utilized to explore the potential correlation between these amounts and diverse conditions, including the shooter's skin color, various physical attributes, hand hair density, hand size, and the presence of sweat or oiliness on the hands.

Analysis of the data revealed no significant disparity in the GSR quantities based on the shooter's skin color. However, discernible fluctuations in the GSR levels were observed in relation to the shooter's physical characteristics. These findings are anticipated to offer practical insights for experts engaged in GSR analysis using the swab technique, facilitating a more comprehensive assessment of the occurrence.

Toal et al. [40], Red X Defense has introduced an automated field presumptive lead test, utilizing a sampling pad designed to function as a red-light/green-light indicator. This pad can subsequently undergo processing within a scanning electron microscope (SEM) for the purpose of confirming the presence of gunshot residue (GSR). The XCAT's sampling card is specifically employed to collect samples from a suspect's hands at the crime scene, enabling investigators to swiftly ascertain the potential presence of lead, likely originating from primer residue. Notably, positive outcomes can be obtained after the discharge of as few as one shot.

Furthermore, the same sampling card can be forwarded to a crime laboratory for SEM-based GSR analysis, aligning with the procedures outlined in the ASTM E-1588-10 Standard Guide for gunshot residue analysis by scanning electron microscopy/energy-dispersive X-ray spectrometry. This processing method is akin to the current utilization of tape lifts within the field. Notably, the system can detect GSR-characteristic particles, including fused lead, barium, and antimony, as small as 0.8 microns with a resolution of 0.5 microns. This detection is achieved through the utilization of a JEOL JSM-6480LV SEM, equipped with an Oxford Instruments INCA EDS system featuring a 50mm² SDD detector. The system operates at 350X magnification, with analyses conducted in both low-vacuum and high-vacuum modes, following carbon coating *via* a sputter coater.

The GSR particles demonstrate stability on the sampling pad for at least 2 months subsequent to chemical exposure, with ongoing assessments exploring their long-term stability. The immediate actionable intelligence provided by the XCAT's presumptive result empowers law enforcement in expediting their investigations without compromising the necessity of a confirmatory test crucial for bolstering legal and investigative proceedings.

3.2.2 Firearms

Scanning electron microscopy (SEM) serves as a valuable instrument for assessing and comparing impressed or striated toolmarks, especially in cases concerning rimfire and centerfire cartridge cases, as well as striated marks on bullets. Notably, SEM provides a significantly superior depth of field compared to a light microscope, eliminating the need for side lighting to visualize the object's surface topography [41].

With the advances in the EM, the field of study has increased which enables to examine the bullets and that bullets shot from the same firearm leave unique marks related to the gun's barrel shape. Matching these distinct marks on bullets can help determine if they were fired from the same gun. Additionally, the firing pin on the bullet's cartridge case can create similar markings, providing another way to link a bullet to a specific firearm. While optical techniques can sometimes be used to match

bullets, they may lack the ability to reveal fine details at higher magnifications and lack the necessary depth of focus for clear visibility [42].

SEM series possesses three key features that offer significant advantages in comparing bullet markings: With a backscattered electron detector, the contrast of markings can be amplified while irrelevant information like dust contamination is suppressed. Carl Zeiss semiconductor manufacturing technology (SMT) provides a specially designed sub-stage for comparing bullets. This sub-stage can securely hold bullets or cartridge cases, allowing each bullet to be rotated independently for precise matching. The capability to cut and paste images, or segments of images, facilitates the alignment of various images to assist in the matching process.

Korda et al. [43] stated that various distinguishing marks can be identified on cartridge cases, including impressions left by the firing pin and imprints created by the breechblock, extractor, and ejector of the firearm. Given that intricate details in such markings are typically situated at the bottom of impressions, the notable depth of focus offered by the SEM presents a clear advantage over other microscopic examination techniques. Hence, the scanning electron microscope (SEM) can be effectively utilized to directly investigate the surface topography of forensic evidence. Its significant depth of focus and high resolutions in the emissive mode enables the detection of crucial microstructural details that are often inaccessible using other microscopic methods. Although not employed in this specific study, the luminescent and conductive modes of the SEM might also hold value in the field of criminalistic investigations.

Similarly, Bíró et al. [44] stated that in the field of forensic medicine, the use of scanning electron microscopy with energy-dispersive X-ray microanalysis (EDX) offers crucial insights into the morphology of injuries and the instruments causing them. The research conducted aims to validate the efficacy of employing scanning electron microscopy in conjunction with X-ray microanalyzer EDX to assess the interaction of a bullet passing through human tissue. The study involved the SEM and EDX analysis of skin tissue samples obtained from bullet wound sites and brain tissue from the depths of bullet wounds in cases of firearm-related injuries to the head. The research team successfully identified the presence of light particles on the surface of the samples and within the bullet wound canal. Analysis of these particles revealed the presence of various elements, including Mg, Al, Si, P, S, Cl, Ca, Cu, and Zn, in both the skin and brain tissue samples. The abundance of micro-particles was notably higher at the bullet wound site, while their presence was minimal in the deeper regions of the wound canal. The study concludes that the utilization of scanning electron microscopy in combination with EDX analysis represents a suitable approach for forensic investigations of firearm-related wounds. This integrated technique facilitates the determination of projectile parameters and allows for an approximate estimation of the distance between the firearm and the target.

Hopkins et al. [45] stated that with 45 recorded instances of confirmed shootings of hen harriers in the UK since the commencement of records (data unpublished, Royal Society for the Protection of Birds), this study presents the results of a pathological examination conducted on a hen harrier, wherein suspected ballistic fragments were identified *via* radiographic imaging. The researchers elaborate on the application of scanning electron microscopy and energy-dispersive X-ray spectroscopy (SEM–EDX) to verify two critical aspects: (i) the composition of a particular ballistic fragment and (ii) its trajectory causing bone damage. Additionally, the authors discuss the utilization of post-analysis software to discern potential irregularities arising from the proprietary SEM–EDX software package. The study also addresses the broader applications of SEM–EDX in the investigation of wildlife-related criminal activities.

3.2.3 Gemstones and jewelry

Scanning electron microscopes (SEMs) have become fundamental instruments within the domain of gemstone and jewelry examination, enabling thorough analyses of diverse materials and structures. In the context of gemstone identification, SEMs facilitate the scrutiny of both internal and external features of gemstones at amplified magnifications, aiding gemologists in their evaluation of genuineness and caliber. These instruments facilitate the identification of surface irregularities, inclusions, and structural imperfections that may signify origins, whether natural or synthetic, thereby augmenting the capability to differentiate between natural gemstones and their synthetic counterparts. Moreover, SEMs yield significant insights into the surface morphology, elemental composition, and crystalline arrangement of gemstones, thereby supporting the assessment of their geological provenance and potential treatment history. In the field of jewelry forensics, SEMs assume a critical role in examining surface coatings, plating thickness, and material constitution, thereby contributing to the validation of precious metals and the discernment of counterfeit jewelry. Through their capacity to generate images of exceptional resolution and conduct elemental analyses, scanning electron microscopes persist in innovating the exploration and evaluation of gemstones and jewelry, safeguarding the integrity and worth of these treasured artifacts.

Cartier et al. [46] showed that by utilizing scanning electron microscopy, the cross-sectional view of pearl nacre exposes the distinct aragonite tablets, as shown in **Figure 12**. It is believed that DNA is present within the organic substance situated amid these individual tablets.

According to Tiwari et al. [47], a report was filed at the police station in Raipur City, Chhattisgarh state, pertaining to a case of fraudulent activity. The victim had been deceived into purchasing gold beads amounting to nearly 16 lakhs. Owing to the nature of the case falling under the purview of forensic physics, involving the analysis and comparison of physical properties, it was duly registered at the State Forensic Science Laboratory in Raipur. This study aimed to apply fundamental principles of physics in resolving unresolved cases and foster awareness regarding the purchase of

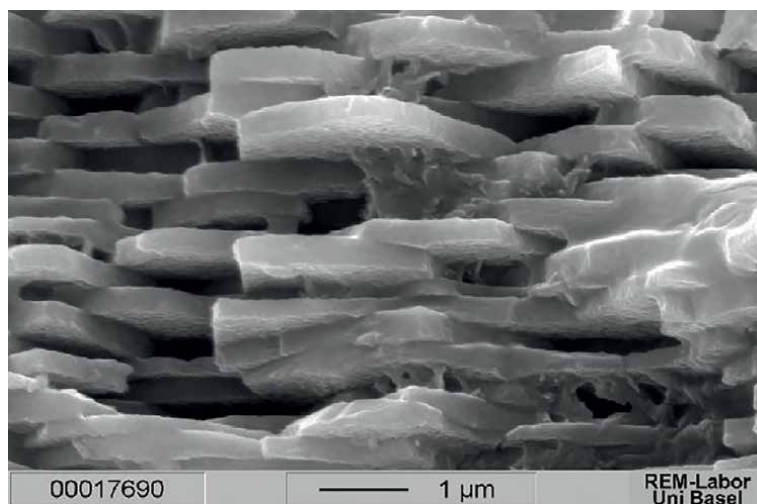


Figure 12.
Aragonite tablets [47].

precious ornaments. In this specific instance, a strand of numerous spherical golden beads was submitted for examination to assess the gold content under the assumption that the gold possessed a lower purity level. To this end, scanning electron microscope (SEM) examination and energy-dispersive X-ray analysis (EDAX) were performed in the laboratory. The findings indicated a notable absence of gold (Au) in all the gold beads within the strand. Instead, the analysis revealed the presence of copper (Cu) and zinc (Zn) in a ratio of Cu:Zn::2:1.

Troalen et al. [48] stated that the National Museums Scotland (NMS) houses approximately 6000 artifacts originating from Ancient Egypt and Sudan, which notably encompass gold and electrum jewelry that has previously received limited attention in terms of scientific scrutiny. The assemblage represents various periods ranging from the Predynastic era to the Roman Empire, with a substantial portion of these items originating from reputable archeological excavations conducted during the nineteenth and twentieth centuries. In an effort to conduct an initial exploration into the diverse alloys and production methodologies employed in Ancient Egypt, the study focused on the examination of the Qurneh jewelry alongside a small selection of other gold items dating between the nineteenth and thirteenth centuries BC. As such, for the examination of gold PGE (platinum group element) inclusions, ranging from a few to a few hundred microns in diameter, as shown in **Figure 13**, this is a characteristic analysis for golden jewelry, and different concentrations may reveal that the source for the golden metal was different. The examination of these objects took place at the NMS, utilizing a stereo-microscope (Olympus SZX12 \times 7–90) integrated with a digital camera (Olympus DP70), as well as CamScan scanning electron microscopy in secondary electron mode (SEI). Furthermore, their structural composition was investigated by employing a 300 kV Pantak X-radiography system. Evident signs of wear were observed across all the jewelries, notably prominent in the Qurneh girdle and one of the Amarna finger-rings (A.1883.49.2). Notably, observations revealed loose decorative elements in the girdle, along with deformations on the edges of the beads and within the holes of the wallet spacers, particularly where they make contact with the beads.

Burat et al. [49], the analysis of a representative sample was conducted using scanning electron microscopy alongside energy-dispersive X-ray spectroscopy (SEM-EDS). This study outlines the process of concentrating and extracting Au and Ag from the waste generated during floor-sweeping activities at jewelry workshops.

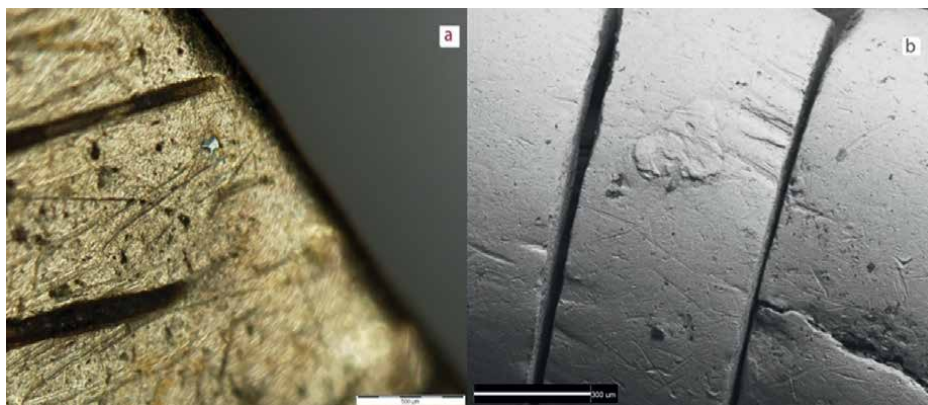


Figure 13.
PGE inclusions in pendant (A.1914.1081) from el-Harāgeh by OM [48].

The concentration and recovery procedures involved both physical methods, such as shaking table, multi-gravity separator (MGS), Knelson, and Falcon concentrators, as well as physicochemical methods like froth flotation. Experimental findings highlighted the effectiveness of gravity-based beneficiation techniques in the removal of a significant portion of the waste matrix. Notably, the employment of a shaking table separator yielded a heavy fraction with a content of 701 and 6017 g/t Ag, obtained from a feed assaying 183 Au and 1835 g/t Ag. To further enhance the beneficiation process, the middlings from tabling were subjected to centrifugal separation, resulting in an increase in the Ag grade from 848 to 7812 g/t. Additionally, the tailings from gravity and centrifugal separations, containing the discharged Au and Ag fractions, were effectively concentrated using froth flotation, ultimately leading to an overall recovery rate of approximately 92% for both Au and Ag.

3.2.4 Paints and fiber

The application of scanning electron microscopes (SEMs) has significantly advanced forensic analysis, specifically in the scrutiny of paint and fiber specimens. In the context of paint analysis, SEMs facilitate an intricate exploration of the layers of paint and their constituent components, aiding in the discernment of diverse pigments and supplementary substances. These instruments enable the visualization of the layer arrangement and the identification of distinctive morphological attributes, thereby contributing to the differentiation of paint samples obtained from varying sources. Furthermore, SEMs play a pivotal role in the analysis of fibers, allowing for the examination of fiber structure, surface properties, and elemental constitution. They facilitate the identification of fiber categories, encompassing both natural and synthetic varieties, while assisting in the detection of any modifications or contamination. By offering capabilities in high-resolution imaging and elemental analysis, scanning electron microscopes continue to serve as indispensable tools in the comprehensive scrutiny and verification of paint and fiber evidence within the domain of forensic investigations.

Schreiner et al. [50], the utilization of scanning electron microscopy (SEM), particularly in conjunction with energy-dispersive X-ray microanalysis (SEM/EDX), has been significantly prevalent in the comprehensive examination of materials found in artifacts of both artistic and archeological significances. A series of case studies illustrate the benefits and limitations of SEM/EDX. These include the analysis of pigments within cross-sectional views of paint layers, the quantitative assessment of archeological glass from the Roman era excavated in Ephesos, Turkey, and investigations into glasses with compositions characteristic of the medieval period, focusing on their susceptibility to weathering and degradation phenomena. The integration of scanning electron microscopy, along with energy-dispersive X-ray microanalysis, has played a pivotal role in the extensive exploration of items comprising our cultural heritage. Moreover, it has served as an indispensable tool in unraveling the processes of deterioration affecting ancient materials as well as contemporary materials utilized in art and archaeology. Recent advancements in techniques, such as environmental SEM (ESEM) or low-voltage SEM (LV-SEM), have broadened the scope of material analysis, eliminating the prerequisites of electrical conductivity and resistance to high-vacuum conditions in samples. However, the findings underscore the necessity of conducting scientific investigations through the amalgamation of multiple analytical methods, wherein conventional microscopy and micro-chemical spot tests are implemented alongside sophisticated techniques utilizing synchrotron radiation.

Mahlting and Grethe [51] provide a comprehensive examination of various high-performance fibers like polyester filament fiber, as shown in **Figure 14**, and functional fiber materials, offering insights into their properties and applications. Microscopic imagery obtained through scanning electron microscopy (SEM) is introduced for fiber materials and fabrics, complemented by electron-dispersive spectroscopy (EDS) analyses performed on the fiber materials, with an overview of the resulting EDS spectra. The distinctive attributes of SEM images and EDS spectra are thoroughly discussed, primarily aimed at aiding professionals engaged in fiber analytics. To furnish a comprehensive understanding of both analytical techniques, SEM and EDS, the review also delineates the challenges and common errors encountered during SEM measurements on textiles. Collectively, the review presents a valuable survey of advanced high-tech fiber materials and their examination using the analytical methods of SEM and EDS, enabling the elucidation and discussion of material properties and composition. It also delves into the analysis and discussion of the composition of industrial fiber materials, as well as the treatments applied to fibers to achieve specific functional properties. Ultimately, the review strives to serve as a practical resource for professionals engaged in fiber and textile analytics and identification.

Jaques et al. [52] stated that scanning electron microscopy (SEM) represents a prevalent technique employed for the analysis of micro-samples derived from paintings. Notably, this method's heightened resolution allows for meticulous surface

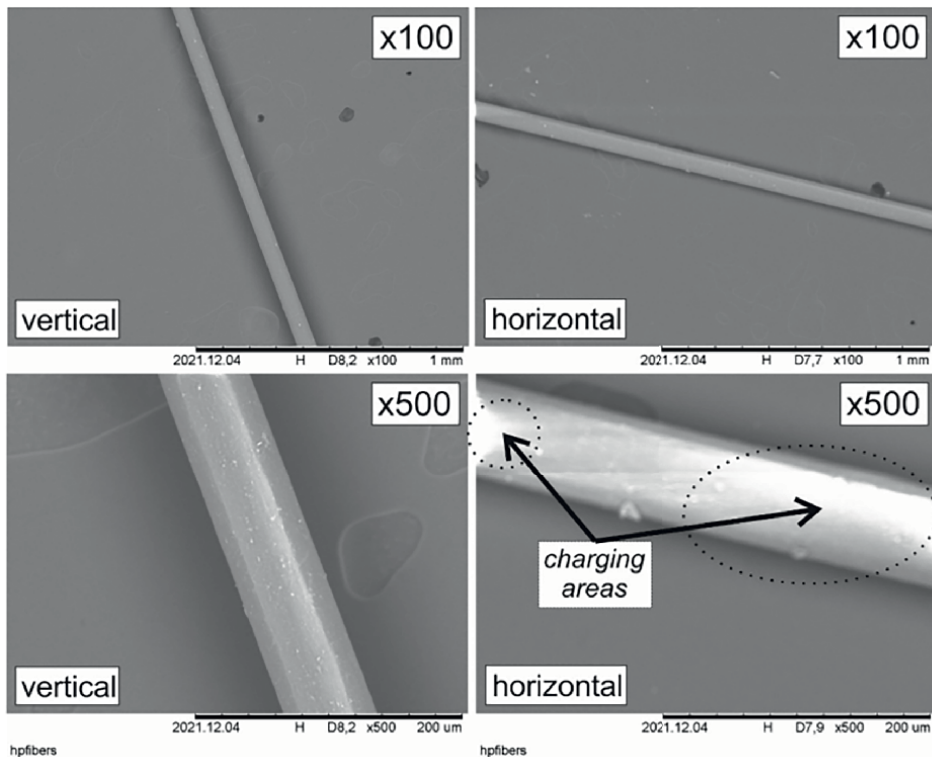


Figure 14.
SEM images of a polyester filament fiber. The SEM images are recorded with two different magnifications ($\times 100$ or $\times 500$) and with two different fiber arrangements on the sample holder [52].

analysis and can be augmented with an energy-dispersive spectrometer to gather elemental composition data. In the context of light microscopy and SEM analysis, painting micro-samples are commonly prepared as cross sections, where the micro-sample is embedded in resin and subsequently polished to reveal the sequential layers. In instances pertinent to cultural heritage, the cross section's polished surface is typically coated with a conductive layer, although in this specific domain, measurements are predominantly conducted using a low-vacuum SEM (LV-SEM). Despite the reduced occurrence of the charging effect in LV-SEM, this issue may still arise and remains challenging to mitigate, even with the application of carbon tape or paint. This research introduces two distinct methods for preparing conductive cross sections from non-conductive samples, thereby mitigating charging effects while preserving the integrity of the samples.

News-Medical.net [53] states that the market for fibers and fiber materials, including natural options like hemp fibers, remains extensive. Hemp fibers have served various purposes over the years, finding application in the production of papers, ropes, clothing, and canvas. More recently, these fibers have been integrated into the automotive industry to enhance paint strength. However, hemp phloem contains wax, pectin, lignin, hemicelluloses, and other impurities, typically removed during the degumming process. To assess the impact of enzymatic degumming on the quality of hemp fibers, a combination of scanning electron microscopy (SEM) and fluorescent microscopy was employed to examine untreated and treated hemp fibers. The primary aim of this investigation was to ascertain the protein content and quality of hemp fibers, evaluating the efficacy of the enzymatic degumming procedure. The findings suggest that the biochemical degumming process under scrutiny offers a viable solution with favorable environmental and economic implications, thereby presenting itself as a feasible candidate for industrial-scale implementation.

According to (Paint Analysis, n.d.) [54], methods such as scanning electron microscopy (SEM) offer the capability to investigate both contemporary and historical paint and polychrome samples. Energy-dispersive X-ray analysis enables the identification and examination of inorganic fillers, pigments, and organic components within distinct paint layers. This information facilitates the comprehensive characterization of each layer, including insights into its formulation and thickness.

Park et al. [55], in electron microscopy (EM), the issue of non-conductive biological samples experiencing charging from focused electron beams has hindered the achievement of high-resolution imaging. Commonly employed solutions, such as the application of gold or platinum coatings, have proven effective in preventing sample charging. However, these coatings pose limitations on the feasibility of conducting further quantitative and qualitative chemical analyses, including energy-dispersive spectroscopy (EDS). This study presents findings indicating that the implementation of graphene-coating on biological samples allows for non-destructive high-resolution imaging through EM, alongside facilitating chemical analysis through EDS. The utilization of graphene is supported by its transparency to electron beams and high conductivity, as shown in **Figure 15** on biological samples as well as its remarkable mechanical strength and flexibility. It is believed that the introduction of graphene-coated imaging and analytical methods will provide a novel avenue for exploring various biological phenomena previously unseen due to limitations in sample preparation and image resolution, thereby enriching our comprehension of the life mechanisms inherent in diverse living organisms.

In a study, a compact, untextured multifilament nylon fabric with a plain woven structure was specifically chosen for the experimental evaluation. The generation of

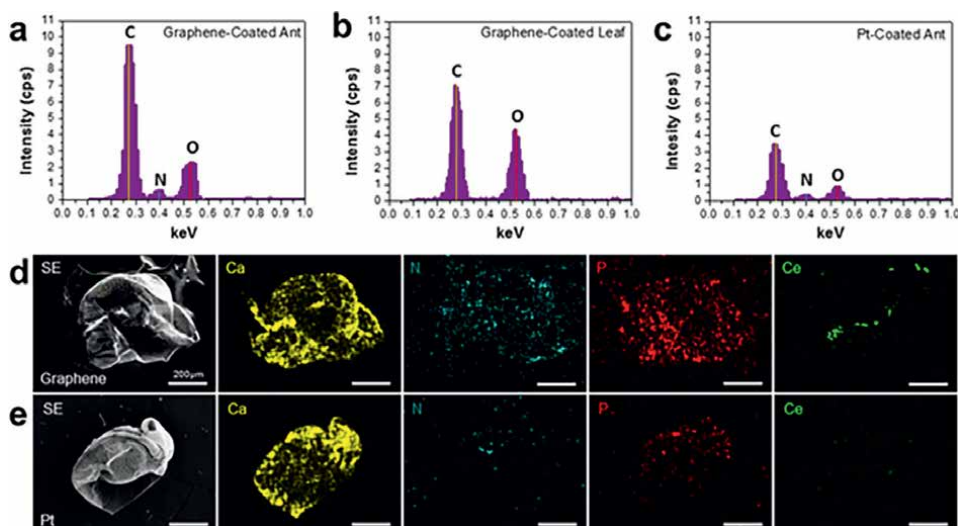


Figure 15.
 SEM and EDS analyses of biological samples coated with graphene [55].

damaged samples involved the use of a precise carving knife, a finely honed pair of dressmaker's shears, and an Elmendorf tear tester. Written guidelines were distributed to 14 panelists, instructing them on the examination of fiber end impairment through comparisons with theoretical models and scanning electron microscopy (SEM) micrographs featuring distinct fiber end appearances resulting from knife cuts, scissor cuts, and impacts causing tears and ductile fractures. Findings indicated a limited probability of accurately identifying the underlying cause of damage, as the fiber ends resulting from various damage mechanisms exhibited overlapping characteristics. Given these outcomes, the study advocates for further exploration into fiber damage, cautioning researchers and practitioners in the forensic domain against relying solely on SEM analyses to ascertain the root cause of fabric damage in forensic investigations [56].

Examining paint chips or flakes is a routine procedure aimed at gathering significant insights. These paint samples are instrumental in deducing essential particulars such as the hues, brands, and models of any vehicle implicated in a crime scene or an incident. Automobile producers typically apply multiple coats of primer, color, and clear finishes to achieve the intended appearance. Unveiling the composition of these paint layers is made feasible through energy-dispersive spectroscopy (EDS), which enables the elemental makeup of each layer to be revealed and cross-referenced against a database of known layer compositions. This analysis can also be utilized for direct comparison with a suspect's vehicle.

3.2.5 Investigation of filament bulb in traffic accidents

Scanning electron microscopy (SEM) is a helpful way to look closely at filament bulbs that were in car crashes. It can take detailed pictures of the inside of the bulbs, helping investigators understand what happened during the crash. By studying how the surface of the broken parts looks and what they are made of, SEM can find important clues about why the bulb stopped working during the accident. This careful study can find signs of pressure, how the materials changed shape, or if there were any problems with the materials that might explain what happened. Also, SEM can

find any other things that should not be there or things that might have affected how the bulb worked. Using SEM to look at the filament bulbs helps investigators learn important things about what caused the car accident.

Thorsen et al. [57] assessed the lighting conditions of a vehicle during an accident as a crucial task in forensic investigations, achieved through the examination of lamps and their remnants. Optical and scanning electron microscopy are two valuable techniques used for this purpose, with the latter gaining prominence due to its high resolution, extensive depth of focus, and the option for EDS microanalysis. To enhance the reliability of light bulb analysis as an investigative tool, it is essential to fully comprehend bulb design, the materials involved, and the functionality of the bulb, particularly its response to impact. This review aims to consolidate the existing but dispersed literature pertaining to these aspects, aiming to facilitate a more systematic and comprehensive approach to light bulb analysis in forensic investigations.

Horvat et al. [58] introduced a novel technical and technological approach for examining automotive light bulbs to detect trace particles of shattered glass in cases involving minimal inertia forces resulting from a traffic accident. Given the limited prior investigations into light bulbs in such accidents, the study focuses on analyzing the filaments of light bulbs used in cars for illuminating the road and signaling, incorporating a new technical procedure utilizing the SEM/EDX method. The research significantly enhances the investigative process for analyzing automotive light bulbs, aiding in the determination of whether the vehicle's regulatory lights were in operation at the time of the accident. Such findings can be critical in establishing the liability of the parties involved in causing the traffic incident.

Grafiati [59] carried out research in order to introduce the benefits of using surveying techniques in traffic accident investigations and show their impacts on evidence documentation and scene clearance. This is done by focusing on the advantages and the disadvantages of each method based on the relevant works of literature and comparing them. Although comparison result shows that the traditional method (coordinate method) is simpler and cheaper than other methods, surveying technique methods are safer and faster in clearing the accident scene, fewer investigators are needed, the scale can be provided directly, high accuracy measurements can be obtained, and three dimensions' models can be produced. So, it is worth using the surveying equipment in car accident investigations.

3.2.6 Handwriting and print examination

Scanning electron microscopy (SEM) has emerged as a versatile tool in the realm of handwriting and print examination, with particular relevance in cases involving forgery. Through the utilization of SEM, forensic professionals can conduct a meticulous analysis of the minute features of ink, paper, and other writing materials utilized in various documents. This thorough examination enables the discernment of distinctive handwriting attributes, encompassing aspects such as pen pressure, ink dispersion, and the unique traits of individual pen strokes. SEM aids in the identification of any modifications, insertions, or erasures present in documents, unveiling subtle alterations in surface texture and ink properties. Moreover, SEM facilitates the recognition of diverse printing methodologies, encompassing disparities in ink absorption, patterns in paper fiber, and the presence of printing artifacts. The high-resolution imaging capacity of SEM offers valuable insights into the genuineness and credibility of documents, significantly contributing to the verification process and the detection of potential falsifications.

Wang et al. [60] performed handwriting authentication as a pivotal domain within the field of forensic science. In this study, diverse types and brands of pen ink samples originating from China can be scrutinized using non-invasive micro-identification techniques. The utilization of scanning electron microscopy and energy spectrum (SEM-ES) enabled the examination of micro-elements and the comprehensive analysis of the written traces, with a particular emphasis on the function of spectral mapping (surface scanning). The precise evaluation of elements within the handwriting traces facilitated the differentiation of subtle disparities among various types and brands of ink in handwritten text. This approach introduced a novel avenue for the analysis and exploration of pen handwriting identification in the realm of forensic science.

Verma et al. [61] detected that computer-generated document forgeries have always posed a significant challenge for forensic document examiners (FDE). To assist in the examination process, researchers have explored the use of Schottky field emission scanning electron microscopy with energy-dispersive X-ray spectroscopy (FE-SEM-EDS) as a modern tool for analyzing black toners sourced from laser printers and photocopier machines. A total of 40 samples from each of the laser printer and photocopier machines were obtained and subjected to an analysis of morphological characteristics, elemental profiles, and multivariate analysis. The acquired SEM images and spectra were scrutinized to distinguish and categorize toners originating from different sources. Multivariate analysis was employed to develop a classification model that successfully categorized the printed documents based on the similarities and differences in their composition. Hierarchical cluster analysis (HCA) differentiated the printouts into distinct groups based on their chemical composition, resulting in 11 clusters for the laser printer printouts and 8 clusters for the photocopier printouts. Cross-validation was additionally conducted to assess the capabilities of the developed principal component analysis (PCA) and linear discriminant analysis (LDA) models for examining printouts of unknown origin.

In the field of forensic document examination, a significant obstacle is the meticulous scrutiny of minute details that remain imperceptible to the unaided eye. Electron microscopy has emerged as a potent solution to tackle this challenge. The use of scanning electron microscopy (SEM) or transmission electron microscopy (TEM) empowers forensic document examiners to capture intricate elements such as ink pigments, paper fibers, and surface topography with remarkable precision. This detailed view offers vital evidence necessary for verifying the legitimacy of a document and uncovering potential modifications or counterfeits. Furthermore, the high-resolution imaging capabilities of electron microscopy enable examiners to distinguish unique attributes of different writing tools. Each pen, for instance, leaves behind a distinct mark due to variations in its nib, ink flow, and the pressure applied during writing. Moreover, the scrutiny of paper fibers can unveil patterns and textures that correspond to specific manufacturing techniques or historical periods, thereby further contributing to the authentication and provenance determination of a document. (AZoOptics.com, 2023) [62].

The examination of ink holds significant importance in forensic document analysis, with electron microscopy playing a crucial role in this domain. Through this technique, analysts can investigate ink samples derived from various documents and assess their chemical makeup, particle distribution, and microstructure, all of which can serve as distinct identifiers. By incorporating energy-dispersive X-ray spectroscopy alongside SEM, specialists can identify unique elements present in the ink, thereby aiding in establishing connections between different documents or highlighting potential disparities. The chemical composition of ink varies depending on its formulation and manufacturing methods. By comparing the ink composition

of different documents, experts can determine if the ink used aligns with a specific brand, batch, or time period, offering pivotal evidence in cases involving falsified documents or forged signatures.

One intriguing application of electron microscopy in forensic document examination lies in its capacity to reveal concealed or modified writing. Indented writing often arises when an individual writes on a piece of paper positioned atop another document, a practice frequently exploited by counterfeiters seeking to manipulate or fabricate documents. Electron microscopy enables analysts to visualize and interpret the indented writing, deciphering its content and contrasting it with the visible writing on the document's surface. This method has proven immensely valuable in uncovering obscured messages, erased text, or alterations made to crucial documents, thereby providing examiners with crucial insights into the document's history and authenticity.

Given the increase in advanced counterfeiting methods, electron microscopy has become an essential instrument for examining counterfeit documents. Such fraudulent documents frequently endeavor to replicate intricate security elements inherent in authentic documents. Through the scrutiny of security features such as watermarks, holograms, and micro-printing, forensic examiners can detect disparities and ascertain the authenticity of a document. Additionally, electron microscopy facilitates thorough analyses of printing methods, surface anomalies, and substrate attributes. By comparing and contrasting these subtle intricacies with those present in verified authentic documents, forensic specialists can furnish compelling evidence to uncover counterfeit endeavors and contribute to legal procedures.

According to Pingitore et al. [63], diagnostic studies were conducted on an ancient coin to determine its authenticity or potential for being a counterfeit. The investigation employed scanning electron microscopy/energy-dispersive X-ray (SEM-EDX) and cathodoluminescence (CL). The coin in question, a Drachma, depicted Poseidon's portrait on the obverse and Amphitrite riding a seahorse with Eros shooting an arrow on the reverse. The coin is widely recognized in numismatic circles, with originals housed in various museums such as those in Catanzaro, Naples, and Milan. The EDX analysis, performed on specific points of the coin's surface, identified Pb and Cu as the primary components on both sides, with 51% Pb and 35% Cu by weight, along with unexpected traces of gold. Gold was detected in small spots measuring around 20 μm , constituting 95% of the total weight. Simultaneously, cathodoluminescence (CL) analysis was conducted to induce luminescent emissions by electron bombardment in these areas. The CL analysis corroborated the SEM findings, highlighting the presence of gold more distinctly than the SEM analysis. In fact, the CL analysis revealed the presence of gold throughout the surface of the sample, albeit in small amounts.

3.2.7 Soil

The implementation of scanning electron microscopy (SEM) has markedly propelled the realm of trace evidence analysis, empowering forensic experts to meticulously examine and discern minute materials of potential significance in criminal inquiries. Through SEM, researchers can investigate the surface morphology and elemental structure of trace evidence, encompassing various substances such as fibers, hair, paint chips, and gunshot residue. The superior imaging capabilities of SEM allow for the meticulous visualization of intricate characteristics and subtle features, facilitating the differentiation of diverse materials and the determination of their origins. Furthermore, the integration of energy-dispersive X-ray spectroscopy (EDS) with SEM permits the identification and spatial mapping of elements present

within trace samples, imparting critical insights into their chemical compositions. These thorough analyses significantly contribute to establishing pivotal associations between physical evidence and crime scenes, thereby streamlining the process of suspect identification and providing robust evidence in legal proceedings.

Soil, an unconsolidated mineral substance found on the Earth's surface, results from the combined effects of organisms, parent material, climate variations, and topography over an extended period. It comprises minerals, organic matter, liquids, and gases, with diverse properties influenced by factors such as vegetation, weather, and solar exposure. The current study delves into the morphology and elemental constituents of soil samples collected from Canterbury (UK), Dubai (UAE), and Kerala (India). Analyzing the samples under a scanning electron microscope involved careful moisture removal *via* controlled heating, considering the distinct water retention capacities of each soil type to prevent any sample combustion. In a comparative assessment, showcasing distinctions in texture, color, and composition across the soils was possible. Backscattered images highlight the unique features of each sample, with elemental composition analysis emphasizing major components as well as trace elements. Notably, variations in elemental composition, particle size, and color emerged, reflecting the geographical diversity of the soil samples. This investigation contributes valuable insights into the distinct characteristics and forensic implications of soil analysis across different regions.

3.2.8 Non-conducting material

Scanning electron microscopy (SEM) has emerged as a critical tool for examining non-conductive materials, revealing important insights into their surface structure, elemental makeup, and overall composition. By employing specialized methods for sample preparation, such as applying a conductive coating or utilizing low-voltage SEM, SEM allows for the effective analysis of materials such as polymers, ceramics, and biological samples that do not conduct electricity. This technique enables the observation of intricate surface features and the detection of subtle structural differences, providing valuable data for evaluating material properties, ensuring quality control, and driving various research endeavors. Additionally, the integration of energy-dispersive X-ray spectroscopy (EDS) with SEM permits the precise identification and mapping of elemental constituents within non-conductive materials, facilitating a comprehensive analysis of their chemical composition and contributing to a deeper understanding of their characteristics and behaviors. With its advanced imaging capabilities and accurate elemental analysis, SEM continues to advance the exploration and comprehension of diverse non-conductive materials across various scientific fields.

Griffin [64] showed that understanding the precise mechanism behind the contrast observed in “environmental” or “gaseous” secondary electron images in the environmental scanning electron microscope remains somewhat unclear. Initially, a straightforward gas amplification model was proposed, suggesting that emitted secondary electrons ionize the chamber gas, leading to signal amplification and subsequent measurement at a biased detector. While this theory is evolving, little attention has been directed toward the factors influencing the actual secondary emission despite the identification of unusual contrast effects in one instance. The conventional perspective implies that the positive ion product resulting from the gas-electron interaction induces charge neutralization at the sample surface. Recent research has indicated the occurrence of charge implantation and trapping in non-conductive materials, particularly in Ref. to electron range measurements. This study showcased the influence of trapped charge on the secondary electron yield, revealing

heightened secondary electron emission above the region where charge is trapped. As a result, the distribution of the trapped charge manifests as a bright circle on the specimen's surface, centered at the point of beam exposure.

Cao et al. [65] showed that with the advancements in science and technology, the field emission scanning electron microscope (FESEM) has become a pivotal tool in nano-material measurements, owing to its notable benefits such as high magnification, high resolution, and user-friendly operation. A high-quality secondary electron image is vital for precise and accurate length measurements. Traditionally, non-conductive materials are treated by coating them with conductive films such as gold, carbon, or platinum to minimize charging effects and achieve high-quality secondary electron images. However, this approach often conceals the authentic microstructures of materials, alters sample composition properties, and introduces significant errors in nanoscale microstructure measurements. This chapter delves into the exploration of methods for minimizing or eliminating the impact of charging effects on image quality to the greatest extent possible without resorting to coating treatments. Adjustments in working conditions, such as voltage, stage bias, and scanning mode, are discussed to uncover genuine and high-quality microstructure information of materials.

Wang et al. [66] performed the examination of surface morphology for non-conducting granular materials was conducted utilizing scanning electron microscopy (SEM) within low-vacuum conditions. An exhaustive investigation was performed to assess the impact of various factors, including incident electron voltage, electronic beam spot size, and atmospheric pressure, on the quality of SEM images and the accuracy of energy-dispersive X-ray (EDX) analysis. The findings from this systematic exploration reveal that the resolution and quality of SEM images demonstrate a decrease in correlation with the escalation of incident electron voltage, electronic beam spot size, and atmospheric pressure. Furthermore, the errors associated with the EDS analysis exhibit a decline when conducted under the specific conditions of low vacuum.

4. Conclusion

Modern scientific investigation is led by electron microscopy, which provides a never-before-seen glimpse into the complex world of microscopic structures that are still out of reach for conventional microscopy. This sophisticated type of microscopy has become an essential tool for forensic investigations analyzing trace evidence because of its remarkable resolution and capacity to examine materials at the nanoscale.

Electron microscopy, such as transmission electron microscopy (TEM) and scanning electron microscopy (SEM), overcomes the constraints of traditional microscopes by utilizing high-resolution imaging and analytical capabilities. It offers unmatched insights into the morphology, structural features, and composition of trace materials—all of which are frequently very important in criminal investigations.

Some of the key findings with respect to both TEM and SEM are as follows.

4.1 Transmission electron microscope

4.1.1 Analysis of paint

- For the purpose of examining paint chips, TEM provides high-resolution imaging that helps detect pigments, binders, layer structures, and elemental makeup.

- Analyses paint and base layers to aid in the authenticity of old artworks. It is vital for recognizing unique properties of car paint, like fillers and primers, which makes possible to image and identify nanoscale particles on paint samples made with focused ion beam technology.

4.1.2 Analysis of soil

- TEM helps to characterize the minuscule soil particles, which makes it easier to comprehend the effects of microbes and elemental changes in soil. Permits the analysis of micrometer-sized micro aggregates, offering information about the functioning of soil and microbial interactions.

4.1.3 An analysis of gunshot residue (GSR)

- TEM, which provides high-resolution imaging and elemental analysis capabilities, is essential for the investigation of nanoscale GSR particles.
- It uses particle analysis to discern between different types of ammunition and their respective geographic origins.

4.1.4 Analysis of fibers

- TEM helps discover asbestos in tissue samples linked to health problems and mineral fibers in lung tissue resulting from industrial dangers.
- Reveals patterns of structural damage in chemically treated fiber, offering information about micro-fibril structure.

4.1.5 Analysis of hair

- Through a deeper understanding of the cellular architecture surrounding hair follicles, TEM helps to uncover biological interactions that may otherwise go undetected.
- It is useful for researching the harm that chemical treatments, such as bleaching, have to the proteins and structure of hair.

4.1.6 Glass evaluation

- To help determine the source of glass pieces (such as shootings or hit-and-run occurrences), TEM looks at the internal microstructure of the broken glass.
- It helps identify glass composition in order to connect broken glass to certain sources, such as bottles or windows.

4.1.7 Nanoparticles

- Nanoparticles discovered as trace evidence are characterized by TEM, which helps to build a reference database for upcoming forensic investigations.

4.1.8 Explosives

- By analyzing explosive residues at the nanoscale, TEM helps with pre- and post-blast analysis and helps determine the type of explosive employed in blast scenarios.
- Essential for researching quantum dots, which are utilized to recognize typical nitro-base explosives.

4.2 Scanning electron microscope

4.2.1 GSR analysis

- GSR particles that have been removed from specimens are thoroughly imaged, and their elemental composition is examined using a combination of SEM and energy dispersion spectroscopy (EDS).
- Predicting firing range and assisting in crime resolution revolutionizes forensic investigations by making it easier to identify GSR particles at far distances.

4.2.2 Gemstone and jewelry analysis

- SEM is a vital tool for the identification and distinction of gemstones, offering information on their internal and exterior characteristics, origin in geology, and possible treatment history.
- SEM supports the analysis of material composition, plating thickness, and surface coatings in jewelry forensics, helping to validate authenticity and identify counterfeits.

4.2.3 Paint and fiber analysis

- SEM developments have a substantial impact on paint analysis. They allow for the detailed examination of paint layers, pigments, and structural characteristics, which makes it easier to distinguish between samples that come from different sources.
- SEM is essential to fiber analysis because it helps identify and detect changes or contamination by analyzing structure, surface characteristics, and elemental constitution.

4.2.4 Filament bulb investigation in traffic accident

- By examining surface characteristics and materials, SEM's thorough imaging aids in the understanding of filament bulb fracture during auto accidents and offers vital hints regarding the cause or impact aspects of the accident.

4.2.5 Handwriting and print inspection

- SEM's use in handwriting analysis helps identify specific writing characteristics, document modifications, and printing techniques, which makes a major contribution to verification and the discovery of forgeries.

4.2.6 Non—Conductive material analysis


- Non conductive materials such as polymer and ceramics can be examined by SEM by integrating energy-dispersive X-ray spectroscopy (EDS) with specialized sample preparation. SEM provides insights into the surface structure, elemental composition, and material properties of these materials.

Author details

Niha Ansari*, Jeet Dasgupta, Shweta Umre and Priya Rajput
School of Forensic Science, National Forensic Sciences University,
Gandhinagar, Gujarat, India

*Address all correspondence to: niha.ansari@nfsu.ac.in

IntechOpen

© 2024 The Author(s). Licensee IntechOpen. This chapter is distributed under the terms of the Creative Commons Attribution License (<http://creativecommons.org/licenses/by/3.0>), which permits unrestricted use, distribution, and reproduction in any medium, provided the original work is properly cited. 

References

- [1] History of the Electron Microscope. 2018. Available from: <https://www.news-medical.net/life-sciences/History-of-the-Electron-Microscope.aspx#:~:text=It%20was%20Ernst%20Ruska%20and,was%20possible%20with%20electron%20microscopy>
- [2] Shaber L, Shaber, L. The History of the Electron Microscope. Advancing Materials. 2018. Available from: <https://www.thermofisher.com/blog/materials/the-history-of-the-electron-microscope/#:~:text=To%20build%20on%20the%20power,The%20solution:%20compound%20microscopes.&text=2>
- [3] Schwab K. What Role Does SEM Play in Trace Evidence Analysis? - Nanoscience Instruments. Nanoscience Instruments. 2023. Available from: <https://www.nanoscience.com/blogs/what-role-does-sem-play-in-trace-evidence-analysis/#:~:text=These%20materials%20can%20include%20fibers,valuable%20information%20in%20criminal%20investigations>
- [4] Twyman R. Microscopy applications: Food. In: Worsfold P, Townshend A, Poole C, editors. Encyclopedia of Analytical Science (Second Edition). London, UK: Elsevier Science; 2005;6:50-57
- [5] Corradini MG, Julian McClements D. Food ☆. In: Reference Module in Chemistry, Molecular Sciences and Chemical Engineering. Vol. 2019. Elsevier; 2017. pp. 47-56
- [6] Australian Microscopy and Microanalysis Research Facility, "My Scope-training for advanced research." Available from: <http://www.ammrf.org.au/myscope/sem/background/> [Accessed: May 3, 2018]
- [7] Mohammed A, Abdullah A. Scanning electron microscopy (SEM): A review. In: Proceedings of 2018 International Conference on Hydraulics and Pneumatics-HERVEX, Baile Govora, Romania, 7-9 November 2018. 2019. pp. 1-9. ISSN 1454 – 8003
- [8] Check out MyScopeTM. n.d. Available from: https://myscope.training/#/TEMlevel_3_1
- [9] Rukari T, Babita A. Review article transmission electron microscopy-an overview. International Research Journal for Inventions in Pharmaceutical Sciences. 2013;1(2):1-7
- [10] Tang H, Martin DC. Microstructural studies of interfacial deformation in painted thermoplastic polyolefins (TPOs). Journal of Materials Science. 2003;37:4783-4791
- [11] Barba C, Andrés MS, Peinado J, Báez MI, Baldonado JL, Andres MS, et al. A note on the characterization of paint layers by transmission electron microscopy. Studies in Conservation. 1995;40(3):194
- [12] Goebel R, Stoecklein W. The use of electron microscopic methods for the characterization of paints in forensic science. Scanning Microscopy. 1987;1(3):16
- [13] Lins A, Giannuzzi LA, Stevie FA, Price B, Tucker M, Gutman N. Fib/tem analysis of paint layers from Thomas Eakins' the crucifixion, 1880. MRS Proceedings. 2002;712:12
- [14] Elsass F, Chenu C, Tessier D. Transmission electron microscopy for soil samples: Preparation methods and use. In: Methods of Soil Analysis Part 5-Mineralogical Methods. Soil Science Society of America. 2015. pp. 235-268

- [15] Watteau F, Villemain G. Soil microstructures examined through transmission electron microscopy reveal soil-microorganisms interactions. *Frontiers in Environmental Science*. 2018;**6**:106
- [16] Watteau F, Villemain G. Soil microstructures examined through transmission electron microscopy reveal soil-microorganisms interactions section soil processes. *Frontiers in Environmental Science*. 2018;**6**:106
- [17] Fitzpatrick RW. Soil: Forensic analysis. In: *Wiley Encyclopedia of Forensic Science*. Chichester, UK: John Wiley & Sons, Ltd; 2004. pp. 1-14
- [18] Warlow TA. *Firearms, the Laws, and Forensic Ballistics*. United Kingdom: Routledge; 1996
- [19] Dalby O, Butler D, Birkett JW. Analysis of gunshot residue and associated materials review. *Journal of Forensic Sciences*. 2010;**55**(4):924-943
- [20] Hill WB. Transmission electron microscopy study of gunshot-residue nanoparticles collected in air samples. *Microscope*. 2012;**60**(3):133-137
- [21] Hill WB. The characterization of nanoparticles using analytical electron microscopy. In: *Proc. Scanning Microscopies 2011. Advanced Microscopy Technologies for Defense, Homeland Security, Forensic, Life, Environmental, and Industrial Sciences*. SPIE Proceedings. 1 June 2011;**80360E**. DOI: 10.1117/12.885115
- [22] Melo LG, Martiny A, Pinto AL. Nano characterization of gunshot residues from Brazilian ammunition. *Forensic Science International*. 2014;**240**:69-79
- [23] Friedrichs KH, Brockmann M, Fischer M, Wick G. Electron microscopy analysis of mineral fibers in human lung tissue. *American Journal of Industrial Medicine*. 1992;**22**(1):49-58
- [24] Reza M, Kontturi E, Jääskeläinen A-S, Vuorinen T, Ruokolainen J. Transmission electron microscopy for wood and fiber analysis—a review. *BioResources*. 2015;**10**(3):6230-6261
- [25] Morioka K. A guide to hair follicle analysis by transmission electron microscopy: Technique and practice. *Experimental Dermatology*. 2009;**18**(7):577-582
- [26] Lee Y, Kim Y, Pi L, Lee SY, Hong H, Lee W. Comparison of hair shaft damage after chemical treatment in Asian, White European, and African hair. *International Journal of Dermatology*. 2013;**53**(9):1103-1110
- [27] Ji JH, Park TS, Lee HJ, Kim YD, Pi LQ, Jin XH, et al. The ethnic differences of the damage of hair and integral hair lipid after ultra violet radiation. *Annals of Dermatology*. 2013;**25**(1):54
- [28] Grosvenor AJ, Deb-Choudhury S, Middlewood PG, Thomas A, Lee E, Vernon JA, et al. The physical and chemical disruption of human hair after bleaching – Studies by transmission electron microscopy and redox proteomics. *International Journal of Cosmetic Science*. 2018;**40**(6):536-548
- [29] Curran JM, Champion TNH, Buckleton JS. *Forensic Interpretation of Glass Evidence*. Boca Raton: CRC Press; 2000
- [30] Schumacher EF. A High-Resolution Look at Glass Delamination Using Transmission Electron Microscopy (TEM). (n.d.). Available from: <https://www.americanlaboratory.com/913-Technical-Articles/134532-A-High-Resolution-Look-at-Glass-Delamination-Using-Transmission-Electron-Microscopy-TEM/>

- [31] Cantu AA. Nanoparticles in forensic science. SPIE Proceedings. 2008;**7119**:71190F-1-8
- [32] Santra TS, Tseng FGK, Barik TK. Biosynthesis of silver and gold nanoparticles for potential biomedical applications—A brief review. Journal of Nanopharmaceutics and Drug Delivery. 2014;**2**(4):249-265
- [33] Hill WB. Forensic applications of the transmission electron microscope. The Microscope. 2016;**57**(4):165-170
- [34] Kashkarov AO, Prueel ER, Ten KA, Rubtsov IA, Gerasimov EY, Zubkov PI. Transmission electron microscopy and x-ray diffraction studies of the detonation soot of high explosives. Journal of Physics: Conference Series. 2016;**774**:012072
- [35] Li Z, Wang Y, Ni Y, Kokot S. A sensor based on blue luminescent graphene quantum dots for analysis of a common explosive substance and an industrial intermediate, 2,4,6-trinitrophenol. Spectrochimica Acta Part A: Molecular and Biomolecular Spectroscopy. 2015;**137**:1213-1221
- [36] Raj AV, Waghmare NP, Monika J, Neelesh T. An experimental investigation of gunshot residue (GSR) evidence: Directly from targeted fabric using sem. International Journal of Medical Toxicology & Legal Medicine. 2020;**23**:233-244
- [37] Brožek-Mucha Z, Jankowicz A. Evaluation of the possibility of differentiation between various types of ammunition by means of GSR examination with SEM–EDX method. Forensic Science International. 2001;**123**(1):39-47
- [38] Reyes LC, López CE, Barrios AB, Soto C, Ibáñez C, Díaz FJ. Development and application of a new nose hairs sample collection device for GSR particles by scanning electron microscopy with energy dispersive X-ray spectroscopy (SEM-EDS). Forensic Science International. 2018;**290**:42-48
- [39] Kara İ. The influence of different skin types on GSR sampling by tape lifting for SEM analysis. Microscopy Research and Technique. 2017;**80**(12):1310-1314
- [40] Toal SJ, Niemeyer WD, Conte S, Montgomery DD, Erikson GS. Confirmatory analysis of field-presumptive GSR test sample using SEM/EDS. Proceedings of SPIE. 2014;92361C. DOI: 10.1117/12.2074212
- [41] Scanlan MD, Reinholz AD. Scanning electron microscopy for firearm and toolmark comparisons. AFTE Journal. 2013;**45**(1):43-47
- [42] Pal A, Debnath S, Pratihari HK. Post Analysis of a Firing Case by Optical and Scanning Electron Microscopy. Journal of Advanced Microscopy Research. 2014;**9**(1):67-70. DOI: 10.1166/jamr.2014.1190
- [43] Korda EJ, MacDonell HL, Williams JP. Forensic applications of the scanning electron microscope. Journal of Criminal Law, Criminology and Police Science. 1970;**61**:453
- [44] Bíró C, Kováč P, Palkovic M, El-Hassoun O, Čaplovičová M, Novotný J, et al. Potentialities of scanning electron microscopy and EDX analysis in bullet wounds. Romanian Journal of Legal Medicine. 2010;**18**(3):225-230
- [45] Hopkins T, Peniche G, Murphy S, Carter I, Shorrock G, Kearns S, et al. Scanning electron microscopy and energy-dispersive x-ray spectroscopy (SEM-EDX) confirms shooting of a hen harrier (*Circus cyaneus*). Veterinary Record Case Reports. 2015;**2015**(3):e000241

- [46] Cartier LE, Krzemnicki MS, Lendvay B, Meyer JB. DNA fingerprinting of pearls, corals and ivory: A brief review of applications in gemmology. *The Journal of Gemmology*. 2018;**36**(2):152-160
- [47] Tiwari S, Sahu DK, Thakur VS, Patel MM, Chandra T. Forensic morphological and elemental analysis of gold jewellery: A case study. *International Journal of Science and Research Archive*. 2023;**9**(2):516-519
- [48] Troalen L, Guerra M, Tate J, Manley B. Technological study of gold jewellery pieces dating from the middle kingdom to the new kingdom in Egypt. *Archeo Sciences*. 2009;**33**:111-119
- [49] Burat F, Baştürkçü H, Özer M. Gold& silver recovery from jewelry waste with combination of physical and physicochemical methods. *Waste Management*. 2019;**89**:10-20
- [50] Schreiner M, Melcher M, Uhlir K. Scanning electron microscopy and energy dispersive analysis: Applications in the field of cultural heritage. *Analytical and Bioanalytical Chemistry*. 2006;**387**(3):737-747
- [51] Mahltig B, Grethe T. High-performance and functional fiber materials—A review of properties, scanning electron microscopy SEM and electron dispersive spectroscopy EDS. *Text*. 2022;**2**(2):209-251
- [52] Jaques VAJ, Zikmundová E, Holas J, Zikmund T, Kaiser J, Holcová K. Conductive cross-section preparation of non-conductive painting micro-samples for SEM analysis. *Scientific Reports*. 2022;**12**(1):19650
- [53] News-Medical.net. Analysing Morphology of Plant Fibers using Scanning Electron Microscopy. 2017. Available from: <https://www.news-medical.net/whitepaper/20170925/Analysing-Morphology-of-Plant-Fibers-using-Scanning-Electron-Microscopy.aspx>
- [54] Paint Analysis. (n.d.). Available from: <https://www.materials.co.uk/paintanalysis.htm>
- [55] Park JB, Kim YJ, Kim SW, Yoo JH, Kim Y, Gorbachev R, et al. Non-destructive electron microscopy imaging and analysis of biological samples with graphene coating. *2D Materials*. 2016;**3**(4):045004
- [56] Using the scanning electron microscope to identify the cause of fibre damage Part II: An exploratory study | Office of Justice Programs. (n.d.). Available from: <https://www.ojp.gov/ncjrs/virtual-library/abstracts/using-scanning-electron-microscope-identify-cause-fibre-damage-0>
- [57] Thorsen KA. Forensic Examination of Bulb Filaments by the SEM. Denmark: Springer eBooks; 1986. pp. 117-147
- [58] Horvat R, Barišić-Jaman B, Mršić G, Špoljarić I, Vrdoljak A, Pehar I. Method of light bulbs analysis on vehicles damaged in traffic accidents. *Promet-Traffic & Transportation*. 2012;**22**(4):259-271
- [59] Grafiati. Journal articles on the topic “Traffic accident investigation.” Grafiati. 2023. Available from: <https://www.grafiati.com/en/literature-selections/traffic-accident-investigation/journal/>
- [60] Wang J, Ren J, Yuan C, Shen Y, Gan Q, Shi J, et al. Non-invasive optical micro-identification of ink verification in pen ink handwriting. *Results in Chemistry*. 2020;**2**:100025
- [61] Verma N, Sharma V, Kumar R, Sharma R, Joshi MC, Umaphathy G, et al. On the spectroscopic examination

of printed documents by using a field emission scanning electron microscope with energy-dispersive X-ray spectroscopy (FE-SEM-EDS) and chemometric methods: Application in forensic science. *Analytical and Bioanalytical Chemistry*. 2019;**411**(16):3477-3495

[62] AZoOptics.com. How is Electron Microscopy Used for Forensic Document Examination? 2023. Available from: <https://www.azooptics.com/Article.aspx?ArticleID=2446>

[63] Pingitore V, Barberio M, Oliva A, Davoli M. A golden drachma from Bruttia: Counterfeit money revealed by scanning electron microscopy and cathodoluminescence. *Mediterranean Archaeology and Archaeometry*. 2008;**8**(2):31-38

[64] Griffin B. A new mechanism for the imaging of crystal structure in non-conductive materials: An application of charge-induced contrast in the environmental scanning electron microscope (ESEM). *Microscopy and Microanalysis*. 1997;**3**(S2):1197-1198

[65] Cao C, Gao R, Shang H, Peng T. Characterization of non-conductive materials using field emission scanning electron microscopy. *Proceedings of SPIE*. 2016;**9903**:990319

[66] Wang ZG, Liu KG, Jiang M, Pang B. SEM analysis of non-conducting materials under low vacuum conditions. *Advanced Materials Research*. 2010;**152-153**:897-901

Perspective Chapter: Predictive Genomics

Jörg Kriegsmann, Sanja Cirovic, Rita Casadonte, Torsten Hansen, Katharina Kriegsmann and Mark Kriegsmann

Abstract

Predictive genomics can support treatment decisions by giving people the chance to act in time to prevent serious illness. Tests based on single nucleotide polymorphism (SNP) can be analyzed by various methods. Matrix-assisted laser desorption/ionization time-of-flight (MALDI-TOF) mass spectrometry technology detects genetic variants based on their individual mass. Standardized workflow, automation, sensitivity, quick turnaround time, and reliability are the main advantages of the MALDI-TOF use in molecular analysis. Beside pharmacogenetics, SNP variation plays a role in various fields of medicine. In the present article importance of various SNPs for nutrigenetics is presented. Especially, various aspects of fat metabolism, vitamin metabolism, and intolerances were discussed.

Keywords: MALDI-TOF (matrix-assisted laser desorption/ionization time-of-flight), SNP (single nucleotide polymorphism), nutrigenetics, predictive genomics, vitamins, intolerances

1. Introduction

Predictive genetics includes various areas of genetics, including nutrigenetics, fitness genetics, and pharmacogenetics. Some authors use the word “lifestyle genetics” because it is different from medical genetics.

Genetic and nongenetic information has to be combined to understand diseases and include this information into personalized preventive medicine.

For the investigation of genetic polymorphisms, mass spectrometry seems to be a very reliable and cost-efficient method compared to next generation sequencing (NGS) technology when investigating not more than 250 SNPs.

We have developed several genetic test panels for various areas of genetic diagnostics and discuss some aspects of nutrigenetics as fat metabolism, vitamins, and intolerances in this report.

2. Mass spectrometry in medicine

Mass spectrometry represents a technology, which is increasingly applied in medical diagnostics. Recently, review articles were analyzed concerning mass spectrometry consisting of microbiological pathogens, diagnosis of diseases, DNA analysis, and small molecules [1].

Matrix-assisted laser desorption/ionization time-of-flight (MALDI-TOF) mass spectrometry is used in everyday routine in clinical diagnostic of microorganism infections. MALDI-TOF technology has many advantages versus traditional techniques, especially fast turnaround time, low amount of hands-on time, and low cost [2]. Direct identification of viruses and bacteria is possible within minutes, allowing the administration of a targeted antimicrobial therapy [3]. Microorganisms were detected by mass spectrometry based on a mass spectrum identifying a characteristic spectrum, which is compared to a large database provided by the manufacturers of the mass spectrometers [4]. Furthermore, the technology may clarify microbial resistance mechanisms [5, 6]. Numerous reports have been published identifying bacteria, fungi [6], and various viruses [7, 8].

Mass spectrometry is able to identify drugs and other metabolites in various body fluids, tissues, and cells [9, 10]. This technique is not only able to identify molecular targets but also their spatial distribution providing a three-dimensional image of the targets. Spatial analysis of drug absorption, distribution, metabolism, and toxicology has been performed using mass spectrometry imaging (MSI) technique [11, 12]. One of the recent developments of MSI is the highly multiplexed immunohistochemistry (IHC) based on MALDI MSI (MALDI-IHC), where up to 30 different antibodies simultaneously can be detected and quantified within a tissue section [13].

Imaging technology was also used in tumor classification providing a tool to identify morphological features of a tissue combined with detection of proteins, glycans, or lipids directly without the limitations and expense of antibodies [14, 15].

The technique of mass spectrometry has been used for the detection of various molecules. The molecular targets for mass spectrometry include proteins [16], peptides [17], lipids [18], glycans [19–22], and metabolites [23]. Application of mass spectrometry in nucleic acid analysis has been shown in various fields [24–26].

A new and growing class of medical tests, differing from conventional medical diagnostic tests, are tests in genetics [27, 28], including pharmacogenetics [29, 30].

3. Mass spectrometry in genetics

Predictive genetic tests represent a new and growing field in medicine that differs from conventional medical diagnostic tests. Unlike testing patients with a disease condition, predictive genetics is applied in asymptomatic people to predict the future risk of disease. Early identification of individuals at risk for a specific condition will lead to reduced morbidity and mortality. Unfortunately, predictive genetic tests carry a degree of uncertainty about whether a condition will develop, when it will develop, and its severity [31].

Various genetic tests were developed and integrated into medical diagnostics, especially in predictive medicine [32].

To date, the medical genetic tests offered are mainly for BRCA1/2 (59, 40%), Lynch syndrome (23, 16%), and newborn screening (18, 12%).

3.1 SNP and GWAS

It is well-known that the DNA sequence at each locus may contain nucleotide bases: A, C, G, and T, which can be similar (homozygous) or different (heterozygous) at each DNA strength.

Single-nucleotide polymorphisms (SNPs) are DNA polymorphisms caused by a single-nucleotide substitution mutation. SNPs are caused by mutation and are present one SNP per thousand bases [33].

SNPs may influence various disease conditions and may alter metabolism of various drugs. The difference between SNP and SNV (single nucleotide variation) is that for the first more than 1% of a population has carry a variant nucleotide at a specific position of the DNA. SNPs can be present in coding (exons) or noncoding regions of DNA (introns). SNPs may cause change in the encoded amino acid or not and may be, therefore, of utmost importance or does not have any effect [34]. Although a particular SNP may not cause a disorder, some SNPs are associated with a disease. Improving knowledge may provide useful SNP markers for medical testing and a safer individualized medication to treat the most common disorders [34].

SNPs may help to provide information to prevent diseases or to give the opportunity of personalized medicine to patients.

In pharmacogenetics specific, SNPs can be used for treatment decisions or to choose the appropriate dosage of a drug. This could save time and could prevent adverse drug effects in patients.

Improved knowledge of the meaning of SNPs comes from genome-wide association studies (GWASs). The principle of GWAS is to compare genetics of two or more different groups of individuals [35, 36]. In the last years, the number of GWAS meta-analysis increased to study various traits in different populations [35].

Genetic analysis of SNPs can be done using various body materials as a source of human DNA such as saliva/buccal smears [37], blood samples [27, 38, 39], bone marrow cell lines [40], cytological liquid samples [41], formalin-fixed paraffin-embedded (FFPE) tissue [24, 26, 42–44].

3.1.1 Mass spectrometry for the detection of SNP (technical considerations)

MALDI-TOF mass spectrometry allows high efficiency in genotyping. An efficient analysis of SNPs is offered by the Agena Bioscience iPLEX® procedure. Automatic extraction of DNA can be performed using Chemagic 360 Instrument (Perkin Elmer). DNA from a variety of biospecimen types (blood, saliva, cells collected by cheek brush, and even from FFPE) can be used for genotyping. Extracted DNA is then processed following manufacturer's instruction for SNP genotyping by Agena Bioscience, described in the multiplex (iPLEX®) assay procedure.

The multiplex (iPLEX®) assay procedure and MassARRAY based on MALDI-TOF mass spectrometry includes several steps [45, 46]. The various steps of this analysis include amplification of targeted DNA sequence by PCR. Then, PCR products are neutralized with shrimp alkaline phosphatase (SAP) for unbound nucleotides. PCR products are then extended by one base. The mass is then measured using a mass spectrometer to produce/calculate a specific mass spectrum of targeted SNPs.

The MassARRAY Analyzer System is built to detect DNA fragments within a mass range of approximately 4500–9000 Da and can easily distinguish between analytes separated by 16 Da. The assay design process is assisted by an online suite of programs that allow for design using “default” settings, as well as “user-defined” settings (more advanced manipulation). Up to two plates of 96 or 384 samples can be genotyped for about 40-plex assay in around 8–12 h, resulting in the generation of more than 30,000 genotypes. Data analysis is performed using MassARRAY Typer Analyzer software from Agena Bioscience. MassARRAY, iPLEX® and SpectroCHIP are registered trademarks of Agena Bioscience, Inc.

3.2 Nutrigenetics

Nutrigenetics attempts to characterize and integrate the relationship between food constituents and gene expression. These approaches for precision nutrition and their relation to disease risk help to identify genetic variants that could modify the effects of dietary intake, affect food metabolism, and influence food preferences [47].

The aim combining genomics and nutrigenomics with clinical data is to get information about genetic variants, which are the basis for personalized nutritional supplementation. The substances of interest for nutritional genetics include lipids, proteins, vitamins, glycose, and iron or calcium [48].

Additionally, in the future, nutrigenetics and nutrigenomics will be combined with data of other omics technologies, such as proteomics and metabolomics, as well as microbiome and data technology [49].

The basic knowledge of emerging nutrigenomics and nutrigenetics can be applied to optimize health, prevention, and treatment of diseases [50]. The increasing number of patients with diabetes and obesity has led focus to these diseases, including genetic risk factors in the last years [51].

Since, these diseases have at least in part a genetic background to explore gene-diet interactions on obesity and diabetes is of utmost interest [52].

Personalized nutrition seems to be necessary because of the substantial variation in the genetic pattern of various human subjects [53].

3.2.1 Fat mass and obesity (FTO) associated gene

FTO gene variants (fat mass and obesity-associated) gene were detected in a GWAS search for genes predisposing for diabetes [36].

This gene is involved in the expression of fat deposition and metabolism-related hormones and genes [54]. For these reasons, investigation of the polymorphism of this gene is included in nearly all specific nutrigenetics and nutrigenomics tests.

Various studies have shown that polymorphisms in this gene lead to a higher body mass index [55, 56].

It has been reported that polymorphisms in the *FTO* gene are associated with other genes involved in adipogenesis. Furthermore, their impact is not solely dependent on the expression of the polymorphisms themselves [57, 58].

The *FTO* rs9939609 has been found to relate to the hormone ghrelin, which is associated with digestive behavior [59].

Childhood metabolic syndrome is prevalent around the world and is associated with increased disease risk, especially of cardiovascular diseases, including hypertension and acute coronary syndrome. Some variants of the human *FTO* gene contribute to the early onset of childhood metabolic syndrome [60].

It must be emphasized that epigenetic influence on the FTO gene is possible as a new approach in the treatment and management of obesity depending on the genetic variant [61].

Figure 1 shows a representative genotyping result of the SNP FTO_rs9939609 using the MassARRAY System.

FTO polymorphisms were reviewed in a minireview, which provides thorough inside into these genetic variants [61].

3.2.2 Lipids

Dyslipidemias are known risk factors, which could require precision nutrition designed according to characteristics, such as diet, phenotype, and genotype [62]. Increased intake of triglycerides and cholesterol is associated with an increased risk of metabolic diseases.

One of the best-studied genetic polymorphisms is that of the Apolipoprotein E (ApoE)-gene.

ApoE plays a key role in the transport of cholesterol. *ApoE* variants are associated with early-onset Alzheimer's disease. Specifically, ApoE4 isoform may be responsible for alterations in insulin- and lipid metabolism, altered gray matter volume, and impaired cerebrovascular functions [63].

The ApoE2 isoform is generally the most favorable and ApoE4 the least favorable for cardiovascular and neurological health. Under metabolic stress, homozygosity for ApoE2 may result in dysbetalipoproteinemia [64].

It is of special interest that omega-3 fatty acid intake and physical activity may modify the impact of ApoE4 on Alzheimer's disease and cardiovascular disease risk [65].

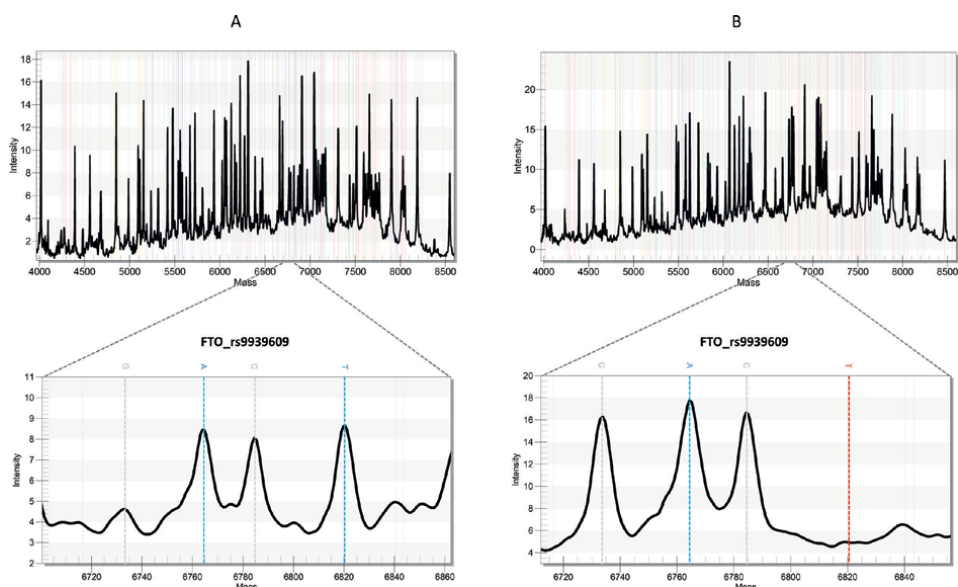


Figure 1. Representative genotyping result of the SNP FTO_rs9939609 with the MassARRAY system. (A) Spectrum showing a representative multiplex assay of a patient with heterozygous genotype for the SNP FTO_rs9939609 (AT). A zoomed view in the mass range 6700–6860 shows two peaks indicated with blue dotted lines representing the heterozygous alleles (AT). (B) Representative spectrum of multiplex assay of a patient with homozygous genotype for the SNP FTO_rs9939609 (AA). A zoomed view in the mass range 6700–6860 shows the detection of one single peak of interest (blue dotted line).

Genotyping for ApoE may help develop a targeted approach to disease prevention. Adherence to Mediterranean diet may lower Alzheimer's disease-related anatomical or clinical symptoms in individuals without ApoE4 genotype [66].

The association of diet rich in saturated fatty acids may increase Alzheimer's risks in ApoE4 carriers [67].

3.2.3 Nonalcoholic fatty liver disease NFLD

Nonalcoholic fatty liver disease (NAFLD) is a chronic condition associated with genetic and environmental factors, obesity, type 2 diabetes, and dyslipidemia in which fat abnormally accumulates in the liver. Different genetic polymorphisms seem to be involved in this context [68].

3.2.4 Vitamins

3.2.4.1 Vitamin A

Retinol (Vitamin A) plays a crucial role in the anti-aging industry, primarily due to its ability to neutralize free radicals in tissues, which subsequently leads to a reduced appearance of wrinkles.

β -carotene 15,15'-monooxygenase 1 (BCMO1) is the most critical enzyme involved in retinoid metabolism [69].

Especially, A379V TT variant was inversely related to vitamin A status [69]. Assessment of the responsiveness to beta-carotene confirmed that carriers of variant alleles had a reduced ability to convert beta-carotene [70].

Individual responsiveness was associated with genetic variants in SNP rs7501331 of the carotenoid metabolizing enzyme BCMO1, resulting of single nucleotide variation (SNV) from C to T [71]. Carriers of T nucleotide have lower ability to convert beta-carotene. Studies shown that only 5% of the population have TT genotypes, while 56% have CC. Having this on mind and knowing that lacking of normal retinol metabolism is responsible for several diseases, supplementation/treatment of vitamin A should be completely personalized in the future in regards to genetic variations in the BCMO1 gene [72, 73].

3.2.4.2 Vitamin B9 (folic acid)

Vitamin B9 is molecule responsible for normal cell growth and development. It is crucial supplement in the prevention of pregnancy complication. Enzyme, which plays a key role in vitamin D metabolisms, is 5,10-methylenetetrahydrofolate reductase (MTHFR), and it regulates around 60% of folic acid metabolism [48].

Mutations in the MTHFR gene can result in abnormal folate metabolism, which is associated with and may contribute to various pathological conditions, including stroke, depression, and reduced cognitive function etc.

Two mutations in SNPs, rs1801131 (SNV, T > G) and rs1801133 (SNV, G > A) have been reported that affect enzymatic activity of MTHFR [74].

Depending in which SNP is the mutation and the state of mutation (is it homozygous or not) several possible phenotypes can be detected. Each phenotype is associated with specific enzyme the activity and function.

Individuals with MTHFR (rs1801133) genotype CC has normal homocysteine levels, on the other hand, patients with TT genotype have high level of homocysteine

and low folate levels. So, autosomal recessive MTHFR polymorphism led to wide range of vascular and neurological unfunctionally [75, 76].

The risk genotype of rs1801133 has been related with various pathological conditions such as deep vein thrombosis, various cardiovascular diseases (CVDs), then cancer, diabetes, etc. [76–78].

TT genotype is also known as C677T MTHFR polymorphism. Supposition of C with T will lead to amino acid change from alanine to valine. If a patient has two defective alleles of the MTHFR gene, enzyme activity can be reduced by 80 to 90%. Recent clinical studies have demonstrated that carriers of these alleles are at a significantly higher risk of ischemic stroke [79].

Studies on MTHFR have been successfully used to develop disease prevention strategies [80]. And therefore, future health education has to be based on personalized nutritional recommendations and prevention strategies in the field of vitamins supplementation.

3.2.4.3 Vitamin D

Vitamin D has been highlighted as a prime example of nutrigenomics. It is a molecule with multiple roles in the human body, including important functions in metabolism and various clinical applications [81, 82].

This vitamin plays a role in numerous system, such as in the immune system [83], skeletal system [84], reproductive system [85], insulin secretion [86], and intestinal system [87].

Vitamin D deficiency is very frequent, with almost 40% of the Europeans presenting levels below 50 nmol/L [88].

Vitamin D receptor (VDR) regulates several target gene transcription processes necessary for various biological functions of vitamin D. VDR will make hormone-receptor complex with active form of vitamin D (1,25(OH)₂D₃) in target cells. This complex interfere with specific DNA sequences of target genes to control the expression of numerous genes [89, 90].

Some genetic variants of the gene encoding VDR modify either its expression or function, with the consequent disruption of the vitamin D signaling pathway. Recent publications on the relationship between VDR genetic variants and the risk of type 2 diabetes, metabolic syndrome, overweight, and obesity were reviewed and give only partial answers to this question [91].

Vitamin D analogs bind to vitamin D receptors in tumor cells and activate downstream pathways to inhibit tumor growth. VDR expression is a prognostic indicator for digestive system tumors. That the intake of vitamin D analogs should be determined according to vitamin D receptor expression was stated in a comprehensive review on tumors of the digestive tract [92].

Findings considering gene polymorphisms in the VDR gene, which are based on the role of VDR SNPs in gene regulation and protein expression, will help to understand the detected role of VDR in various diseases [93].

For personalized medicine and pharmacogenomics new studies of VDR polymorphisms and vitamin D-VDR signaling are necessary for better understanding of role of this complex in various diseases [94].

Individuals who are genetically predisposed to low vitamin D benefit from foods rich in this vitamin [95, 96].

Individuals with genetic changes in the VDR gene may benefit from foods rich in vitamin D and from calcium and/or vitamin D supplementation [97, 98].

3.3 Intolerances

3.3.1 Gluten

Celiac disease (CD) is an autoimmune disorder, affecting about 1% of the population, where individuals are genetically predisposed to gluten intolerance [99, 100]. Gluten is a protein complex present in some cereals such as wheat, barley, and rye, in which gliadins and glutenin proteins are considered to be responsible for the inappropriate immune response of the genetically predisposed individuals. This condition can cause a localized complication in the mucosa of the intestine with toxic effects, leading to villous atrophy and lymphocyte infiltration in the small intestinal mucosa [101]. Typical symptoms include diarrhea, digestive tract pain and discomfort, weight loss, and malabsorption of nutrients [102].

There is a genetic basis at the origin of CD that determines susceptibility to the disease, which is correlated with genes in the human leukocyte antigen (HLA) system. More specifically, genetic testing for CD consists of determining the presence of the HLA DQ2 and DQ8 alleles [103].

Most CD cases (90%) are associated with the presence of the HLA-DQ2 haplotype encoded by (HLA-DQA1*05-DQB1*02). Some patients (5%) carry a second HLA DQ8 heterodimer encoded by (DQA1*03-DQB1*0302), and the remaining 5% of patients hold at least one of the two genes [104]. Six SNPs in HLA-DQ genes are responsible for CD, and in 75% patients CD has hereditary pattern. Sporadic, non -HLA related CD will occur in 68% patients [105].

Screening of single nucleotide polymorphisms by mass spectrometry within HLA region is an efficient method to accurately analyze multiple SNPs at the same time [106]. For example, individuals with CC (around 1% in Caucasian population) genotype in HLA-DQ8 gene (rs7454108) have high risk of gluten intolerance, while CT genotype indicates moderate risk of gluten intolerance. However, the most frequent genotype for this polymorphism in Caucasian population is TT (no risk), around 80% (**Figure 2**), indicating that other genes. SNPs from HLA-DQ system plays key role in gluten intolerance.

3.3.2 Lactose

The most common carbohydrate, which is the main component of milk and milk products, is disaccharide lactose. Necessary enzymes in lactose metabolism (*located at* LCT/MCM6 gene) have role to *cut lactose in glucose and* galactose [107]. The ability to digest and have a normal metabolism of lactose in adults is called lactase persistence/persistent (LP). LP is regulated by five genetic polymorphisms, which have dominant distribution in humans [108].

Lactase non-persistence/intolerance is a worldwide phenomenon, but it affects people with varying degrees of severity. Completely inactive lactase gene is very rare and present in patients with alactasia [109].

Lactose intolerance can manifest as secondary lactase deficiency, which can be either temporary or chronic, depending on the duration and nature of the harmful mediator affecting the small intestinal mucosa cells. Alternatively, it can appear as primary lactase deficiency, typically emerging in adolescence or early adulthood [110].

In the natural condition lactase non-persistence (LPN) in primary lactase deficiency, the activity of the enzyme LCT decreases with age. Various studies have been

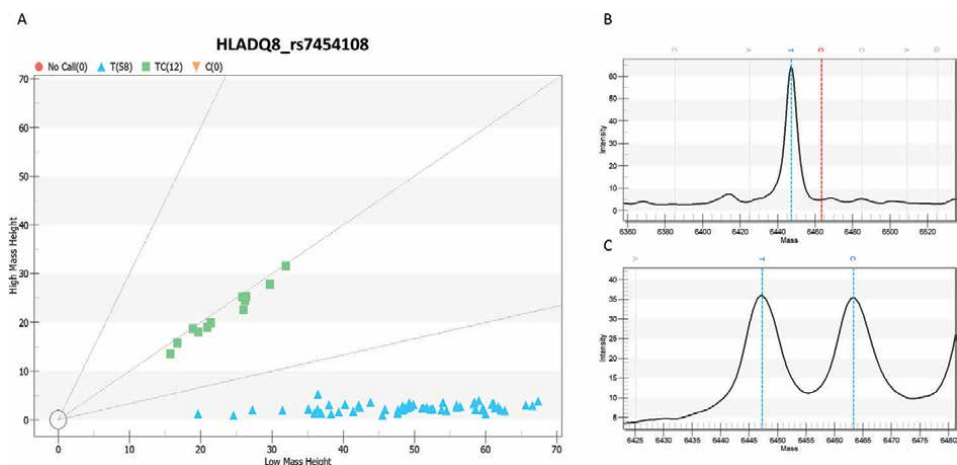


Figure 2.
 (A) Representative cluster plot displaying the SNP HLADQ8_rs7454108 genotypes of 70 samples assayed. Heterozygous region is close to the 45°-line (green squares represent heterozygous (TC) samples. Homozygous region for the low mass allele is close to the X coordinate (blue triangles represent homozygous (TT) samples for the same SNP. (B) Representative spectrum of homozygous genotype (TT) for the SNP HLADQ8_rs7454108 where one single peak of interest (blue dotted line) is indicated for the allele T. (C) Example of a spectrum of heterozygous genotype (TC) for the same SNP HLADQ8_rs7454108 where two peaks of interest are indicated with blue dotted lines representing the heterozygous alleles (AT).

done and shown that genetic alterations are responsible for type of reduced lactase enzyme activity [111].

In the European population polymorphism in gene MCM6 (rs4988235, C > T), which is placed in the promoter region of MCM6 gene is mainly responsible for tolerance or intolerance for lactose.

Lactase intolerance in adults is triggered by a recessively congenital polymorphism of the MCM6 gene, and this phenotype is inherited as an autosomal dominant characteristic. Individuals who carry C allele are likely that will develop lactose intolerance during lifetime, meaning that CT individuals have more chance that they can digest milk in older ages, while TT individuals can digest lactose during all lifetime [112].

The decreased ability of the body to hydrolyze lactose is due to a programmed regulatory phenomenon involving the MCM6 gene intron, 13,14 kb upstream of the MCM6 gene. This gene has several single nucleotide base polymorphisms including the (rs4988235) for which the Thymine (T) allele forms an haplotype that is commonly evaluated in LP studies [113].

The -13,910*T allele is commonly distributed in the European population with an average frequency of 50.8%. However, genetic distribution of T allele is most prevalent in northern Europe, especially England and Scotland (72.0% of the population), while it progressively decreases in the southern Europe with a frequency of 8.9% in Tuscany, Italy [114].

Mutations in the SNP rs4988235 cause intolerance problems [115]. Specifically, a genotype that has two (TT) at position -13,910 results in a lactase persistence (LP), while a homozygous CC genotype in the same position results in a lactase non-persistent (LNP) phenotype [116, 117].

The undigested lactose that remains in the intestine is metabolized by intestinal bacteria with the generation of an osmotic effect causing a recall of water, resulting in

symptoms such as diarrhea, cramping, meteorism, intestinal discomfort, and sometimes nausea and vomiting [118, 119].

Twenty-nine percentage of individuals reported symptoms attributed to the ingestion of fresh milk, with abdominal pain, bloating, and flatulence being the most frequent [120].

Previous studies have shown that gut microbiota may be capable of adapting to lactose consumption in LNP individuals [121].

Mass spectrometry seems to be an ideal method to detect SNPs in the MCM-Gene. By excluding the genetic predisposition to lactose intolerance, people can avoid unnecessary dietary restrictions on dairy products [122].

4. Conclusions

This book chapter aimed to present the application of mass spectrometry for DNA analysis. After a small introduction of application of mass spectrometry in modern medicine methods for the detection of SNPs were discussed. Furthermore, an overview about studies using SNPs as genetic markers related to nutrigenetics, including fat metabolism, vitamins, and intolerances, were provided.

In the last years, MALDI-TOF mass spectrometry technique has been proven to be a versatile tool for the characterization of point mutations. This method allows the detection of SNPs in a rapid, precise, cost-effective, and high-throughput way. MALDI-TOF is a technique, which allows assessment of up to 250 SNPs. For the analysis of a larger amount of SNPs or genome-wide association studies, next-generation sequencing is the method of choice.

Conflict of interest

The authors declare no conflict of interest.

Author details

Jörg Kriegsmann^{1,2*}, Sanja Cirovic^{1,3}, Rita Casadonte¹, Torsten Hansen³, Katharina Kriegsmann⁴ and Mark Kriegsmann⁵

1 Proteopath GmbH, Trier, Germany

2 Faculty of Medicine/Dentistry, Danube Private University (DPU), Krems-Stein, Austria


3 Center for Histology, Cytology and Molecular Diagnostics Trier GmbH, Trier, Germany

4 Laborarztpraxis Rhein-Main MVZ GbR, Limbach Gruppe SE, Frankfurt am Main, Germany

5 Center for Histology, Cytology and Molecular Pathology Wiesbaden, Wiesbaden, Germany

*Address all correspondence to: joerg.kriegsmann@patho-trier.de

IntechOpen

© 2024 The Author(s). Licensee IntechOpen. This chapter is distributed under the terms of the Creative Commons Attribution License (<http://creativecommons.org/licenses/by/3.0>), which permits unrestricted use, distribution, and reproduction in any medium, provided the original work is properly cited. 

References

- [1] Li D, Yi J, Han G, Qiao L. MALDI-TOF mass spectrometry in clinical analysis and research. *ACS Measurement Science Au.* 2022;**2**(5):385-404
- [2] Chen XF, Hou X, Xiao M, Zhang L, Cheng JW, Zhou ML, et al. Matrix-assisted laser desorption/ionization time of flight mass spectrometry (MALDI-TOF MS). Analysis for the identification of pathogenic microorganisms: A review. *Microorganisms.* 2021;**9**(7):1536
- [3] Oviano M, Rodriguez-Sanchez B, Gomara M, Alcala L, Zvezdanova E, Ruiz A, et al. Direct identification of clinical pathogens from liquid culture media by MALDI-TOF MS analysis. *Clinical Microbiology and Infection.* 2018;**24**(6):624-629
- [4] Hou TY, Chiang-Ni C, Teng SH. Current status of MALDI-TOF mass spectrometry in clinical microbiology. *Journal of Food and Drug Analysis.* 2019;**27**(2):404-414
- [5] Oviano M, Bou G. Matrix-assisted laser desorption ionization-time of flight mass spectrometry for the rapid detection of antimicrobial resistance mechanisms and beyond. *Clinical Microbiology Reviews.* 2019;**32**(1):e00037-18
- [6] Vrioni G, Tsiamis C, Oikonomidis G, Theodoridou K, Kapsimali V, Tsakris A. MALDI-TOF mass spectrometry technology for detecting biomarkers of antimicrobial resistance: Current achievements and future perspectives. *Annals of Translational Medicine.* 2018;**6**(12):240
- [7] Wierz M, Sauerbrei B, Wandernoth P, Kriegsmann M, Casadonte R, Kriegsmann K, et al. Detection of severe acute respiratory syndrome coronavirus 2 (SARS-CoV-2) including variant analysis by mass spectrometry in placental tissue. *Viruses.* 2022;**14**(3):604
- [8] Calderaro A, Arcangeletti MC, Rodighiero I, Buttrini M, Montecchini S, Vasile Simone R, et al. Identification of different respiratory viruses, after a cell culture step, by matrix assisted laser desorption/ionization time of flight mass spectrometry (MALDI-TOF MS). *Scientific Reports.* 2016;**6**:36082
- [9] Ren JL, Zhang AH, Kong L, Wang XJ. Advances in mass spectrometry-based metabolomics for investigation of metabolites. *RSC Advances.* 2018;**8**(40):22335-22350
- [10] Fresnais M, Yildirim E, Karabulut S, Jager D, Zornig I, Benzel J, et al. Rapid MALDI-MS assays for drug quantification in biological matrices: Lessons learned, new developments, and future perspectives. *Molecules.* 2021;**26**(5)
- [11] Spruill ML, Maletic-Savatic M, Martin H, Li F, Liu X. Spatial analysis of drug absorption, distribution, metabolism, and toxicology using mass spectrometry imaging. *Biochemical Pharmacology.* 2022;**201**:115080
- [12] Karlsson O, Hanrieder J. Imaging mass spectrometry in drug development and toxicology. *Archives of Toxicology.* 2017;**91**(6):2283-2294
- [13] Yagnik G, Liu Z, Rothschild KJ, Lim MJ. Highly multiplexed Immunohistochemical MALDI-MS imaging of biomarkers in tissues. *Journal of the American Society for Mass Spectrometry.* 2021;**32**(4):977-988

- [14] Casadonte R, Kriegsmann M, Kriegsmann K, Hauk I, Meliss RR, Muller CSL, et al. Imaging mass spectrometry-based proteomic analysis to differentiate melanocytic nevi and malignant melanoma. *Cancers (Basel)*. 2021;**13**(13):3197
- [15] Kriegsmann M, Zgorzelski C, Casadonte R, Schwamborn K, Muley T, Winter H, et al. Mass spectrometry imaging for reliable and fast classification of non-small cell lung cancer subtypes. *Cancers (Basel)*. 2020;**12**(9):1-14
- [16] Yang HC, Li W, Sun J, Gross ML. Advances in mass spectrometry on membrane proteins. *Membranes (Basel)*. 2023;**13**(5):457
- [17] Taha HB, Chawla E, Bitan G. IM-MS and ECD-MS/MS provide insight into modulation of amyloid proteins self-assembly by peptides and small molecules. *Journal of the American Society for Mass Spectrometry*. 2023;**34**(10):2066-2086
- [18] Holzlechner M, Eugenin E, Prideaux B. Mass spectrometry imaging to detect lipid biomarkers and disease signatures in cancer. *Cancer Report (Hoboken)*. 2019;**2**(6):e1229
- [19] Scott DA, Casadonte R, Cardinali B, Spruill L, Mehta AS, Carli F, et al. Increases in tumor N-glycan polylactosamines associated with advanced HER2-positive and triple-negative breast cancer tissues. *Proteomics Clinical Applications*. 2019;**13**(1):e1800014
- [20] Li Y, Wang J, Chen W, Lu H, Zhang Y. Comprehensive review of MS-based studies on N-glycoproteome and N-glycome of extracellular vesicles. *Proteomics*. 2023;**2023**:e2300065
- [21] McDowell CT, Lu X, Mehta AS, Angel PM, Drake RR. Applications and continued evolution of glycan imaging mass spectrometry. *Mass Spectrometry Reviews*. 2023;**42**(2):674-705
- [22] Peng W, Kobeissy F, Mondello S, Barsa C, Mechref Y. MS-based glycomics: An analytical tool to assess nervous system diseases. *Frontiers in Neuroscience*. 2022;**16**:1000179
- [23] Wang Z, Zhu H, Xiong W. Advances in mass spectrometry-based multi-scale metabolomic methodologies and their applications in biological and clinical investigations. *Science Bulletin (Beijing)*. 2023;**68**(19):2268-2284
- [24] Kriegsmann M, Arens N, Endris V, Weichert W, Kriegsmann J. Detection of KRAS, NRAS and BRAF by mass spectrometry – a sensitive, reliable, fast and cost-effective technique. *Diagnostic Pathology*. 2015;**10**:132
- [25] Su KY, Tseng JS, Liao KM, Yang TY, Chen KC, Hsu KH, et al. Mutational monitoring of EGFR T790M in cfDNA for clinical outcome prediction in EGFR-mutant lung adenocarcinoma. *PLoS One*. 2018;**13**(11):e0207001
- [26] Sutton BC, Birse RT, Maggert K, Ray T, Hobbs J, Ezenekwe A, et al. Assessment of common somatic mutations of EGFR, KRAS, BRAF, NRAS in pulmonary non-small cell carcinoma using iPLEX(R) HS, a new highly sensitive assay for the MassARRAY(R) system. *PLoS One*. 2017;**12**(9):e0183715
- [27] Lin Y, Lin CH, Yin X, Zhu L, Yang J, Shen Y, et al. Newborn screening for spinal muscular atrophy in China using DNA mass spectrometry. *Frontiers in Genetics*. 2019;**10**:1255
- [28] Lin Y, Zheng W, Chen Y, Huang C, Fu Q, Chen D, et al. Incorporating second-tier genetic screening for multiple acyl-CoA dehydrogenase deficiency. *Clinica Chimica Acta*. 2022;**537**:181-187

- [29] Williams GR, Cook L, Lewis LD, Tsongalis GJ, Nerenz RD. Clinical validation of a 106-SNV MALDI-ToF MS pharmacogenomic panel. *Journal of Applied Lab Medicine*. 2020;5(3):454-466
- [30] Wollmann BM, Storset E, Kringen MK, Molden E, Smith RL. Prediction of CYP2D6 poor metabolizers by measurements of solanidine and metabolites-a study in 839 patients with known CYP2D6 genotype. *European Journal of Clinical Pharmacology*. 2023;79(4):523-531
- [31] Evans JP, Skrzynia C, Burke W. The complexities of predictive genetic testing. *BMJ*. 2001;322(7293):1052-1056
- [32] Unim B, Pitini E, Lagerberg T, Adamo G, De Vito C, Marzuillo C, et al. Current genetic service delivery models for the provision of genetic testing in Europe: A systematic review of the literature. *Frontiers in Genetics*. 2019;10:552
- [33] International HapMap C, Frazer KA, Ballinger DG, Cox DR, Hinds DA, Stuve LL, et al. A second generation human haplotype map of over 3.1 million SNPs. *Nature*. 2007;449(7164):851-861
- [34] Shastry BS. SNPs: Impact on gene function and phenotype. *Methods in Molecular Biology*. 2009;578:3-22
- [35] Defo J, Awany D, Ramesar R. From SNP to pathway-based GWAS meta-analysis: Do current meta-analysis approaches resolve power and replication in genetic association studies? *Briefings in Bioinformatics*. 2023;24(1):bbac600
- [36] Frayling TM, Timpson NJ, Weedon MN, Zeggini E, Freathy RM, Lindgren CM, et al. A common variant in the FTO gene is associated with body mass index and predisposes to childhood and adult obesity. *Science*. 2007;316(5826):889-894
- [37] Hernandez MM, Banu R, Shrestha P, Patel A, Chen F, Cao L, et al. RT-PCR/ MALDI-TOF mass spectrometry-based detection of SARS-CoV-2 in saliva specimens. *Journal of Medical Virology*. 2021;93(9):5481-5486
- [38] Ramos-Levi A, Barabash A, Valerio J, Garcia de la Torre N, Mendizabal L, Zulueta M, et al. Genetic variants for prediction of gestational diabetes mellitus and modulation of susceptibility by a nutritional intervention based on a Mediterranean diet. *Frontier in Endocrinology (Lausanne)*. 2022;13:1036088
- [39] Ryan DJ, Toomey S, Smyth R, Madden SF, Workman J, Cummins R, et al. Exhaled breath condensate (EBC) analysis of circulating tumour DNA (ctDNA) using a lung cancer specific UltraSEEK oncogene panel. *Lung Cancer*. 2022;168:67-73
- [40] Allinson LM, Potts A, Goodman A, Bown N, Bashton M, Thompson D, et al. Loss of ALK hotspot mutations in relapsed neuroblastoma. *Genes, Chromosomes & Cancer*. 2022;61(12):747-753
- [41] Pedersen H, Ejegod DM, Quint W, Xu L, Arbyn M, Bonde J. Clinical performance of the full genotyping Agena MassARRAY HPV assay using SurePath screening samples within the VALGENT4 framework. *The Journal of Molecular Diagnostics*. 2022;24(4):365-373
- [42] Giannoudis A, Sartori A, Eastoe L, Zakaria R, Charlton C, Hickson N, et al. Genomic profiling using the UltraSEEK panel identifies discordancy between paired primary and breast cancer brain metastases and an association

with brain metastasis-free survival. *Breast Cancer Research and Treatment*. 2021;**190**(2):241-253

- [43] Sirivisoot S, Kasantikul T, Techangamsuwan S, Radtanakantikanon A, Chen K, Lin TY, et al. Evaluation of 41 single nucleotide polymorphisms in canine diffuse large B-cell lymphomas using MassARRAY. *Scientific Reports*. 2022;**12**(1):5120
- [44] Tian HX, Zhang XC, Wang Z, Chen JG, Chen SL, Guo WB, et al. Establishment and application of a multiplex genetic mutation-detection method of lung cancer based on MassARRAY platform. *Cancer Biology & Medicine*. 2016;**13**(1):68-76
- [45] Ellis JA, Ong B. The MassARRAY((R)) system for targeted SNP genotyping. *Methods in Molecular Biology*. 2017;**1492**:77-94
- [46] Oeth P, del Mistro G, Marnellos G, Shi T, van den Boom D. Qualitative and quantitative genotyping using single base primer extension coupled with matrix-assisted laser desorption/ionization time-of-flight mass spectrometry (MassARRAY). *Methods in Molecular Biology*. 2009;**578**:307-343
- [47] Kiani AK, Bonetti G, Donato K, Kaftalli J, Herbst KL, Stuppia L, et al. Polymorphisms, diet and nutrigenomics. *Journal of Preventive Medicine and Hygiene*. 2022;**63**(2 Suppl 3):E125-EE41
- [48] Wang F, Zheng J, Cheng J, Zou H, Li M, Deng B, et al. Personalized nutrition: A review of genotype-based nutritional supplementation. *Frontiers in Nutrition*. 2022;**9**:992986
- [49] Singh V. Current challenges and future implications of exploiting the omics data into nutrigenetics and nutrigenomics for personalized diagnosis

and nutrition-based care. *Nutrition*. 2023;**110**:112002

- [50] Lal MK, Sharma E, Tiwari RK, Devi R, Mishra UN, Thakur R, et al. Nutrient-mediated perception and signalling in human metabolism: A perspective of nutrigenomics. *International Journal of Molecular Sciences*. 2022;**23**(19):11305
- [51] Guevara-Ramirez P, Cadena-Ullauri S, Ruiz-Pozo VA, Tamayo-Trujillo R, Paz-Cruz E, Simancas-Racines D, et al. Genetics, genomics, and diet interactions in obesity in the Latin American environment. *Frontiers in Nutrition*. 2022;**9**:1063286
- [52] Sekar P, Ventura EF, Dhanapal A, Cheah ESG, Loganathan A, Quen PL, et al. Gene-diet interactions on metabolic disease-related outcomes in southeast Asian populations: A systematic review. *Nutrients*. 2023;**15**(13)
- [53] Mitchelson KAJ, Ni Chathail MB, Roche HM. Systems biology approaches to inform precision nutrition. *The Proceedings of the Nutrition Society*. 2023;**82**(2):208-218
- [54] Xu ZY, Jing X, Xiong XD. Emerging role and mechanism of the FTO gene in cardiovascular diseases. *Biomolecules*. 2023;**13**(5):850
- [55] Scuteri A, Sanna S, Chen WM, Uda M, Albai G, Strait J, et al. Genome-wide association scan shows genetic variants in the FTO gene are associated with obesity-related traits. *PLoS Genetics*. 2007;**3**(7):e115
- [56] Sentinelli F, Incani M, Coccia F, Capoccia D, Cambuli VM, Romeo S, et al. Association of FTO polymorphisms with early age of obesity in obese Italian subjects. *Experimental Diabetes Research*. 2012;**2012**:872176

- [57] Grunnet LG, Nilsson E, Ling C, Hansen T, Pedersen O, Groop L, et al. Regulation and function of FTO mRNA expression in human skeletal muscle and subcutaneous adipose tissue. *Diabetes*. 2009;**58**(10):2402-2408
- [58] Smemo S, Tena JJ, Kim KH, Gamazon ER, Sakabe NJ, Gomez-Marin C, et al. Obesity-associated variants within FTO form long-range functional connections with IRX3. *Nature*. 2014;**507**(7492):371-375
- [59] Karra E, O'Daly OG, Choudhury AI, Yousseif A, Millership S, Neary MT, et al. A link between FTO, ghrelin, and impaired brain food-cue responsivity. *The Journal of Clinical Investigation*. 2013;**123**(8):3539-3551
- [60] Song Y, Wade H, Zhang B, Xu W, Wu R, Li S, et al. Polymorphisms of fat mass and obesity-associated gene in the pathogenesis of child and adolescent metabolic syndrome. *Nutrients*. 2023;**15**(12):2643
- [61] Popovic AM, Hudek Turkovic A, Zuna K, Bacun-Druzina V, Rubelj I, Matovinovic M. FTO gene polymorphisms at the crossroads of metabolic pathways of obesity and epigenetic influences. *Food Technology and Biotechnology*. 2023;**61**(1):14-26
- [62] Rivera-Iniguez I, Gonzalez-Becerra K, Ramos-Lopez O, Perez-Beltran YE, Chaguen-Hernandez MS, Martinez-Lopez E, et al. Lipid-related genetic variants for personalized dietary interventions: A systematic review. *Molecular Nutrition & Food Research*. 2023;**67**(14):e2200675
- [63] Jabeen K, Rehman K, Akash MSH. Genetic mutations of APOEepsilon4 carriers in cardiovascular patients lead to the development of insulin resistance and risk of Alzheimer's disease. *Journal of Biochemical and Molecular Toxicology*. 2022;**36**(2):e22953
- [64] Marais AD. Apolipoprotein E in lipoprotein metabolism, health and cardiovascular disease. *Pathology*. 2019;**51**(2):165-176
- [65] Bos MM, Noordam R, Blauw GJ, Slagboom PE, Rensen PCN, van Heemst D. The ApoE epsilon4 isoform: Can the risk of diseases be reduced by environmental factors? *The Journals of Gerontology. Series A, Biological Sciences and Medical Sciences*. 2019;**74**(1):99-107
- [66] Martinez-Lapiscina EH, Galbete C, Corella D, Toledo E, Buil-Cosiales P, Salas-Salvado J, et al. Genotype patterns at CLU, CR1, PICALM and APOE, cognition and Mediterranean diet: The PREDIMED-NAVARRA trial. *Genes & Nutrition*. 2014;**9**(3):393
- [67] Kivipelto M, Rovio S, Ngandu T, Kareholt I, Eskelinen M, Winblad B, et al. Apolipoprotein E epsilon4 magnifies lifestyle risks for dementia: A population-based study. *Journal of Cellular and Molecular Medicine*. 2008;**12**(6B):2762-2771
- [68] Vasconcellos C, Ferreira O, Lopes MF, Ribeiro AF, Vasques J, Guerreiro CS. Nutritional genomics in nonalcoholic fatty liver disease. *Biomedicine*. 2023;**11**(2):319
- [69] Zumaraga MPP, Arquiza J, Concepcion MA, Perlas L, Alcudia-Catalma MN, Rodriguez M. Genotype effects on beta-carotene conversion to vitamin A: Implications on reducing vitamin A deficiency in the Philippines. *Food and Nutrition Bulletin*. 2022;**43**(1):25-34
- [70] Leung WC, Hessel S, Meplan C, Flint J, Oberhauser V, Tourniaire F,

- et al. Two common single nucleotide polymorphisms in the gene encoding beta-carotene 15,15'-monooxygenase alter beta-carotene metabolism in female volunteers. *The FASEB Journal*. 2009;**23**(4):1041-1053
- [71] Wang TT, Edwards AJ, Clevidence BA. Strong and weak plasma response to dietary carotenoids identified by cluster analysis and linked to beta-carotene 15,15'-monooxygenase 1 single nucleotide polymorphisms. *The Journal of Nutritional Biochemistry*. 2013;**24**(8):1538-1546
- [72] Moran NE, Thomas-Ahner JM, Fleming JL, McElroy JP, Mehl R, Grainger EM, et al. Single nucleotide polymorphisms in beta-carotene oxygenase 1 are associated with plasma lycopene responses to a tomato-soy juice intervention in men with prostate cancer. *The Journal of Nutrition*. 2019;**149**(3):381-397
- [73] Feigl B, Morris CP, Voisey J, Kwan A, Zele AJ. The relationship between BCMO1 gene variants and macular pigment optical density in persons with and without age-related macular degeneration. *PLoS One*. 2014;**9**(2):e89069
- [74] Goyette P, Christensen B, Rosenblatt DS, Rozen R. Severe and mild mutations in cis for the methylenetetrahydrofolate reductase (MTHFR) gene, and description of five novel mutations in MTHFR. *American Journal of Human Genetics*. 1996;**59**(6):1268-1275
- [75] Goyette P, Frosst P, Rosenblatt DS, Rozen R. Seven novel mutations in the methylenetetrahydrofolate reductase gene and genotype/phenotype correlations in severe methylenetetrahydrofolate reductase deficiency. *American Journal of Human Genetics*. 1995;**56**(5):1052-1059
- [76] Li WX, Cheng F, Zhang AJ, Dai SX, Li GH, Lv WW, et al. Folate deficiency and gene polymorphisms of MTHFR, MTR and MTRR elevate the hyperhomocysteinemia risk. *Clinical Laboratory*. 2017;**63**(3):523-533
- [77] Liew SC, Gupta ED. Methylenetetrahydrofolate reductase (MTHFR) C677T polymorphism: Epidemiology, metabolism and the associated diseases. *European Journal of Medical Genetics*. 2015;**58**(1):1-10
- [78] Raghubeer S, Matsha TE. Methylenetetrahydrofolate (MTHFR), the one-carbon cycle, and cardiovascular risks. *Nutrients*. 2021;**13**(12):4562
- [79] Zhao L, Li T, Dang M, Li Y, Fan H, Hao Q, et al. Association of methylenetetrahydrofolate reductase (MTHFR) rs1801133 (677C>T) gene polymorphism with ischemic stroke risk in different populations: An updated meta-analysis. *Frontiers in Genetics*. 2022;**13**:1021423
- [80] Huo Y, Li J, Qin X, Huang Y, Wang X, Gottesman RF, et al. Efficacy of folic acid therapy in primary prevention of stroke among adults with hypertension in China: The CSPPT randomized clinical trial. *Journal of the American Medical Association*. 2015;**313**(13):1325-1335
- [81] Bikle DD. Vitamin D metabolism, mechanism of action, and clinical applications. *Chemistry & Biology*. 2014;**21**(3):319-329
- [82] Szymczak-Pajor I, Miazek K, Selmi A, Balcerzyk A, Sliwinska A. The action of vitamin D in adipose tissue: Is there the link between vitamin D deficiency and adipose tissue-related metabolic disorders? *International Journal of Molecular Sciences*. 2022;**23**(2):956

- [83] Wimalawansa SJ. Infections and autoimmunity-the immune system and vitamin D: A systematic review. *Nutrients*. 2023;**15**(17):3842
- [84] Wu F, Fuleihan GE, Cai G, Lamberg-Allardt C, Viljakainen HT, Rahme M, et al. Vitamin D supplementation for improving bone density in vitamin D-deficient children and adolescents: Systematic review and individual participant data meta-analysis of randomized controlled trials. *The American Journal of Clinical Nutrition*. 2023;**118**(3):498-506
- [85] Mohan A, Haider R, Fakhor H, Hina F, Kumar V, Jawed A, et al. Vitamin D and polycystic ovary syndrome (PCOS): A review. *Annals of Medical Surgery (Lond)*. 2023;**85**(7):3506-3511
- [86] Upadhyay PK, Thakur N, Vishwakarma VK, Srivastav RK, Ansari TM. Role of vitamin D in management of diabetes and unresolved cardiovascular diseases. *Current Diabetes Reviews*. 2024;**20**:e010923220647 [Online ahead of print]
- [87] Santa K, Watanabe K, Kumazawa Y, Nagaoka I. Phytochemicals and vitamin D for a healthy life and prevention of diseases. *International Journal of Molecular Sciences*. 2023;**24**(15)
- [88] Cashman KD, Dowling KG, Skrabakova Z, Gonzalez-Gross M, Valtuena J, De Henauw S, et al. Vitamin D deficiency in Europe: Pandemic? *The American Journal of Clinical Nutrition*. 2016;**103**(4):1033-1044
- [89] Nurminen V, Seuter S, Carlberg C. Primary vitamin D target genes of human monocytes. *Frontiers in Physiology*. 2019;**10**:194
- [90] Valdivielso JM, Fernandez E. Vitamin D receptor polymorphisms and diseases. *Clinica Chimica Acta*. 2006;**371**(1-2):1-12
- [91] Fronczek M, Osadnik T, Banach M. Impact of vitamin D receptor polymorphisms in selected metabolic disorders. *Current Opinion in Clinical Nutrition and Metabolic Care*. 2023;**26**(4):316-322
- [92] Zhao M, Liu Z, Shi H, Song J. Prognostic role of vitamin D receptor in digestive system tumours: A systematic review and preliminary meta-analysis. *PLoS One*. 2023;**18**(8):e0289598
- [93] Morrison NA, Qi JC, Tokita A, Kelly PJ, Crofts L, Nguyen TV, et al. Prediction of bone density from vitamin D receptor alleles. *Nature*. 1994;**367**(6460):284-287
- [94] Tourkochristou E, Mouzaki A, Triantos C. Gene polymorphisms and biological effects of vitamin D receptor on nonalcoholic fatty liver disease development and progression. *International Journal of Molecular Sciences*. 2023;**24**(9):8288
- [95] Bouillon R. Comparative analysis of nutritional guidelines for vitamin D. *Nature Reviews. Endocrinology*. 2017;**13**(8):466-479
- [96] Wang TJ, Zhang F, Richards JB, Kestenbaum B, van Meurs JB, Berry D, et al. Common genetic determinants of vitamin D insufficiency: A genome-wide association study. *Lancet*. 2010;**376**(9736):180-188
- [97] Arabi A, Zahed L, Mahfoud Z, El-Onsi L, Nabulsi M, Maalouf J, et al. Vitamin D receptor gene polymorphisms modulate the skeletal response to vitamin D supplementation in healthy girls. *Bone*. 2009;**45**(6):1091-1097
- [98] Morrison NA, George PM, Vaughan T, Tilyard MW, Frampton CM, Gilchrist NL. Vitamin D receptor genotypes influence the success

of calcitriol therapy for recurrent vertebral fracture in osteoporosis. *Pharmacogenetics and Genomics*. 2005;**15**(2):127-135

[99] Caio G, Volta U, Sapone A, Leffler DA, De Giorgio R, Catassi C, et al. Celiac disease: A comprehensive current review. *BMC Medicine*. 2019;**17**(1):142

[100] Fasano A, Catassi C. Current approaches to diagnosis and treatment of celiac disease: An evolving spectrum. *Gastroenterology*. 2001;**120**(3):636-651

[101] Kagnoff MF. Celiac disease: Pathogenesis of a model immunogenetic disease. *The Journal of Clinical Investigation*. 2007;**117**(1):41-49

[102] Sapone A, Bai JC, Ciacci C, Dolinsek J, Green PH, Hadjivassiliou M, et al. Spectrum of gluten-related disorders: Consensus on new nomenclature and classification. *BMC Medicine*. 2012;**10**:13

[103] Wolters VM, Wijmenga C. Genetic background of celiac disease and its clinical implications. *The American Journal of Gastroenterology*. 2008;**103**(1):190-195

[104] Louka AS, Moodie SJ, Karel K, Bolognesi E, Ascher H, Greco L, et al. A collaborative European search for non-DQA1*05-DQB1*02 celiac disease loci on HLA-DR3 haplotypes: Analysis of transmission from homozygous parents. *Human Immunology*. 2003;**64**(3):350-358

[105] Kuja-Halkola R, Lebwohl B, Halfvarson J, Wijmenga C, Magnusson PK, Ludvigsson JF. Heritability of non-HLA genetics in coeliac disease: A population-based study in 107 000 twins. *Gut*. 2016;**65**(11):1793-1798

[106] Tsai SH, Chang PY, Wen YH, Lin WT, Hsu FP, Chen DP. Screening of

single nucleotide polymorphisms within HLA region related to hematopoietic stem cell transplantation using MassARRAY technology. *Scientific Reports*. 2023;**13**(1):5913

[107] Montgomery RK, Mulberg AE, Grand RJ. Development of the human gastrointestinal tract: Twenty years of progress. *Gastroenterology*. 1999;**116**(3):702-731

[108] Fabre A, Fabre A, Bon C, Guerry P, Segurel L. Proposed mechanism for the selection of lactase persistence in childhood. *BioEssays*. 2023;**45**(7):e2200243

[109] Kowalowka M, Kosewski G, Lipinski D, Przyslawski J. A comprehensive look at the -13910 C>T LCT gene polymorphism as a molecular marker for vitamin D and calcium levels in young adults in central and Eastern Europe: A preliminary study. *International Journal of Molecular Sciences*. 2023;**24**(12):10191

[110] Porzi M, Burton-Pimentel KJ, Walther B, Vergeres G. Development of personalized nutrition: Applications in lactose intolerance diagnosis and management. *Nutrients*. 2021;**13**(5):1503

[111] Lukito W, Malik SG, Surono IS, Wahlqvist ML. From 'lactose intolerance' to 'lactose nutrition'. *Asia Pacific Journal of Clinical Nutrition*. 2015;**24**(Suppl 1):S1-S8

[112] Ugidos-Rodriguez S, Matallana-Gonzalez MC, Sanchez-Mata MC. Lactose malabsorption and intolerance: A review. *Food & Function*. 2018;**9**(8):4056-4068

[113] Guimaraes Alves AC, Sukow NM, Adelman Cipolla G, Mendes M, Leal TP, Petzl-Erler ML, et al. Tracing the distribution of European lactase persistence genotypes along

the Americas. *Frontiers in Genetics*. 2021;**12**:671079

[114] Auton A, Brooks LD, Durbin RM, Garrison EP, Kang HM, Korbel JO, et al. A global reference for human genetic variation. *Nature*. 2015;**526**(7571):68-74

[115] Catanzaro R, Sciuto M, Marotta F. Lactose intolerance: An update on its pathogenesis, diagnosis, and treatment. *Nutrition Research*. 2021;**89**:23-34

[116] De Luca P, Iaconis D, Biffali E, Enza C, de Magistris L, Riegler G, et al. Development of a novel SNP assay to detect lactase persistence associated genetic variants. *Molecular Biology Reports*. 2021;**48**(11):7087-7093

[117] Enattah NS, Sahi T, Savilahti E, Terwilliger JD, Peltonen L, Jarvela I. Identification of a variant associated with adult-type hypolactasia. *Nature Genetics*. 2002;**30**(2):233-237

[118] Hammer HF, Fox MR, Keller J, Salvatore S, Basile G, Hammer J, et al. European guideline on indications, performance, and clinical impact of hydrogen and methane breath tests in adult and pediatric patients: European Association for Gastroenterology, Endoscopy and Nutrition, European Society of Neurogastroenterology and Motility, and European Society for Paediatric Gastroenterology Hepatology and Nutrition consensus. *United European Gastroenterology Journal*. 2022;**10**(1):15-40

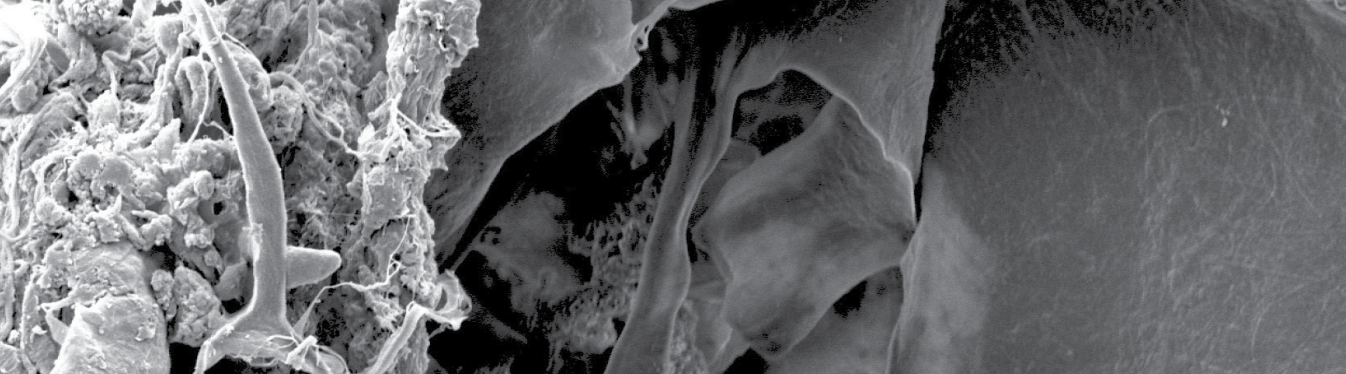
[119] Segurel L, Bon C. On the evolution of lactase persistence in humans. *Annual Review of Genomics and Human Genetics*. 2017;**18**:297-319

[120] Gaudin RGN, Figueiro G, Flores-Gutierrez S, Mut P, Vega-Requena Y, Luna-Andrada L, et al. DNA polymorphisms associated with

lactase persistence, self-perceived symptoms of lactose intolerance, milk and dairy consumption, and ancestry, in the Uruguayan population. *American Journal of Human Biology*. 2023;**35**(6):e23868

[121] Kable ME, Chin EL, Huang L, Stephensen CB, Lemay DG. Association of estimated daily lactose consumption, lactase persistence genotype (rs4988235), and gut microbiota in healthy adults in the United States. *The Journal of Nutrition*. 2023;**153**(8):2163-2173

[122] Chengolova Z, Ivanova R, Gabrovska K. Lactose intolerance – single nucleotide polymorphisms and treatment. *Journal of American Nutrition Association*. 2023;**2023**:1-8



Edited by Guillermo Huerta Cuellar

This book explores the use of electronic microscopes and spectroscopic techniques to solve different problems. Delve into the intricate details of these powerful tools as they reveal some of the hidden mysteries of the microscopic realm. From exploring the inner workings of cells to analyzing the composition of materials at the atomic level, this book offers an engaging and motivating journey into the realm of cutting-edge scientific exploration in electron microscopy and spectroscopy techniques with emerging trends in the field. Whether you are an experienced researcher or a curious enthusiast, this book will motivate your scientific thinking to discover and expand your understanding of the microscopic world, inviting you to continue working in these areas to obtain more interesting results.

Published in London, UK

© 2024 IntechOpen

© Thomas Spaeter / iStock

IntechOpen

